Republic of Iraq
Ministry of Higher Education and Scientific Research
University of Kerbala -College of Science
Chemistry Department

Preparation, Characterization and Application of Zinc Oxide for Treatment of Methyl Green Dye

A thesis
Submitted to the Council of the College of Science, University of Kerbala as a Partial Fulfillment of the Requirements for M.Sc in Chemistry

By

Eitemad Saleh Fadhil Al Hussnawe

Supervisor

Assist.prof.Dr. Luma Majeed Ahmed

2015 AD 1436AH

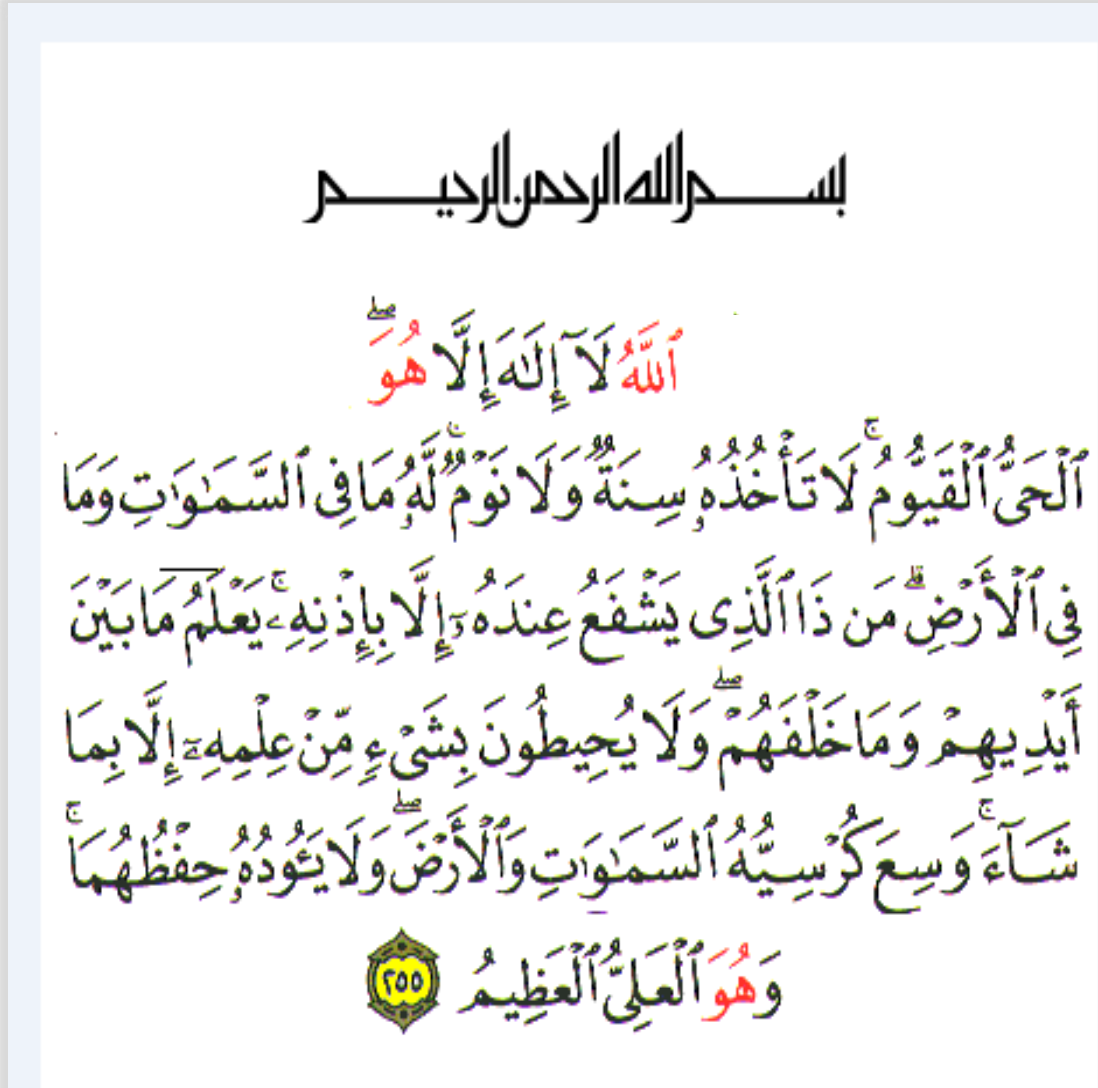

صدق الله العلي العظيم

سورة البقرة الآية (255)

Dedication

To Imam Mahdi (calf God reappearance)

To my parents who make my Dreams possible...

To to my husband…

To to my friends…

Who enhance me all the time

Eitemad /2015

Acknowledgments

First, I would like to express my great appreciation to the almighty Allah for his support enabling me to complete this work. A special thanks to my supervisor, **Assistant Professor Dr. Luma Majeed Ahmed** for his irreplaceable suggestions, wonderful contribution, and continuing support to start and complete this scientific research.

Also, I would like to thank all people who introduced direct or indirect assistance for me, and my gratitude is due to all faculty members of Department of Chemistry– College of Science in Kerbala University, for their constant support.

Finally, I would like to thank my family and friends for their continuous support through this process. Their voices of encouragement and support guided me along the way.

Eitemad

Abstract

This work consists of three parts, **the first one** is focused on the preparation of ZnO and calcination at 500 ^{o}C. Moreover, metallized commercial and prepared ZnO by different amounts of Co and Ag were prepared by photo deposition method.

The properties of naked and metalized commercial and prepared ZnO were estimated by Fourier transform infrared (FT-IR) analysis, X-ray diffraction (XRD) analysis and Atomic force microscope (AFM) analysis. Moreover, the Atomic absorption (A.A) analysis for metalized commercial and prepared ZnO was done.

FT-IR analysis for prepared ZnO was obtained by stretching vibrations of the OH at 3446 cm^{-1} and a strong band around 500 cm^{-1} that assigned to find the stretching band of Zn-O. So these results refer to the creation of ZnO.

The new band around 1383-1384 cm^{-1} occurred when cobalt was loaded on commercial and prepared ZnO surfaces. From the other hand, the new band around (1386-1388) cm^{-1} was formed when silver was loaded on both commercial and prepared ZnO surfaces.

XRD data was utilized to calculate the mean crystallite sizes and crystallite sizes of naked and metalized commercial and the prepared ZnO by employing the Scherer equation and the modified Scherer equation.

The mean crystallite sizes and crystallite sizes for naked commercial ZnO were increased when loading 0.5%Co and decreased when loading 2%Ag. However, the mean crystallite sizes and crystallite sizes data for naked prepared ZnO were increased with loading 1%Co and 2%Ag.

The AFM images indicated that most of the shapes of naked and metalized commercial and prepared ZnO were semi spherical. Moreover, the most particle sizes were less than the mean crystalline size and crystalline size.

The second part includes studying the effect of different parameters on photo decolourization of methyl green dye with the presence of naked and metalized commercial of ZnO. The parameters involved with the amount and the type of loading metals, dose of catalyst, concentration of dye, initial pH of solution and temperature. However, **the third part** includes the same parameters studied in the second part but the catalyst is different (naked and metalized prepared ZnO that calcination at 500 ^{o}C).

The photo catalytic decolourization of methyl green in the presence of the naked and the metalized commercial ZnO included decolourization process of it at optimum conditions.

The effect of initial concentration of methyl green was studied by employing different concentrations from (25-100) ppm. The reaction is obeyed a pseudo first order.

The dosage of naked and metalized commercial ZnO is determined and the optimum value is equal to 0.7 g/200 mL. on the other hand, the optimum dosage for prepared ZnO is equal to 0.6 g/200 mL, while the value is slightly increased with loading of 2%Ag on prepared ZnO surface.

The best initial pH of aqueous solution for photo catalytic decolourization of methyl green is equal to 10 with commercial ZnO and 5.40 for 2% Ag /commercial ZnO, prepared ZnO and 2% Ag /prepared ZnO respectively.

The effect of temperature was investigated by utilizing Arrhenius equation and found it is the rise in the temperature of (278.15 to 293.15) K was increased the rate of reaction, hence the photo-decolourization of methyl green was endothermic reaction. Moreover, the activation energy found to be (24.910) kJ/mol with the presence of commercial ZnO, while it is equal to (6.185) kJ/mol with the presence of Ag (2.00)/ commercial ZnO and equal to (19.690, 10.375) kJ/mol with presence of prepared ZnO and Ag (2.00)/prepared ZnO respectively. The change in entropy was found to be fewer, which that indicated an increase of randomness, while the reaction was non spontaneous.

Contents

Contents

List of Figures

Abbreviation and Symbols	The Meaning
AFM	Atomic Force Microscopy
AOPs	Advanced Oxidation Processes
CB	Conduction Band
C_o	Initial Concentration
C_t	Concentration of substrate at time t of irradiation.
CV	Valance Band
e^-	Negative Electron
E_a	Activation Energy
E_f	Fermi Level
E_g	Energy gap
eV	Electron Volt
F_{cc}	Face centered cubic
FLM	Fermi Energy Level of Metal
FLS	Fermi Energy Level of Semiconductor
FT-IR	Fourier transform infrared
FWHM	Full width half -maximum
g	gram
h^+	Positive Hole
HOMO	Highest occupied molecular orbital
I_o	Light intensity
K	Kelvin
k	Rate constant
kJ	Kilo Joule
L	Mean Crystallite Size
Ĺ	Crystallite Size
mL	milli liter
Mol	Mole
Nm	Nanometer
PDE	Photo decolourization efficiency
pH_{zpc}	Zero Point Charge
T	Temperature
t	Time of irradiation
UV	Ultraviolet
UV(A)	Ultra violet light in the range from 315 to 380nm
XRD	X-Ray Diffraction
λ	Wavelength

CHAPTER ONE INTRODUCTION

1.1 General Introduction:

Photocatalysis is a process that accelerated the rate of the photochemical reactions in existence of a photocatalyst (usually a photo- semiconductor) that illuminated under ultraviolet or visible light [1].

Many chemical reactions take place only when the molecule is has or provided by the suitable activation energy. In case of the photochemical reactions, the light usually provides the activation energy while the thermal reactions can take place even in the absence of light [2]. Photocatalysis usually involves two reactions: oxidation and reduction. These reactions need to be balanced which is regarded as an essential requirement of catalysis [3].

Photocatalysis is widely employed in water and air purification [4], cleaning surfaces [5-7], self-sterilizing surfaces [7], self- photocatalytic lithography [8-10], microchemical systems [11-18], synthesis of some organic compounds [15] and the production of hydrogen [19]. And the most important applications in photocatalysis is an environmental cleanup that becomes one of the most active areas. Hence air, water and solid waste pollution have a detrimental effect. Thereby many researches were used for the decolourization of organic compounds to CO_2 and H_2O by a mineralization process, depression of toxic metal ions to them non-toxic states, decomposition of pollutants in air and water such as CO, NOx and NH_3[1, 20-22].

1.2 Photochemical and Thermal reactions:

In photochemical processes, the solar photons are directly absorbed by reactants with /or without a catalyst that will lead to a reaction (see scheme1-1). This way causes a chemical reaction that generated by the energy of the sun's photons [2]. Photochemical reaction is required [23]:

a. involved absorption of light.

b. produced materials that should be easy to store and transport.
c. the effect of temperature is very little on the photochemical reaction rate.
d. The free energy change (ΔG) of a photochemical reaction may not be negative.

In thermochemical processes, the some solar radiation is converted into thermal energy that leads to a chemical reaction(see scheme1-1). In the other word, the chemical reaction is generated by a thermal energy that-is produced by the sun for the general purpose of substituting fossil fuels [23].The requirements for Thermo-chemical reaction are[2,3]:

a. The thermochemical reaction mostly endothermic.
b. They are accelerated by the presence of a catalyst.
c. These reactions involve absorption or evolution of heat.
d. Temperature is clearly affected at thermochemical reaction rate.
e. The free energy change (ΔG) of a thermochemical reaction is always negative.

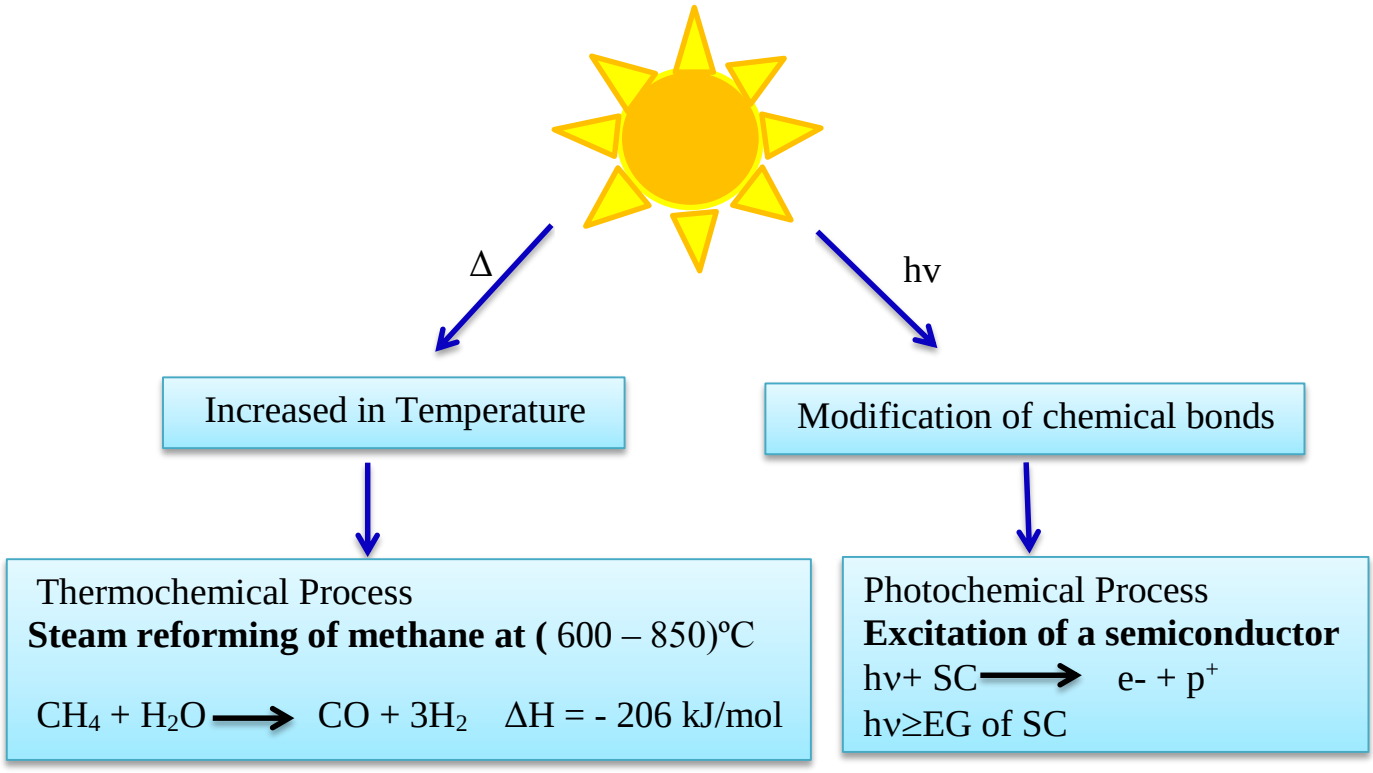

Scheme1-1: Solar Chemical Applications (modified from reference [23]).

1.3 Solar Systems

Solar spectrum consists of a small part of ultraviolet radiation between (3.5 – 8)% of the solar spectrum (note the figure 1-1). In the solar reactor, the knowledge of the amount of the photon flux incident is very important for the economic comparison between the solar radiation and the artificial electric lamps as a different types of UV photon source[23].

The solar photocatalytic decolourization process is having a possible mineralization of toxic organics, remove and recover toxic metals. Recently, The most important applications of solar photocatalysis are disinfection of drinking water (SODIS) that performed without the use of chlorine but by employing a UV transparent solar collector [24]. SODIS is regarded a simple, cheap technique and can be enhanced by the existence of semiconductors [25]. It used for disinfection of drinking water by putting the infected drinking water in transparent containers and displaying to direct sunlight [25].

Sunlight can widely used to remove more pollutants (mostly organic compound) from water. So the removal of color compounds from wastewater (mostly textile dyes) is regarded as more important than the removal of the other colorless chemicals materials [26]. when finished the decolourization process, the compounds such as CO_2, H_2O, NO_3^-, SO_3 were resulted, these compounds is regarded as non-toxic or at less toxic than the degraded original compound [27].

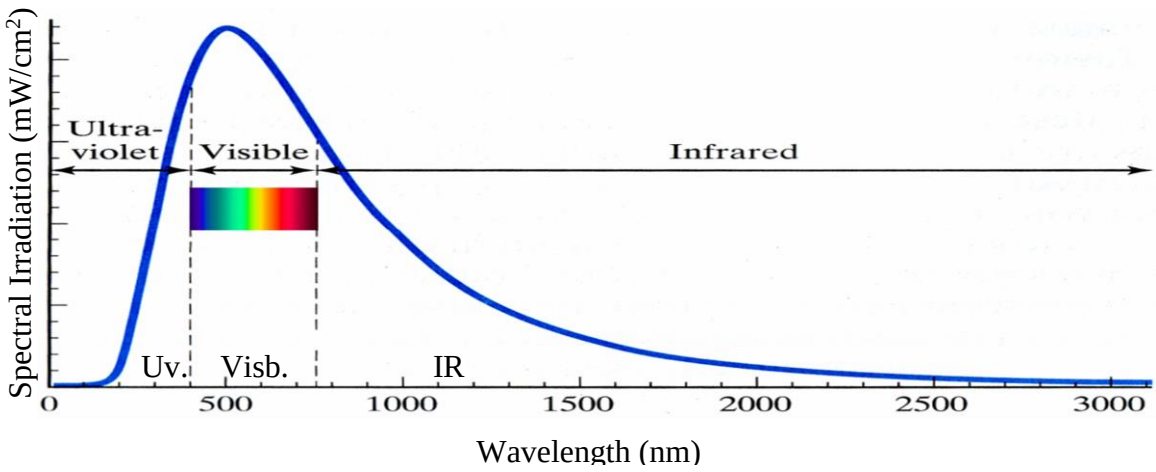

Figure1-1: Solar spectrum diagram (modified from references [28])

1.4 Semiconductors:

A semiconductors can be defined as crystalline or amorphous solid materials, that have an intermediate value which lies between a metal and an insulator. They can be changed by altering: the impurity, the temperature, size in quantum dot and Illumination with light [29]. In general, to the account of the semiconductor properties, one must understand the Band Theory for electrical conductivity. (According to the band theory, each solid can be characterized by two energy bands: a valence band (VB) that has a lower energy, completely filled with electrons (at least at 0°K); and a conductivity band (CB) with higher energy, that be empty at 0°K). The energetic distance between them amounts to 0.7-3.5 eV for semiconductors and is called a forbidden band or a band gap, (E_g). While in metals (VB) overlaps (CB), and in isolators Eg amounts to 6-7 eV) [30]. Table 1-1 shows the band gaps values of some photo-semiconductors.

Table 1-1: Forbidden bandwidths of some more popular photo-semiconductors [30 -31]

Semiconductors	Eg (eV)
Si	1.1
Fe_2O_3	2.3
WO_3	2.8
TiO_2 (rutile)	3.0
TiO_2 (anatase)	3.2
ZnO	3.37
SnO_2	3.5

In general, the band gap values of photo-semiconductor also refer to the colour of the semiconductors, because of the semiconductors absorb certain light spectrum when it is having energy equal to or higher than E_g energy. So light absorption leads to electron transfer from a valence band (VB) to a conductive band (CB).

So, the energy of visible light lies in the region of 1.5 eV (red) to 3.0 eV (violet). Thereby, the semiconductors are having a narrow band gap of about 1.5 eV (black), but they are having a band gap of about 3.0 eV (white), (e.g. CdS, absorbs part of the wavelength from the visible region, are yellow colour [30]. Semiconductor materials are very sensitive to impurities in the crystal lattice. Hence the controlled addition of these impurities is known "a doping". The properties of a pure semiconductor are called "intrinsic", while the "extrinsic" are referred to dopants semiconductors [32].In general, the semiconductors have two types: n-type semiconductor and p-type semiconductor, according to figure 1-2. These types of semiconductors depended on the position of the Fermi level (The Fermi level is defined as the highest occupied molecular orbital(HOMO) in the valence band at 0.0 K or can be defined as the energy at which the probability of an energy level being occupied by an electron is exactly 1/2). In semiconductor the Fermi level is located in the band gap. In an intrinsic semiconductor, the Fermi level approximately lies between conduction band energy (EC) and valence band energy (EV). From other the hand, at n-type doping, the Fermi level shifts toward the conduction band (negatively charged) edge, while p-type doping shifts toward the valence band (positively charged) edge [33,34].

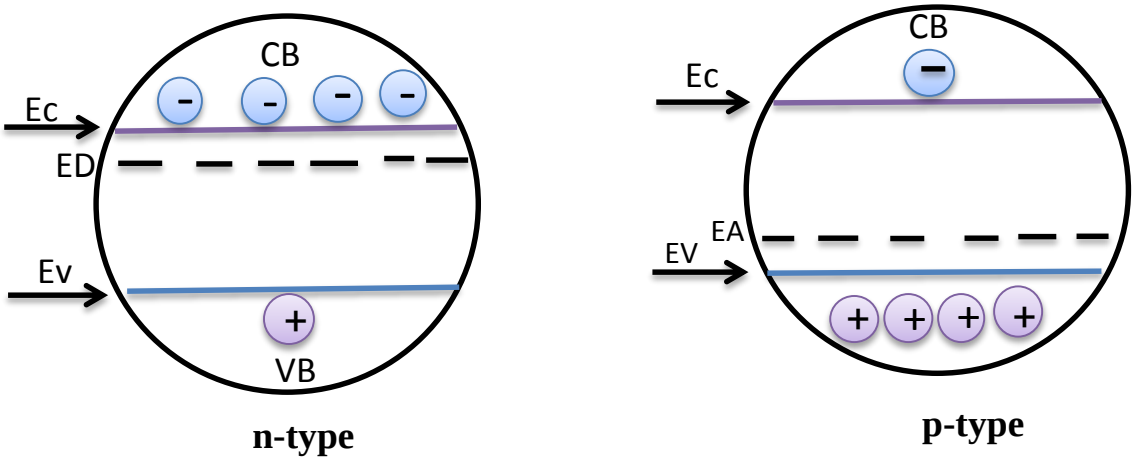

ED → energy level of donor impurity EA → energy level of acceptor impurity

Figure1-2: Energy level diagram for n-type and p-type semiconductors.

During the last few years, semiconductor nanoparticles have drawn much attention because of their have a novel optical and transport properties that give have great potential for many optoelectronic applications [35].

1.5 Advanced Oxidation Processes (AOPs):

Advanced oxidation processes are regarded as one of the most important methods to destroy the organic pollutants and form a friendly products [36-39].The AOPs can be divided into two groups: abiotic decolourization and photo decolourization[40, 41]. See figure 1-3.

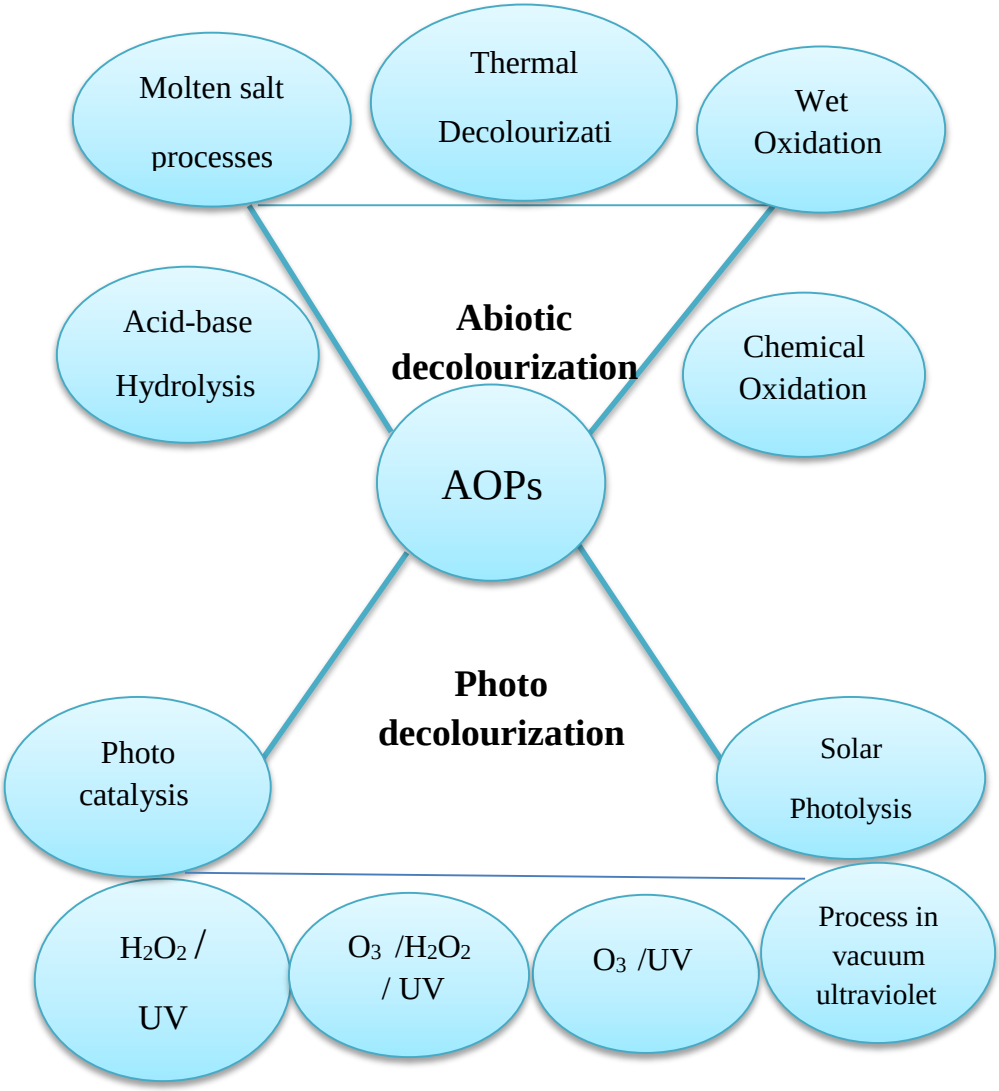

Figure 1-3: Schematic diagram to obtain the some examples on the photo decolourization and abiotic decolourization

Generally, the reactivity of the photo catalysts like (TiO_2, ZnO and CdS) depends on the surface charge property and the nature of dye molecules [42,43].

The essential mechanism of AOPs function is formed of highly reactive free radicals such as hydroxyl radical . Hydroxyl radicals ($HO^{\bullet}$) are high effective in breaking down the organic chemicals (such as dyes) because $HO^{\bullet}$ is a high reactive electrophiles and regards as a second strong oxidant (has value 2.80 V) as shown in table 1-2. The reactivity of $HO^{\bullet}$ that will be react rapidly and non-selectively with nearly all electron-rich organic compounds[44].

Table 1-2 : Hydroxyl radical as the second strongest oxidant [45].

Oxidant	E^{o} / V
Fluorine (F_2)	3.03
Hydroxyl radical ($^{\bullet}OH$)	2.80
Atomic oxygen (O)	2.42
Ozone (O_3)	2.07
Hydrogen peroxide(H_2O_2)	1.78
Hydro-peroxyl radical ($O_2H^{\cdot}$)	1.70
Potassium permanganate ($KMnO_4$)	1.67
Chlorine (Cl_2)	1.36
Bromine (Br_2)	1.09
Iodine (I_2)	0.54

The advantages of AOP_S are greater than from the disadvantages. The advantages of AOPs are summarized as follows [39]:

1.Cut down the reaction time.

2. Have low economic cost.

3. Have a pertinent potential to reduce the toxicity of organic pollutant compounds by forming $CO_2 + H_2O$ in mineralization process.

But, AOP is quenching some application by increasing the amount of peroxide[46].

$$H_2O_2 + h\nu \longrightarrow 2^{\bullet}OH \qquad 1\text{-}1$$

$H_2O_2 + {}^{\bullet}OH \longrightarrow H_2O + HO^{\bullet}{}_2$ 1-2

$HO^{\bullet}{}_2 + {}^{\cdot}OH \longrightarrow H_2O + O_2$ 1-3

1.5.1 Photocatalysis:

The photocatalysis word is consisted of two parts: the prefix "photo" defined as "light" [47], and "catalysis" is the process when a substance shares in altering the rate of a chemical transformation of the reactants without consumed it in the final. Mostly, the catalyst increases the rate of reaction by depressing the activation energy (E_a). Hence, the photocatalysis is a reaction that employs the light to activate a catalyst which alters the rate of a chemical reaction without being involved itself.

Photocatalysis is regarded as more advanced technique than the conventional organic synthesis, that due to following reasons:-

1. In photocatalytic reactions, oxidation and reduction process occur simultaneously on the photocatalyst particles, while in conventional reactions, the reaction needs different oxidizing agent and reducing agent.

2. The photochemical reaction mostly is a single step reaction, so the product has just produced by mixing the reactant and irradiating, but the conventional reactions are multi-step reactions.

3. During the photochemical reactions, the common solvent used is water while in conventional reactions many solvents are employed.

4. The photocatalytic reactions occur at ambient temperature and pressure, but the conventional reactions don't need to maintain drastic conditions.

The requirements of photocatalysis are summarized as [23]:

1. The photocatalysis process must be an endothermic reaction, cyclic, and without any side reactions to prevent the decolourization of photochemical reactants.

2. The photochemical reaction should use in a large range of light, i.e., UV, visible, and part of IR, hence, the solar spectrum is suitable economically.

3. The back reaction must be very slow to help the storage of the products, while, the reaction must be rapid to recover the energy content.

4. The products of the photochemical reaction must be not difficult to save and transport.

The photocatalysis process is classified into two basic types: homogenous photocatalysis and heterogeneous photocatalysis. These classified depend on the kind of phase for the catalyst and the reactants[38, 39].

1.5.1.1 Homogeneaus Photocatalysis:

This process is carried out with catalyst and reactants have analogous phases (single-phase) under near UV irradiation, and production ·OH radical which plays a crucial role in demolition of organic pollutants mostly in water, such as textile dyes. The employed of UV light via photodecolourization of organic pollutants can be classified into two kinds [23]:

1. Direct photodecolourization (photolysis), it's depended on the direct excitation of the organic pollutant by using UV light like (Dye +light).

2. Photooxidation, that deals with the use of UV light with an oxidant to produce hydroxyl radicals, which attack the organic pollutants and damage them like (H_2O_2 /UV).

1.5.1.2 Heterogeneous Photocatalysis:

Heterogeneous photocatalysis is defined as a catalytic process which take place through one or more reaction steps when the semiconductor materials irradiated by light of suitable energy and the electron–hole pairs are photogenerated on the surface of them [48]. During the previous years, the processes of heterogeneous photocatalysis on semiconductors evolved, in outset it regarded as potential methods for hydrogen photo production from water [49, 50]. However, some papers concerned on the photo oxidation of some inorganic (e.g. CN^- ions) and organic compounds [4, 51]. The scientists care for application of the heterogeneous photocatalytic methods to detoxification of waste water. Many semiconductor materials can be used for heterogeneous photocatalysis, including ZnO, ZnS, Fe_2O_3 and TiO_2 [52]. The irradiation process of a semiconductor catalyst is an essential process to photo excitation it, which promoted photoelectron from the valence band (VB) to the conductance band (CB), that will create a positive photohole in the valence band. The creation of photo electro- hole pair is separated by an energy distance (band gap (E_g)). In outset, the photon energy of illuminated light is equal to or more than the band gap energy. From other the hand, the photoelectron-hole pair may recombine and generate heat. The photo-reduction process occurs on the conductance band by electron-acceptor species such as O_2, while the photo-oxidation process occurs on the valence band by electron- donor species such as ^-OH which the H_2O originally, and produces the hydroxyl radical that used for decolourization and mineralization of pollutants [1,45,53,54]. The essential processes under illumination of semiconductor particles are shown in the Figure 1-4.

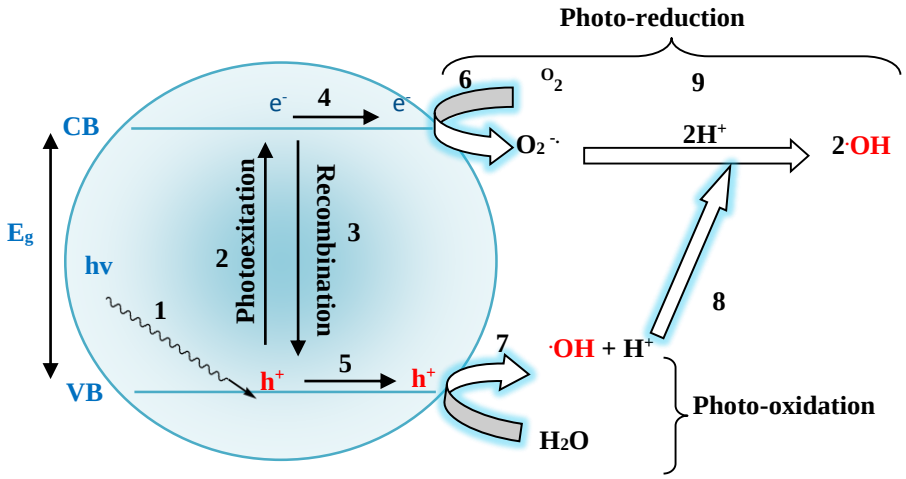

Figure 1-4: Essential Processes under Illumination of semiconductor particles.

The advantages of the heterogeneous photocatalysis process are low cost, high stability, high activity, has a high conversion efficiency and quantum yield, widely used in an industry and an environmental, and works in the high range of spectra (UV and visible light), or solar light [55,56].

on the other side, the recombination process is regarded as disadvantage of the heterogeneous photocatalysis process, due to loss in the energy as heat. In photocatalysis process, the efficiency of the photo-catalyst rises with increases in the surface species which acts as traps by adsorbing them on the photocatalyst surface.

There are three important mechanisms of recombination [45, 57, 58]:

1. Direct recombination, in this kind, the photo electron in the conductive band drops directly into an unoccupied state in the valence band and combines with the photo hole by electrostatic attraction.

2. Surface recombination is regarded a lower probability than others types, due to the surface species which can capture the photogenerated charge carriers (photo electron-hole) and undergo the chemical reaction at the end.

3. Recombination at recombination centers, which is called volume recombination. It is having a high probability compared with the other

type , because the recombination centers lie in the lattice site's transition within the bulk of the crystal and the transition beyond to initial ground state.

Generally, most metal oxide photocatalysts are having a wide band-gap, thereby they will depress the efficiency of the photo-catalyst. However, the essential prerequisite to rise the efficiency of the photo-catalyst is modified the surface of photo-semiconductor [23].

1.7 Modification of Photocatalyst Surface:

There are three essential methods for modification of photocatalytic surface to depress the recombination process: surface sensitization, composite semiconductor and metal-semiconductor modification. These modified is an important to increase the charge separation and the life time of photo hole, thereby that will raise the efficiency of the photoreaction and raise the ability to absorb the large range of the wavelengths [1].

1.7.1 Surface Sensitization:

The surface sensitization favours for a wide band gap semiconductor via physical or chemical adsorption of coloured materials like dye, which absorbs the visible or solar light after irradiation, to excite it either singlet or triplet excited state, then injected the electron via the conductive band of semiconductor which more negative than dye, this modification reports in references [59-61]. Like ruthenium complexes [62] .All of these can be displayed in Figure 1-5.

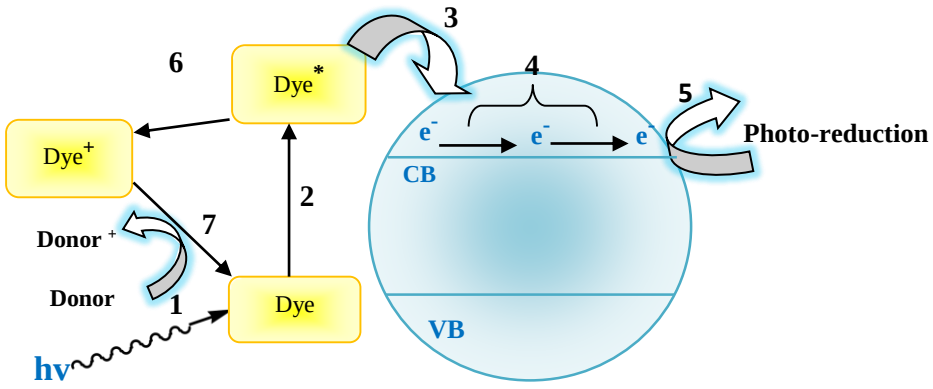

Figure 1-5 : Excitation Steps Using Dye Molecule Sensitizer.

1.7.2 Composite Semiconductor:

This method is used, when the energy of the irradiated light is not enough to excite the semiconductor because it has a big band gap, but the other semiconductor has a small band gap, thereby the coupled process of two semiconductors will raise the efficiency with the use near UV or visible or utilize from solar light. See Figure 1-6. This process has two advantages:

1. Increasing the response of semiconductor that has a large band gap exists in UV by coupling within other that has a small band gap exists in visible light [59].
2. Depressing the recombination of photo electron-hole by injecting the electrons from the higher laying of the conductive band which beyond to semiconductor has a small band gap into the lower laying of conductive band of large band gap semiconductor [63].like TiO_2- SnO_2[64].

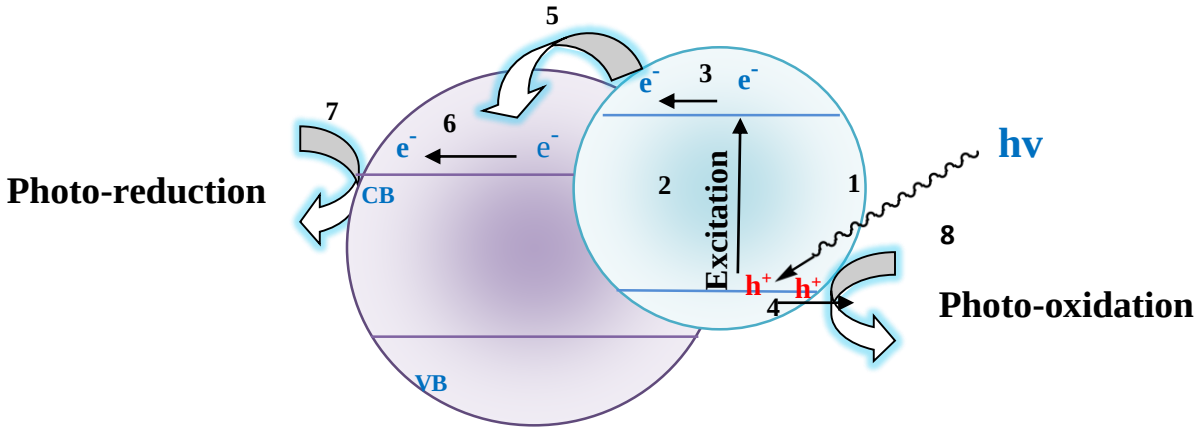

Figure 1-6: Photo-excitation in Composite Semiconductor Photocatalysts.

1.7.3 Metal-Semiconductor Modification (Metalized ZnO Surfaces):

Considerable efforts have been made to modify ZnO nanoparticles to improve the catalytic efficiency in the visible light region. Hence, the advantages of this modifications are [65,66]:

1. To delay the electron–hole recombination.
2. To broaden the absorption spectrum.

3. To facilitate some specific reactions on the surface of catalysts.
4. To improve the photo stability

The metal is deposited on the surface of the semiconductor, this modification is shown in Figure (1-7), which raises the selectivity and the efficiency of photoreaction. This is attributed to the use of the metal as a sink of electrons, hence the lifetime of photo hole increases too. Most of metals in the periodic table can be deposited on the photo semiconductor such as, Li, Al, Mn and Cr loaded on ZnO Surface [67-69]. That depends on the work functions of both (metal and semiconductor). Some values of work functions for some metals at fcc(111) are listed in table1-3. The Miller indices (111) has most compact atomic arrangement and is most stable. This indicates, is Schottky barrier formed.

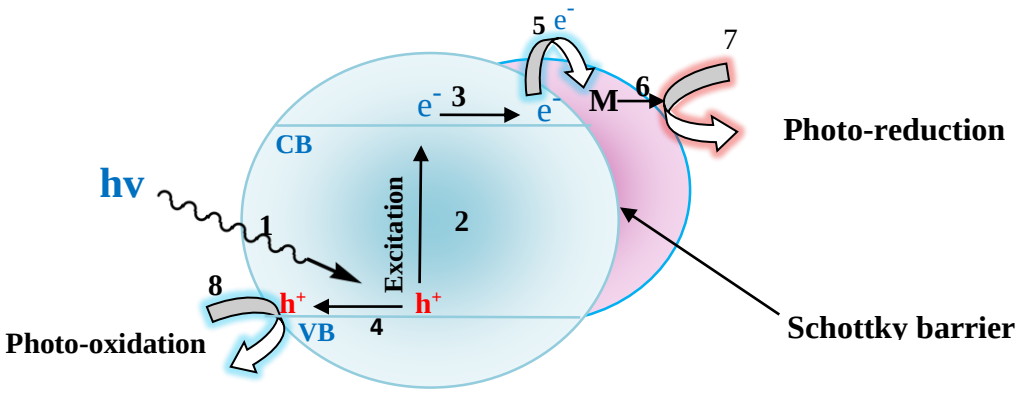

Figure 1-7 : Metal-modification Semiconductor Photocatalyst Particle.

Table 1.3 : Work Functions of Some Metals [70,71].

Metals	Surface	Work functions (eV)
Pt	fcc(111)	5.93
Pd	fcc(111)	5.6
Au	fcc(111)	5.31
Co	fcc(111)	5.0
Ag	fcc(111)	4.74
Zn	fcc(111)	4.22

1.8 Schottky Barrier

It is a potential barrier generated at a metal - semiconductor junction formed. This barrier is formed if the work function of metal (Φm) is higher than the function of semiconductor (Φs) and the Fermi energy level of metal (FL_M) is lower than that for semiconductor (FL_S). In the other word, when the semiconductor illuminates by light, the photoelectron–hole pair created, and the photoelectrons in the semiconductor conductive band will spontaneously flow from the semiconductor to the surface of the metal (metal acts as an electron sank) until the Fermi levels of both are nearer to each other and becomes equal. Moreover, the excess positive charge is accumulates on the surface of the semiconductor, thereby the energy band of semiconductor bends upwards, and forming Schottky barrier (Φb). So, the electrons will flow from semiconductor to metal until Fermi levels of both becomes equal [72 ,73] .

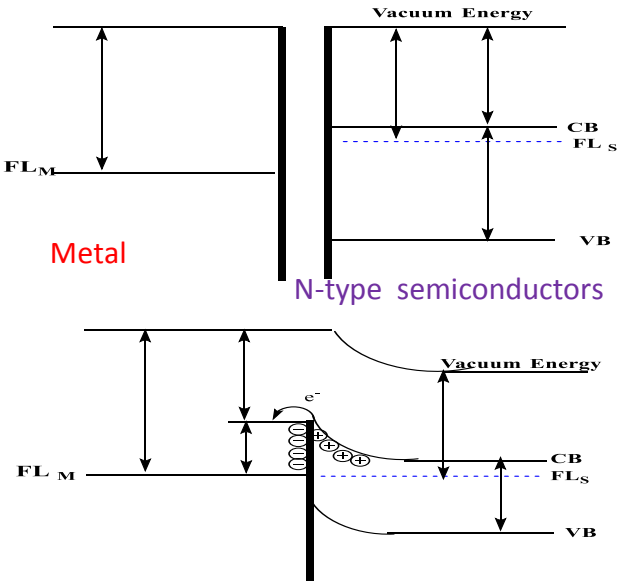

Figure 1-8: Band diagram of a metal and a semiconductor (a) Before and (b) after Being Brought into Contact. (Modified and Redrawn from Reference [74].

1.9 General View of Zinc Oxide

Zinc oxide (ZnO) is an inorganic compound. It is found in the earth's crust as a mineral zincite, so the most ZnO employed commercially is manufactured synthetically. In materials science, "ZnO is often called a II-VI semiconductor because zinc and oxygen lie in the 2^{nd} and 6^{th} groups of the periodic table, respectively". ZnO usually finds as a white powder and a slight soluble in water. It plays an important role in a vast range of applications (show figure 1-9). The powder is widely used in industries including medical, electronic and chemical industries. It is used as an additive material with many compounds like plastics, first aid tapes, food (source of Zn nutrient), ceramics, fire retardants, lubricants, glass, cement, paints and batteries. It is also utilized as filler for rubber goods and in coating processes for paper. Moreover, the Chinese white is used in artists' pigments that regarded a special grade of zinc white. Such the crystalline of ZnO is a light sensitive thereby it absorbs the ultraviolet light, so it can be employed in manufacture of creams, lotions, and ointments to protect the skin from the sunburn. [75-79].

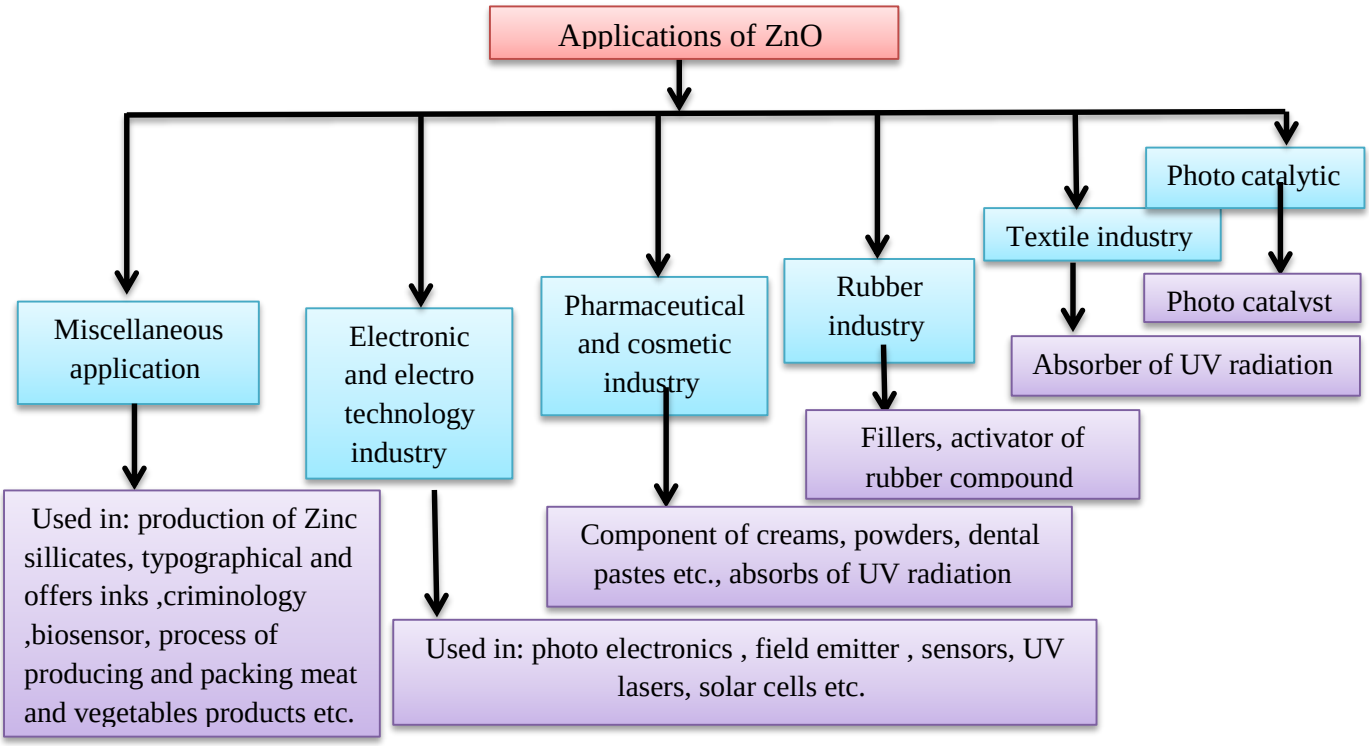

Figure 1-9: Schematic representation all the application of ZnO [80-82].

ZnO has several favorable properties that make it a good photo semiconductor such as: wide band gap (3.37eV), good transparency, high electron mobility, large exciton binding energy (60 m eV), thermal stable, nontoxic, a low cost, higher quantum efficiency, and more active alternative photocatalyst to titanium dioxide (TiO_2) for decolourization of organic pollutants in aqueous solutions [31].

1.9.1 Chemical properties:

Zinc oxide is an amphoteric oxide. So its reaction depends on the pH of the media and the type of adsorption materials on the surface of semiconductor like solvent molecule, substrate (pollutants) and the charged radicals formed, hence the electrostatic force is most dominated on the adsorption between the pollutants and the semiconductor[83]. In general, ZnO surface is having a net surface charge equal to zero, that concept is called zero point charge (pH_{ZPC}). The pH_{ZPC} of ZnO is 9.0, hence, at pH less than pH_{ZPC}, the surface becomes positively charged, while, at pH more than pH_{ZPC}, the surface becomes negatively charged. In acid media, ZnO can be undergo photocorrosion by self- oxidation according to equations 1-4 and 1-5

In acids: $ZnO + 2h^+ \longrightarrow Zn^{2+} + 1/2O_2$ 1-4

$ZnO + 2H^+ \longrightarrow Zn^{2+} + H_2O$ 1-5

While, at basic media, ZnO can be undergo dissolution, that obtained in equation 1-6 [84].

In bases: $ZnO + H_2O + 2OH^- \longrightarrow [Zn(OH)_4]^{2-}$ 1-6

1.9.2 Physical properties:

ZnO is having three forms : cubic rock salt, hexagonal wurtizite and cubic zincblende. The anion is surrounded by four cations at the corners of tetrahedron. This tetrahedral coordination is typical of sp3 Ionic bonding. That is shown in Figure 1-10 [85].

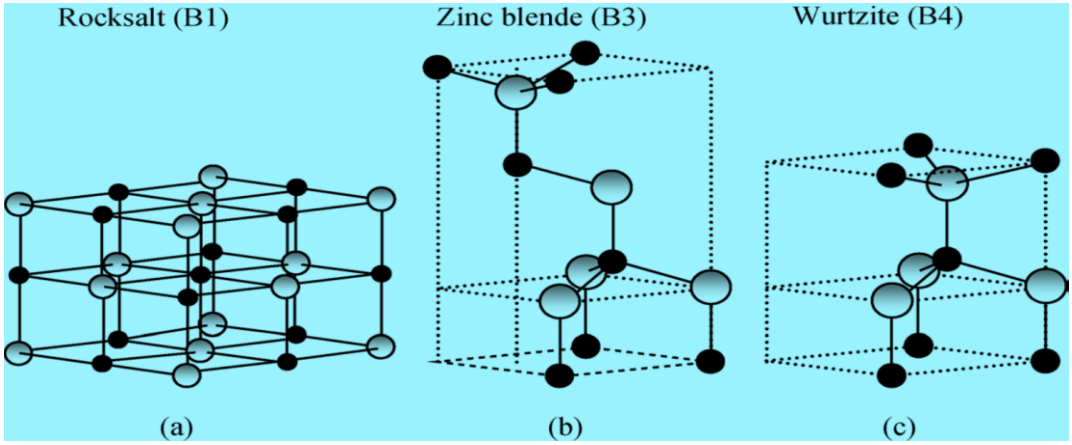

Figure 1-10 : Stick-and-ball representation of ZnO crystal structures:

(a) cubic rock salt (B1), (b) cubic zinc blende (B3), and(c) hexagonal wurtzite (B4). Shaded gray and black spheres denote Zn and O atoms, respectively.

The wurtzite (B4) structure is the most stable and the most common. The zinc blende (B3) structure can be stabilized by growing zinc oxide on substrates with cubic lattice structure. The zinc and oxide centers are tetrahedral in B3 and B4 strictures. Moreover, the zinc blende and wurtzite are polymorphs. At relatively high pressures, zinc oxide can be crystallised in the rock salt **(**B_1**)** motif [86]. The bonds in Zn-O are polar because zinc and oxygen planes naked electric charge (positive and negative, respectively). Thereby, to conserve on the electrical neutrality[87].

1.9.3 Electronic properties:

At room temperature, ZnO has a direct band gap that equal to 3.37 eV, so the pure ZnO is colorless and transparent. Most zinc oxide types has a n-type character [88]. The electron mobility of ZnO is strongly alters with temperature and equal to ~2000 $cm^2/(V{\cdot}s)$ at ~80 K. While, the hole mobility is scarce with values in the range 5– 30 $cm^2/(V{\cdot}s)$[87].

1.10 ZnO Nanoparticles

Nanometric zinc oxide structure shows that the ZnO can be classified in to: one- (1D), two- (2D) and three-dimensional (3D) structures. The one-dimensional structures make up the largest group, including nanorods [89–91], -needles [92], -helixes, -springs and -rings [93], -ribbons [94], -tubes [95–97] -belts [98], -wires [99–101] and -combs [102]. Zinc oxide can be occurred in 2D structures, such as nanopellets, nanoplate and nanosheet [103,104]. Moreover, 3D structures of it consist of snowflakes, dandelion, flower, coniferous urchin-like, *etc.* [105–108]. ZnO nanoparticle (ZnO-NPs) can be a synthesis of different preparation methods. These different methods will produce various morphologies, sizes and characteristics. Among these preparation methods, as shown in scheme 1-2. The precipitation method is widely used, because it provides a simple growth process for nano-scale production, and it is an efficient and inexpensive way [109-119] (see scheme 1.2)

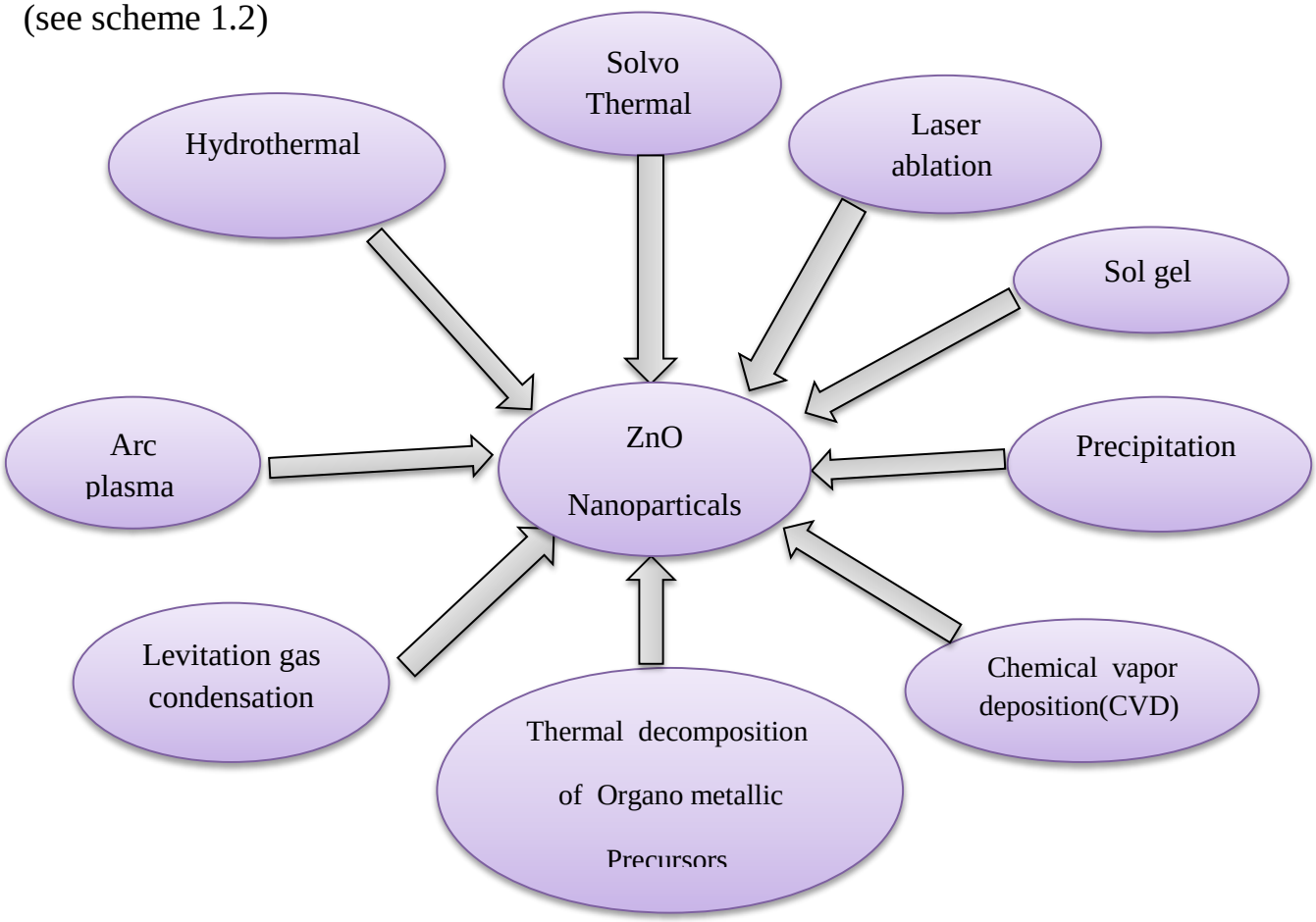

Scheme 1.2: Some synthesis methods of ZnO nanostructures.

1.11 Adsorption:

Adsorption can be defined as the association of molecules (either liquid or vapor) on the surface of other molecules (mostly solid). The liquid-solid or vapor-solid system are called adsorbate and adsorbent respectively .While the reverse process of adsorption that called "desorption"[120,121].The adsorption process has gained importance in the treatment process of the waste water. Because it's recognized as an effective, efficient and economical method for removing the water decontamination. One of the important factors of photocatalytic decolourization is the adsorption process that affect on the photocatalytic oxidation reaction [122]. As any process, adsorption has some important advantages and disadvantage. The advantage can be summarized as :

1. The high ability of removing the toxic organic compounds from wastewater.
2. Finding different types of catalyst.

But the disadvantages are summarized as [123]:

1. The catalyst losses the actionable step by step.
2. The active sites of catalyst are blocked with the present high amount of macromolecular compounds like (dyes) in solution.
3. Some types of catalyst are high cost.

1.11.1 Adsorption on Catalyst Surface

Adsorption occurs when the molecule contacts with the surface that depends on the attractive and repulsive forces between this molecule and the surface at a short distance. The bonding between the surface and the molecules can be either Van der Waals force (physisorption) or chemical bond (chemisorptions) depending on the reactivities of surface and the molecule [124].

In general, when the reaction took place on the catalyst surface, that will form strong interactions (chemical bonds) with the intermediates. These intermediates react to give products and then the separation process (desorption) between the

reactants and the catalyst surface occurs after the reaction is completed [125]. The efficiency of the photocatalytic decolourization raises with the increase the adsorption of organic pollutants on the catalyst surface [126].

1.11.2 Water Adsorption

The splitted of water on semiconductor surface in to hydrogen and oxygen is difficult process. This process was depended on the form of water molecules or dissociated it. The water molecular exists on the surface that will be adsorption and produce hydroxyl group. The hydroxyl group is detected on the surface after H_2O adsorption at 300 K [127]. The adsorbed H_2O molecule reacts with a bridging oxygen atom (as a lattice oxygen) to produce two hydroxyl groups[128]:

$$H_2O + O_L \longrightarrow 2{\cdot}OH \qquad 1\text{-}7$$

where $O_{(L)}$ is a lattice oxygen atom and OH is a hydroxyl group, respectively. Oxygen vacancy on the semiconductor surface is nature strongly adsorbed water. on the other hand, the molecular water is adsorbed at below 160 K and the hydroxyl group produced by water dissociation is found in heating the phyisorbed layer at above 200 K [129]. During illumination the H_2O molecule or ^{-}OH group adsorbed on the surface of catalyst that reacts with the holes in the valence band forming illumination to give hydroxyl radical, but the electrons react with lattice oxygen and not with adsorbed oxygen[130].

$$\text{Semiconductors } (h_{VB}{+}) + H_2O_{ads.} \longrightarrow \text{Semiconductors} + {\cdot}OH_{(ads)} + H^{+} \qquad 1\text{-}8$$

$$\text{Semiconductors} + {}^{-}OH_{(ads)} . \longrightarrow \text{Semiconductors} + {\cdot}OH \qquad 1\text{-}9$$

The existence of water vapor on the catalyst surface depresses the reaction rate by "competitive adsorption" that causes to compete of water vapor with pollutants for adsorption sites on the photocatalyst, thus will reduce the pollutant removal rate [131].

1.11.3 Adsorption of Oxygen:

Purified oxygen is necessary for some applications such as wastewater treatment, chemical processing, etc. [132]. So, the increase of oxygen concentrations leads to raise the decomposition rate of pollutants. The competitive adsorption between pollutants and molecule of oxygen is weak, because the adsorbed oxygen molecules are independent on the electron-trapping [133].While the presence of O_2 or the addition of electron acceptors such as H_2O_2 leads to improve the rate of photocatalytic decolourization of organic compounds, that beyond to reduce the rate of photocatalytic decolourization by recombination of electron-hole pairs. In general, the adsorbed oxygen on the photocatalyst surface leads to trapping the photogenerated electrons and enhances the separation of electron- hole pairs, thereby increasing ·OH concentrations [134]. The surface oxygen types adsorb in the active site of a surface catalyst to produce O_2, O^- and $O_2^{\cdot-}$. These types are detected by using electronic spin resonance (ESR) spectroscopy and give by the following equations [135,136].

$$O_{2(gas)} \longrightarrow O_{2(ads.)} \qquad 1\text{-}10$$

$$O_{2(ads.)} + e^- \longrightarrow O_2^{\cdot-}{}_{(ads.)} \qquad 1\text{-}11$$

$$O_2^{\cdot-}{}_{(ads.)} \longrightarrow O^-_{(ads.} + O_{(ads.)} \qquad 1\text{-}12$$

Where O_2•- is super oxide anion radicals, that is regarded as an one of the strongest reactive species among the free radicals. Superoxide anion reacts with other molecules like (H_2O ,H_2O_2 ,….) according to the following equations [137].

$$O_2^{\cdot-}{}_{(ads.)} + H_2O \longrightarrow 2^-OH + {}^{\cdot}O^+ \qquad 1\text{-}13$$

$$2\cdot OH_2 \longrightarrow H_2O_2 + 2H^+ \qquad 1\text{-}14$$

The two superoxide anions can be reacted with a self and ^+H to form H_2O_2 and O_2 as follows:

$O_2^{\cdot-} + O_2^{\cdot-} + 2H^+ \longrightarrow O_2 + H_2O_2$ 1-15

H_2O_2 reacts with $O_2^{\cdot-}$ by Haber Weiss reaction [138].equation (1-16)

$H_2O_2 + O_2^{\cdot-} \longrightarrow O_2 + {}^{\cdot}OH + {}^{-}OH$ 1-16

On the other hand, the photo holes are trapped by the surface absorbed group (organic molecule) and electrons will be rapped by molecular of oxygen as follows:

$h^+ + RH \longrightarrow R^+ + H$ 1-17

The oxygen anion (O^-) can produce more free organic molecule or hydrocarbon radicals [139]:

$O^- + RH \longrightarrow R^{\cdot} + {}^{\cdot}OH$ 1-18

The interaction between adsorbed oxygen and catalyst surfaces has been extensively studied [138,139]. The charge transfer processes take place between the adsorbed O_2 species such as ($O_2^{\cdot-}$, O^-) and the photoexcited catalyst substrate material. The neutral O_2 molecules adsorb as O^{-2} on catalyst surfaces [140](see figure 1-11), where the electrons are found in the conduction and or from localized semiconductors sites as measured by EPR spectroscopy [141].

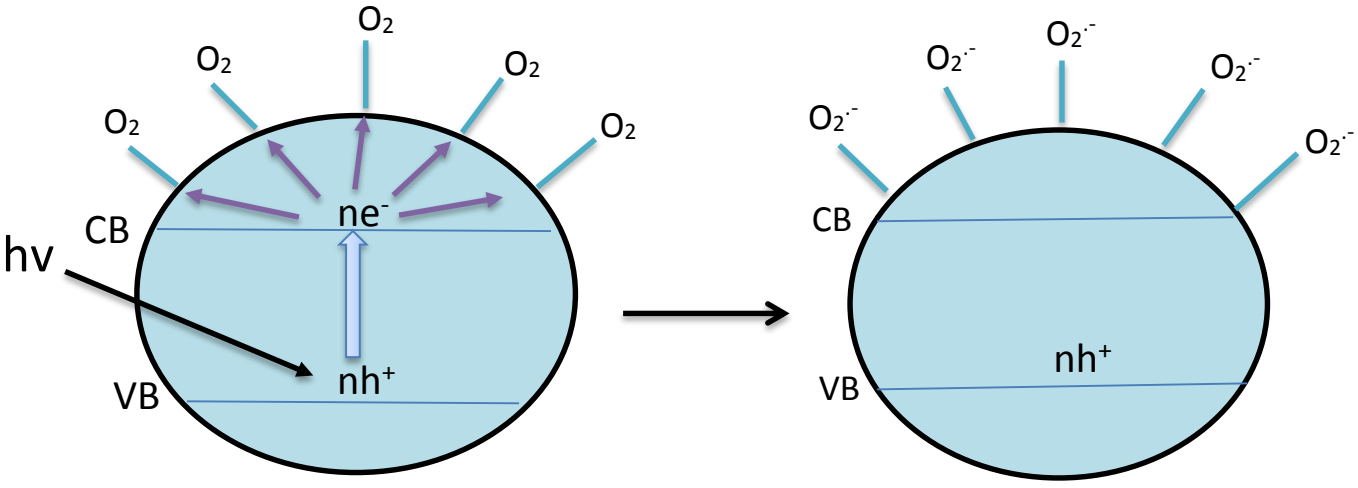

Figure 1-11: Schematic diagram showing the active range of sites for hole trapping.

1.10.4 Dyes adsorption

Many industries, like textile, plastics, dyestuffs and paper, utilize from dyes in color their products that lead to consume a high volumes of water. As a result, that generates a high amounts of colored wastewater. Color is regarded as a first contaminant that formed a wastewater[142]. The presence of slight that amounts to (less than 1 ppm for some dyes) of dyes in water is recognized a highly visible and an undesirable[143] .Water pollutants occur in trace amounts in industrial wastewater. Hence, the indication of the scale of this problem is given by the fact that 2% of dyes that produced are discharged directly in aqueous effluent [144]. So, it is necessary to remove the dyes from wastewater before it is discharged. The most types of the dyes are toxic, carcinogenic and this poses a serious hazard to aquatic living organisms [145]. However, the wastewater containing dyes has a difficult methods for treatment, since the dyes are recalcitrant organic molecules, resistant to aerobic digestion, and stable toward an oxidizing agents, a light and a heat [146]. Some chemical and physical methods are employed to remove the dye. So, the adsorption process is deemed as one of the high effective techniques that is successfully employed for dye to remove dye from wastewater [147,148]. The removal by adsorption is distinguished as an effective and simple technique for dye treatment but it usually generates a large amounts of sludge, that may cause a secondary pollution for water. The individual treatment technique is not enough to wholly remove for the dyes from wastewaters. Hence, the combining for two or more treatment techniques such as employing the adsorption with the photo decolourization (or photo degradation) technique leads to get on a high efficiency for removal of dyes from the wastewater [149].

1.12 Dyes

Dyes can be defined as an organic molecules that have a selective absorb wavelengths of light within the electromagnetic spectra between 400 nm and

800nm (visible range). They contain on chromophores, delocalized electron systems with conjugated double bonds, auxochromes and electron-donating substitutes in stractures that cause or intensify the color of the chromophore by changing the overall energy of the electron system. Chromophores usually are $-C=C-, -C=N-, -N=N-$ and -NO_2. While the auxochromes are -NH_2, -COOH, -SO_3H and -OH group. Large amounts of dyes are widely used in different types of industries, like textile dye, food, cosmetic, paper printing and pharmaceutical. The textile industry is regarded the largest consumer of dyes [150,151]. The dye can be applied in solution, in suspension, by any chemical or physical method . But it imparts a definite colour to the fabric and its colour is retained against the attack of light, moisture, dilute acids, washing soda and soaps. It dose not only adher the surface, while penetrates into the fabrics.The fastness properties, however,vary from dye to dye.

1.13 Classification of Dyes :

Dyes may be broadly classified according to their application in to: chemical structure, and by their method of application to the fiber. In many cases, a chemical class may include dyes of several application classes [152].

1.13.1 Chemical Classification

Under the chemical classification, the range of structural variations is quite difficult to classify them into distinct groups, it is likely that a dye may be placed in more than one group (see scheme 1.3).

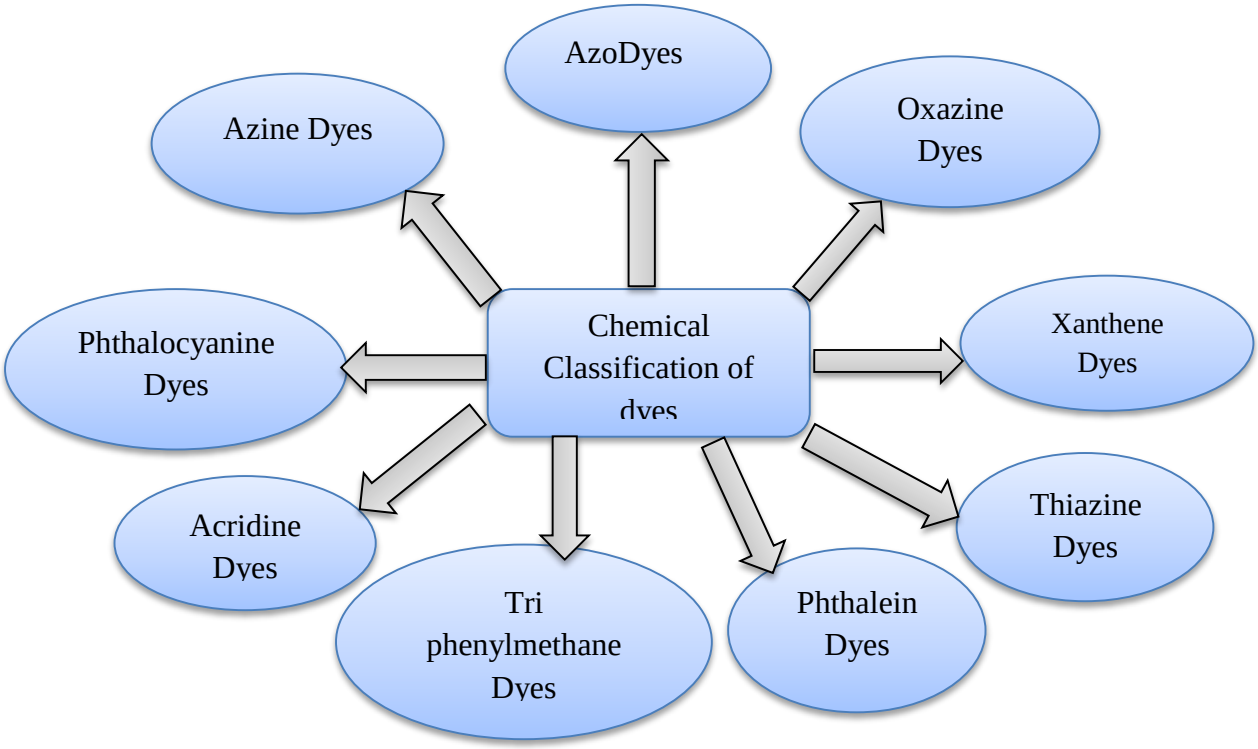

Scheme 1.3 : Chemical Classification of dyes [152].

1.13.2 Classification by application as in the down Scheme below:

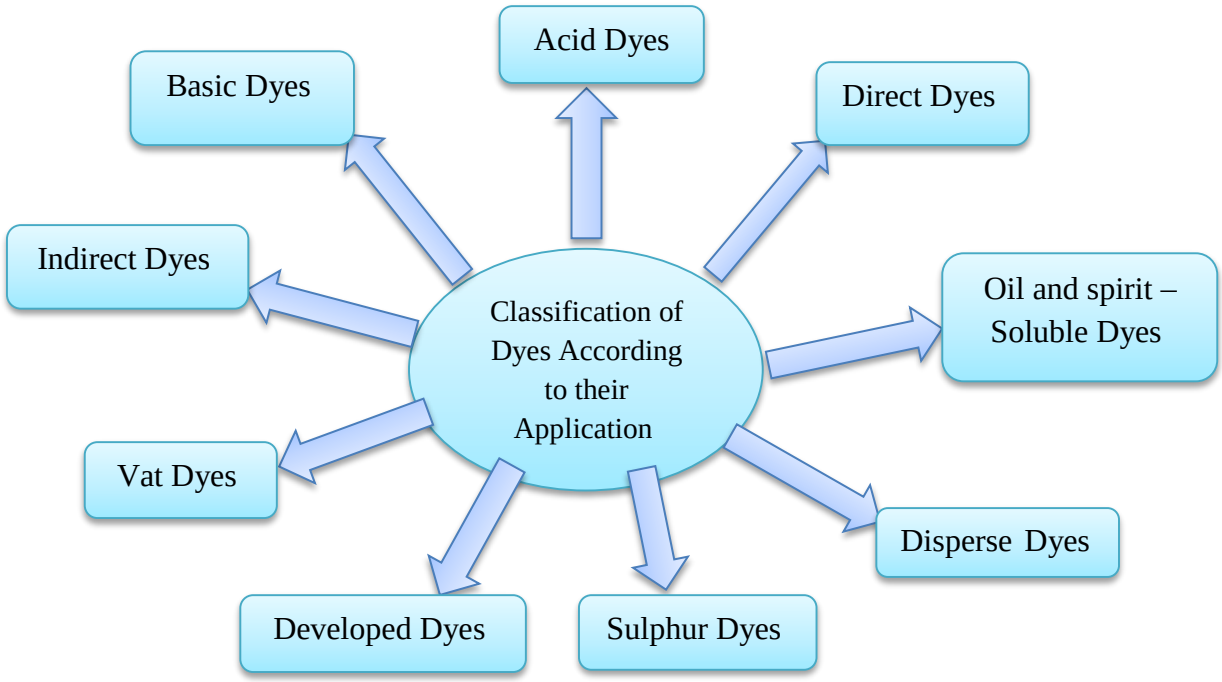

Scheme 1.4: Classification of Dyes According to their Application [152].

1.14 Tri phenylmethane Dyes

Triphenylmethane dyes are derivatives of triphenyl methyl cation. They are represented in the chemical classes. They are basic dyes for wool, silk colouring paper, printing inks, cosmetics, coping papers, food stuffs or for suitably tannin-mordanted cotton but dyes of other classes with better fastness properties. The earliest synthetic dyes were cationic. Many dyes now manufactured were discovered in the nineteenth or early twentieth century. All of these are characterized by exceptional brilliance, high tinctorial strength and low fastness to light [152] . Figure 1.12 shows the derivatives of triphenyl methane Dyes.

Methyl Green Dye

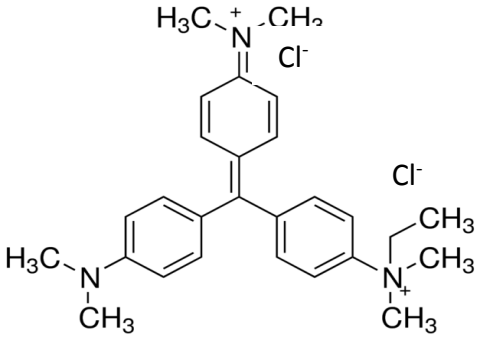

Crystal Violet Dye

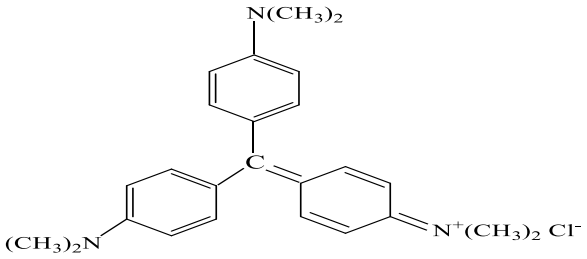

Malachite Green

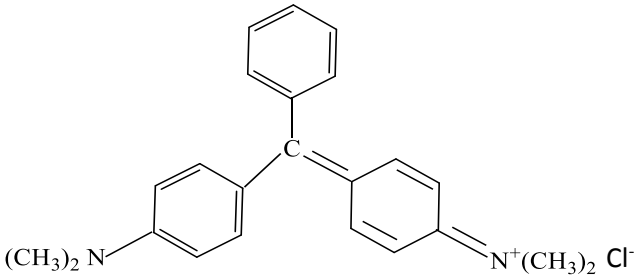

Triphenylmethane

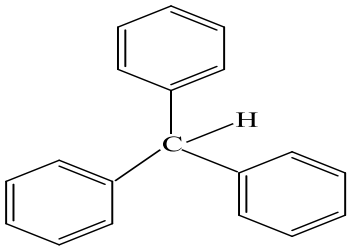

Figure 1.12: The derivatives of tri phenyl methane Dye.

1.14.1 Methyl Green (MG)

Methyl Green (Molecular Formula: $C_{27}H_{35}Cl_2N_3 \cdot ZnCl_2$ is a basic triphenylmethane-type dicationic dye (see figure 1.13). Methyl green may be employed as a pH indicator. So, it is a yellow at pH 1, green at pH 2, blue at pH equal or greater than 3. The more applications of Methyl Green are usually used in staining solutions that utilized in medicine and biology [153], and as photochromophore to sensitize gelatinous films [154].

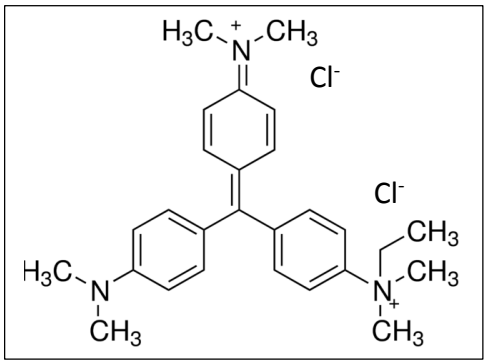

Figure 1.13 : The structure of Methyl Green.

1.15 Photocatalytic Reaction Parameters:

The photocatalysis process on catalyst surface is utilized by raising the redox capability via forms the photoelectrons-photoholes, and controlled in the recombination process between both. Moreover, this increases the decolourization of organic pollutant substrates, by counting on different parameters such as mass of adsorbent catalyst, initial dye concentration, initial pH of the solution and temperature(note figure 1.14) [155,156, 157,158].

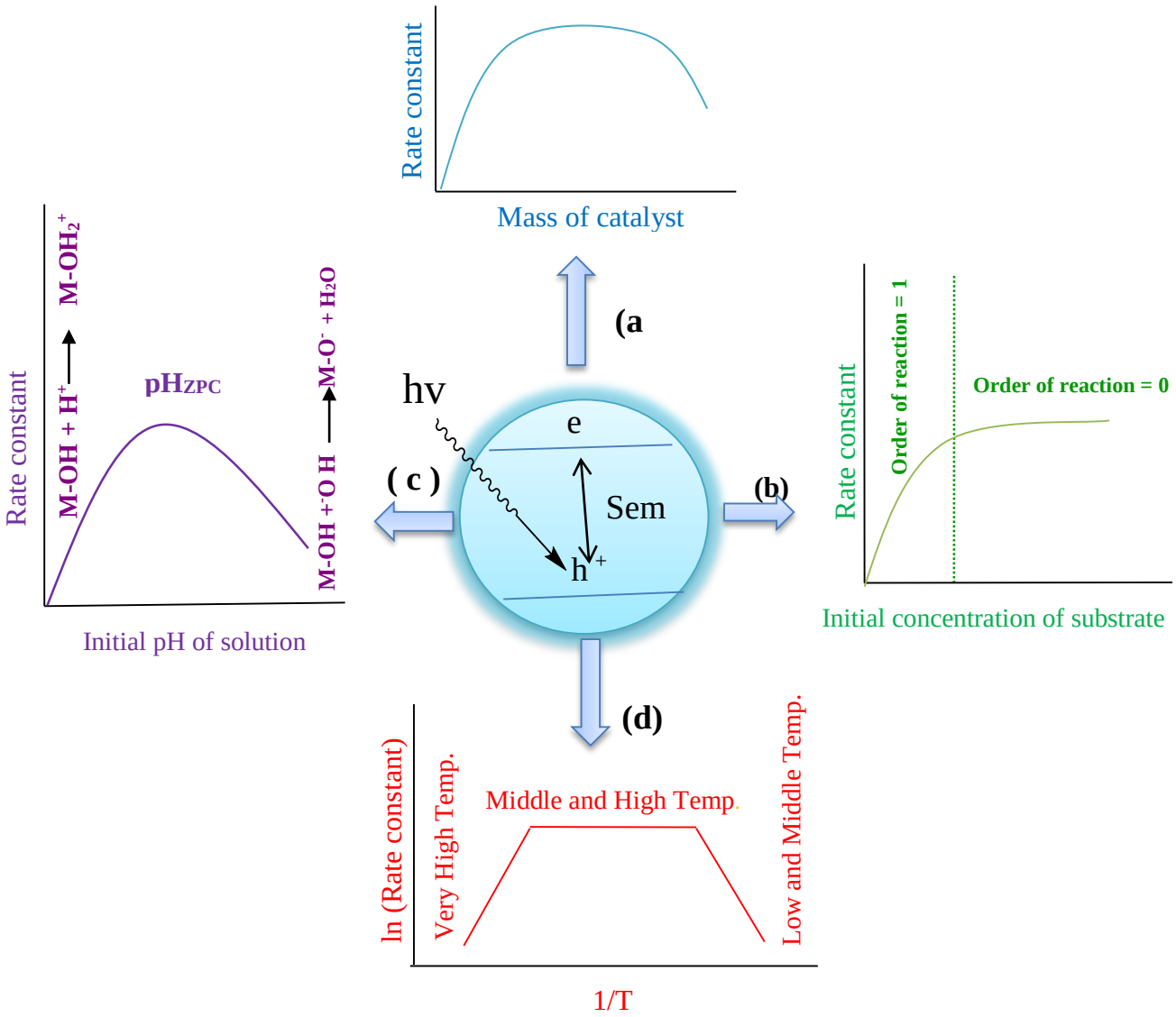

Figure1.14: Rate of photocatalytic Reaction as Function of Common Different Parameters: (a) Mass of Catalyst, (b) Initial Concentration of Substrate, (c) Initial pH of Solution, (d) Temperature

1.15.1 Mass of Catalyst

In order to avoid the needless excess of catalyst and to take care a wholly absorption of light without loss, figure(1.14 a) shows the rate of reaction is directly proportional with the mass of catalyst; this behavior reflects the increment of the numbers of the active sites on catalyst surface. However, above

a certain level of catalyst mass, the reaction rate becomes flat and is not dependent on the mass; this limit relies on the geometry and the conditions of photoreactor and the type of the UV lamp[158]. At a high mass of catalyst, the rate of reaction and the penetration of light will inhibit that attitude to scattering effect [159, 156].

1.15.2 Initial Concentration of Substrate

In photocatalytic or photoadsorption reactions, the decolourization rate of reaction depends on the substrate concentration. From other the word, the formed active species ($^{\cdot}OH$ and $O_2^{\cdot-}$) over the catalyst surface essentially enhances this process. The decolourization rate of photocatalytic reaction of the substrate or organic pollutants in the presence the illuminated catalyst is suitable for the Langmuir-Hinshelwood (L-H) kinetics model (see equation (1-19)). Langmuir-Hinshelwood equation assuming that adsorption -desorption kinetics is faster than the photochemical reaction [160,161].

$$r = -\frac{dC}{dt} = \frac{k\,KC}{(1+KC)} \qquad (1\text{-}19)$$

where: r is the rate of reaction, k is the rate constants, K is the Langmuir constant reflecting the adsorption/desorption equilibrium between the substrate and the photocatalyst surface, C is the concentration of substrate and t is the time of illumination. When the concentration of substrate goes towards to be zero (low concentration), the equation (1-20) must be improved to give an apparent first order equation [162,158]:

$$\ln\left[\frac{C_o}{C}\right] = k\,K.t = k_{app}\,.t \qquad (1\text{-}20)$$

where (k_{app}) is an apparent first order constant.While, with the large

concentrations of substrate, the rate of reaction is maximum and of the zero order (Figure 1. 14 (b)).

The Langmuir-Hinshelwood (L-H) kinetics model has four possible states[158, 163, 164], according to the following schematic (1-5).

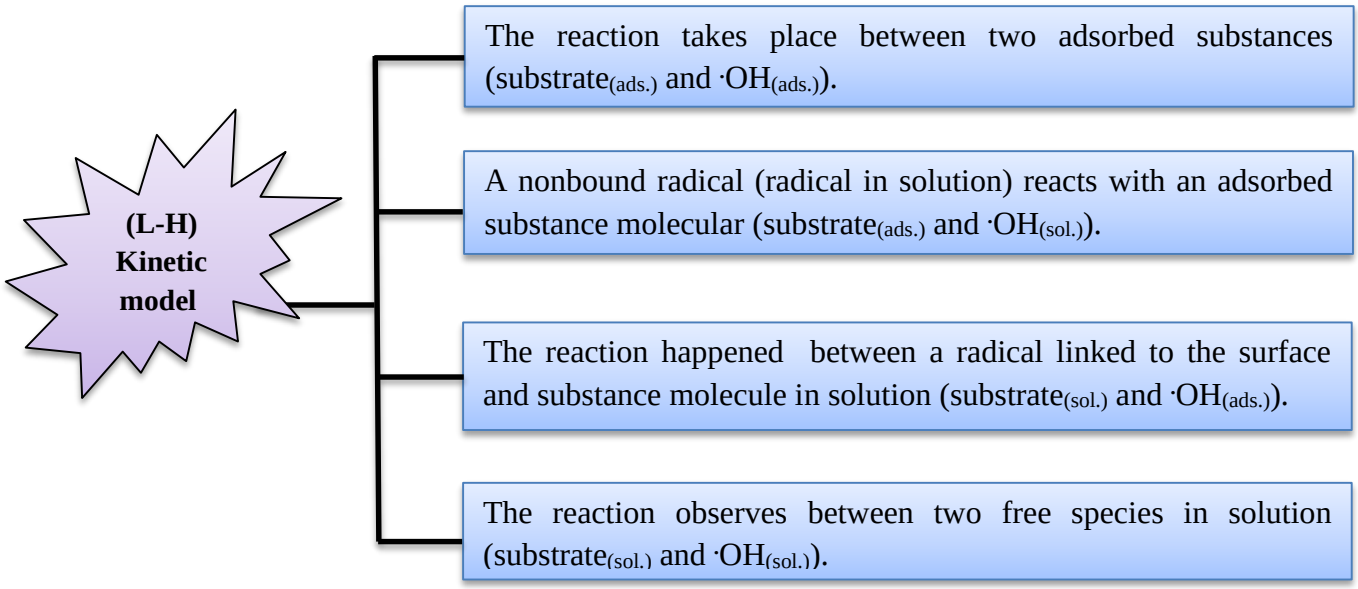

Scheme 1.5: The possible of L- H Kinetic model.

In all top suggested cases. The expression of the reaction rate equation is similar and the process takes place either on the surface in solution or at the interface.

1.15.3 Initial pH of Solution

The pH is regarded as one of the most benefit parameters that effect on the surface charge of catalyst, hence it enhances the photodecolouriz-ation of the organic pollutants in the presence of photocatalyst.

The relationship between the apparent rate constant and pH is shown in Fig. 1.14 (c). It is clearly seen that the apparent rate constant increases with increasing of pH in the range about 6-10, that depends on the type of the used photo semiconductors and the properties of the organic pollutants.

Equations (1-21) indicate that at low pH, ZnO is dissolved in solution and at high pH ZnO is deprotonated or dissoluted [165-169].

$Zn - OH + H^+ \longrightarrow Zn - OH_2^+$ (Acidic pH) …(1-21)

or

$ZnO + 2\ H^+ \longrightarrow Zn^{2+} + H_2O$ (Acidic pH) …(1-22)

$Zn - OH + OH^- \longrightarrow Zn - O^- + H_2O$ (Basic pH) …(1-23)

or

$ZnO + H_2O + 2\ OH^- \longrightarrow [Zn(OH)_4]^{2-}$ (Basic pH) …(1-24)

1.15.4 Temperature

In photocatalytic system, the room temperature is enough to active the photoreaction. Hence, the true activation energy Et is nil. However , the apparent activation energy Ea is defined as a minimum amount of energy that is required to promote the photoelectron from trapping centers to conductive band of photocatalyst [157,158, 170].

The apparent activation energy is calculated by Van't Hoff-Arrhenius plot employing the ln rate constant (k) verse (1/temperatures of reaction) [171].

$$\ln k = \frac{-E_a}{RT} + \ln A \qquad (1\text{-}25)$$

where: k is the rate constant, E_a is an apparent activation energy, R is a gas constant, T is a temperature of reaction, and A is a Pre-exponential (frequency) factor.The catalytic reaction is a slightly affected with the temperature change. Temperature dependent steps in adsorption or photocatalytic reaction are sorption of reactants and products on the surface of photocatalyst [172]. Generally, raising the temperature of solution will enhance the recombination process of charge carriers and the desorption process of adsorbed reactant species, at final, that will cause to decrease of photocatalytic activity.

If the adsorption process is endothermic, the uptake of dye solution is increased with the rise in the solution temperature due to increase in the mobility of number of the dye molecules with temperature, that interacts with the active sites in the

defected surface [173]. At medium temperature range, which approximately has values more than 20 ^{o}C and less than 80 ^{o}C, the apparent activation energy has very small values, i.e., a few kJ/mol and near zero. This behavior reflects the closed in the rate of reaction and the reaction is independent on the temperature [158, 171].

1-16 The Aims of the Present Work

The work is composed of three main parts.

1. The first deals investigates the synthesis of nanoparticles semiconductor (ZnO-NPs) using direct precipitation method, then metalized the prepared ZnO and commercial ZnO by using photo deposition method with different percentage of Ag and Co.
2. The second part includes characterizations of all samples by employing FTIR, XRD and AFM analysis, then it compares the characterizations of prepared (naked and metalized ZnO) with the commercial (naked and metalized ZnO).
3. The third part is to study the effects for various parameters, such as:

a. Dose of catalyst.
b. Dye concentration.
c. Initial pH of solution
d. Temperature of solution.

which are done to estimate the best (optimum) condition for decolorization of Methyl green dye.

CHAPTER TWO

Experimental

2.1 Chemicals

The used chemicals in this work are listed in Table 2-1. All of the chemicals were obtained without further purification.

Table 2-1: **Chemicals**

No	**Chemicals**	**Company supplied**
1	Absolute ethanol (99.98%)	Hayman ,England.
2	Hydrochloric acid (HCl) 99%	SD Fine_Chemical limited- India.
3	Nitric Acid(HNO_3) 98%	Riedel-De-Haen AG, Seelze, Hannover, Germany.
4	Sulphuric acid (99.00%)	Himedia Chemical Company .
5	Zinc Oxide (ZnO) 99.78%	Fluka AG, Switzerland .
6	Zinc sulfate heptahydrate ($ZnSO_4.7H_2O$)	Labochemie, India.
7	Methyl green	GEORGE T. GURRL TD., London , S.W.6 , ENGLAND.
8	Cobalt nitrate hexahydrate $Co(NO_3)_2.6H_2O$	BDH Laboratory reagents.
9	Silver nitrate (Ag NO_3)	Appli- Chem- GmbH
10	Iron (II) sulfate ($FeSO_4$)	Fluka AG, Switzerland.
11	Iron (III) sulfate ($Fe_2(SO_4)_3$)	Evans medical LTD
12	Magnesium Sulphate ($MgSO_4$)	Fluka –Garantie.
13	Magnesium Chloride ($MgCl_2$)	Hazardous .
14	Potassium oxalate ($K_2C_2O_4$)	Riedel-De-Haen AG, Seelze, Hannover, Germany.
15	1,10- Phenonethroline.	Riedel-De-Haen AG, Seelze, Hannove, Germany.
16	Sodium hydroxide 99%	Sigma Chemical Company .
17	N_2 gas cylinder, 99.995 %	Emirates Industrial gasses /Dubai.

2.2 Instruments

The instruments used in this study with its companies are shown in Table 2-2.

Table 2-2: Instruments.

No.	Instrument	Company
1	Sensitive balance	BL 210 S, Sartorius- Germany
2	UV-Visible spectrophotometer	Cary 100Bio, shimadzu (Varian)-Germany
3	Atomic absorption spectrophotometer	AA-6300, Shimadzu-Japan
4	Fourier Transform Infrared spectrophotometer	8400S, Shimadzu- Japan
5	X-Ray Diffraction Spectroscopy	Lab X XRD 6000, Shimadzu-Japan
6	Scan Probe Microscope	AFM model, AA 3000, Advanced Angstrom Inc.,-USA
7	Ultrasonic	FALC-Italy
8	High Pressure Mercury Lamp -UV (A)	Philips-Germany
9	Hot plate Stirrer	LMS1003/Labtech/DaihanlabTechco, LTD
10	pH meter	WTW Inolab pH720 –Germany
11	Centrifuge	Hettich- Universall II- Germany
12	Oven	Memmert-Germany

2.3 Photocatalytic Reactor Set up

The general diagram of the experimental set-up (Photocatalytic Reactor Unit) is shown in Scheme 2-1.

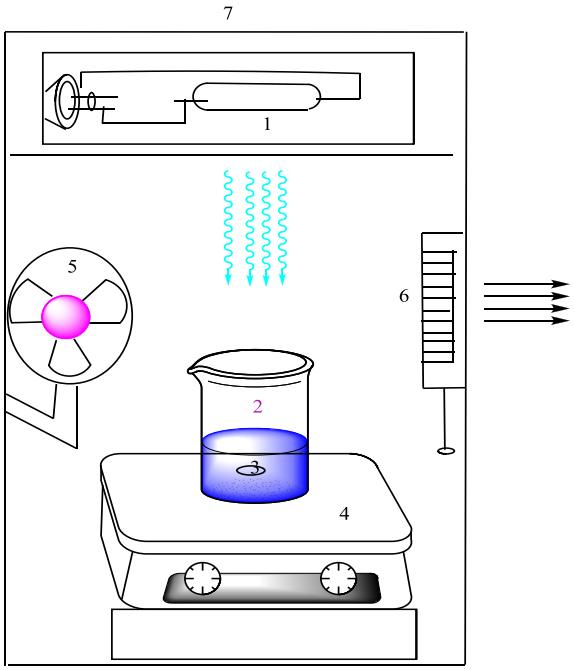

Scheme 2-1 : Schematic Diagram of Experimental Set-up (Photocatalytic Reactor Unit), Where: Mercury lamp type high pressure (400 W)(1), Pyrex glass beaker size 400 cm^3 (2), Teflon bar (3), magnetic stirrer (4), fan (5), pump fan (6) and wooden box (7).

2.4 Preparation of ZnO Nanoparticles

ZnO-NPs have been prepared by direct precipitation method .[174]

The direct precipitation method is briefly summarized in figure (2-1). Zinc sulphate heptahydrate ($ZnSO_4.7H_2O$) and sodium hydroxide (NaOH) were used as precursors of the ZnO-NPs. The aqueous solution of metal sulphate was prepared from pure metal salt by dissolving in distilled water. A certain quantity of NaOH was dissolved in distilled water and added to the aqueous solution of zinc sulfate. Then sodium hydroxide solution was added drop by drop as a molar ratio of 1:4 under vigorous stirring for 15min. The produced precipitate was filtered and washed several times with distilled water to remove all the

impurities. The white formed precipitate was dried in an oven at 86 °C. The powder obtained from the above method was calcined at different temperatures such as 300°C, 500°C,and 700°C for 2 h.

$$ZnSO_4.7H_2O + 2NaOH \longrightarrow Zn(OH)_2 + Na_2SO_4 + 7H_2O \quad (2\text{-}1)$$

$$Zn(OH)_2 + 2H_2O \longrightarrow (Zn(OH)_4)^{2-} + 2H^+ \longrightarrow 3H_2O + ZnO \quad (2\text{-}2)$$

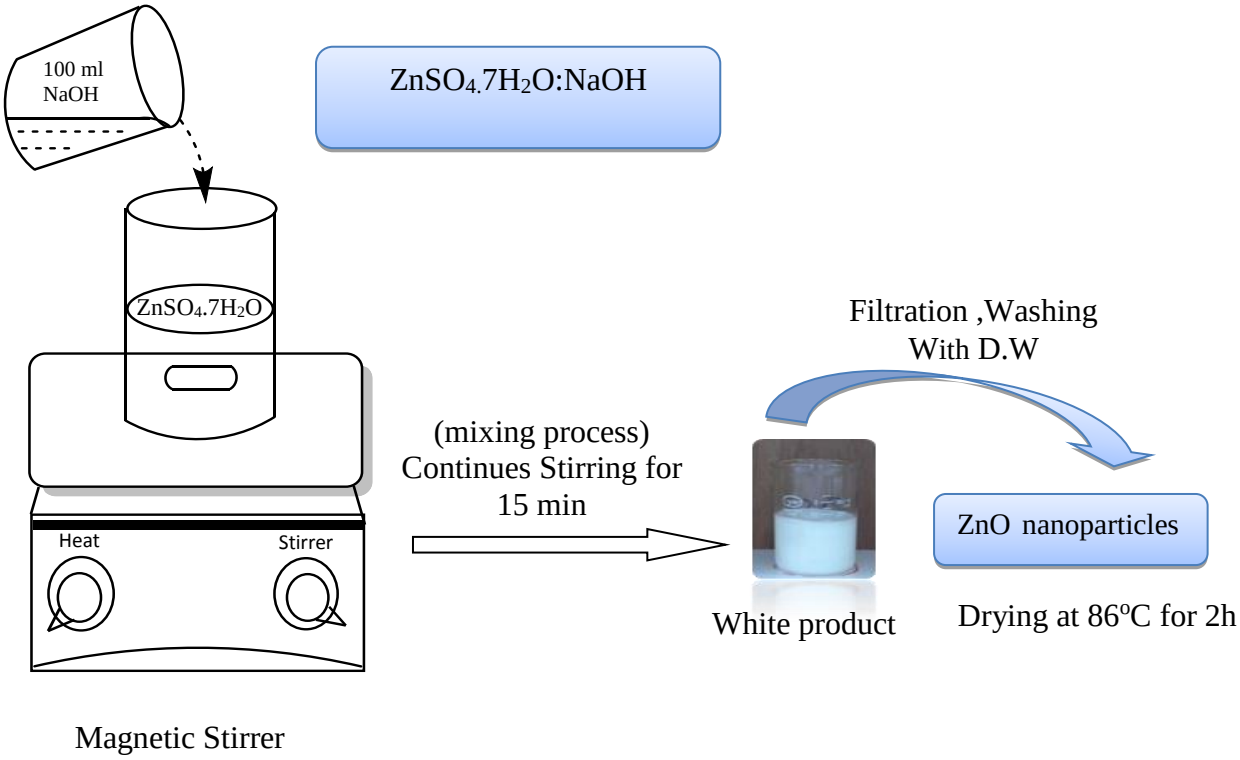

Figure (2-1) : Schematic of direct precipitation

2.5 Preparation of Metallized ZnO

Different percentages of cobalt and silver ZnO surface were loaded by photo deposition method [157, 175]. In all experiments, 2 g of zinc oxide (commercial or prepared) and 20 mL of absolute ethanol were mixed, then followed by the addition of the desired amount of as-prepared solution from Co(0.5-2 % $Co(NO_3)_2.6H_2O$/ 0.1M HNO_3) or Ag (0.5-4 % $AgNO_3$/0.1M HNO_3), under continuous magnetic stirring at 700 rpm as shown in the tables (2-3) and (2-4),. The reaction vessels were irradiated with UV-A light on light intensity equal to $6x10^{-5}$ Ens $.s^{-1}$ in the present inert environment by purging with N_2 gas for 3h for

loading each Co and Ag respectively. The produced solutions were beige colour for Co loaded and leaden colour for Ag loaded on ZnO, as shown in Figure (2-2). The produced suspension solutions were filtered by using two filtration papers together type (Chm - CHEMLAB GROUP, size 150 mm) under vacuum, repeated the filtration process until the filter solution was become colourless, then washed by absolute ethanol, and threw overnight in disiccator that contained $MgSO_4$ to remove the ethanol.

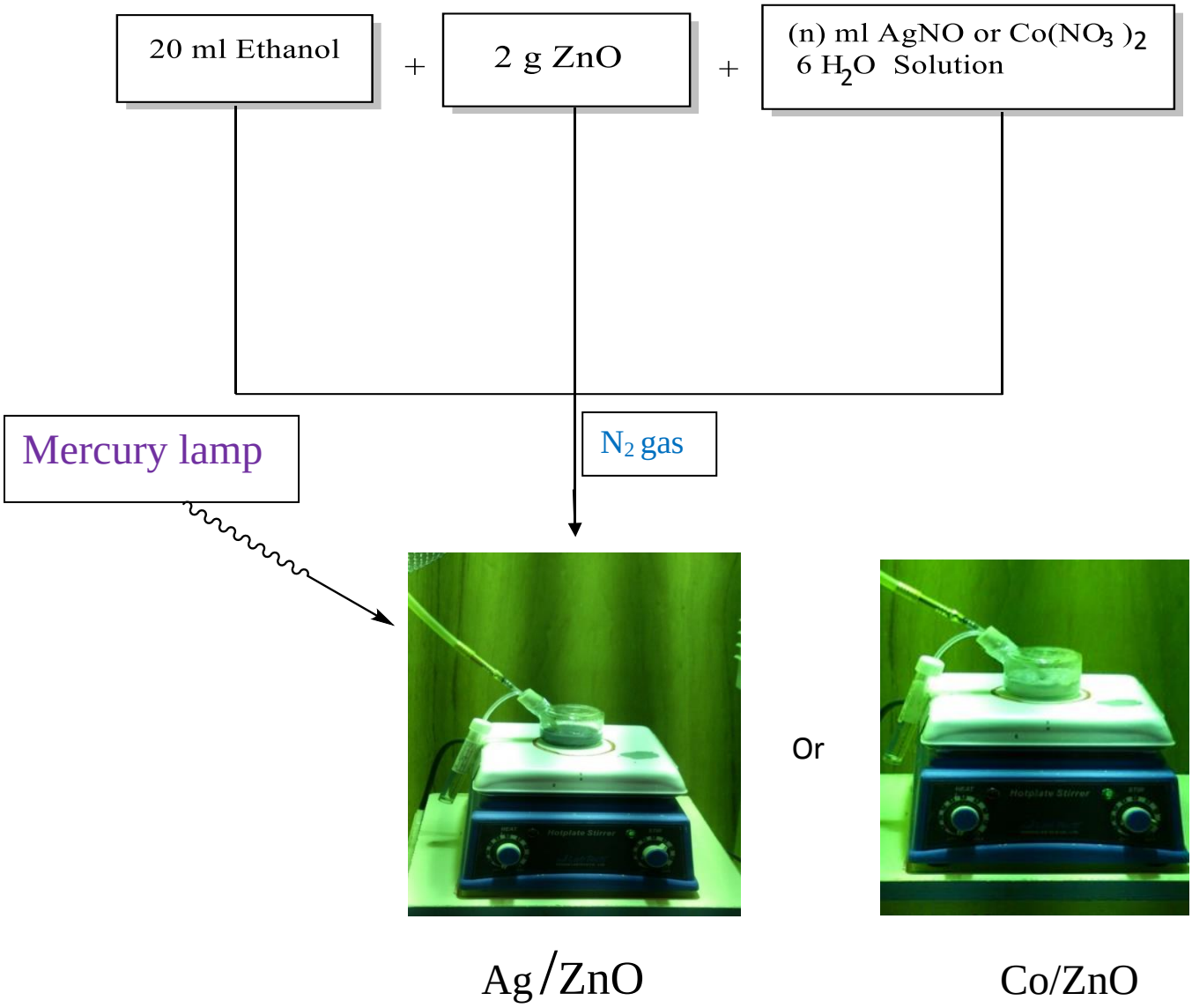

Figure (2-2) : Schematic of the photo deposition of Co and Ag loaded on ZnO.

Table 2-3: Loaded Calculations of Co on ZnO Surface.

$Co(NO_3)_2$ .6 H_2O concentrations /(g/100 mL)	Wt. of ZnO /g	Co%	Volume of Co aqueous solution /mL
2.000	2.000	0.500	2.48
2.000	2.000	1.000	4.935
2.000	2.000	2.000	9.85

Table 2-4: Loaded Calculations of Ag on ZnO Surface.

$AgNO_3$ concentrations/ (g/100 mL)	Wt. of ZnO /g	Ag %	Volume of Ag aqueous solution /mL
2.000	2.000	0.500	0.79
2.000	2.000	1.000	1.5
2.000	2.000	2.000	3.14
2.000	2.000	4.000	6.55

2.6 Atomic Absorption Spectrophotometry

Atomic absorption instrument was used to find the reside amount of Co or Ag in solution after loading them on commercial or prepared ZnO with passing mixture of air and acetylene via the flame using (Shimadzu-AA-6300) instrument. The analyzed samples were measured before and after 3h of irradiation for Co or Ag respectively. The calibration curves data are shown in Table 2- 5 and plotted in Figures 2-3 and 2- 4 for Co and Ag Solutions .

Table 2- 5: Calibration Curve Data of Co and Ag Concentrations.

Metals concentrations /ppm	Intensity of Co	Intensity of Ag
0	0.000	0.000
1	1.13	0.85
5	4.75	4.66
10	10.04	10.47
15	15.13	15.51
20	19.92	19.46

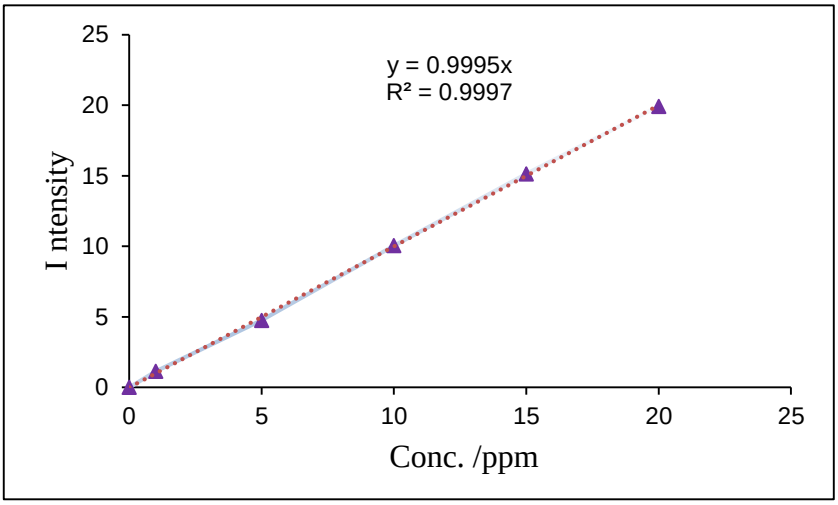

Figure 2- 3 : Calibration Curve at Different Concentration of Cobalt (II) .

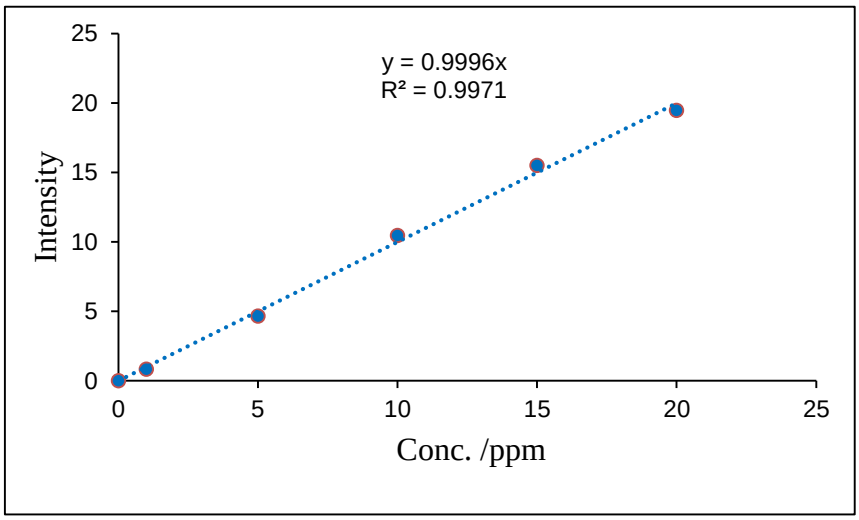

Figure 2- 4 : Calibration Curve at Different Concentration of Silver (I) .

2.7 Fourier Transform Infrared Spectroscopy (FTIR)

Fourier Transform Infrared spectra of naked and loaded Co or Ag on commercial or prepared ZnO were recorded. The analysed samples were measured in the range of 4000-400 cm^{-1} on palletised with KBr dise at room temperature.

2.8 X-Ray Diffraction Spectroscopy (XRD)

X-Ray diffraction (XRD) data were analysed by Lab X XRD 6000 instrument equipped. This instrument was employed Cukα1 as a target source (wave length 1.54060 Å, voltage 40.0 kV and current 30 mA), slit (divergence 1.00000º, scatter 1.00000º and receiving 0.30000º), 2θ range from 20 to 80º, speed

12.0000 (deg/min) and reset time 0.10 sec. The mean crystallite sizes (L) calculated by utilized from XRD data and using Scherrer's formula in the following equation [176, 177].

$$L = \frac{k\ \lambda}{\beta \cos \theta} \qquad 2\text{-}3$$

where: k is the Scherrer's constant (0.94) which depends on the shape of the crystal, λ is the wavelength of the x-ray radiation (0.15406 nm for Cukα), β is the full width of half-maximum (FWHM) intensity expressed in radians (originally, β is measured in degrees then multiply by (π/180) to convert to radians), and θ is a diffraction (Bragg) angle. On the other hand, the more accurate crystallite sizes (Ĺ) were estimated using modified Scherrer's equation by Monshi and co-workers [178], that also utilized from XRD data.

$$\beta = \frac{(k\ \lambda)}{\acute{L}} \cdot \left(\frac{1}{\cos \theta} \right) \qquad 2\text{-}4$$

By making logarithm on both sides:

$$\ln \beta = \ln \left(\frac{(k\ \lambda)}{\acute{L}} \right) + \ln \left(\frac{1}{\cos \theta} \right) \qquad 2\text{-}5$$

By plotting lnβ against ln(1/cosθ), the slope equal 1 and the intercept is ln (kλ/ Ĺ). The exponential of the intercept is obtained:

$$\exp \left(\ln \left(\frac{(k\ \lambda)}{\acute{L}} \right) \right) = \frac{k\ \lambda}{\acute{L}} \qquad 2\text{-}6$$

where: k and λ are substituted 0.94 and 0.15406 nm respectively.

2.9 Atomic Force Microscopy (AFM)

The Atomic Force Microscopy image was recorded with Scanning Probe Microscopy employing software WSxM (nanotech). The glass slides were cut to 1 x 2 cm and cleaned by putting them in (1:1) (ethanol: deionised water) solution

and treated by ultrasonic (Ultrasound, FALC) instrument at 3 min in power equal 25 kHz.

All sample solutions of naked and Co^{2+} or Ag^{1+} loaded on commercial or prepared ZnO were prepared by adding very small amounts (about 0.001g) of Co^{2+} or Ag^{1+} to distal water, then shaked by ultrasonic instrument at the same conditions to get on colloidal solution. These solutions were left for about 1 h to give a fine colloidal solutions. The produced solutions poured on the glass slides as drop by drop, then left to dry in the air,(notes: this step was continuously repeated until a good spot occurred).

The Crystallinity Index was calculated by using the following equation[179].

$$\text{Crystallinity Index} = \frac{D_p}{L \text{ or } \acute{L}} \qquad 2\text{-}7$$

where: D_p is the particle size which is measured by the AFM analysis and L is the mean crystallite size or Ĺ is the crystallite size that is calculated by Scherrer equation and modified Scherrer equation of XRD data respectively.

2.10 Apparatus for the Photocatalytic decolourization of Methyl Green Dye:

All photocatalytic experiments were performed in a batch photoreactor using the radiation UV-A source type Philips (Germany), high pressure mercury lamp (HPML) with 400 W. The aqueous suspensions of commercial or prepared zinc oxide containing Methyl Green dye in a beaker under magnetic stirring were irradiated in light of wavelength 365 nm with an irradiation intensity of $6x10^{-5}$ ensien.s^{-1}. The used lamp was positioned perpendicularly above the beaker of reaction. Before commencing a reaction, this lamp must be allowed to warm up for 5 minutes to reach the intensity of light to stable state.

In all experiments, the required amount of the catalyst either naked or metallized ZnO was suspended in 200 mL of methyl green dye solution . After illumination, 5mL was pulled from the reaction suspension solution, then centrifuged at 4000 rpm for 10 minutes, and filtered for two times to remove the all particles of ZnO.

The second centrifugal was very important to remove of the fine particle of the ZnO. Then, the absorbance at the maximum wavelength of the Methyl Green dye was measured with using UV-visible spectrophotometer at 298.15 ^{o}K. The apparatus used for photocayalytic reaction is shown in figure2-5,and the apparatus used of solar reactor is shown in figure 2-6

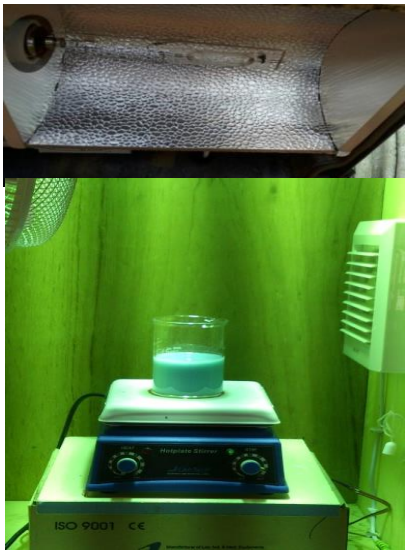

Figure 2-5: Photocatalytic reactor. **Figure 2-6 : The solar reactor**

Photocatalytic reactions on the surface of naked or metallized of commercial or prepared ZnO can be expressed by the Langmuir–Hinshelwood model (see quation 2-8) [180]. After the adsorption equilibrium, the reaction rate can be expressed as:

$$- \ln \left(\frac{Ct}{Co}\right) = kt \qquad 2\text{-}8$$

where: C_t and C_o are the reactant concentration at time $t = t$ and $t = 0$, respectively, k is the apparent reaction rate constant and t is a time. A plot of $ln(C_o/C_t)$ versus t will yield a slope as a value of k.

The photocatalytic decolorization (P.D.E) was calculated using the following equations [181]:

$$P.D.E\ \% = \frac{(Co - Ct)}{Co} \times 100 \qquad 2\text{-}9$$

where: C_o and C_t are the initial concentrations of the MG dye before and after t/min UV irradiation, respectively.

2.11 Calibration Curve

The calibration curve was performed by using standard Methyl Green (MG) aqueous solutions. The absorbance was measured at 630 nm. Typical calibration values are given in the table 2-6 and plot is given in figure 2-7 .

Table 2-6: Absorbance at different concentration.

[MG] /ppm	Absorbance at 630 nm
0	0
10	0.437
20	0.912
30	1.267
40	1.549
50	1.731
60	1.788
70	1.813
80	1.821
90	1.819
100	1.823

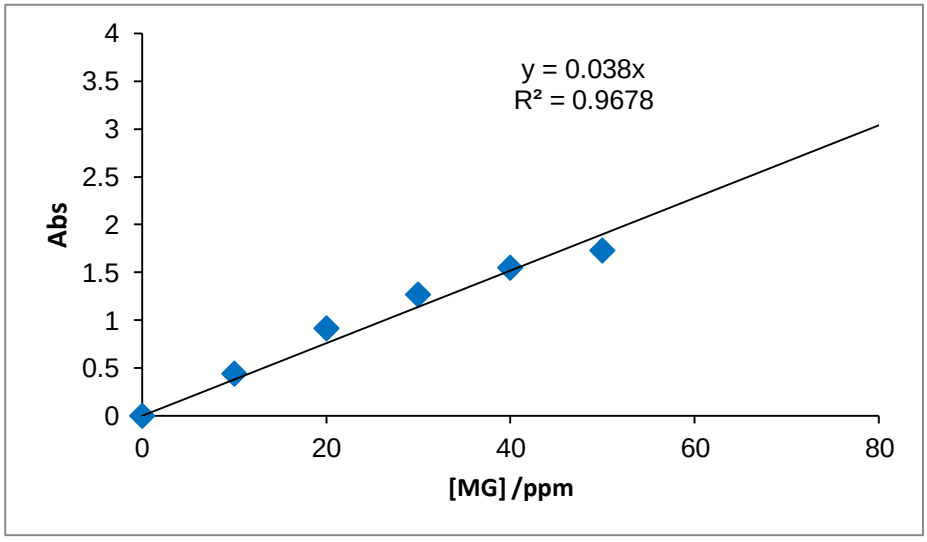

Figure 2-7 : Calibration curve at different concentration of MG Dye .

2.12 Light Intensity Measurements

The light flux density was calculated. The actinometric method was used to measure the light flux density by using the same photocatalytic reactor with the same volume of the reaction mixture (200 mL) of actinometric solution. The ferrioxalate actinometric solution was prepared by mixing 80 mL of 0.15 M of

$Fe_2(SO_4)_3.7H_2O$ with 100 Ml of 0.45 M of $K_2(C_2O_4)$ and 20 mL of 0.05 M of H_2SO_4 in photocatalytic reactor, then irradiated under atmospheric oxygen. The colour of the solution was changed to yellowish green to indicate the production of $K_3[Fe(C_2O_4)_3].3H_2O$, as in shown in Figure (2-8).

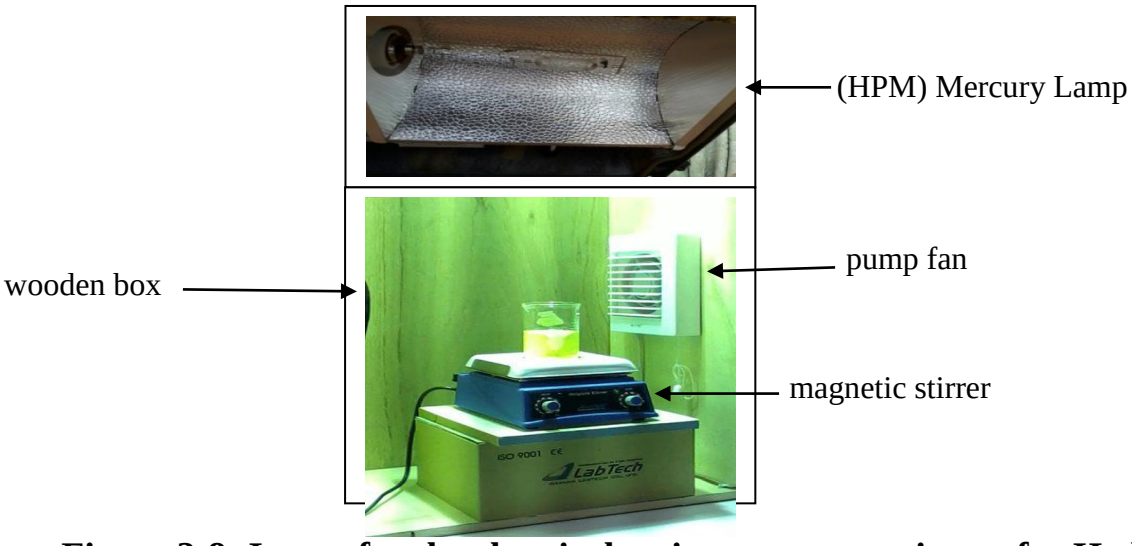

Figure 2-8: Image for the chemical actinometry experiment for Hg lamp setup reactor.

3 mL of irradiated solution was collected in regular intervals at (5, 10 and 15) min by test tubes and centrifuged (2000 rpm, in 10 min). 2.5 mL of filtered solutions was added to 0.5 mL of 1,10-phenonethroline to produce reddish orange complex which absorbed at 510 nm.

The photolysis process of ferrioxalate solution produces was recognized according to the following equations [182-185]:

$$[Fe^{3+}(C_2O_4)_3]^{3-} \xrightarrow{h\nu} [Fe^{2+}(C_2O_4)_2]^{2-} + C_2O_4^{\cdot -} \qquad 2\text{-}10$$

$$[Fe^{3+}(C_2O_4)_3]^{3-} \xrightarrow{h\nu} Fe^{2+} + 2(C_2O_4)^{2-} + C_2O_4^{\cdot -} \qquad 2\text{-}11$$

$$[Fe^{3+}(C_2O_4)_3]^{3-} + C_2O_4^{\cdot -} \longrightarrow [Fe^{2+}(C_2O_4)_2]^{2-} + C_2O_4^{\cdot -} + 2CO_2 \qquad 2\text{-}12$$

$$[Fe^{3+}(C_2O_4)_3]^{3-} + C_2O_4^{\cdot -} \xrightarrow{\Delta} Fe^{2+} + 2CO + 3C_2O_4^{2-} \qquad 2\text{-}13$$

$$2[Fe^{3+}(C_2O_4)_3]^{3-} \longrightarrow 2[Fe^{2+}(C_2O_4)_2]^{2-} + C_2O_4^{2-} + 2CO_2 \qquad 2\text{-}14$$

The light intensity (I_o) was calculated by depending on the calculation of the amount of quantity of producing ferrous ions that formed during an irradiation time by depending on the following equations [182]:

$$\text{moles of } Fe^{2+} = \frac{V_1 \times V_3 \times A_{(510\ nm)}}{V_2 \times l \times \varepsilon_{(510\ nm)} \times 10^3} \qquad 2\text{-}15$$

$$I_o = \frac{\text{mole of } Fe^{2+}}{\Phi_\lambda \times t} \qquad 2\text{-}16$$

$$I_o = 6 \times 10^{-5} \text{ Enstine. } S^{-1}$$

where:V_1 is total of irradiation volume (200 cm^3), V_3 is the volume of irradiation solution mixed with 1,10-phenonethroline (3 cm^3), V_2 is the volume of irradiation solution (2.5 cm^3), l is the optical path length (1 cm), ε is the molar absorptivity 1.045 x 10^4 L. mol^{-1}. cm^{-1} , A_{510} is the average absorbance of solution after irradiation in different internals time with 1,10-phenonethroline, (t) is the average of irradiation time and Φ_λ is the quantum yield (1.2) [182].

2.13 Thermodynamic Parameters:

The $\Delta H^{\#}$ and $\Delta S^{\#}$ values can be calculated from the plot of the Eyring equation [186]:

$$\text{Ln}\frac{k_{app}}{T} = \frac{-\Delta H^{\#}}{RT} + \left(\ln\frac{K_B}{h} + \frac{\Delta S^{\#}}{R}\right) \qquad 2\text{-}17$$

where: k_{app} is apparent rate constant , k_B is Boltzmann's equation, T is the temperature of reaction, R is the gas constant, and h is Plank's constant. The free energy $\Delta G^{\#}$ is calculated by equation (2-18) :

$$\Delta G^{\#} = \Delta H^{\#} - T\Delta S^{\#} \qquad 2\text{-}18$$

2.14 Activation Energy

In a range of 278.15-293.15 ^oK, a linear relationship fitting for the graph of Arrhenius equation, that calculated for photo decolourization reaction of methyl green dye.

$$\ln k_{app} = \frac{-Ea}{RT} + \ln A \qquad 2\text{-}19$$

where : k_{app} is apparent rate constant, T is temperature of reaction, E_a is the apparent activation energy, R is the gas constant, and A is a frequency constant.

The equation (2-19) was used to calculate the apparent activation energy [186].

CHAPTER THREE

RESULTS

3.1 Physical Characterizations of Catalysts

3.1.1 Atomic Absorption Spectrophotometry (A.A)

The atomic absorption spectroscopy was used to deduce the presence of silver ions (Ag^{1+}) and cobalt ions (Co^{2+}) that were loaded on the surface of ZnO surface as silver atoms at percentages ranged between (0.50 - 4.00), and as Co atoms at percentages ranged (0.50 - 2.00). The Ag and Co amounts were measured before and after irradiation. These results were shown in Tables 3-1 and 3-2.

Table 3-1: Loaded Calculations of Ag on ZnO Surface.

Ag % added as Ag NO3	[Ag] added/ppm	[Ag]/ppm measured by A.A after 3 h from irradiation with Commercial ZnO	[Ag]/ppm measured by A.A after 3 h from irradiation with prepared ZnO
0.5	482.587	Zero	Zero
1	886.046	Zero	0.43
2	1723.336	0.053	0.36
4	3133.145	Zero	Zero

Table 3-2: Loaded Calculations of Co on ZnO Surface.

Co % added as Co(NO3)2	[Co] added /ppm	[Co]/ppm measured by A.A after 3 h from irradiation /ppm with Commercial ZnO	[Co]/ppm measured by A.A after 3 h from irradiation /ppm with prepared ZnO
0.5	882.5	Zero	Zero
1	1583.3	Zero	0.13

3.1.2 UV-visible absorption spectra

These spectra were pictured to investigate the ability of naked and metallized of commercial and prepared ZnO to make the photocatalytic decolourization of methyl green in aqueous solution, as show in Figures from 1 to 6(in Appendix (A)

3.1.3 Fourier Transform Infrared Spectroscopy (FTIR)

Fourier Transform Infrared spectra were measured to detect the changes in the intensity of peaks with the increasing in the amount of Co and Ag loaded on Commercial ZnO surfaces and prepared ZnO that calcined at (500) ^{o}C surfaces. The spectra are displayed in Figures 7 and 8 (in Appendix (A)) .

3.1.4 X-Ray Diffraction Spectroscopy (XRD)

XRD was employed to study the phase stability and the transformation phase of naked and metallised ZnO as percentage ranged from 0.50 to 2.00 for Co and from (0.50) to (4.00) for Ag respectively. The mean crystallite sizes (L) in nm were calculated by using Scherrer's formula (see equation 2-3). The crystallite sizes (Ĺ) in nm was determined by plotting the modified Scherrer's equation (see equations 2-4 and 2-5) and Figures from 9 to 10 (in Appendix (A)), that depends on the full width at half maximum (FWHM) for the peak and diffraction (Bragg) angles [194-195]. The calculated results are illustrated by Tables from (3-3) to(3-6) .

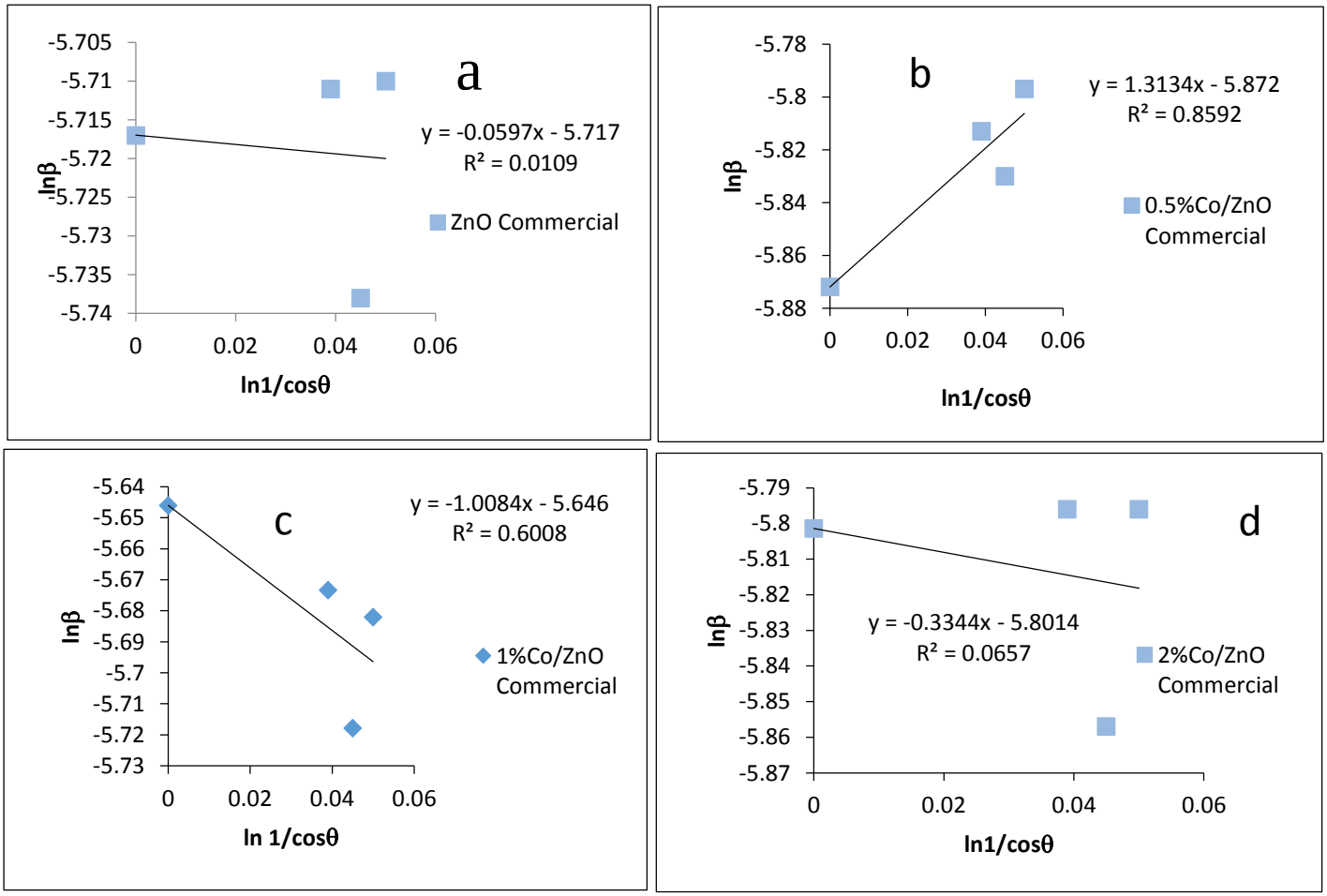

Figure 3- 1: Modified Scherrer Equation of Naked and Co Loaded on Commercial ZnO Plot, at a) Naked Commercial ZnO , b) Co(0.50)/Commercial ZnO , c)Co(1.00)/Commercial ZnO and d)Co (2.00)/ Commercial ZnO .

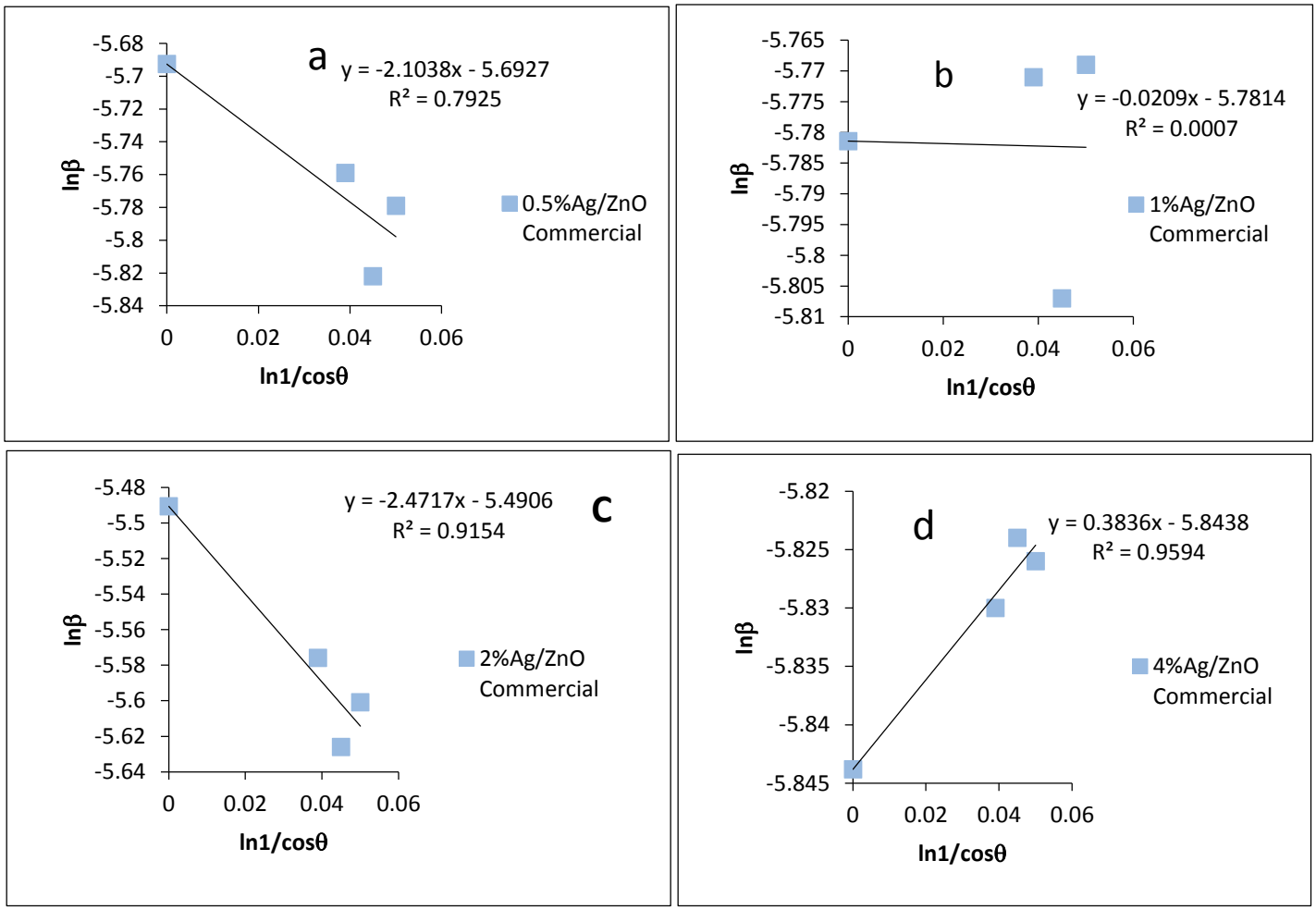

Figure 3-2 : Modified Scherrer Equation of Ag Loaded on ZnO Plot, at a) Ag (0.50)/Commercial ZnO , b) Ag (1.00)/Commercial ZnO , c) Ag (2.00)/ Commercial ZnO and d) Ag (4.00)/Commercial ZnO .

Table 3-3 : Mean Crystallite Sizes and Crystallite Sizes of Naked ZnO and Co Loaded on Commercial ZnO .

Crystallite Sizes (Ĺ)/nm	Mean Crystallite Sizes (L)/nm	Co %	Crystal Components
42.27	44.116	0	ZnO Commercial
49.51	48.446	0.5	Co-ZnO
39.27	42.896	1	Co-ZnO
45.91	48.446	2	Co-ZnO

Table 3-4 : Mean Crystallite Sizes and Crystallite Sizes of Naked ZnO and Ag Loaded on Commercial ZnO .

Crystallite Sizes (Ĺ)/nm	Mean Crystallite Sizes (L)/nm	Ag%	Crystal Components
42.27	44.116	0	ZnO Commercial
41.14	47.213	0.5	Ag-ZnO
45.00	36.995	1	Ag-ZnO
33.65	39.3	2	Ag-ZnO
47.97	49.34	4	Ag-ZnO

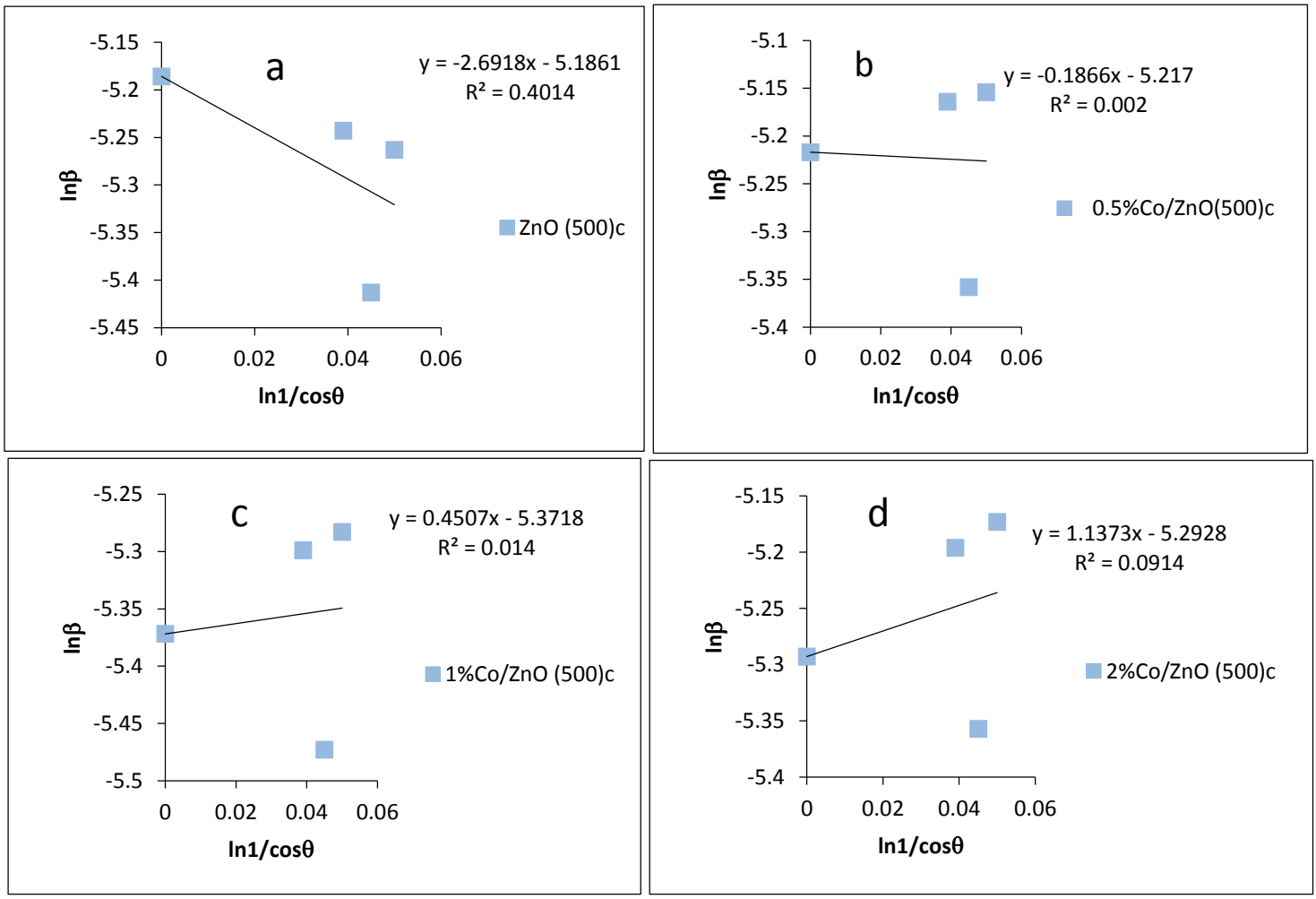

Figure 3-3 : Modified Scherrer Equation of Naked and Co Loaded on ZnO Calcination at (500)^{O}C Plot, at a) Naked ZnO Calcination at (500)^{O}C, b) Co(0.50)/ZnO Calcination at (500)^{O}C, c)Co(1.00)/ZnO Calcination at (500)^{O}C and d)Co (2.00)/ ZnO Calcination at (500)^{O}C .

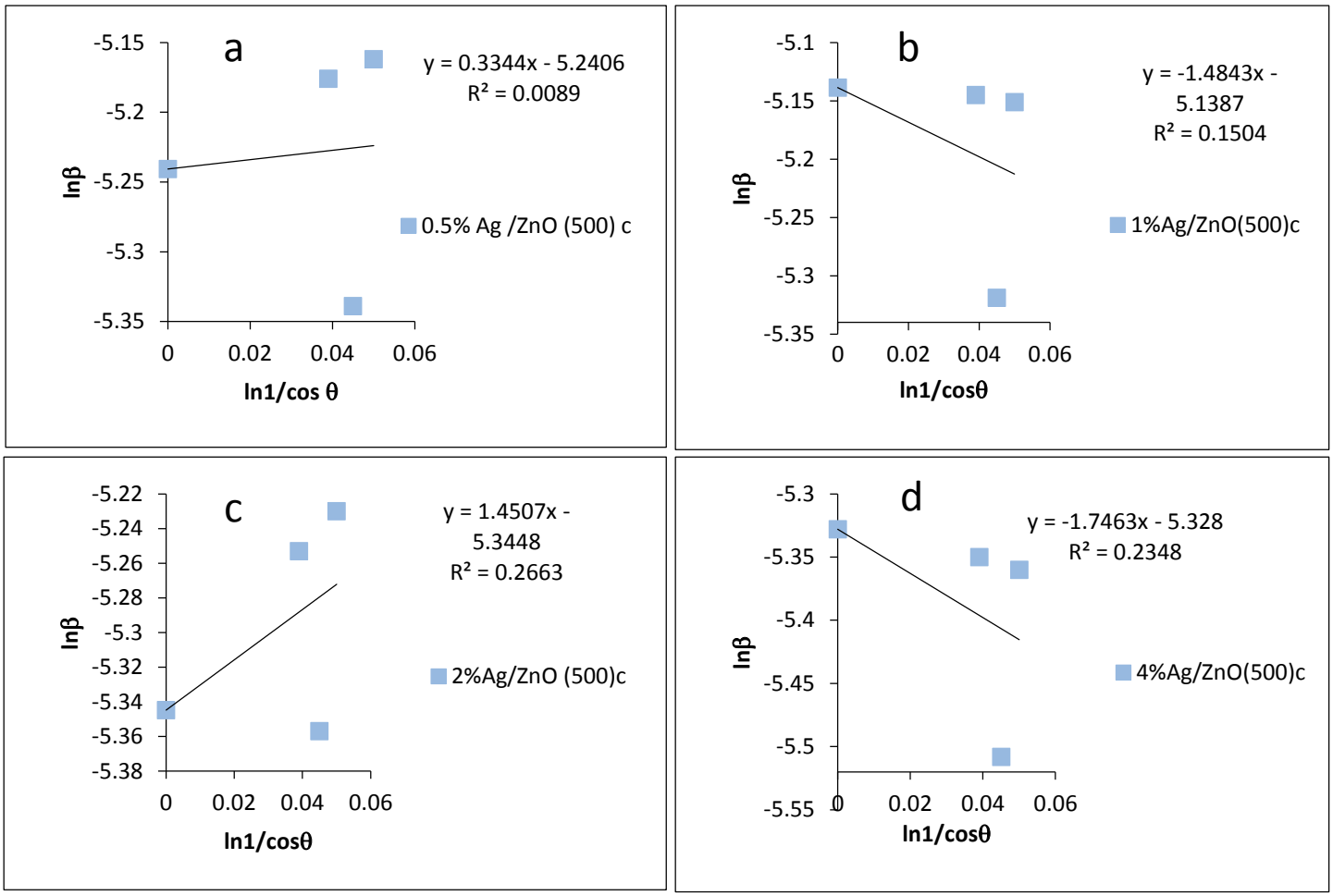

Figure 3-4: Modified Scherrer Equation of Ag Loaded on ZnO Calcination at (500)^{O}C Plot, at a) Ag (0.50)/ZnO Calcination at (500)^{O}C, b) Ag (1.00)/ZnO Calcination at (500)^{O}C , c) Ag (2.00)/ ZnO Calcination at (500)^{O}C and d) Ag (4.00)/ZnO Calcination at (500)^{O}C .

Table 3-5: Mean Crystallite Sizes and Crystallite Sizes of Naked ZnO (500)^{o}C and Co Loaded on ZnO (500)^{o}C .

Crystallite Sizes (Ĺ)/nm	Mean Crystallite Sizes (L)/nm	Co %	Crystal Components
24.80	29.009	0	ZnO
25.58	26.655	0.5	Co-ZnO
29.88	30.262	1	Co-ZnO
27.62	27.119	2	Co-ZnO

Table 3-6 : Mean Crystallite Sizes and Crystallite Sizes of Naked ZnO and Ag Loaded on ZnO (500)ºC

Crystallite Sizes (Ĺ)/nm	Mean Crystallite Sizes (L)/nm	Ag%	Crystal Components
24.80	29.009	0	ZnO
26.21	26.667	0.5	Ag-ZnO
23.66	26.168	1	Ag-ZnO
29.06	28.201	2	Ag-ZnO
28.58	32.022	4	Ag-ZnO

3.1.5 Atomic Force Microscopy (AFM)

AFM images were utilized to determine the particle sizes of naked ZnO and Co and Ag loaded on commercial and prepared ZnO surface. Crystallinity index was calculated by divided on particle size on mean crystallite size or crystallite size that noted in equation 2-7.

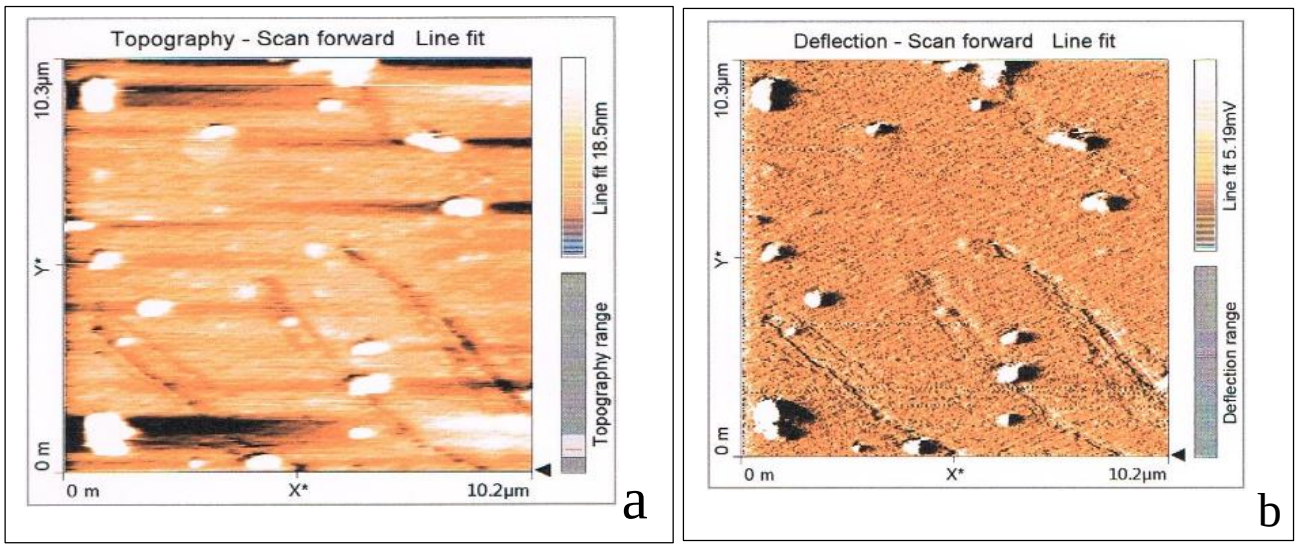

Figure 3- 5 : AFM Image of Commercial ZnO,

a) 2- Dimensions Image (Topography) b) 2- Dimensions Image (Deflection)

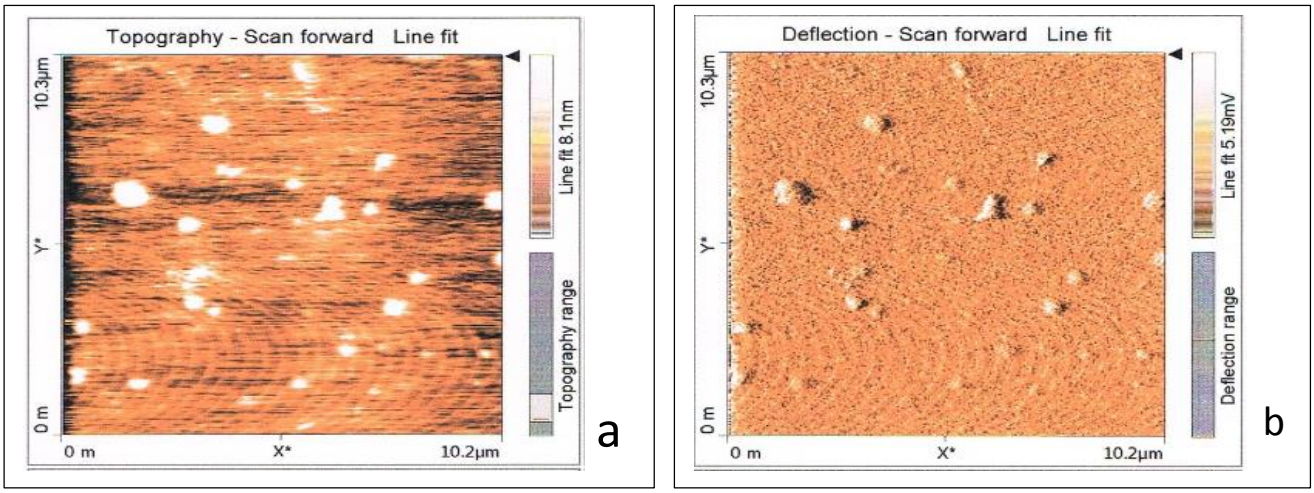

Figure 3-6: AFM Image of 0.5%Co Loaded on Commercial ZnO, a) 2-Dimensions Image (Topography) b) 2- Dimensions Image (Deflection)

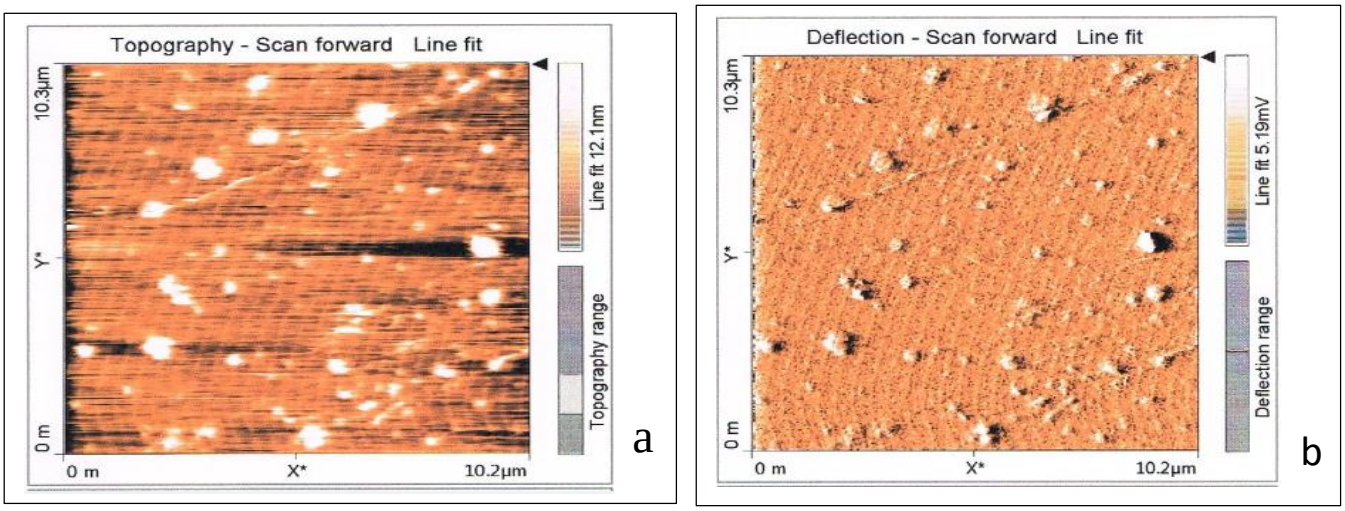

Figure 3- 7 : AFM Image of 1%Co Loaded on Commercial ZnO, a) 2- Dimensions Image (Topography) b) 2- Dimensions Image (Deflection)

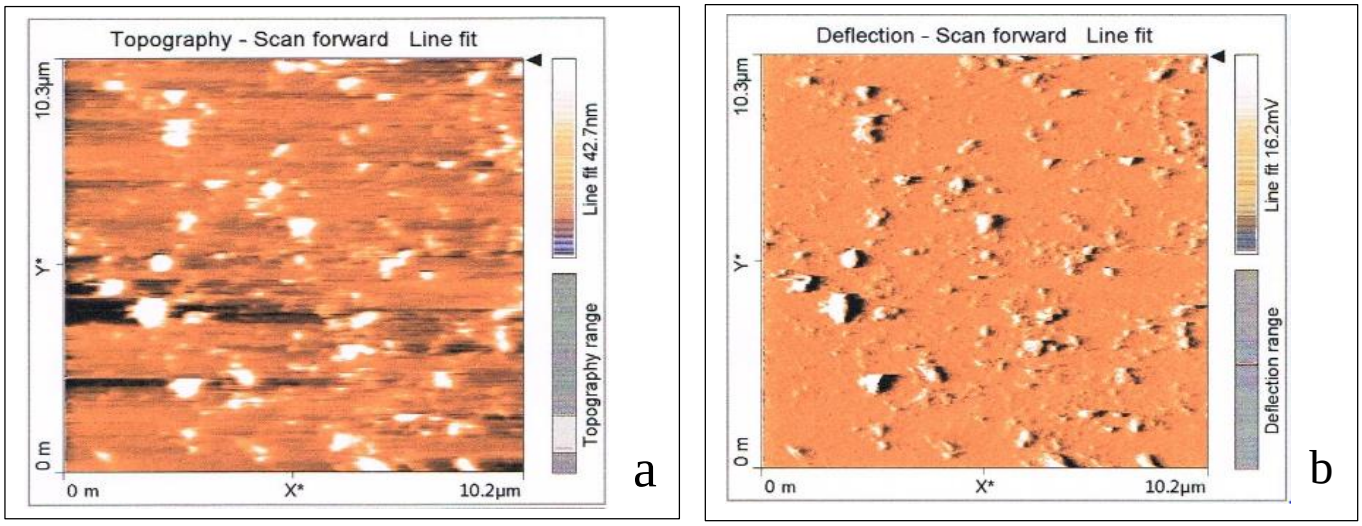

Figure 3-8 : AFM Image of 2%Co Loaded on Commercial ZnO, a) 2- Dimensions Image (Topography) b) 2- Dimensions Image (Deflection)

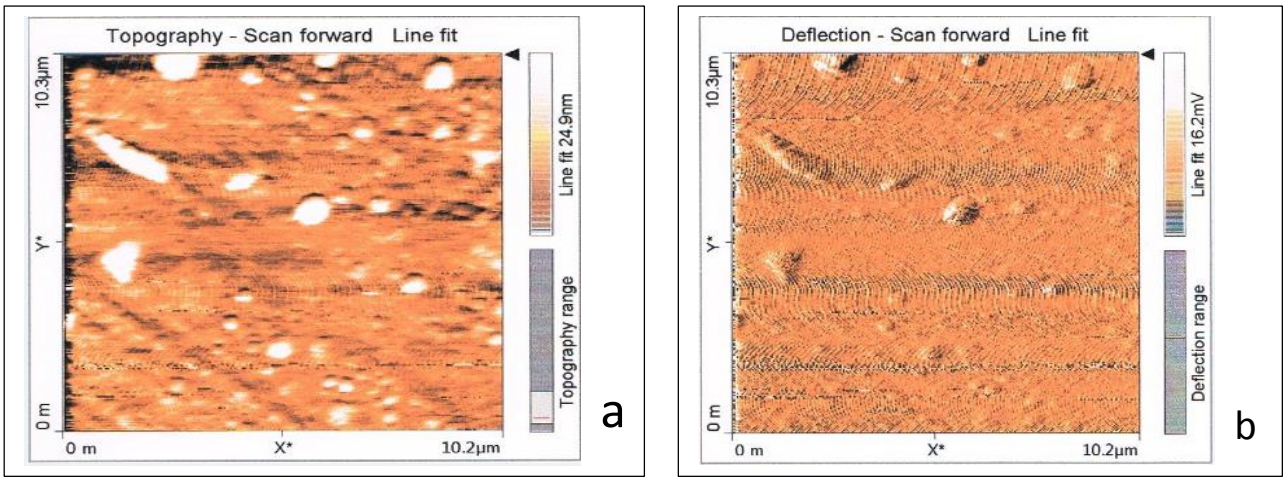

Figure 3- 9 : AFM Image of 0.5%Ag Loaded on Commercial ZnO,

a) 2- Dimensions Image (Topography) b) 2- Dimensions Image (Deflection)

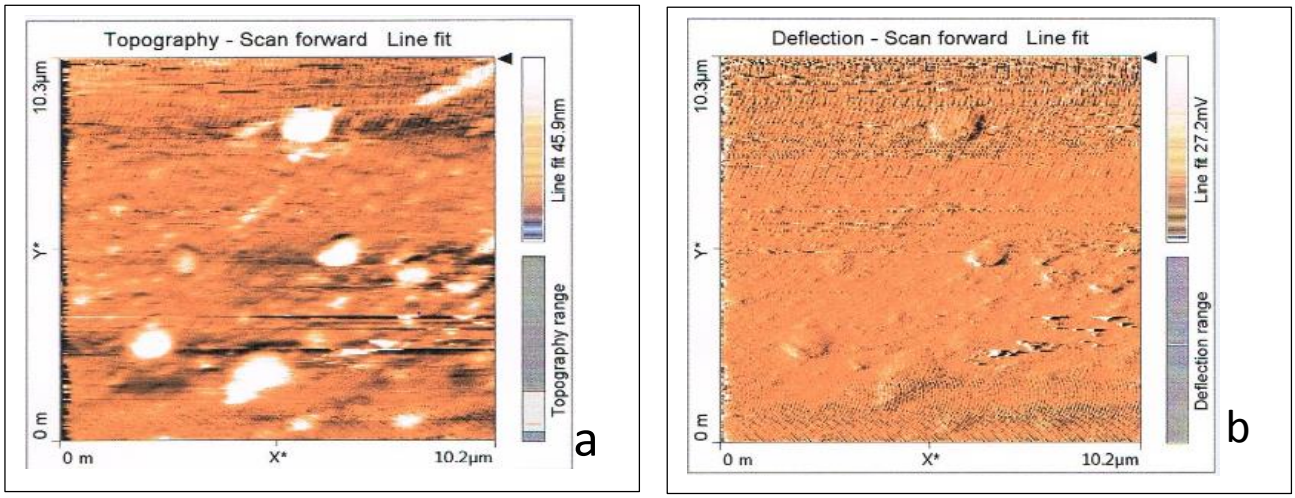

Figure 3- 10 : AFM Image of 1%Ag Loaded on Commercial ZnO,

a) 2- Dimensions Image (Topography) b) 2- Dimensions Image (Deflection)

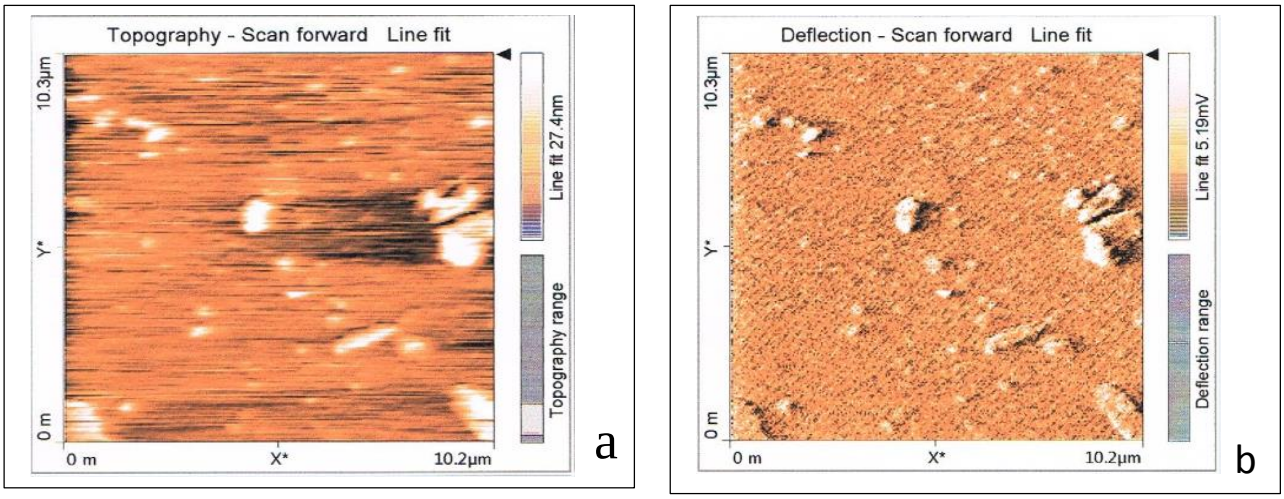

Figure 3- 11 : AFM Image of 2%Ag Loaded on Commercial ZnO,

a) 2- Dimensions Image (Topography) b) 2- Dimensions Image (Deflection)

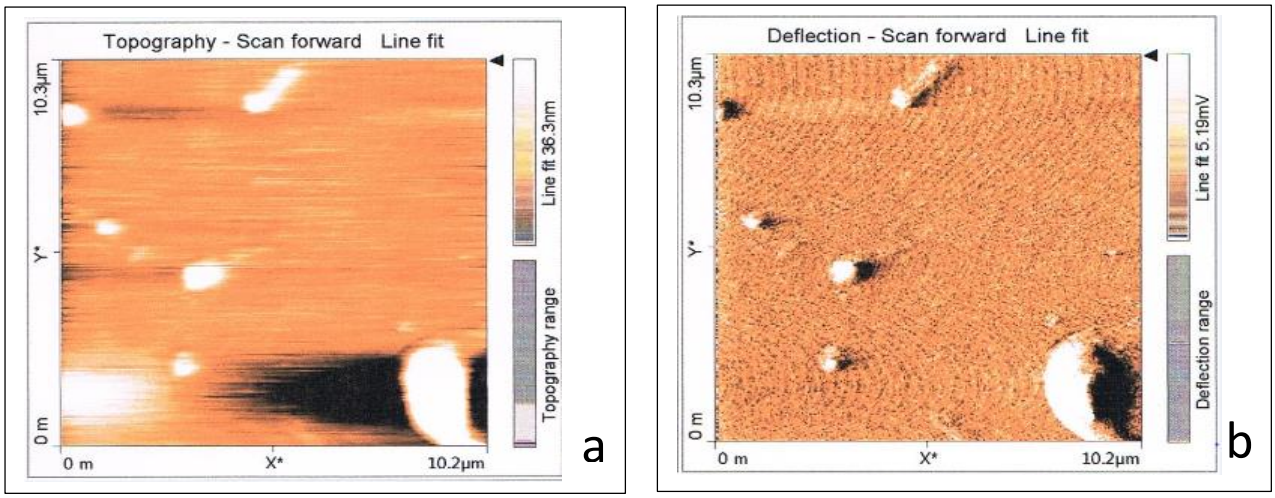

Figure 3-12 : AFM Image of 4%Ag Loaded on Commercial ZnO,

a) 2- Dimensions Image (Topography) b) 2- Dimensions Image (Deflection)

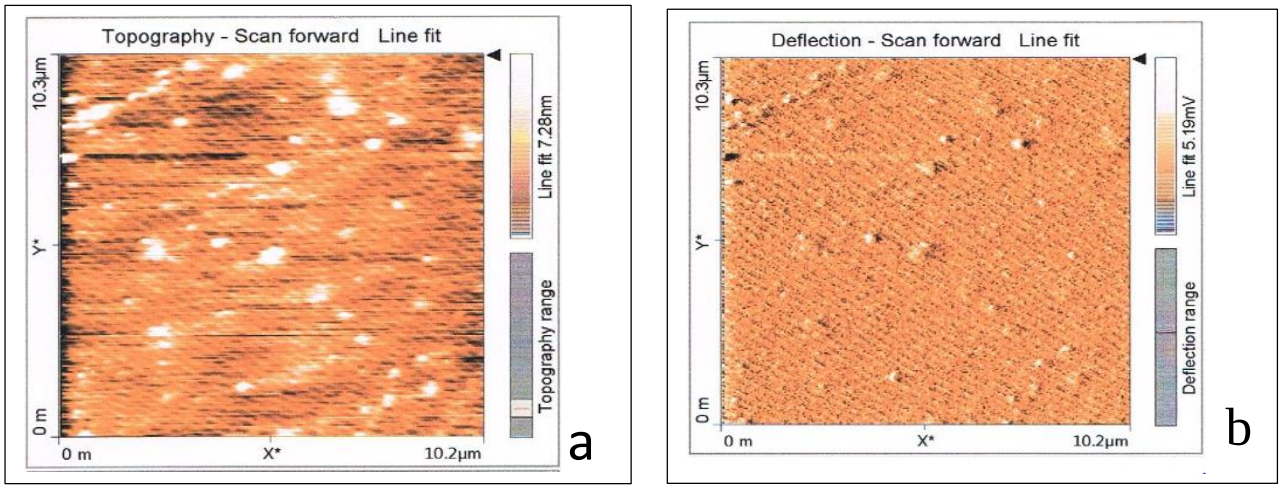

Figure 3-13 : AFM Image of ZnO Calcination at (500) °C,

a) 2- Dimensions Image (Topography) b) 2- Dimensions Image(Deflection)

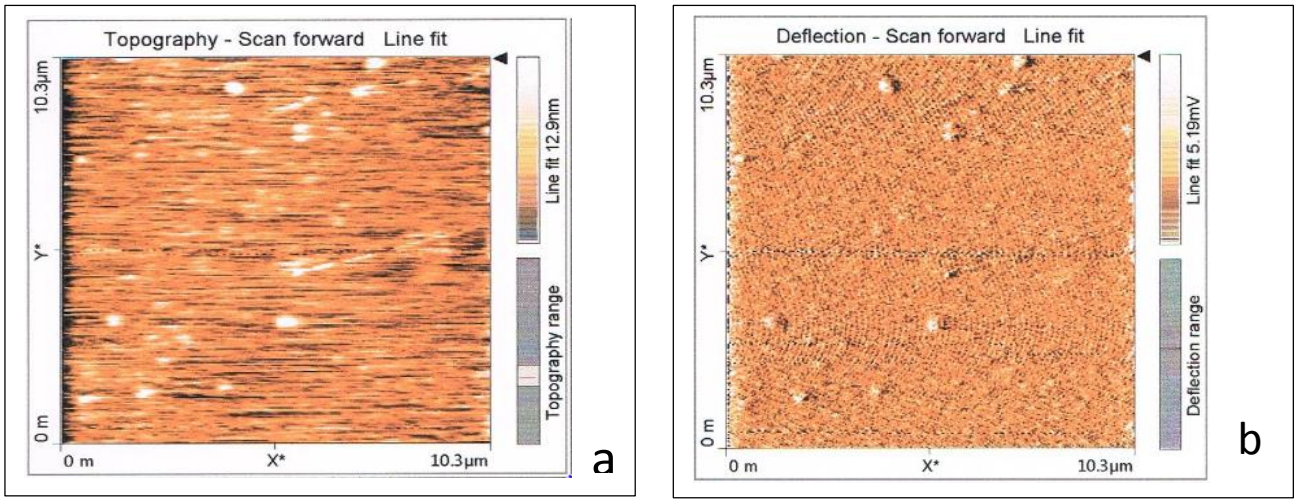

Figure 3- 14 : AFM Image of 0.5% Co Loaded on ZnO Calcination at (500)°C,

a) 2- Dimensions Image (Topography) b) 2- Dimensions Image (Deflection)

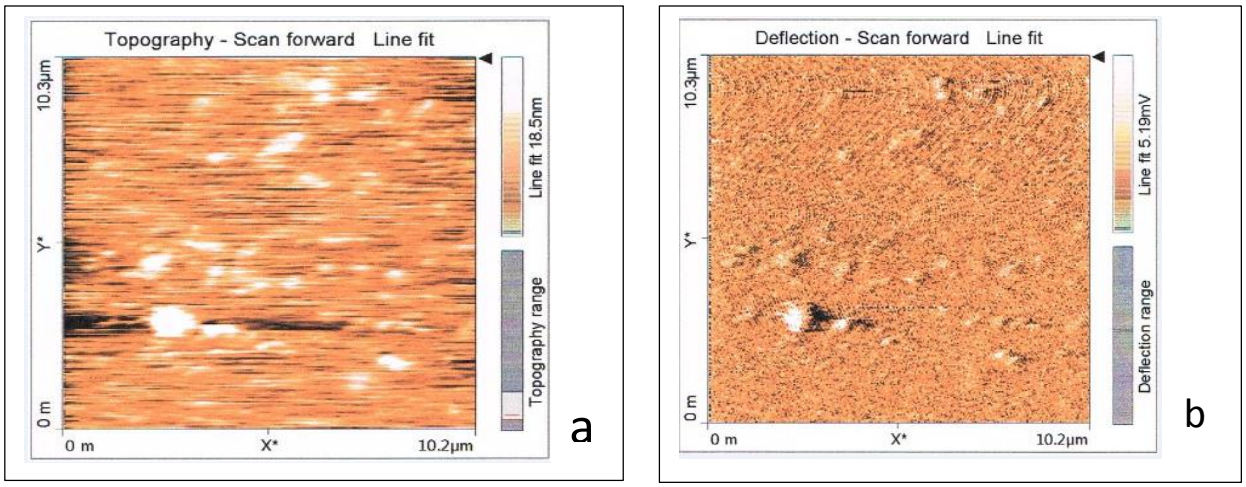

Figure 3-15 : AFM Image of 1% Co Loaded on ZnO Calcination at (500)^{o}C,

a) 2- Dimensions Image (Topography) b) 2- Dimensions Image (Deflection)

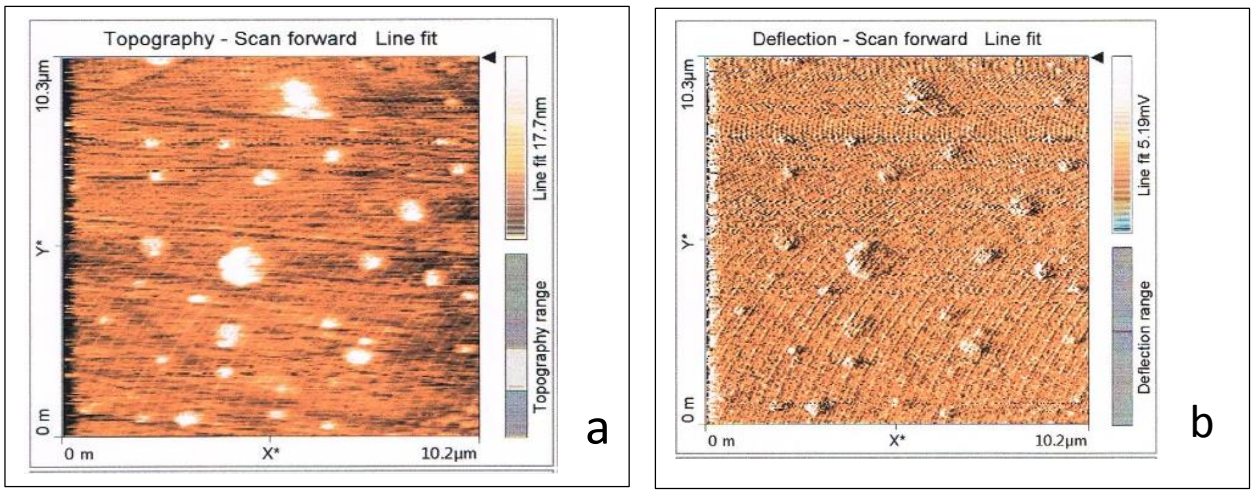

Figure 3- 16 : AFM Image of 2% Co Loaded on ZnO Calcination at (500)^{o}C,

a) 2- Dimensions Image (Topography) b) 2- Dimensions Image (Deflection)

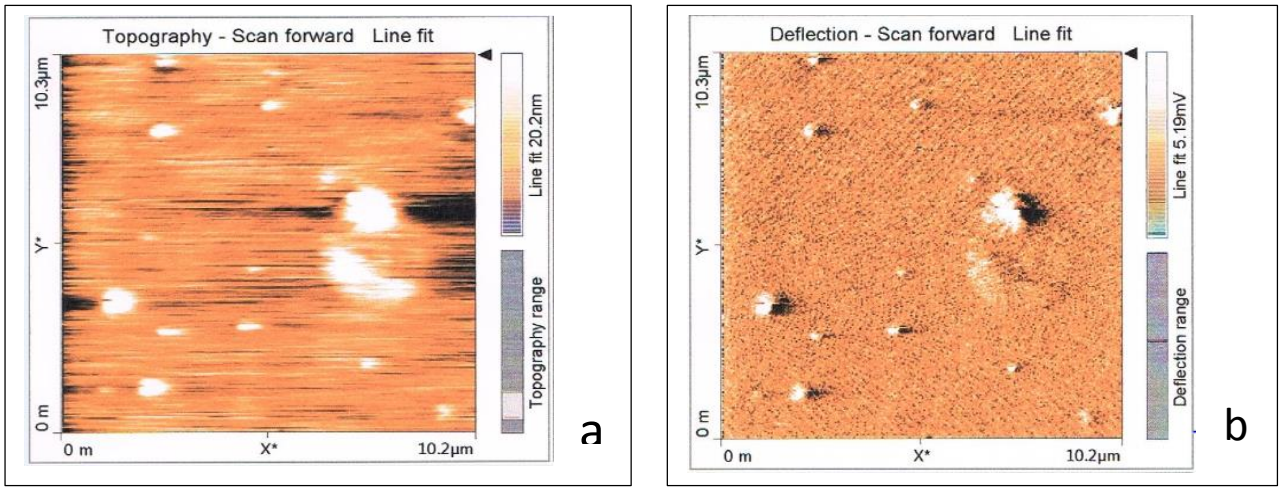

Figure 3- 17 : AFM Image of 0.5% Ag Loaded on ZnO Calcination at (500)^{o}C,

a) 2- Dimensions Image (Topography) b) 2- Dimensions Image (Deflection)

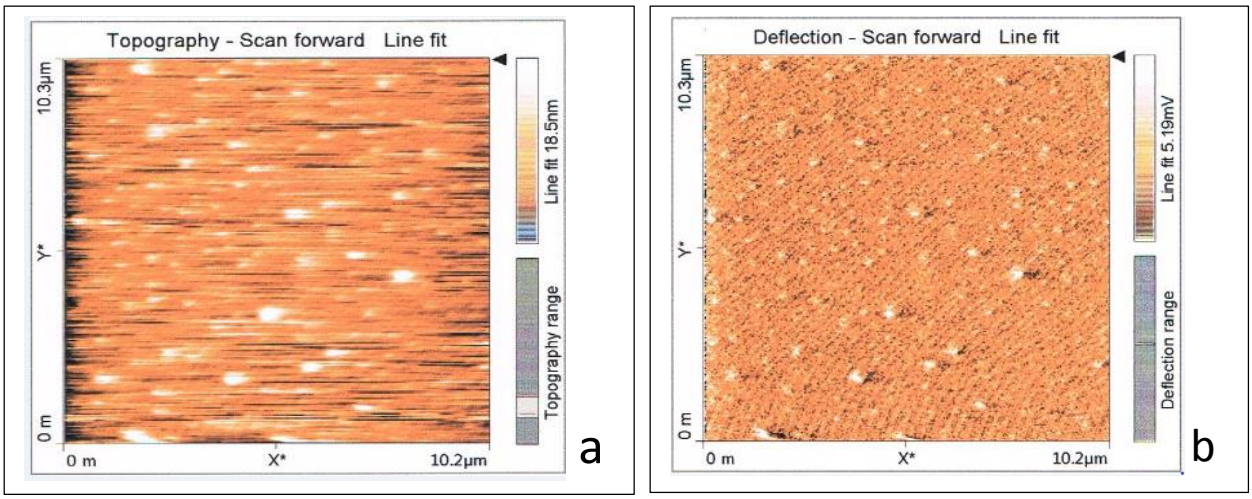

Figure 3- 18 : AFM Image of 1.0 % Ag Loaded on ZnO Calcination at (500)^{o}C,

a) 2- Dimensions Image (Topography) b) 2- Dimensions Image (Deflection)

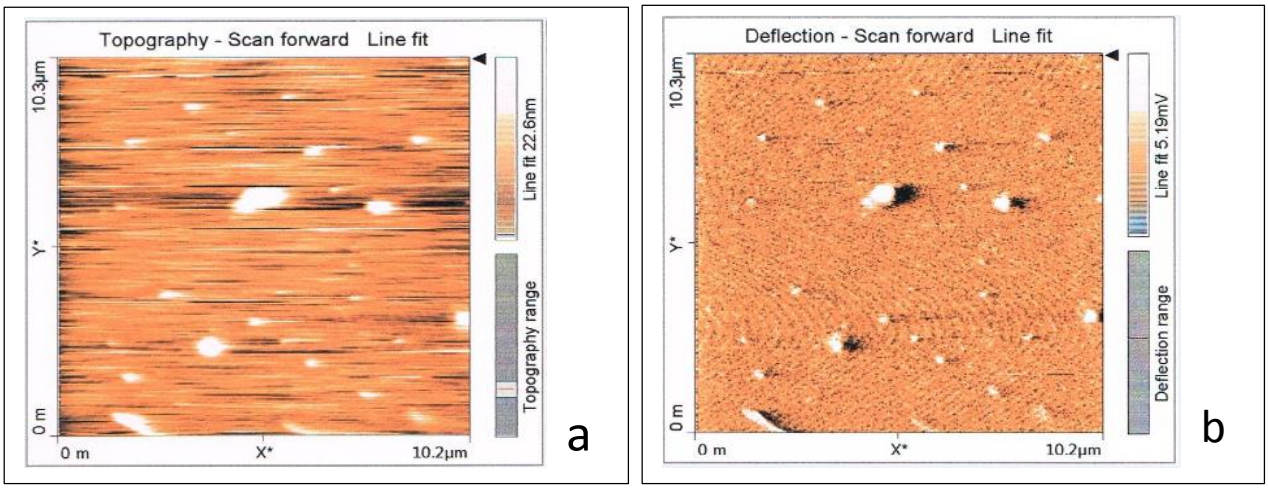

Figure 3- 19 : AFM Image of 2% Ag Loaded on ZnO Calcination at (500)^{o}C,

a) 2- Dimensions Image (Topography) b) 2- Dimensions Image(Deflection)

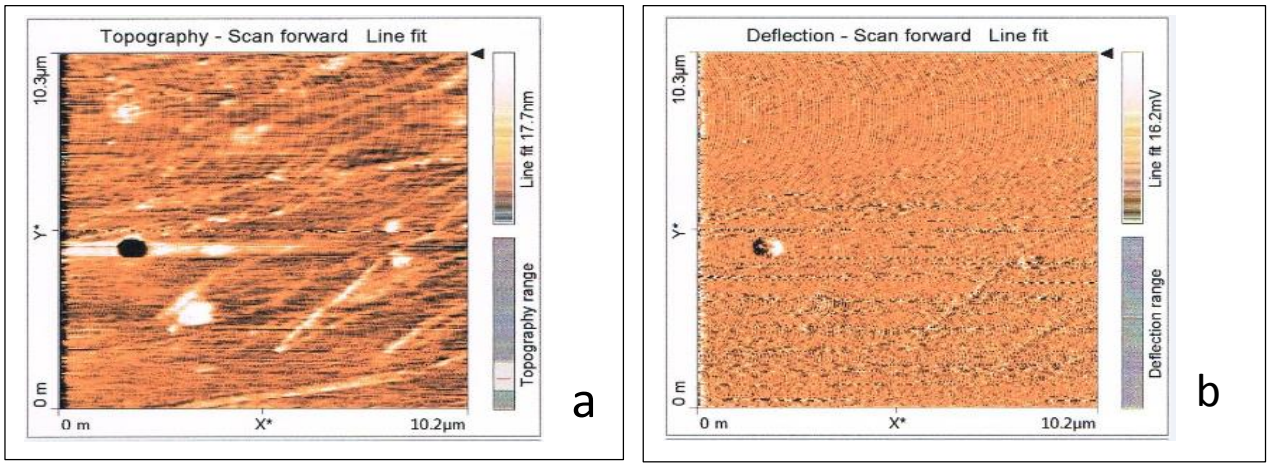

Figure 3- 20 : AFM Image of 4% Ag Loaded on ZnO Calcination at (500)^{o}C,

a) 2- Dimensions Image (Topography) b) 2- Dimensions Image (Deflection)

Table 3-7: Particle Size Measured by AFM and Crystallinity Values of Naked ZnO and Metalized ZnO.

Samples	Particle size /nm	*Crystallinity Index	**Crystallinity Index	Average of Crystallinity Index
ZnO Commercial	18.5	0.419	0.437	0.428
Co(0.50)/ZnO	8.1	0.167	0.163	0.165
Co(1.00)/ZnO	12.1	0.282	0.308	0.295
Co(2.00)/ZnO	42.7	0.881	0.93	0.9055
Ag(0.50)/ZnO	24.9	0.527	0.605	0.566
Ag(1.00)/ZnO	45.9	1.24	1.02	1.13
Ag(2.00)/ZnO	27.4	0.697	0.814	0.755
Ag(4.00)/ZnO	36.3	0.735	0.756	0.745
ZnO(500) **ºC**	7.28	0.25	0.293	0.271
Co(0.50)/ZnO(500) **ºC**	12.9	0.483	0.504	0.493
Co(1.00)/ZnO(500) **ºC**	18.5	0.611	0.619	0.615
Co(2.00)/ZnO(500) **ºC**	17.7	0.652	0.640	0.646
Ag(0.50)/ZnO(500) **ºC**	20.2	0.757	0.770	0.763
Ag(1.00)/ZnO(500) **ºC**	18.5	0.706	0.781	0.743
Ag(2.00)/ZnO(500) **ºC**	22.6	0.801	0.777	0.789
Ag(4.00)/ZnO(500) **ºC**	17.7	0.552	0.619	0.585

*****Crystallinity index calculated by divided particle size on mean crystallite size.
**Crystallinity index calculated by divided particle size on crystallite size.

3.2 Preliminary Experiments

A series of experiments were done at light intensity $6x10^{-5}$ Ens s^{-1}.

3.2.1 Dark Reaction (Adsorption Reaction)

These experiments were carried out in the absence of the ultraviolet radiation by using (50 ppm of MG dye with 0.7g commercial ZnO) and (25ppm of MG dye with 0.6g prepared ZnO that calcinated at 500 ^{o}C). The results are listed in table 1 (in Appendix (B)) and plotted in figure 3-21. These results show that there is no reaction in the absence of ultraviolet radiation.

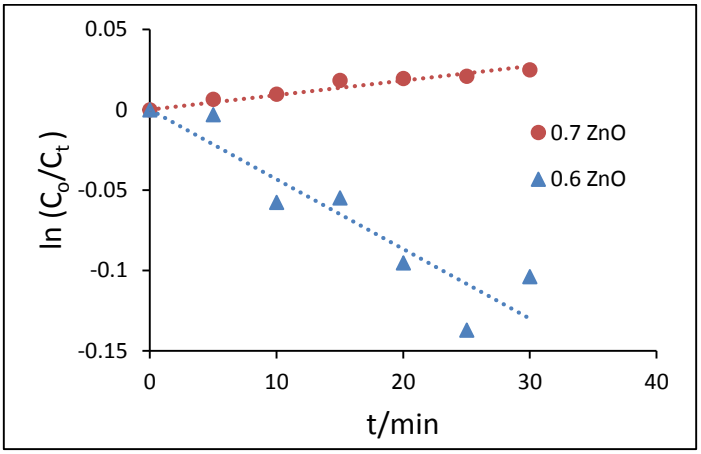

Figure 3-21: The change of adsorption time in absence of radiation with ln (C_o/C_t)

3.2.2 Photolysis Reaction

The photolysis reaction for 200 mL of (25, 50) ppm MG dye at 303 K, under purged O_2 and at irradiation time are equal 30 min. That was done in the absence of catalyst. The results are listed in table 2 (in Appendix (B)) and plotted in figure 3-22.

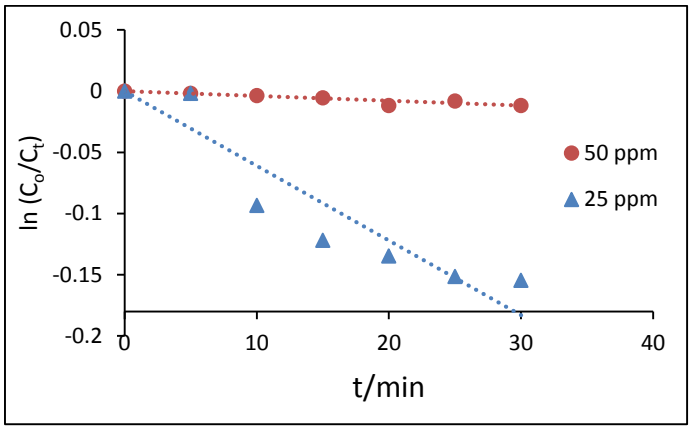

Figure 3- 22: The change of adsorption time in presence of radiation with ln (C_0/C_t).

3.3Effect of Different Parameters on Photocatalytic Decolourization of Methyl green dye for Commercial ZnO.

3.3.1 Effect of Initial Dye Concentration.

In these experiments a series of different concentrations for MG dye in the range (25-100) ppm were used. These results shown in table 3 (in Appendix (B)) and plotted in figure 3-23, indicate the experimental condition light intensity equal to ($6x10^{-5}$ Enstine s^{-1}), commercial ZnO dosage (0.7g/200 mL), the initial pH of solution equal to 5.40 and temperature equal to 288.15 K .

The results listed in table 4 (in Appendix (B)) and plotted in figure 3-24 show a pseudo first order reaction according to Langmuir Hinshelwood relationship.

The results listed in table5 (in Appendix (B)) and plotted in figure 3-25 show the relationship between the apparent rate constant of reaction and initial Methyl green dye concentration. It is found that the apparent rate constant of reaction decrease with increasing of initial dye concentration. (PDE) was calculated then listed in table 6 (in Appendix (B)) and plotted in figure 3-26 .

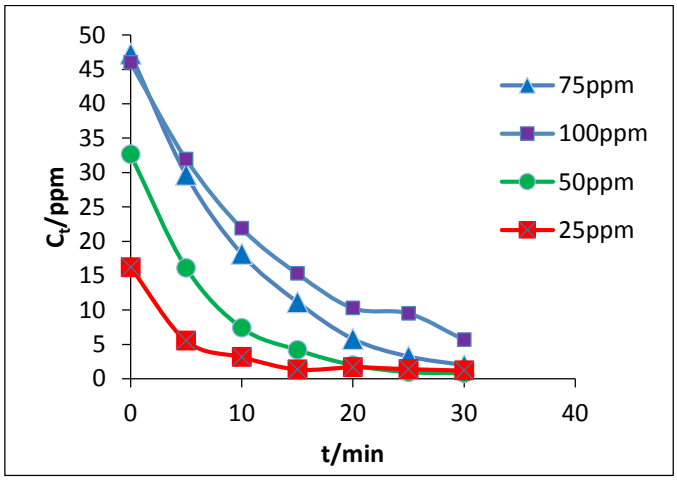

Figure 3-23 : Relationship between C_t and the change of irradiation time on different MG concentrations with commercial ZnO

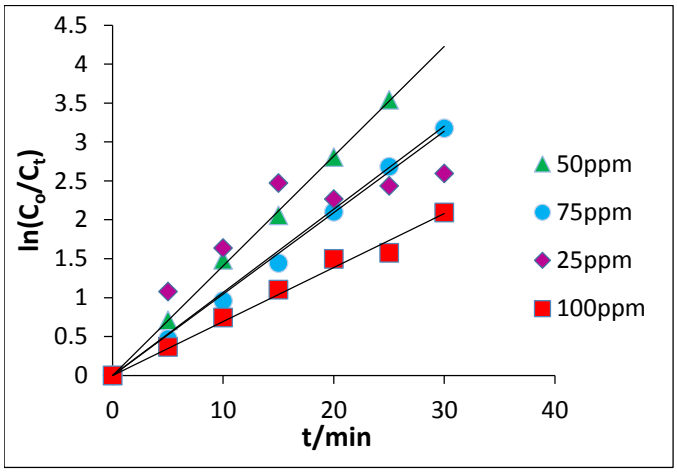

Figure 3-24 : Relationship between $\ln(C_o/C_t)$ and the change of irradiation time on different MG concentrations with commercial ZnO .

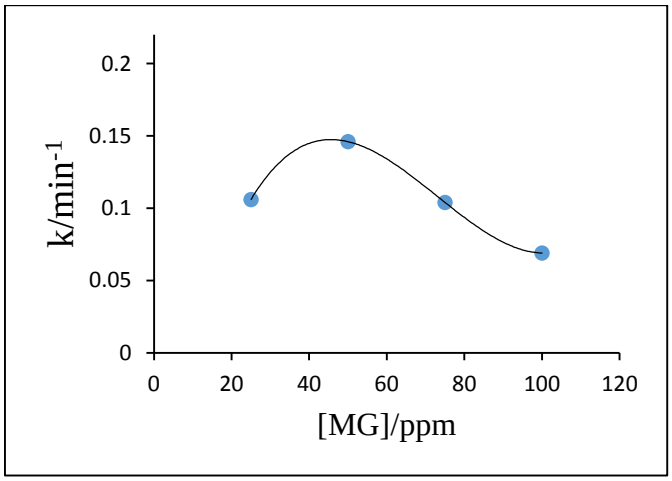

Figure 3- 25 : Relationship between apparent rate constant with commercial ZnO and initial MG

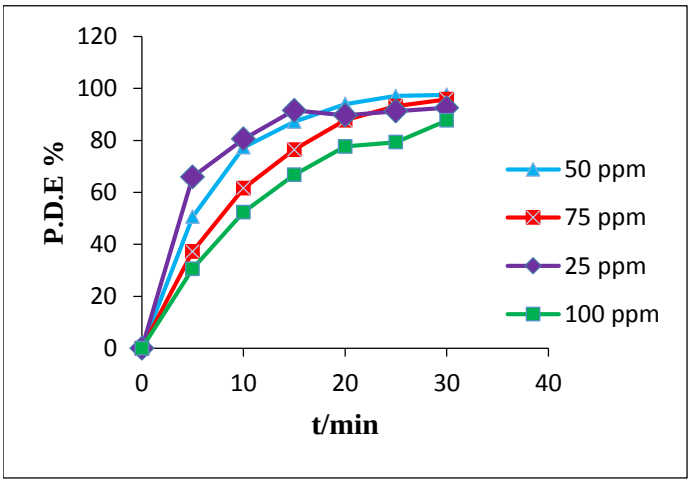

Figure 3-26 : The change of PDE and irradiation time on different concentrations of MG with commercial ZnO .

3.3.2 Effect of dosage of commercial ZnO.

These experiments were carried out by using different dosages of ZnO with MG dye. The results are shown in table 7 (in Appendix (B)) and plotted in figure 3-27. Other factors were kept constant for all these experiments (light intensity ($6x10^{-5}$ Enstine s^{-1}), initial MG dye concentration 50 ppm, initial pH solution 5.40 and

temperature 288.15 K. From these experiments, it was found that 0.7 g of ZnO/200 mL of MG dye gives the optimum photocatalytic activity. The results shown in table 7 (in Appendix (B)) are plotted in figure 3-27 as C_t against time/min. where C_t represent the concentration of MG dye at different times of irradiation and the results shown in table 8 (in Appendix (B)) are plotted in figure 3-28 as ln (C_o/C_t) against time/min. Apparent rate constant expressed in min^{-1} was calculated from the slopes of such linear reaction plots. These results reaction are listed in table 9 (in Appendix (B)) and plotted in figure 3-29 . (PDE) was calculated then listed in table 3- 10 and plotted in figure 3-30 .

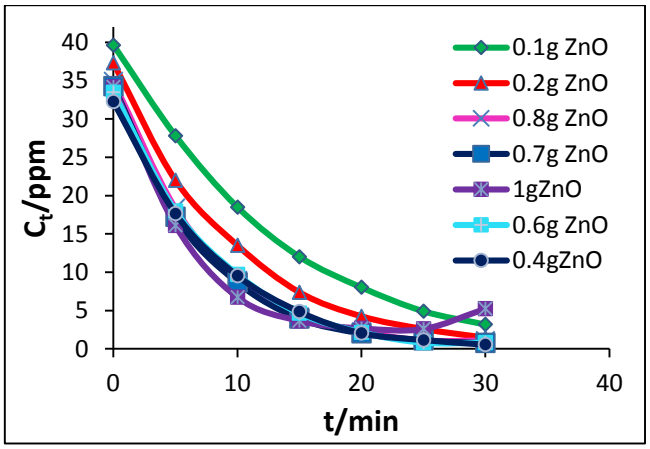

Figure 3-27 : Relationship between C_t and the change of irradiation time on different dosages of commercial ZnO .

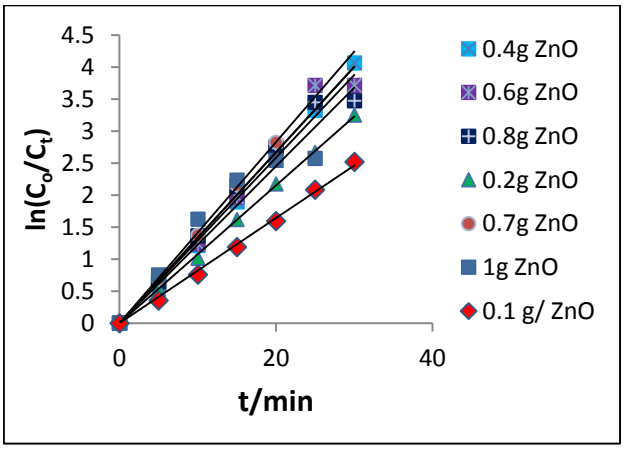

Figure 3-28 : Relationship between $ln(C_o/C_t)$ and the change of irradiation time at different dosage of commercial ZnO

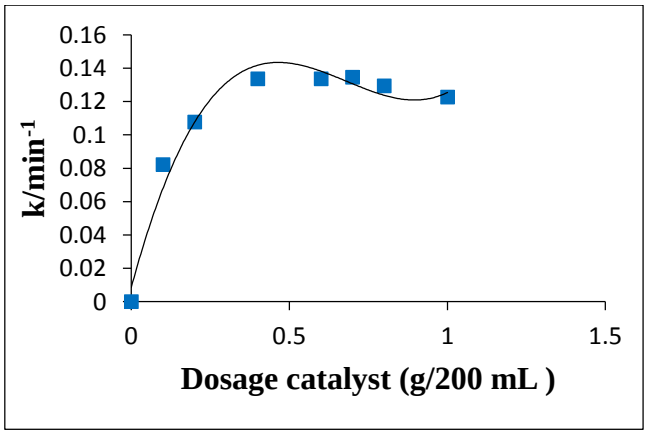

Figure 3-29: Relationship between apparent rate constant for photodecolourization of MG and dosage of commercial ZnO .

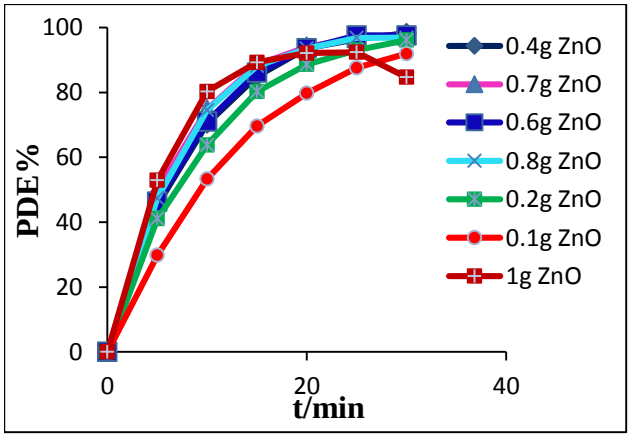

Figure 3-30: The change PDE and irradiation time on different dosage of commercial ZnO

3.3.3 Effect of Initial pH Solution for commercial ZnO.

pH plays an important role in the production of hydroxyl radicals. These experiments used ZnO as photocatalyst to decolorize of MG dye in the aqueous suspensions under the determined experimental condition, light intensity equal to ($6x10^{-5}$ Enstine s^{-1}), initial MG dye concentration of 50 ppm, ZnO concentration (0.7g/200mL) and temperature as equal to 288.15K. Using the pH range between (2 –10) is shown in table 11 (in Appendix (B)) and plotted in figure 3-31 . The results listed in table 12 (in Appendix (B)) and plotted in figure 3-32 show a pseudo first order reaction according to Langmuir Hinshelwood relationship. The results listed in table 13 (in Appendix (B)) and plotted in figure 3-33 show that the apparent rate constant of reaction increases with increasing of the initial pH solution up to the maximum level at pH 10 and then decreases. The decolurization rate of MG dye increases with the increases the initial pH, it is found that the best pH of ZnO is at pH 10 . (PDE) was calculated then listed in table 14 (in Appendix (B)) and plotted in figure 3- 34.

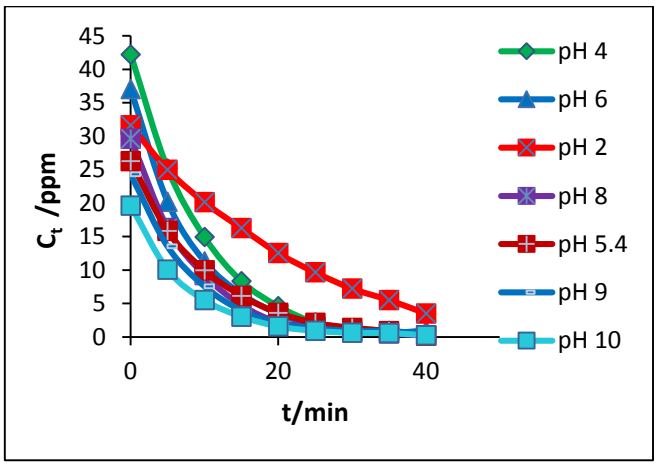

Figure 3-1: Relationship between C_t and the change of irradiation time at different values of initial pH with commercial ZnO.

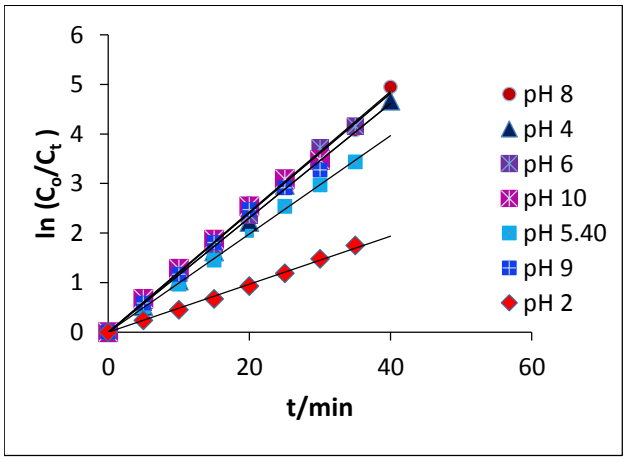

Figure 3-32: Relationship between ln (C_o/C_t) and the change of irradiation time at different values of initial pH with commercial ZnO

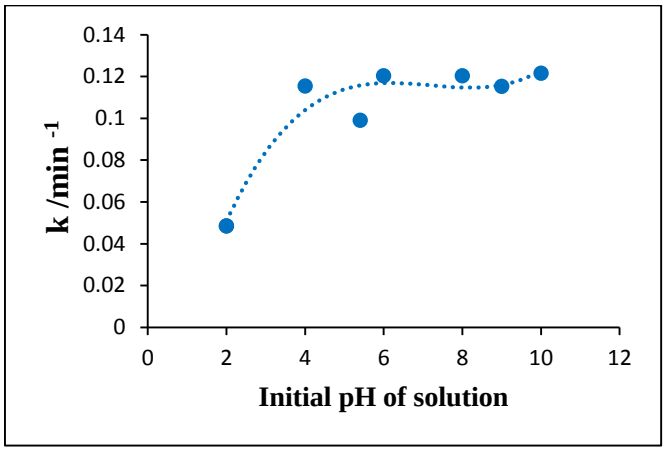

Figure 3- 33 Relationship between ln (C_o/C_t) and the change of irradiation time at different values of initial pH with commercial ZnO

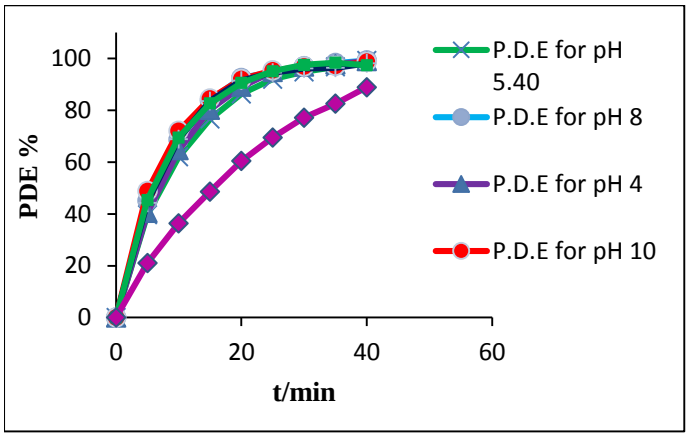

Figure 3-34: The change of PDE and irradiation time at different values of initial pH with commercial ZnO.

3.3.4 Effect of Temperature for Commercial ZnO.

The results in table 15 (in Appendix (B)) which plotted in figure 3- 35 show that the higher temperature had faster decolorization rate of MG dye under experimental conditions, light intensity equal to ($6x10^{-5}$ Enstine s^{-1}), initial MG dye concentration of 50 ppm, ZnO dosage (0.7g/200mL) and initial pH solution equal to 5.40. These experiments used different temperature for ZnO in the range 278.15-293.15 K. It is found that the decolorization rate of MG dye increases when increasing temperature. The results in table 16 (in Appendix (B)) which plotted in figure 3-36 show a pseudo first order reaction according to Langmuir Hinshelwood relationship. The results in table 17 (in Appendix (B)) which plotted in figure 3-37 show Arrhenius relationship which gives activation energy of 24.914 kJ mol^{-1} for photocatalytic decolurization efficiency of MG dye by using commercial ZnO. The results in table 18 (in Appendix (B)) which plotted in figure 3-38 show Eyring relationship which gives thermodynamics parameters. (PDE) was calculated then listed in table 20 (in Appendix (B)) and plotted in figure 3-39.

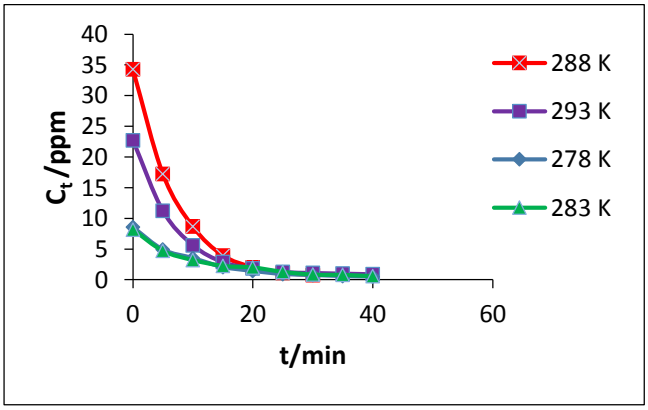

Figure 3-35 : Relationship between C_t and the change of irradiation time at different temperature of MG solution with commercial ZnO .

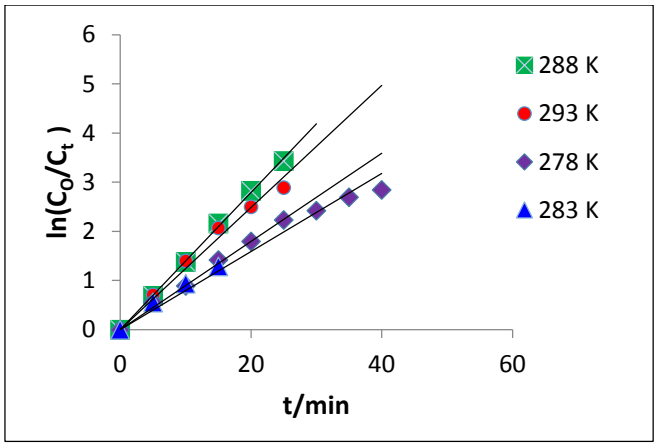

Figure 3-36 : Relationship between ln (C_o/C_t) and the change of irradiation time at different values of temperature with commercial ZnO

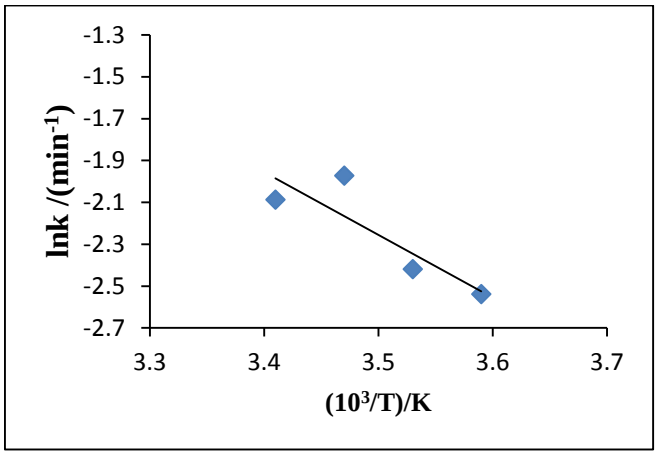

Figure 3-37: Arrhenius plot with commercial ZnO.

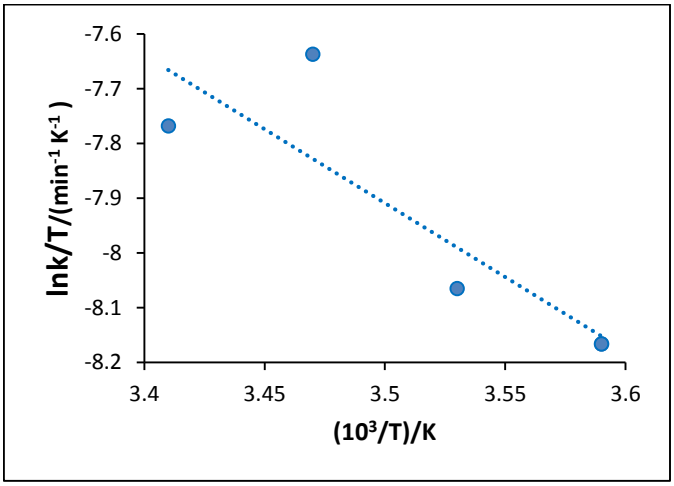

Figure 3-38 : Eyring plot of (ln(k/T) vs. 1/T

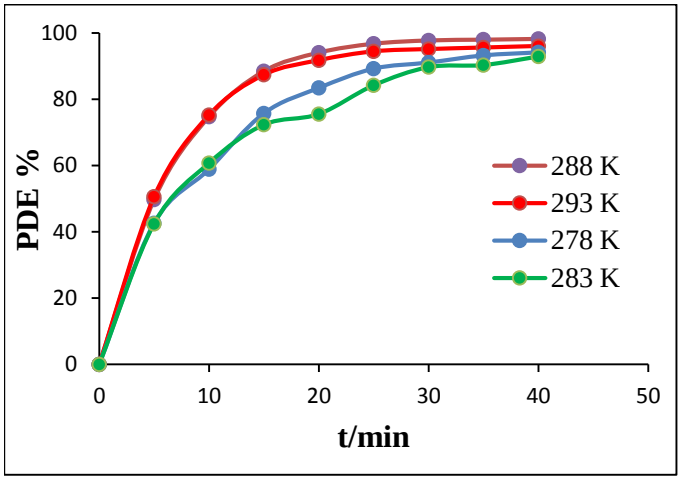

Figure 3-39 : The change of (PDE) and irradiation time on different Temperatures of MG solution with commercial ZnO

3.3.5 Effect the Percentage Loaded Metals

Metals loaded on ZnO as Co%(0.5-2.00) and Ag%(0.50-4.00) were prepared in order to increase the photocatalytic activity of 50 ppm of MG dye in 200 mL. Catalyst dosage of 0.7g was used for all the prepared metalized catalysts at 298.15 K throughout the experiments. The results are listed in Tables 21 and 22 (in Appendix (B)), and plotted in Figures 3- 40 , 3-41.

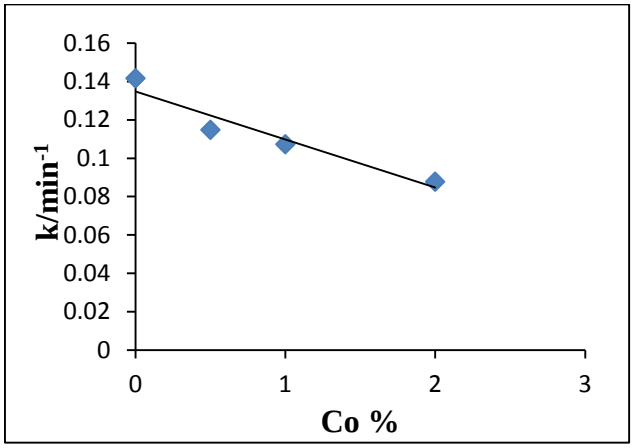

Figure 3-40: The Relationship between the apparent rate constant and the Different Percentage of Co Loaded on commercial ZnO Surface.

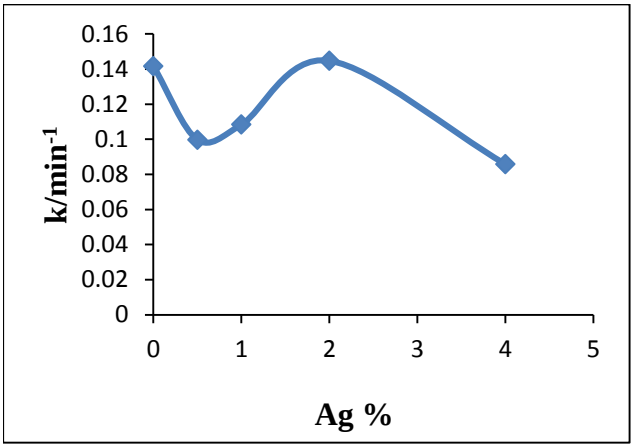

Figure 3-41 : Relationship between the apparent rate constant and the Different Percentage of Ag Loaded on commercial ZnO Surface .

3.4-Effect of Different Parameters on Photocatalytic Decolourization of MG dye for Ag(2.00)/commercial ZnO.

3.4.1- Effect of Initial Dye Concentration.

In these experiments, a series of different concentrations for MG dye in the range (25- 100 ppm) were used .These results are shown in table 23 (in Appendix (B)) and plotted in figure 3- 42 within the experimental conditions light intensity equal to ($6x10^{-5}$ Enstine s^{-1}), pH of solution equal to 5.40 , temperature equal to 303.15 K and commercial ZnO dosage (0.7g/200mL).

The results listed in table 24 (in Appendix (B)) and plotted in figure 3-43 show a pseudo first order reaction according to Langmuir Hinshelwood relationship.

The results listed in table 25 (in Appendix (B)) and plotted in figure 3-44 show the relationship between the apparent rate constant of reaction and initial MG dye concentration . It is found that the apparent rate constant of reaction decrease with increasing of initial dye concentration. (PDE) was determined, then listed in table 26 (in Appendix (B)) and plotted in figure 3- 45 .

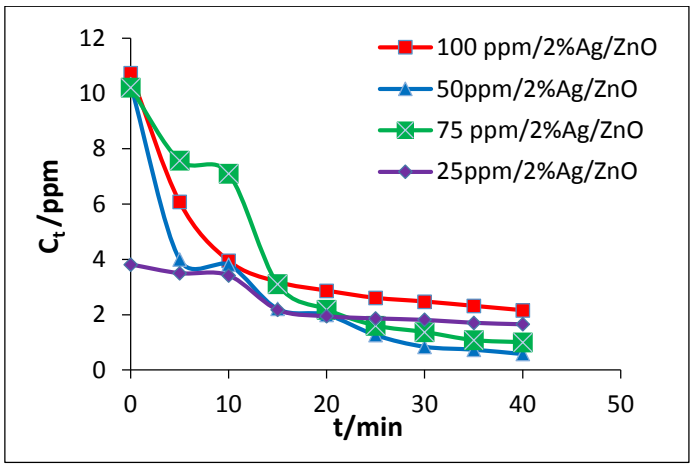

Figure 3-42 : The change of C_t and irradiation time on different MG concentrations with Ag(2.00)/Commercial ZnO .

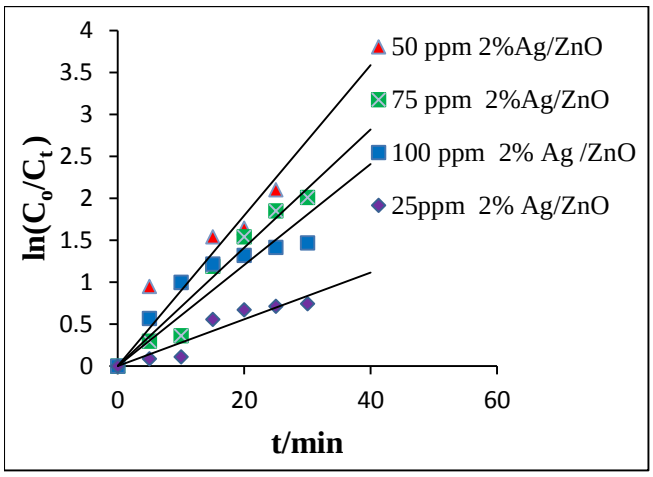

Figure 3-43 : Relationship between ln (C_o/C_t) and irradiation time on different MG concentrations with Ag(2.00)/ commercial ZnO

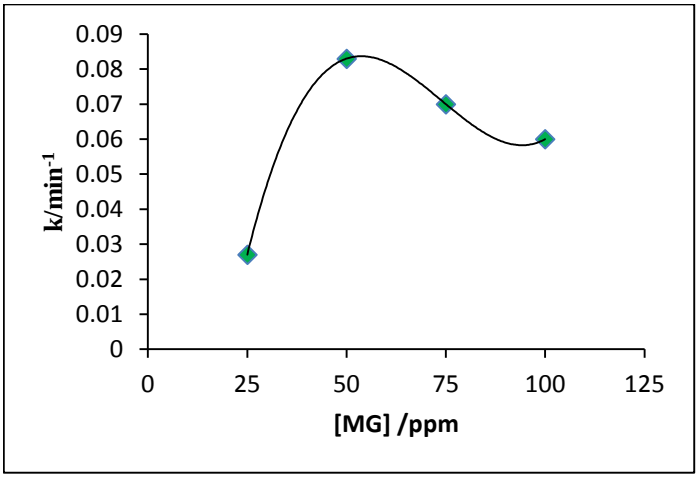

Figure 3-44: Relationship between apparent rate constant and Concentration of MG with Ag (2.00)/commercial ZnO.

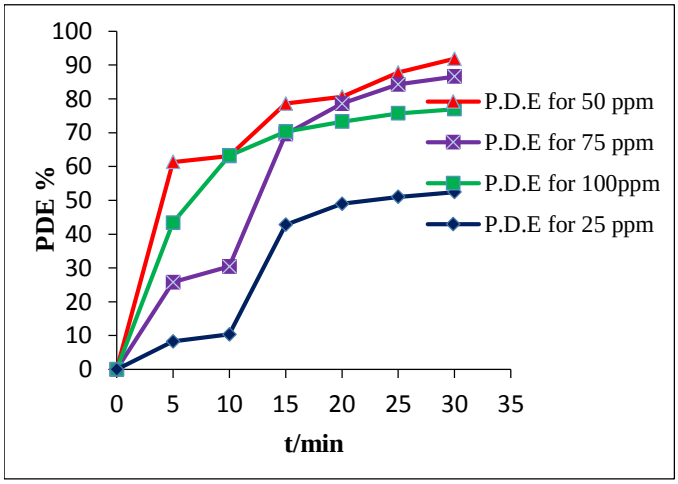

Figure 3-45 : Relationship between irradiation time on different concentration of with Ag (2.00)/Commercial ZnO and (PDE)

3.4.2 Effect of dosage Catalyst as Ag (2.00)/ commercial ZnO.

These experiments were carried out by using different dosages of Ag (2.00)/ZnO with MG dye. The results are shown in table 27 and plotted in figure 3-46. Other factors were kept constant for all these experiments (light intensity ($6x10^{-5}$ Enstine s^{-1}), initial MG dye concentration 50 ppm, pH solution 5.40 and temperature 303.15K). From these experiments, the optimum dosage of Ag (2.00)/ZnO was found to be 0.7 g/200 mL with photocatalytic activity of MG dye solution. The

results are shown in table 27 (in Appendix (B)) and plotted in figure 3-46 as C_t against time/min, where C_t represent the concentration of MG dye at different times of irradiation .The results listed in table 28 (in Appendix (B)) and plotted in figure 3-47 show a pseudo first order reaction according to Langmuir Hinshelwood relationship. Apparent rate constant expressed in min^{-1} was calculated from the slopes of such linear reaction plots. These results reaction are listed in table 29 (in Appendix (B)) and plotted in figure 3-48. (PDE) was calculated then listed in table 30 (in Appendix (B)) and plotted in figure 3-49 .

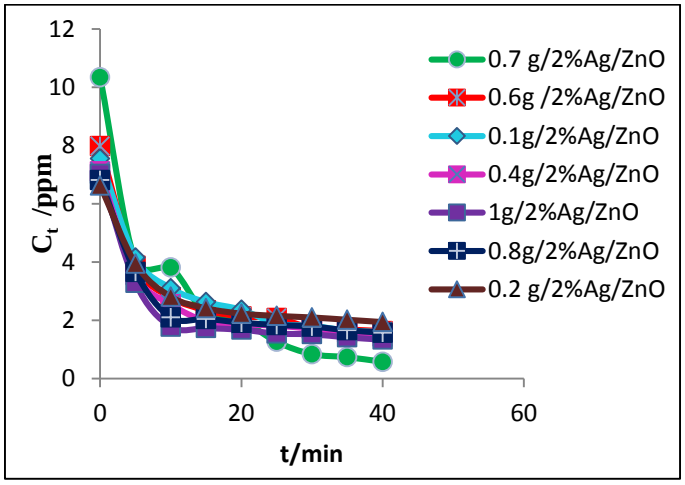

Figure 3-46 : Relationship between C_t and irradiation time on different dosages of Ag (2.00)/ commercial ZnO .

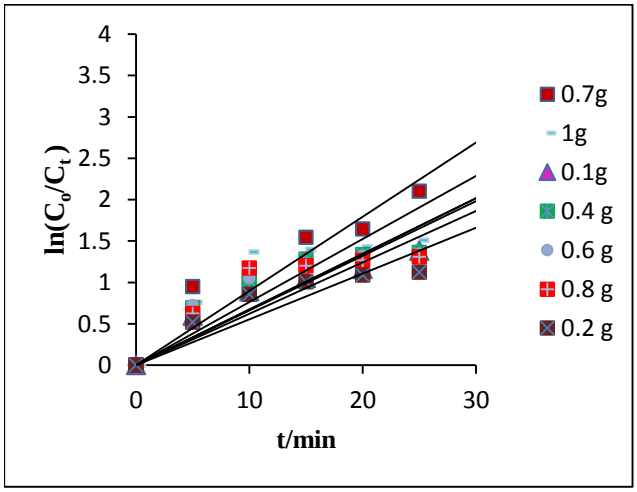

Figure 3-47 : Relationship between $ln(C_o/C_t)$ and irradiation time with different dosages of Ag (2.00)/ commercial ZnO .

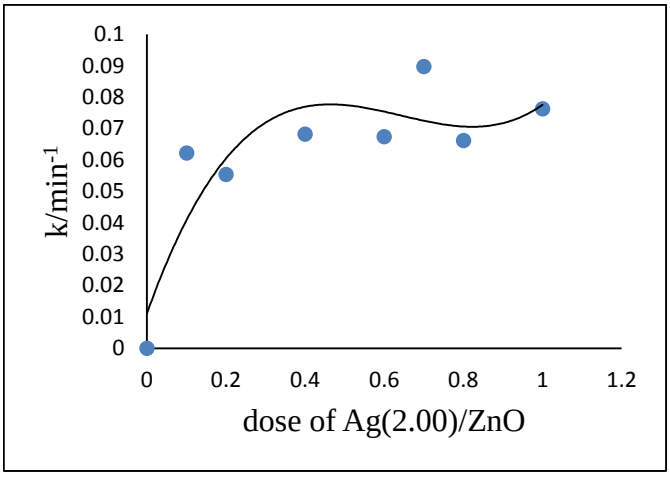

Figure 3-48 : Relationship between apparent rate constant and dosages of Ag(2.00)/ ZnO commercial .

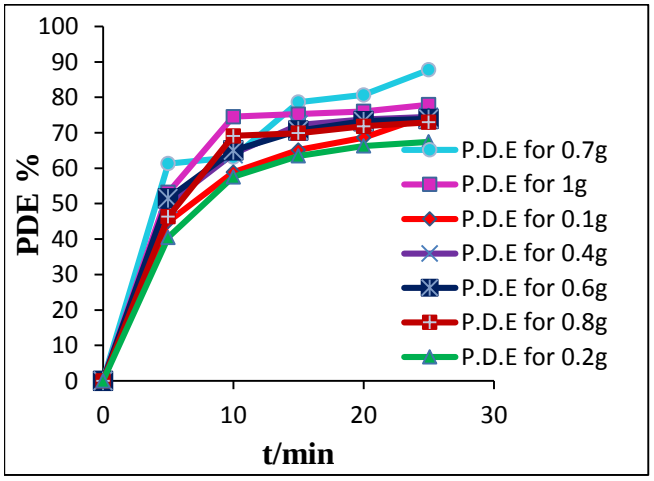

Figure 3-49 : Relationship between (PDE) and irradiation time on different dosages of Ag (2.00)/commercial ZnO.

3.4.3 Effect of initial pH of Solution with Ag (2.00)/ commercial ZnO.

pH is an important factor in the production of hydroxyl radicals. These experiments used ZnO as photocatalyst to decolorize of Methyl green dye in the aqueous suspensions under the determined experimental condition, light intensity equal to ($6x10^{-5}$ Enstine s^{-1}) , ZnO dosage (0.7g/200mL), initial Methyl green dyeconcentration of 50 ppm and temperature equal to 303.15 K. Using the pH range between (2– 10) is shown in table 31 (in Appendix (B)) and plotted in figure 3-50. The results listed in table 32 (in Appendix (B)) and plotted in figure 3- 51 show a pseudo first order reaction according to Langmuir Hinshelwood relationship. The results listed in table 33 (in Appendix (B)) and plotted in figure 3-52 show that the apparent rate constant of reaction increases with increasing of the pH of solution up to the maximum level at pH 5.40 and then decreases. The decolurization rate of Methyl green dye increases with increasing of pH, it is found that the best pH of ZnO at pH 5.40. (PDE) was calculated, then listed in table 34 (in Appendix (B)) and plotted in figure 3-53.

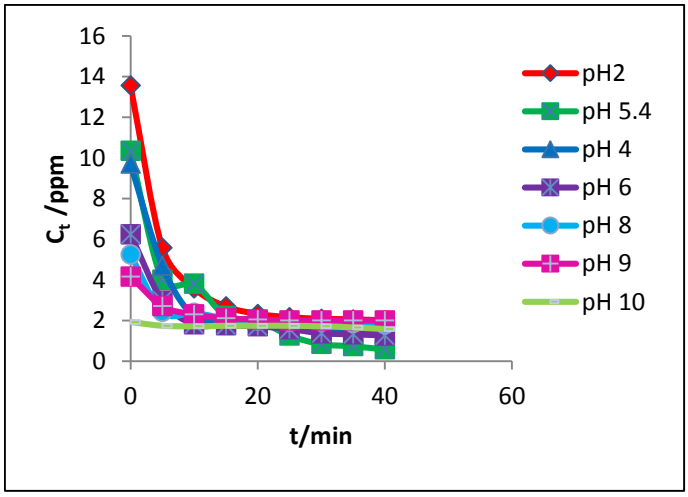

Figure 3-50 : Relationship between C_t and irradiation time at different value of pH with Ag(2.00)/ commercial ZnO.

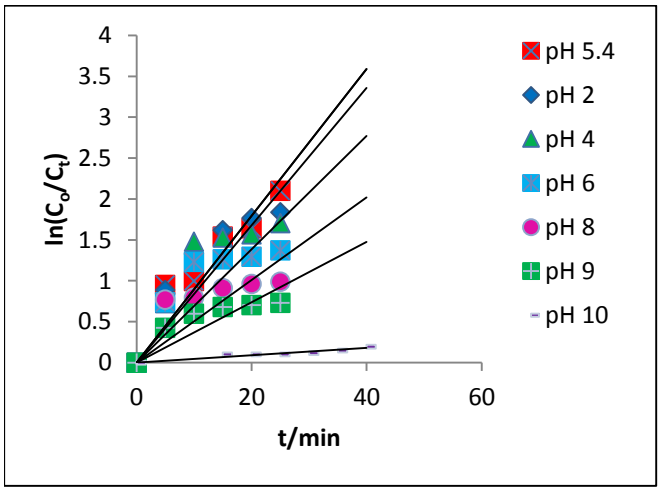

Figure 3-51 :The Relationship between $\ln(C_o/C_t)$ and irradiation time at different value of pH and with Ag (2.00)/ commercial ZnO.

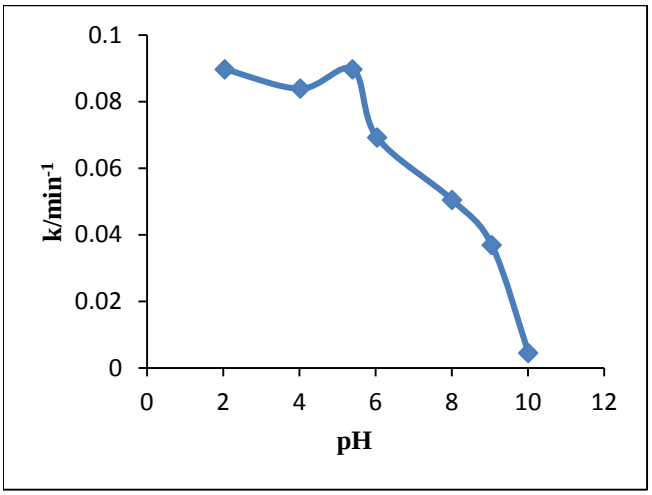

Figure 3-52 : The Relationship between apparent rate constant and initial pH with Ag (2.00)/ commercial ZnO.

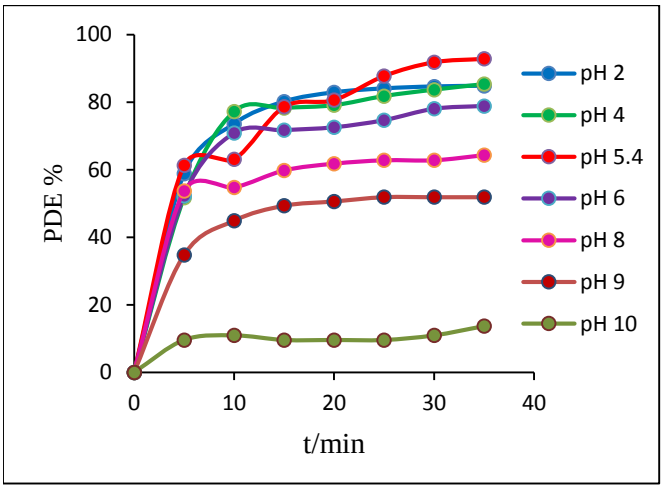

Figure 3-53: The Relationship between (PDE) and irradiation time on different initial pH with Ag (2.00)/commercial ZnO.

3.4.4 Effect of Temperature for dye solution with Ag (2.00)/ commercial ZnO.

The results in table 35 (in Appendix (B)) which plotted in figure 3- 54 show that the higher temperature has faster decolurization rate of MG dye under the experimental conditions, light intensity equal to ($6x10^{-5}$ Enstine s^{-1}), initial MG dye concentration of 50 ppm, initial pH Solution equal to 5.40 and Ag(2.00)/ ZnO dosage (0.7g/200mL).

These experiments used different temperature with Ag (2.00)/ commercial ZnO and dye solution in the range 278.15-293.15 K. It is found that the decolurization rate of MG dye increases with increase of temperature.

The results listed in table 36 (in Appendix (B)) and plotted in figure 3- 55 show a pseudo first order reaction according to Langmuir Hinshelwood relationship .The results in table 37(in Appendix (B)) which plotted in figure 3-56 show Arrhenius relationship which gives activation energy of (6.185) kJ mol^{-1} for photocatalytic decolurization efficiency of MG dye by using Ag (2.00)/commercial ZnO . The results in table 38 (in Appendix (B)) which plotted in figure 3-57 show Eyring relationship which gives thermodynamics parameters. (PDE) was calculated then listed in table 40 (in Appendix (B)) and plotted in figure 3-58 .

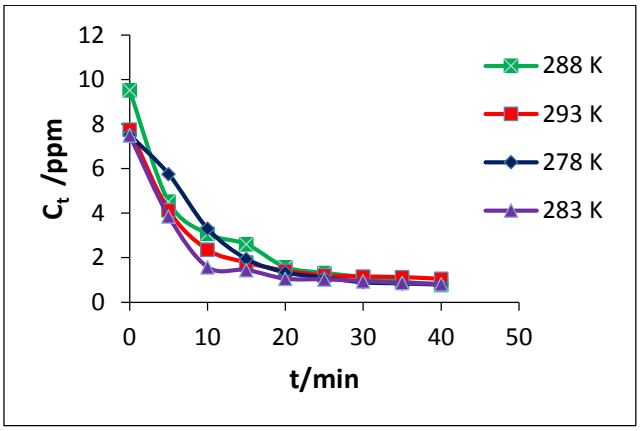

Figure 3- 54: Relationship between C_t and irradiation time at different temperatures of solution with Ag (2.00)/ commercial ZnO .

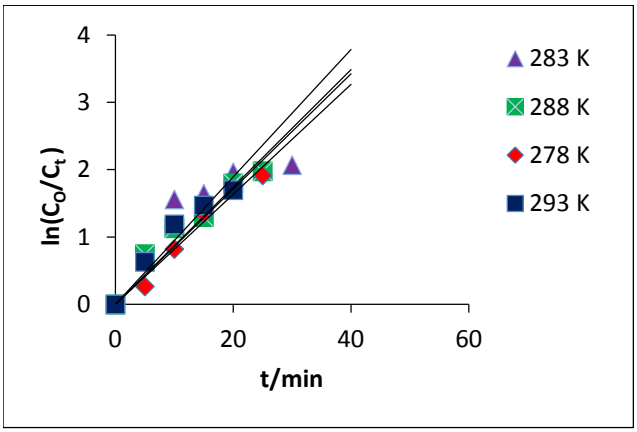

Figure 3-55: Relationship between $\ln(C_0/C_t)$ and irradiation time at different temperatures of solution with Ag (2.00)/commercial ZnO.

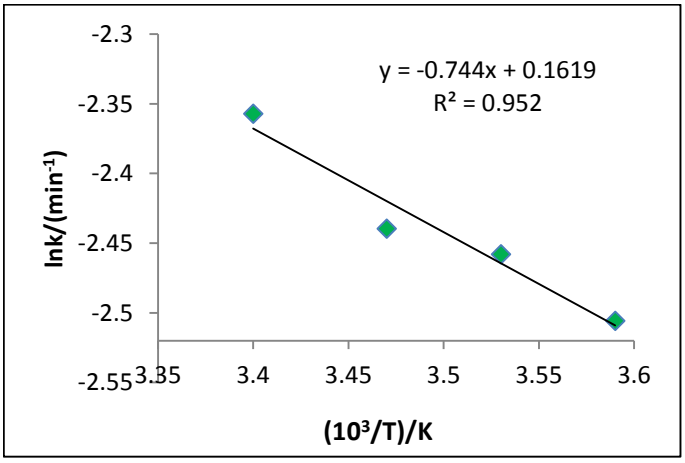

Figure 3-56: Relationship between lnk and temperature for MG solution with Ag (2.00)/commercial ZnO.

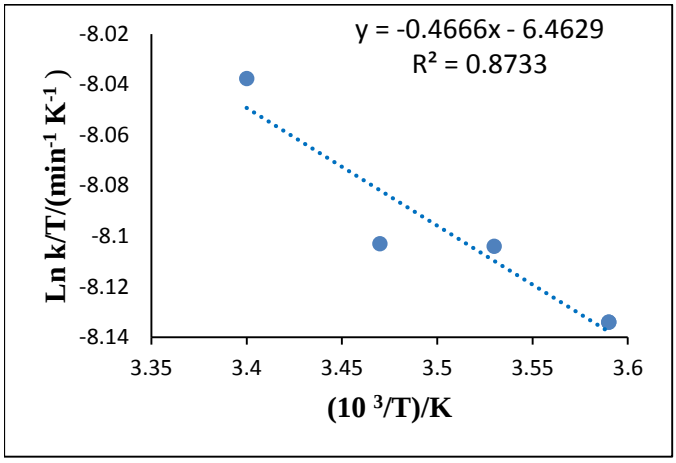

Figure 3-57: Eyring plot of (ln(k/T) vs.1/T

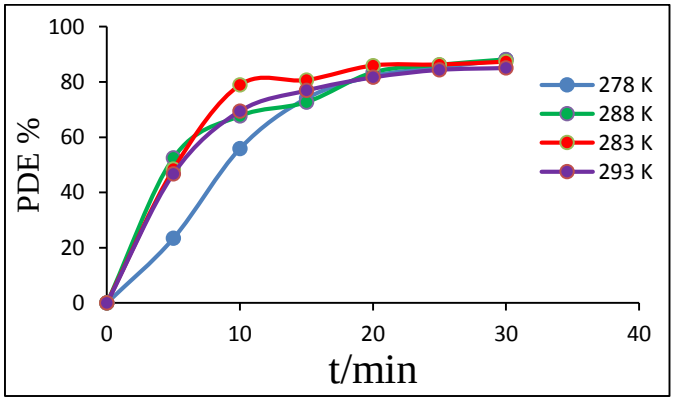

Figure 3-58 : Relationship between(PDE) and irradiation time on different tempertures of solution with Ag (2.00)/ commercial ZnO.

3.5 Effect of Calcination on prepared ZnO

These experiments, series of different temperatures of Calcination for prepared ZnO in the range (300°C, 500 °C and 700 °C) were used .These results are shown in table 41(in Appendix(B)) and plotted in figure 3- 59. Within the experimental conditions, light intensity equal to ($6x10^{-5}$ Enstine s^{-1}), and prepared ZnO dosage (0.7g/200mL), initial pH of solution is equal to 5.40 and temperature equal to 298.15K. The results listed in table 42 (in Appendix(B)) then plotted in figure 3-60 show the reaction of this dye is a pseudo first order reaction according to Langmuir Hinshelwood relationship. Moreover, the results listed in table 43 (in Appendix(B)) then plotted in figure 3-61 show the relationship between apparent rate constant of reaction and the temperature of calcination. It is found that the apparent rate constant of reaction increase with increasing of temperature of calcination and the best temperature is 500°C. (PDE) was calculated then listed in table 44 (in Appendix (B)) and plotted in figure 3-62.

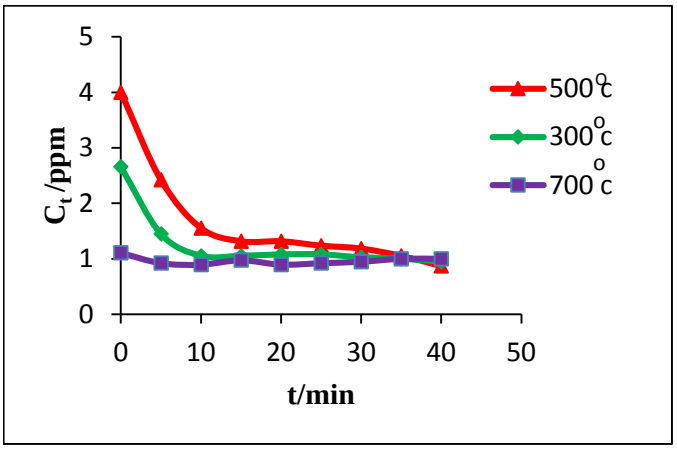

Figure 3-59 :Relationship between C_t and irradiation time on different temperatures of calcination with prepared ZnO .

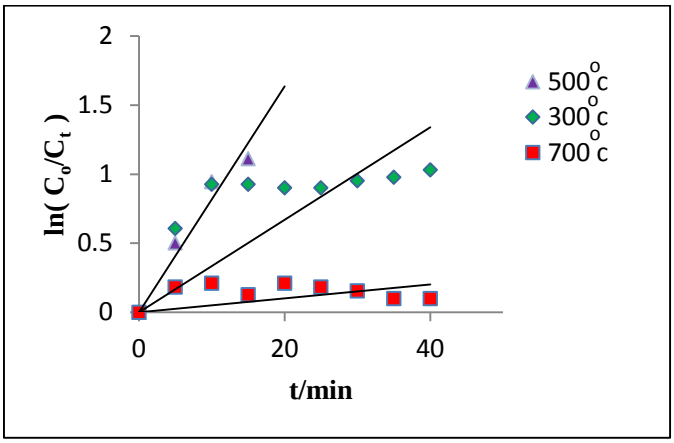

Figure 3-60 : Relationship between ln (C_o/C_t) and irradiation time on different temperatures of calcination with prepared ZnO.

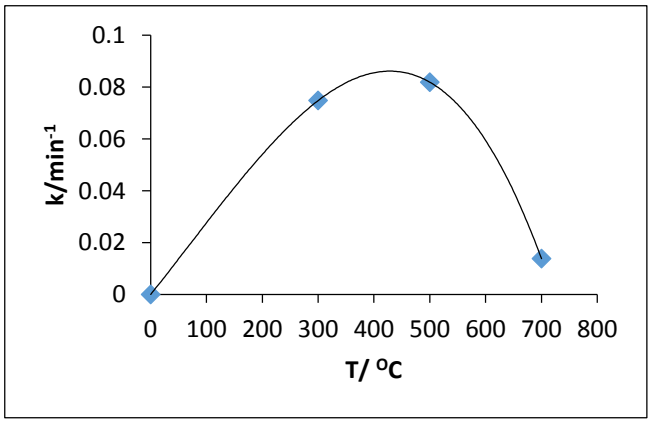

Figure 3-61: The Relationship between the apparent rate constant with prepared ZnO and the temperatures of calcination .

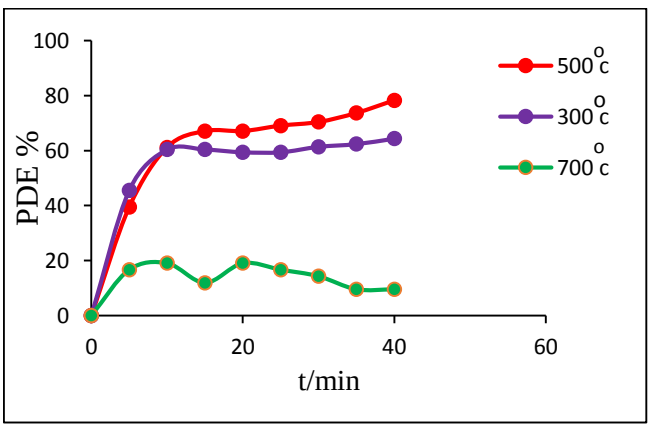

Figure 3-62:The Relationship between (PDE) and irradiation time on different temperatures of calcination with prepared ZnO.

3.6- Effect of Different Parameters on Photocatalytic Decolourization of MG dye with prepared ZnO and calcination at 500 ºC.

3.6.1 Effect of Initial Dye Concentration.

Different concentrations for MGdye in the range (25-100 ppm) were prepared. These results are shown in table 45 (in Appendix(B)) and plotted in figure 3-63. Within the experimental condition, light intensity is equal to ($6x10^{-5}$ Enstine s^{-1}), initial pH of solution equal to 5.40, temperature equal to 298.15K and (0.6g/200mL) as dosage of ZnO calcinated at (500)ºC. So, the optimum initial MG dye concentration is 25 ppm. The results listed in table 46 and plotted in figure 3-64 show a pseudo first order reaction according to Langmuir Hinshelwood relationship. The results listed in table 47 (in Appendix(B)) and plotted in figure 3-65 show the relationship between the apparent rate constant of reaction and initial MG dye concentration. It is found that the apparent rate constant of reaction decreases when increasing of initial dye concentration. (PDE) was calculated then listed in table 48 (in Appendix(B)) and plotted in figure 3-66.

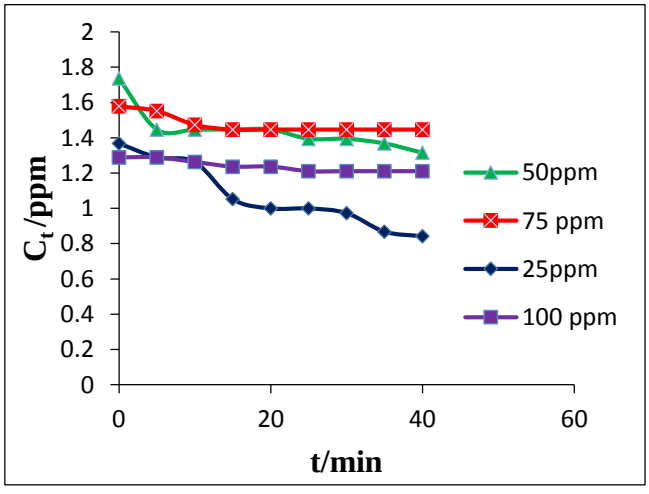

Figure 3-63 : The Relationship between C_t and irradiation time on different MG concentrations with prepared ZnO and calcinated at (500)ºC .

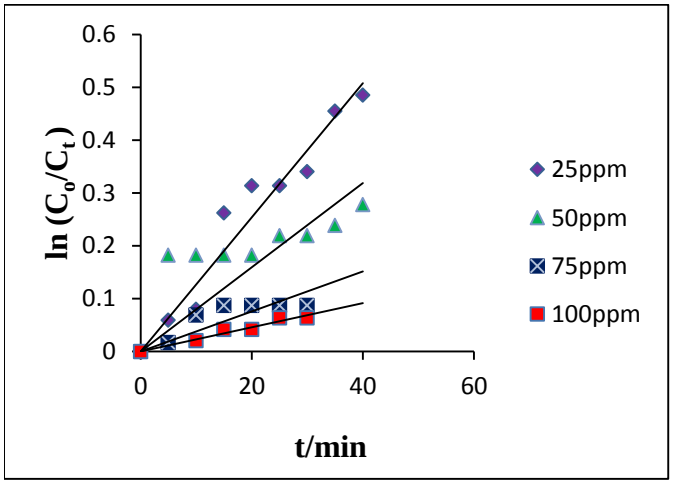

Figure 3-64 :Relationship between ln (C_o/C_t) and irradiation time on different MG concentrations for prepared ZnO and calcinated at (500) ºC .

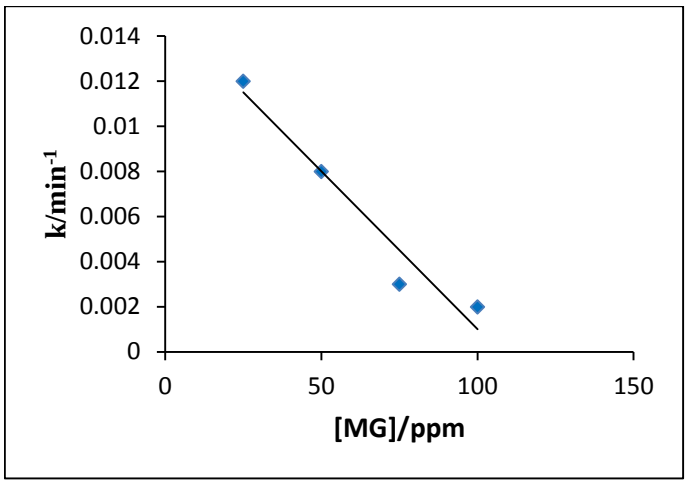

Figure 3-65 : Relationship between apparent rate constant and concentration of MG for prepared ZnO and calcinated at (500)^{o}C .

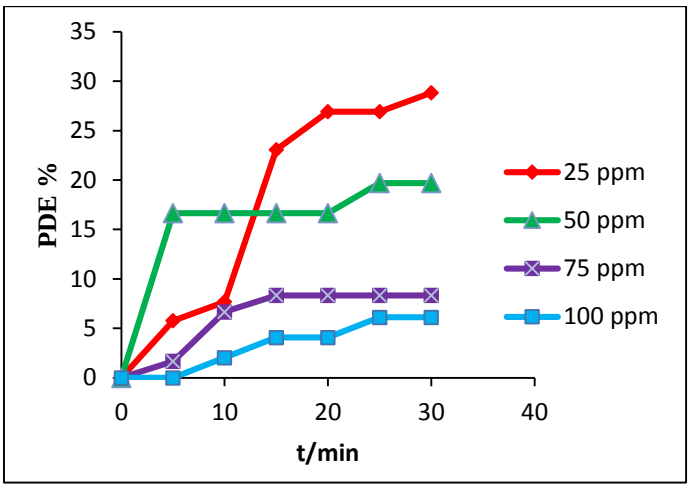

Figure 3-66: Relationship between (PDE) and irradiation time on different concentration of MG for prepared ZnO and calcinated at (500)^{o}C .

3.6.2 Effect of dosage of prepared ZnO and calcinated at (500) ^{o}C .

These experiments were carried out by using different dosages of prepared ZnO (500)^{o}C with MG dye. The results are shown in table 49 (in Appendix(B)) and plotted in figure 3-67.Other factors were kept constant for all these experiments (light intensity ($6x10^{-5}$ Enstine s^{-1}), initial MG dye concentration 25 ppm, initial pH solution 5.40 and temperature 298.15K). From these experiments, it is found that 0.6 g of prepared ZnO and calcinated at 500 ^{o}C /200 mL of MG dye gives the optimum photocatalytic activity.

The results shown in table 49 (in Appendix(B)) are plotted in figure 3-67 as C_t against time/min. The results listed in table 50 and plotted in figure 3-68 show a pseudo first order reaction according to Langmuir Hinshelwood relationship. Reaction rate constants expressed in min^{-1} were calculated from the slopes of such linear reaction plots. These results reaction are listed in table 51 (in Appendix(B)) and plotted in figure 3-69. (PDE) was calculated then listed in table 52 (in Appendix(B)) and plotted in figure 3-70 .

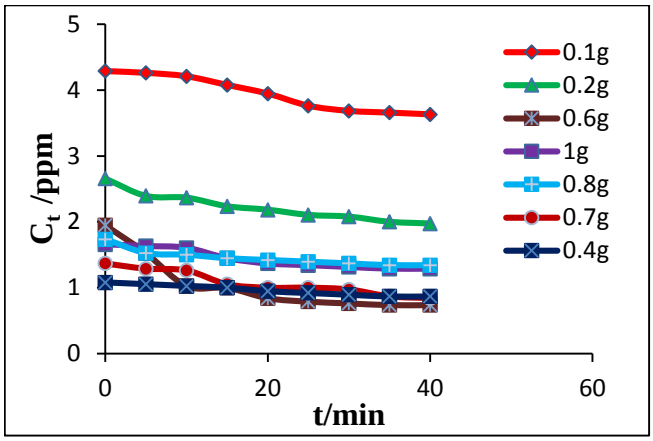

Figure 3-67: Relationship between C_t and irradiation time on different dosages with prepared ZnO and calcinated at (500) °C .

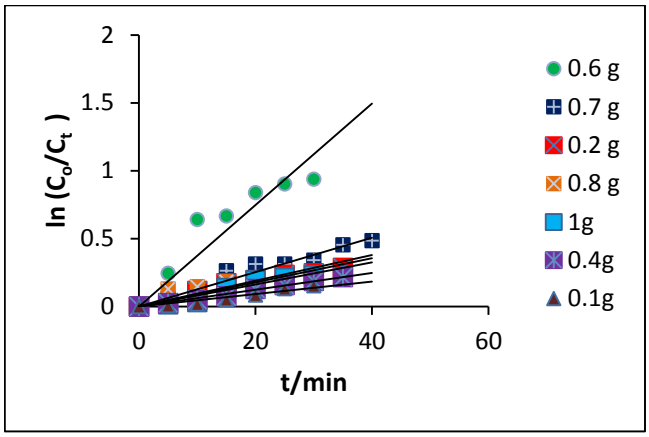

Figure 3-68 : Relationship between ln(C_o/C_t) and irradiation time on different dosages with prepared ZnO and calcinated at (500)°C .

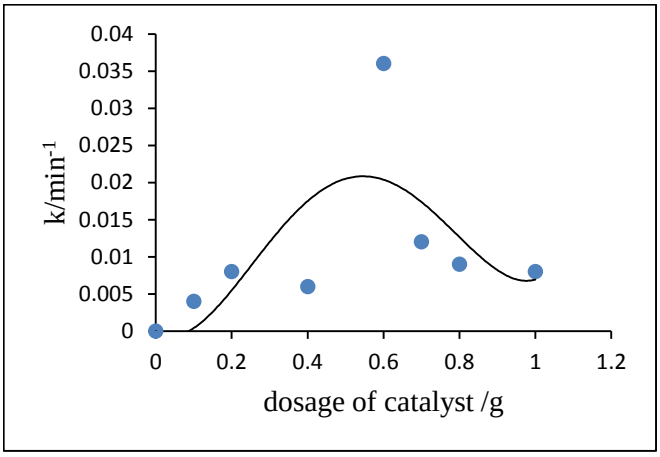

Figure 3- 69 : Relationship between apparent rate constant and dosage with prepared ZnO and calcinated at (500)°C .

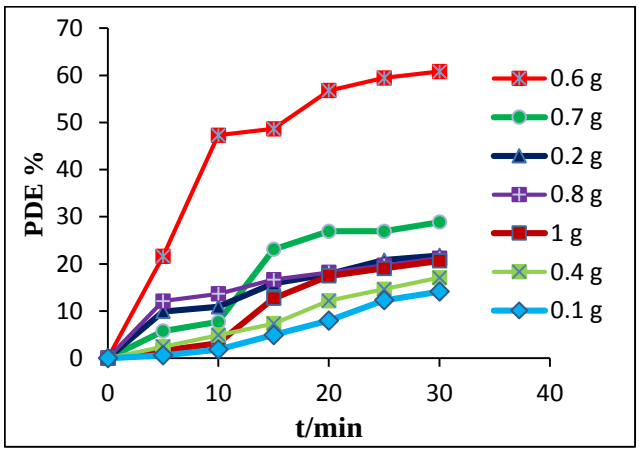

Figure 3-70: Relationship between (PDE) and irradiation time on different dosage for prepared ZnO and calcinated at (500)°C.

3.6.3 Effect of initial pH of Solution for prepared ZnO and calcination at (500)°C .

In general, the initial pH of solution plays an important role in the production of hydroxyl radicals. These experiments used the prepared ZnO as photocatalyst to remove the color of MGdye in the aqueous suspensions under the determined experimental condition, light intensity equal to ($6x10^{-5}$ Enstine s^{-1}), initial MG dye concentration of 25 ppm, prepared ZnO (500) °C dosage (0.6 g/200mL) and temperature equal to 298.15K. Using the pH range between (2 –10) is shown in table 53 (in Appendix(B)) and plotted in figure 3- 71. The results listed in table 54

(in Appendix(B)) and plotted in figure 3- 72 show a pseudo first order reaction according to Langmuir Hinshelwood relationship. The results listed in table 55 (in Appendix(B)) and plotted in figure 3-73 show that the apparent rate constant of reaction increases with the increase of the initial pH solution up to the maximum level at pH 5.40 and then decreases. The decolourization rate of MG dye increases with the increase of pH . It is found that the best pH of solution with used prepared ZnO at pH 5.40. (PDE) was calculated then listed in table 56 (in Appendix(B)) and plotted in figure 3- 74.

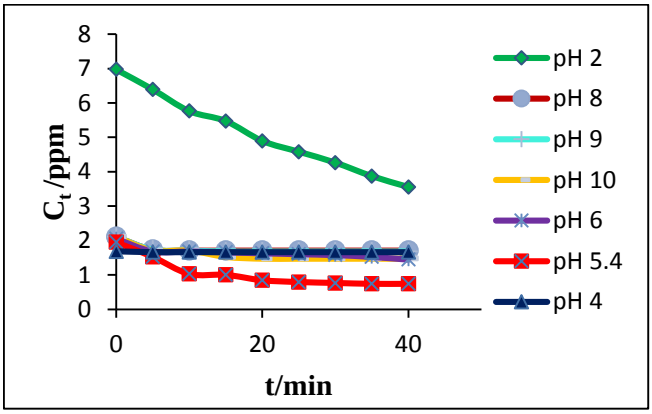

Figure 3-71 : Relationship between C_t and irradiation time at different value of pH with prepared ZnO and calcination at (500)ºC.

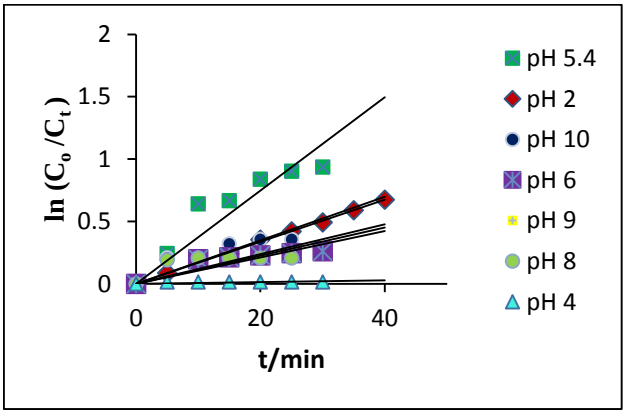

Figure 3-72 : Relationship between ln(C_o/C_t) and irradiation time at different value of pH with prepared ZnO and calcinated at (500) ºC .

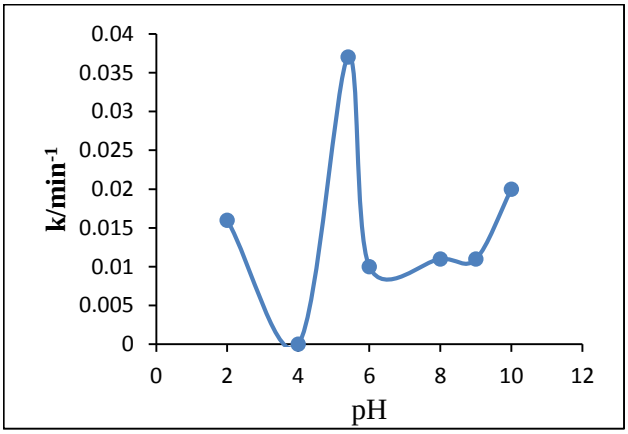

Figure 3-73: Relationship between apparent rate constant with prepared ZnO and calcinated at (500) ºC and initial pH of solution .

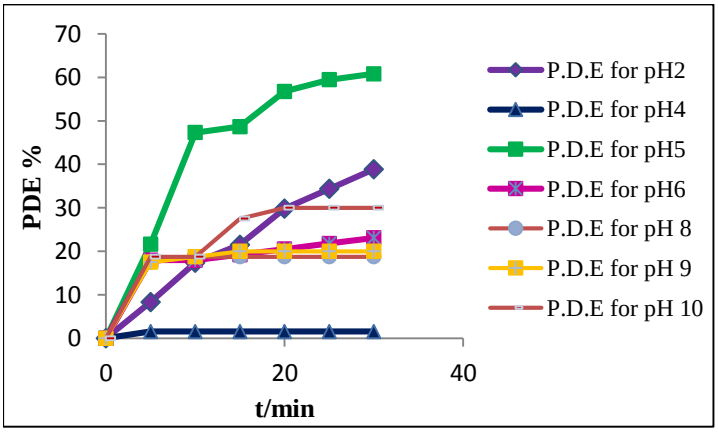

Figure 3-74 :Relationship between (PDE) and irradiation time on different pH with prepared ZnO and calcinated at (500) ºC .

3.6.4 Effect of Temperature for prepared ZnO and calcinated at (500) ^{o}C.

The results in table 57 (in Appendix(B)) which plotted in figure 3-75 show that the higher temperature had faster decolurization rate of MGdye under experimental conditions, light intensity equal to ($6x10^{-5}$ Enstine s^{-1}), initial MG dye concentration of 25 ppm, initial pH solution equal to 5.40 and ZnO dosage 0.6 g. These experiments used different temperature for solution of prepared ZnO and calcinated at (500) ^{o}C in the range (278.15-293.15) K. It is found that the decolourization rate of MG dye increases with increasing of temperature. The results listed in table 58 (in Appendix(B)) and plotted in figure 3-76 show a pseudo first order reaction according to Langmuir Hinshelwood relationship. The results in table 59 (in Appendix(B)) which plotted in figure 3-77 show Arrhenius relationship which gives activation energy of (19.690) kJ mol^{-1} for photocatalytic decolurization efficiency of MG dye by used prepared ZnO and calcinated at (500)^{o}C. The results in table 60 (in Appendix (B)) which plotted in figure 3-88 show Eyring relationship which gives thermodynamics parameters. (PDE) was calculated then listed in table 62 (in Appendix(B)) then plotted in figure 3-79.

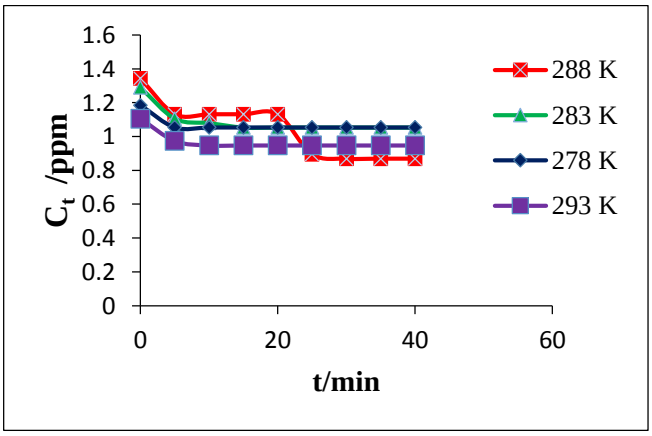

Figure 3- 75 : Relationship between C_t and irradiation time at different temperatures for prepared ZnO and calcinated at (500)^{o}C.

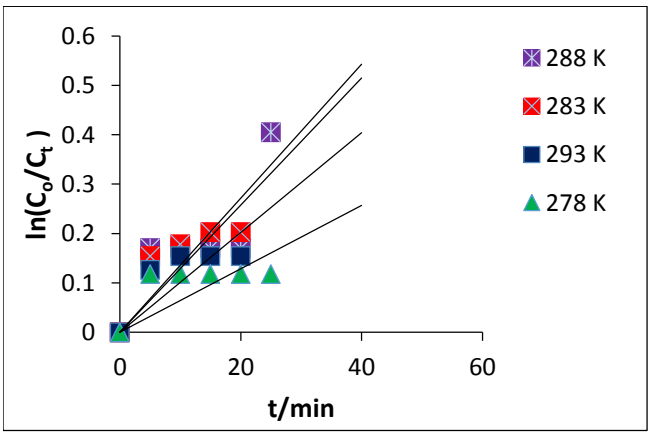

Figure 3-76 : Relationship between $\ln(C_o/C_t)$ and irradiation time at different temperatures with prepared ZnO and calcinated at (500)^{o}C .

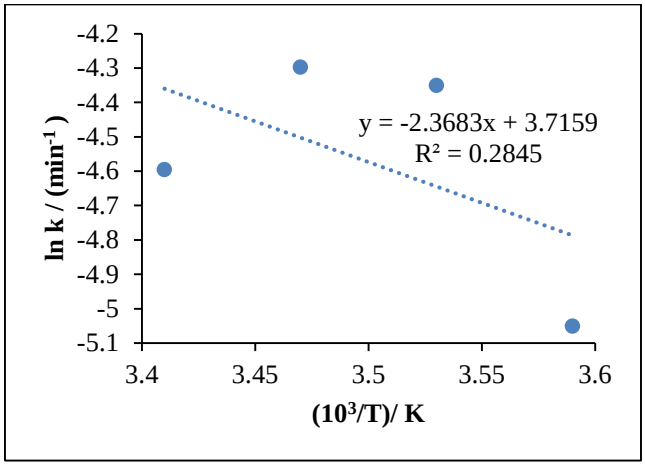

Figure 3-77 : Relationship between lnk and (10^3/T) K for solution with prepared ZnO and calcinated at 500 ºC.

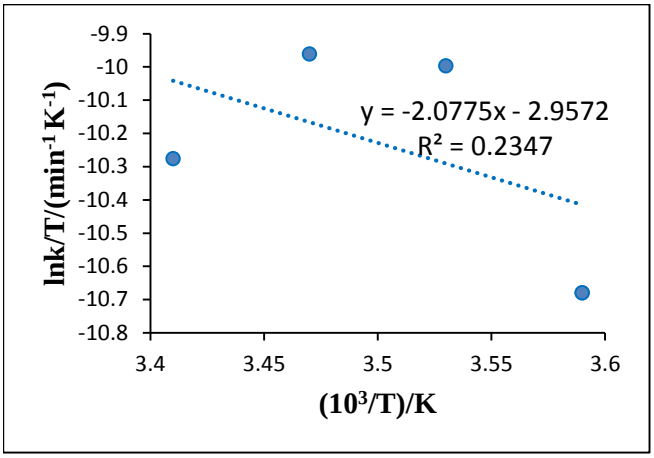

Figure 3-78 : Eyring plot of (ln(k/T) vs.1/T.

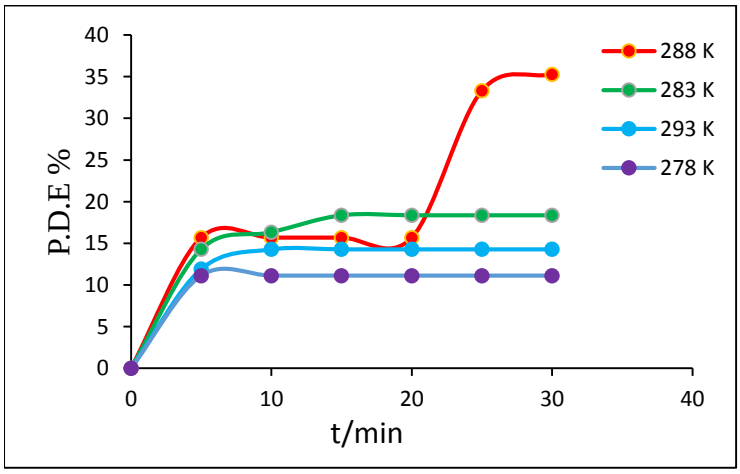

Figure 3-79 : Relationship between(PDE) and irradiation time on different temperatures with prepared ZnO and calcinated at (500)ºC and .

3.6.5 Effect of the percentage of Loaded Metals

Metals loaded on ZnO as Co % (0.5-2.00) and Ag % (0.50-4.00) were prepared in order to increase the photocatalytic activity of 50 ppm of MG dye in 200 mL with 0.7 g Catalyst which were used for all prepared catalysts at 298.15 K throughout the experiments. The results are listed in Tables 63 and 64 (in Appendix(B)), then plotted in Figures 3-80,3-81.

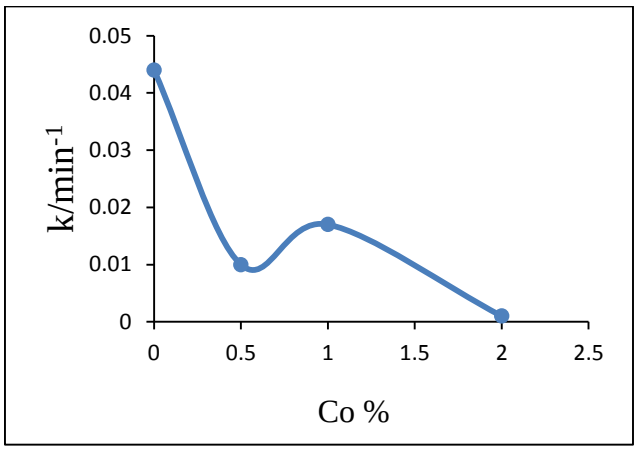

Figure 3-80: Relationship between apparent rate constant and Different Percentage of Co Loaded on surface of prepared ZnO and calcinated at (500) ºC

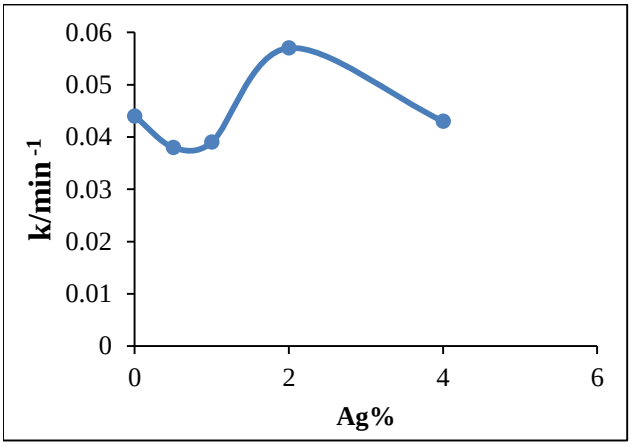

Figure 3-81: Relationship between apparent rate constant and Different Percentage of Ag Loaded on prepared ZnO and calcinated at (500)ºC Surface .

3.7- Effect of Different Parameters on Photocatalytic Decolourization of MG dye with Ag(2.00)/ prepared ZnO and calcinated at (500)ºC.

3.7.1- Effect of Initial Dye Concentration.

Different concentrations for MG dye in the range (25-100 ppm) were also used. These results are shown in table 65 (in Appendix(B)) and plotted in figure 3-82 within the experimental conditions light intensity is equal to ($6x10^{-5}$ Enstine $.s^{-1}$), initial pH solution equal to 5.40, temperature equal to 306.15 K and (0.7g/200mL) dosage of Ag (2.00)/ prepared ZnO that was calcinated at (500) ºC. The results listed in table 66 (in Appendix(B)) and plotted in figure 3-83 show, the photocatalytic decolorization of MG dye is a pseudo first order reaction according to Langmuir Hinshelwood relationship. The results listed in table 67 (in Appendix(B)) and plotted in figure 3-84 show the relationship between the apparent rate constant of reaction and initial MG dye concentration. It is found that the apparent rate constant of reaction decrease with increasing of initial dye concentration. (PDE) was calculated then listed in table 68 (in Appendix(B)) and plotted in figure 3-85.

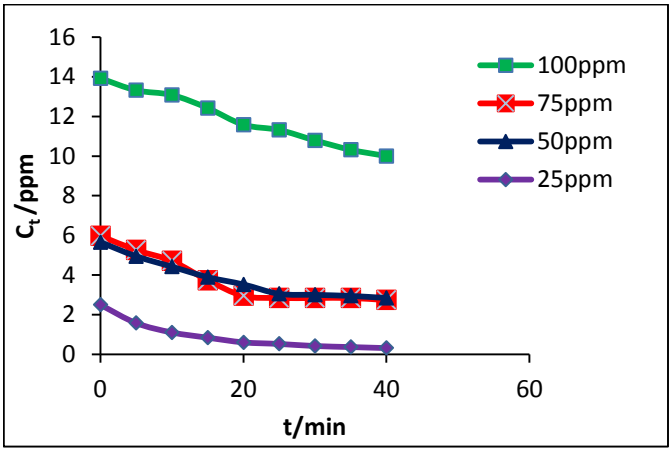

Figure 3-82: Relationship between C_t and irradiation time on different dye concentrations with Ag (2.00)/prepared ZnO and calcinated at (500)^{O}C .

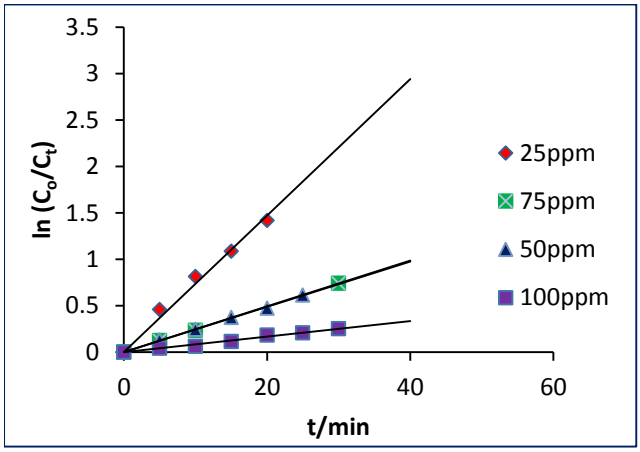

Figure 3-83 : Relationship between ln (C_o/C_t) and irradiation time at different dye concentrations with Ag (2.00)/ prepared ZnO that calcinated at (500) ^{o}C.

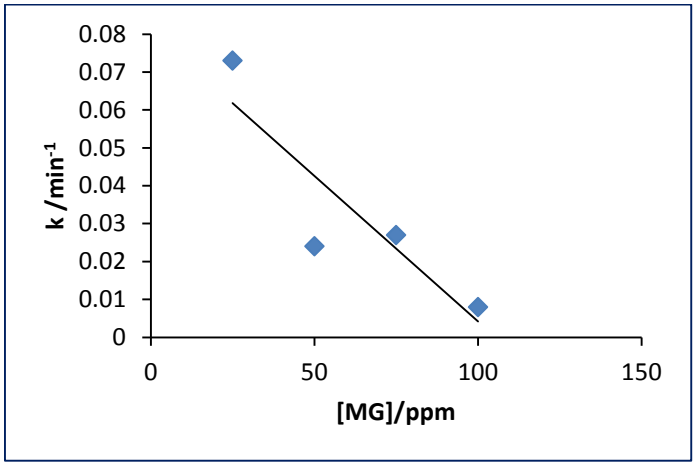

Figure 3-84 : Relationship between apparent rate constant and concentration with Ag (2.00)/ prepared ZnO that calcinated at (500) ^{o}C.

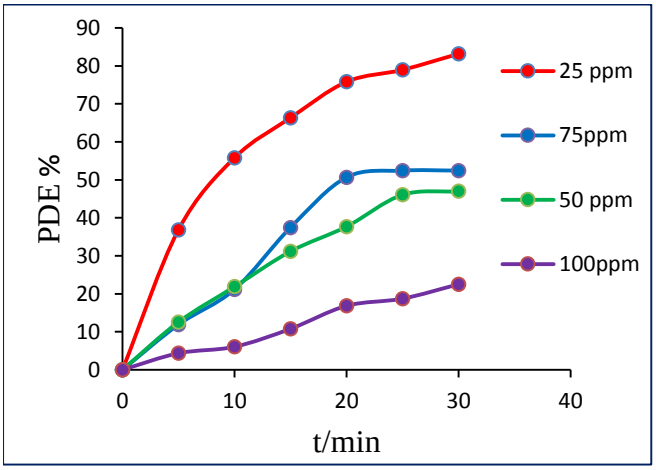

Figure 3-85 : Relationship between (PDE) and irradiation time on different concentration with Ag(2.00)/ prepared ZnO that calcinated at (500)^{o}C.

3.7.2 Effect of dosage of Ag (2.00)/ prepared ZnO that calcinated at (500) ^{o}C .

This effect was carried out by using different dosages of Ag (2.00)/ prepared ZnO that was calcinated at (500) ^{o}C in aqueous solution of MG dye. The results are shown in table 69 (in Appendix(B)) then plotted in figure 3-86. Other factors were kept constant for all these experiments (light intensity ($6x10^{-5}$ Enstine s^{-1}), initial MGdye concentration 25 ppm, pH of solution 5.40 and temperature 306.15K). From these experiments, it is found that 0.7 g of Ag (2.00)/ prepared ZnO that calcinated at (500) ^{o}C /200 mL of MG dye gives the optimum

photocatalytic activity. The results are shown in table 69 (in Appendix(B)) that plotted in figure 3-86 as C_t against time/min, where C_t represents the concentration of MG dye at different times of irradiation. The results listed in table 70 (in Appendix(B)) and plotted in figure 3-87 show a pseudo first order reaction according to Langmuir Hinshelwood relationship.Reaction rate constant expressed in min $^{-1}$ are calculated from the slopes of such linear reaction plots. These results of reaction are listed in table 71 (in Appendix(B)) and plotted in figure 3-88. (PDE) was calculated and then are given in listed in table 72 (in Appendix(B)) and plotted in figure 3-89 .

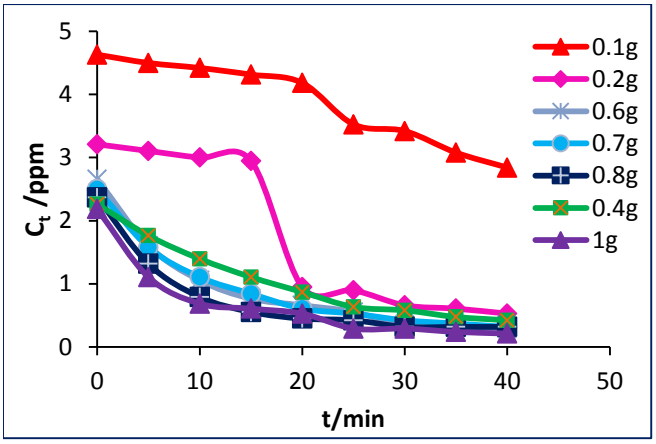

Figure 3-86 : Relationship between C_t and irradiation time on different dosages of Ag (2.00)/ prepared ZnO that calcinated at (500)°C.

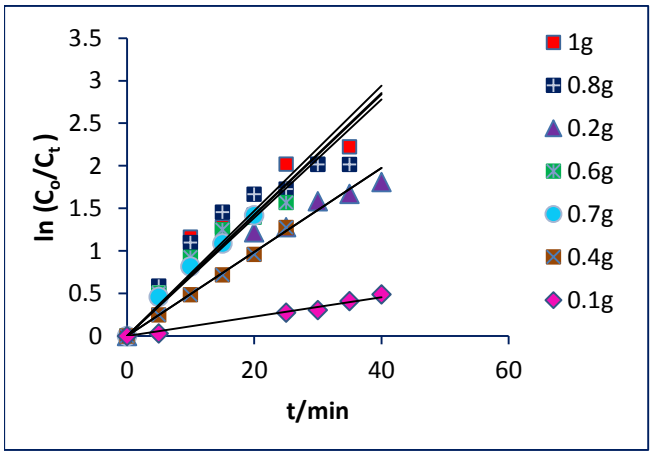

Figure 3-87 : Relationship between ln(C_o/C_t) and irradiation time on different dosages of Ag (2.00)/ prepared ZnO that calcinated at (500)°C.

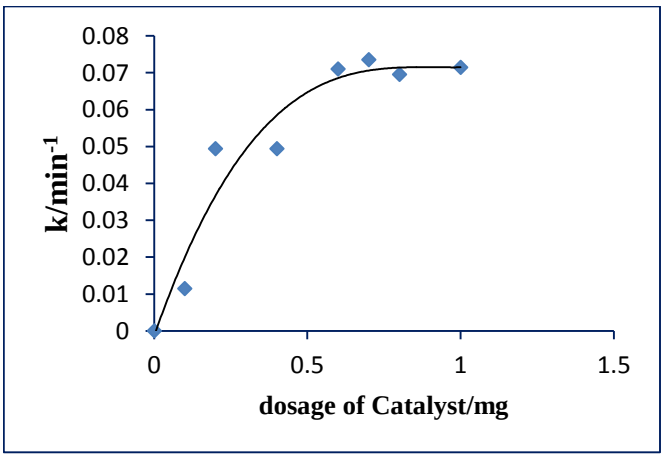

Figure 3-88 : Relationship between apparent rate constant and dosage with Ag (2.00)/prepared ZnO that calcinated at (500)°C .

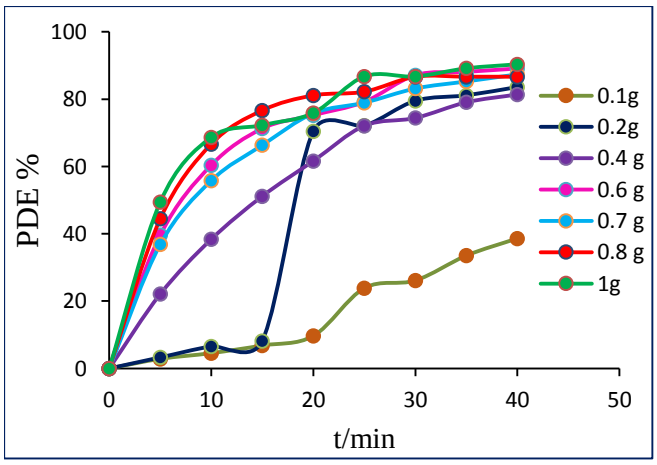

Figure 3-89 : Relationship between (PDE) and irradiation time on different dosages of Ag (2.00)/prepared ZnO that calcinated at (500)°C.

3.7.3 Effect of Initial pH Solution for Ag (2.00)/ prepared ZnO that calcinated at (500) ºC .

The pH of solution is regarded as an important factor in the generation of hydroxyl radicals. These experiments used prepared ZnO that calcinated at (500) ºC as photocatalyst to decolorize of MGdye in the aqueous suspensions under the determined experimental condition, light intensity equal to ($6x10^{-5}$ Enstine s^{-1}), temperature equal to 306.15 K, ZnO dosage (0.6g/200 mL) and initial MGdye concentration of 25 ppm. Using the pH range between (2 –10) is shown in table 73 (in Appendix(B)) then plotted in figure 3-90.

The results listed in table 74 (in Appendix(B)) and plotted in figure 3-91 show a pseudo first order reaction according to Langmuir Hinshelwood relationship. The results listed in table 75 (in Appendix(B)) and plotted in figure 3-92 show that the apparent rate constant of reaction increases with increase of the initial pH solution up to the maximum level at pH 5.4 and then decreases. The decolourization rate of MG dye increases with the increase of pH .It is found that the best pH of ZnO at pH 5.40. (PDE) was calculated and are given listed in table 76 (in Appendix(B)) and plotted in figure 3-93 .

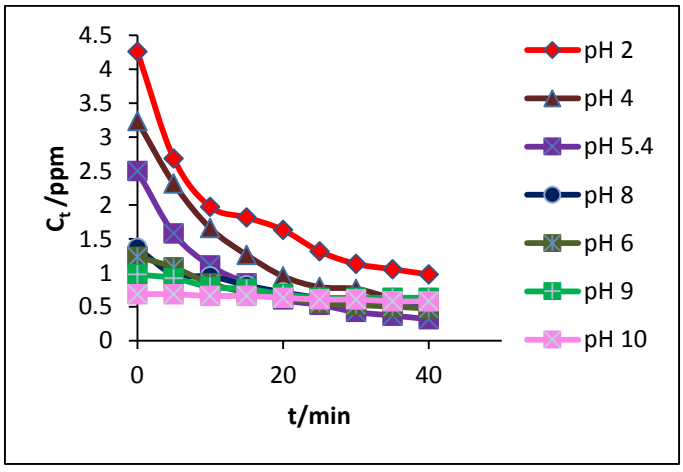

Figure 3-90 : Relationship between C_t and irradiation time at different value of pH for Ag (2.00)/ prepared ZnO that calcinated at (500)ºC.

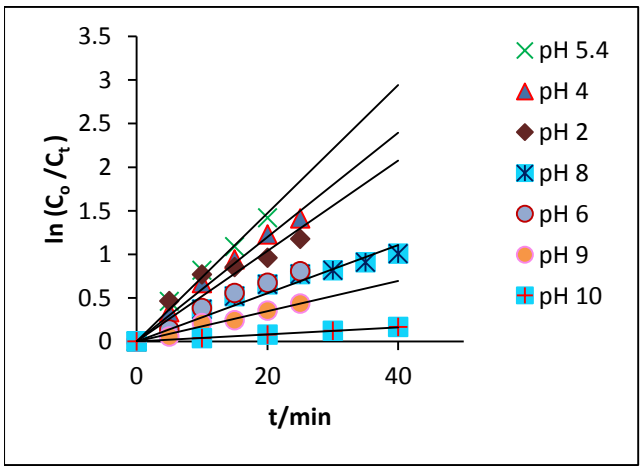

Figure 3-91 : Relationship between ln(C_o/C_t). irradiation time at different value of pH with Ag (2.00)/prepared ZnO that calcinated at (500) ºC.

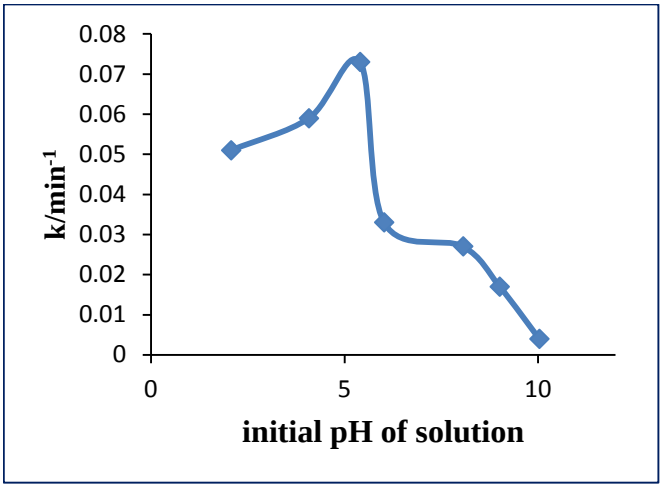

Figure 3-92: Relationship between apparent rate constant and initial pH of Ag(2.00)/ prepared ZnO that calcinated at (500) ºC.

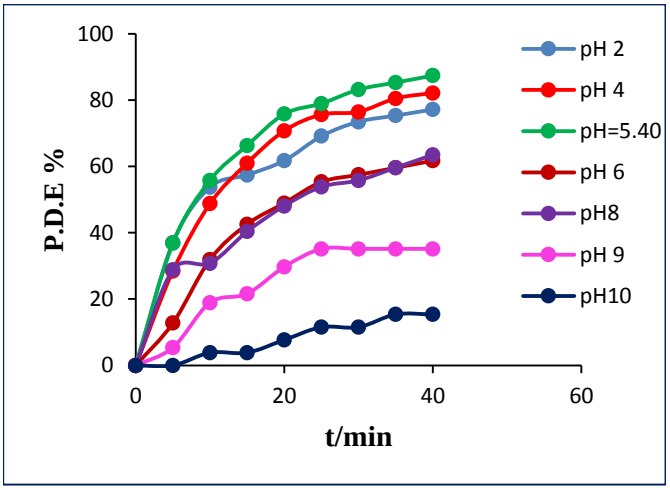

Figure 3- 93 : Relationship between(PDE) and irradiation time on different pH of Ag (2.00)/ prepared ZnO that calcinated at (500)ºC .

3.7.4 Effect of Temperature of Ag (2.00)/prepared ZnO that calcinated at (500) ºC .

The results in table 77 (in Appendix(B)) which plotted in figure 3-94 show that the higher temperature has faster decolourization rate of MG dye under experimental conditions, light intensity equal to ($6x10^{-5}$ Enstine s^{-1}), initial MG dye concentration of 25 ppm, initial pH Solution equal to 5.40 and Ag (2.00)/prepared ZnO that calcinated at (500) ºC dosage 0.7g.

These experiments used different temperature for Ag (2.00)/ prepared ZnO that was calcinated at (500) ºC in the range 278.15-293.15 K. It is found that the decolourization rate of MG dye increases with increasing of temperature.

The results listed in table 78 (in Appendix(B)) and plotted in figure 3-95 show a pseudo first order reaction according to Langmuir Hinshelwood relationship

The results in table 79 (in Appendix(B)) which plotted in figure 3-96 show Arrhenius relationship which gives activation energy of (10.223) kJ mol^{-1} for photocatalytic decolourization efficiency of MG dye by using prepared ZnO and calcinated at (500)ºC. The results in table 80 (in Appendix (B)) which plotted in figure 3-97 show Eyring relationship which gives thermodynamics parameters. (PDE) was calculated then listed in table 82 (in Appendix(B)) then plotted in figure 3-98 .

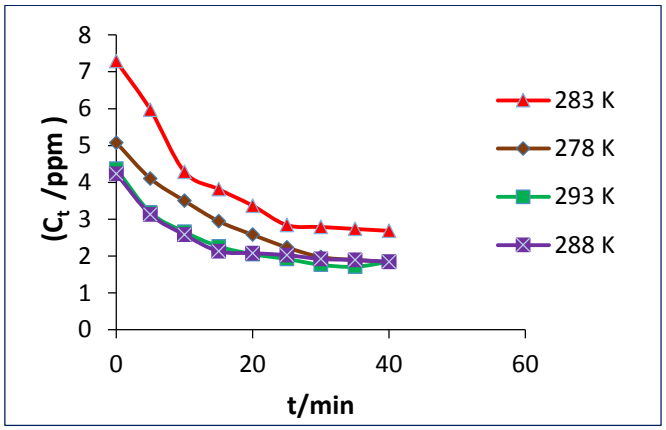

Figure 3-94: Relationship between C_t of Ag (2.00)/prepared ZnO that calcinated at (500)ºC and irradiation time at different temperatures.

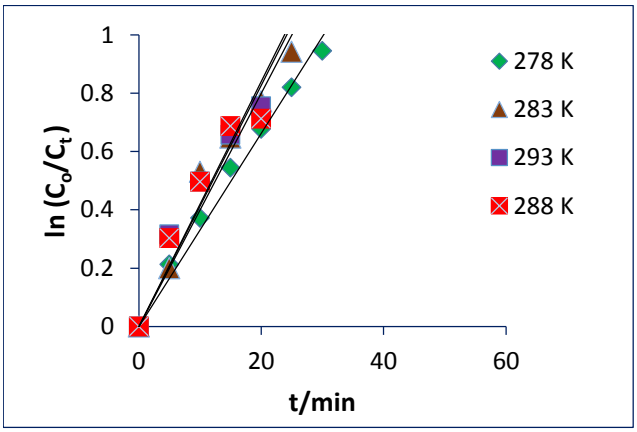

Figure 3-95 : Relationship between ln(C_o /C_t) and irradiation time at different temperatures of Ag (2.00)/ prepared ZnO that calcinated at (500)ºC.

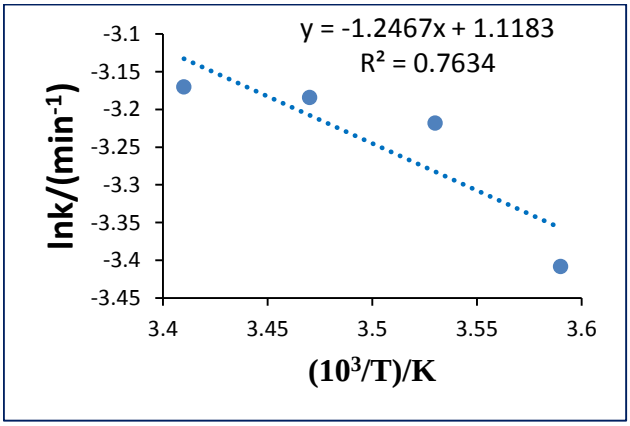

Figure 3-96 : Relationship between lnk and (1/T) with Ag (2.00)/prepared ZnO that calcinated at 500 ºC .

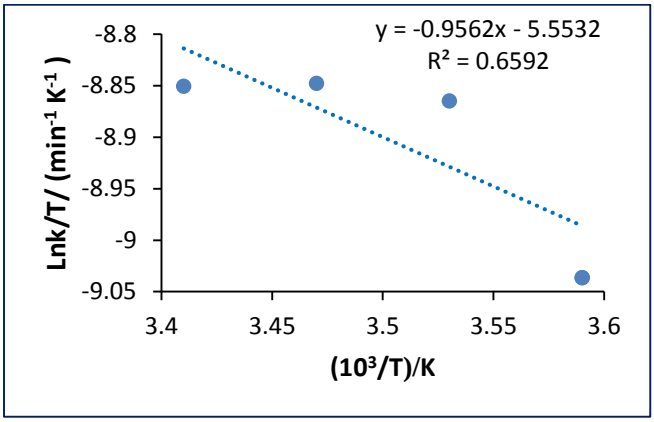

Figure 3-97: Eyring plot of (ln(k/T)) vs.1/T.

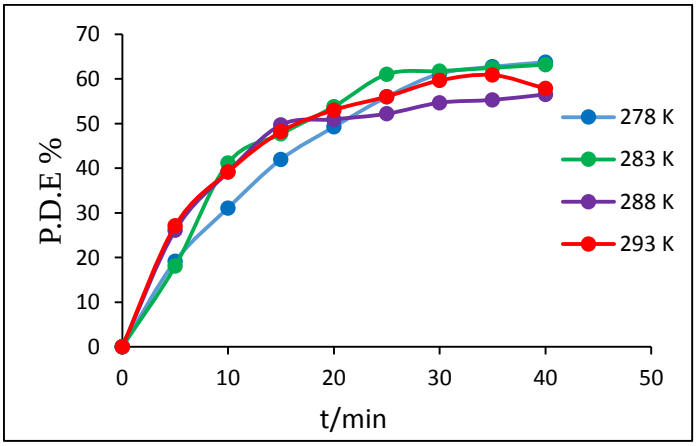

Figure 3-98 : Relationship between (PDE) and irradiation time on different Tempertures of Ag (2.00)/ prepared ZnO that calcinated at (500)ºC.

3.8.1 Effect of solar irradiation with presence prepared ZnO and metalized ZnO calcination at (500)°C.

The results are shown in table 83 (in Appendix(B))then plotted in figure 3-99 .They show the experiment conditions for all these experiments (light intensity 5.4 $x10^{-5}$ Enstine s^{-1}), initial MG dye concentration 25 ppm, initial pH of solution 5.40, temperature 309.15 K, prepared ZnO and metalized ZnO calcination at (500) °C dosage (0.6g/200 mL) . The results are shown in table 83 (in Appendix(B)) are plotted in figure 3-100 as C_t against time/min. where C_t represent the concentration of MG dye at different times of irradiation. The results listed in table 84 (in Appendix(B)) and plotted in figure 3-101 show a pseudo first order reaction according to Langmuir Hinshelwood relationship. Reaction apparent rate constant expressed in min $^{-1}$ are calculated from the slopes of such linear reaction plots. These results of reaction are listed in table 85(in Appendix(B))and plotted in figure 3-102. Photocatalytic decolourization efficiency (PDE) was calculated then listed in table 86 (in Appendix(B)) and plotted in figure 3-103.

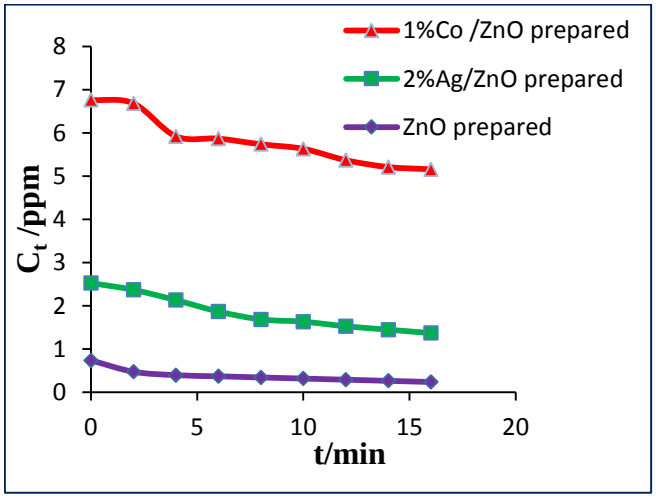

Figure 3-99: Relationship between C_t of dye with prepared and metalized ZnO calcination at (500)°C and irradiation time with using solar irradiation.

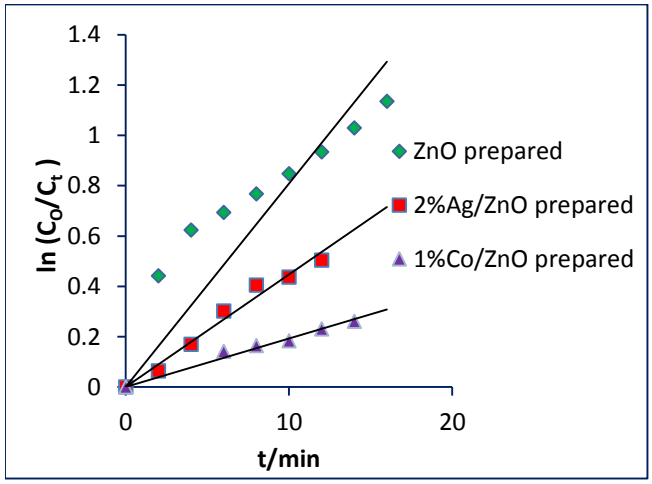

Figure 3-100 : Relationship between ln (C_o/C_t) and irradiation time with prepared and metalized ZnO calcination at (500)°C with using solar irradiation .

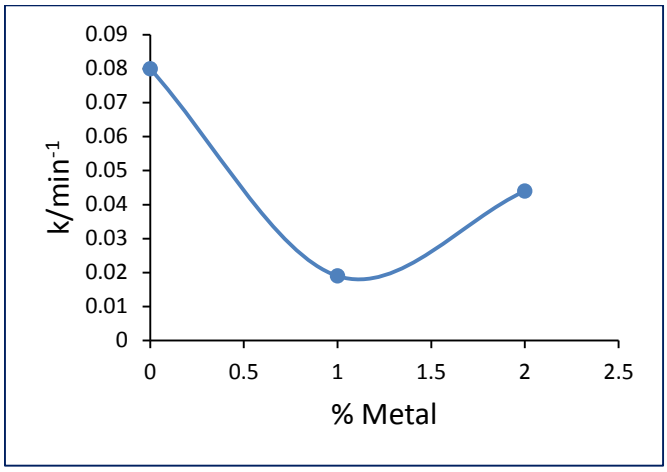

Figure 3-101 : Relationship between apparent rate constant and % Metal and with prepared and metalized ZnO calcination at(500)^{O}C with using solar irradiation.

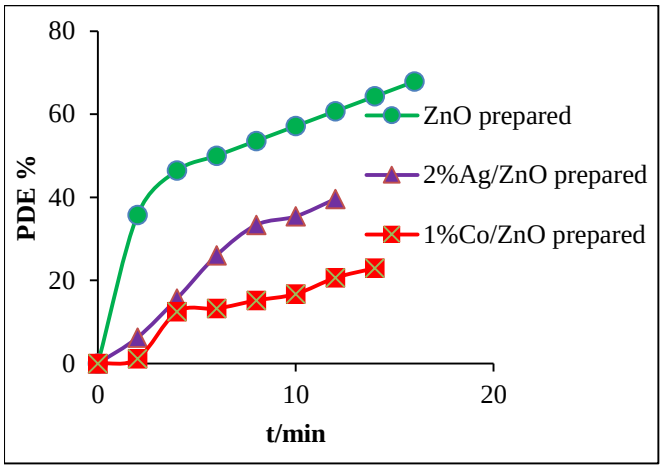

Figure 3-102 : Relationship between PDE and irradiation time with prepared and metalized ZnO calcination at(500)$^{\zeta}$C with using solar irradiation .

3.8.2 Effect of solar irradiation in presence of naked ZnO and Metalized Commercial ZnO .

The results are shown in table 87 (in Appendix(B)) then plotted in figure 3-103. They show the experiment conditions for all these experiments (light intensity 5.4 x10^{-5} Enstine s^{-1}) , initial MG dye concentration 50 ppm, initial pH solution 5.40, temperature 309.15 K, and dose of naked ZnO and metalized Commercial ZnO 0.7g/200 mL) . The results are shown in table 87 (in Appendix(B)) are plotted in figure 3-103 is C_t against time/min, where C_t represents the concentration of MGdye at different times of irradiation. The results listed in table 88 (in Appendix(B)) and plotted in figure 3-104 show a pseudo first order reaction according to Langmuir Hinshelwood relationship. Reaction rate constants expressed in min^{-1} are calculated from the slopes of such linear reaction plots. These results of reaction are listed in table 89 (in Appendix(B)) and plotted in figure 3-105. (PDE) was calculated then listed in table 90 (in Appendix(B)) and plotted in figure 3-106.

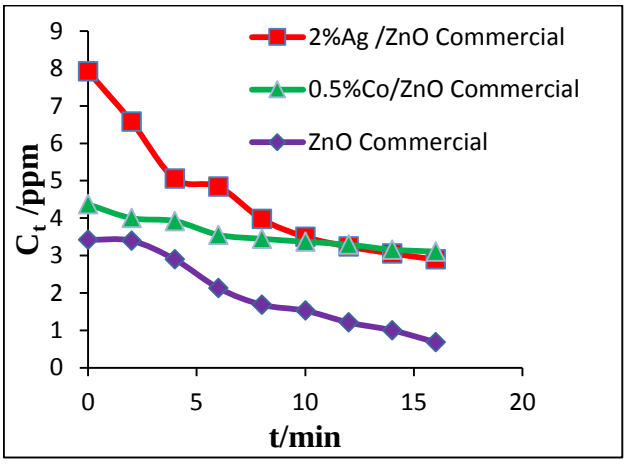

Figure 3-103: Relationship between C_t and irradiation time with naked ZnO and metalized commercial ZnO with using solar.

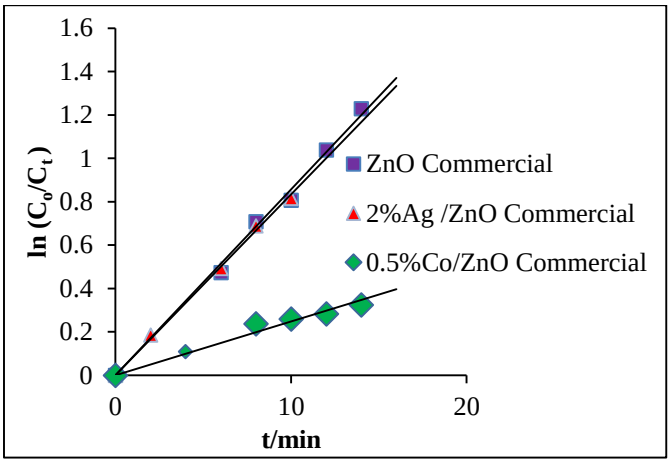

Figure 3-104 : Relationship between ln (C_o/C_t) and irradiation time with naked ZnO and metalized commercial ZnO with using solar.

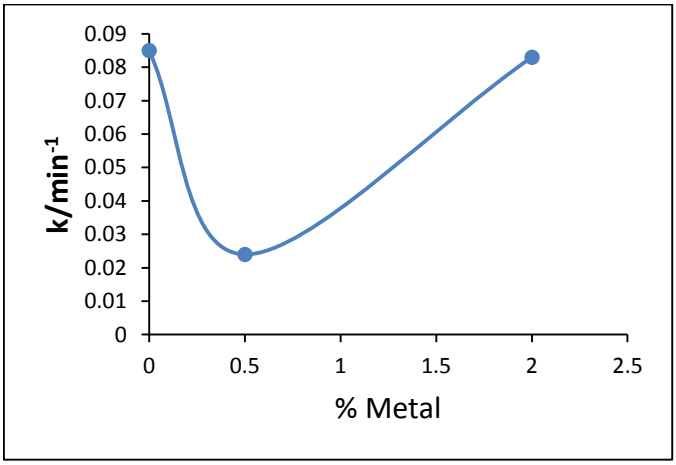

Figure 3-105 : Relationship between apparent rate constant with using solar irradiation and % Metal .

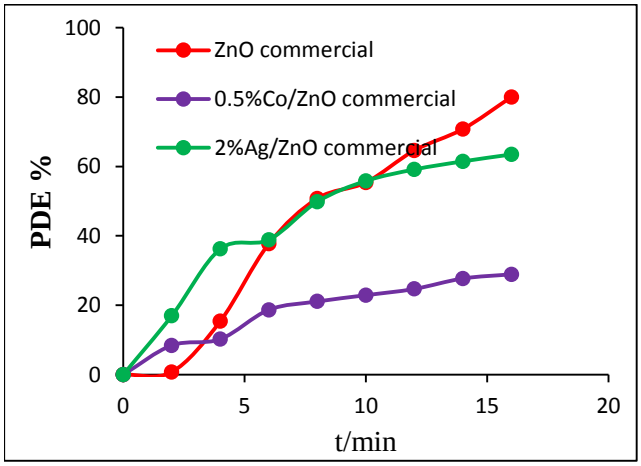

Figure 3-106 : Relationship between (PDE) and irradiation time with naked ZnO and metalized ZnO with using solar irradiation.

CHAPTER FOUR
DISCUSSION

4.1 Preliminary Experiments:

Series of experiments had performed in Figures (4-1 and 4-2).

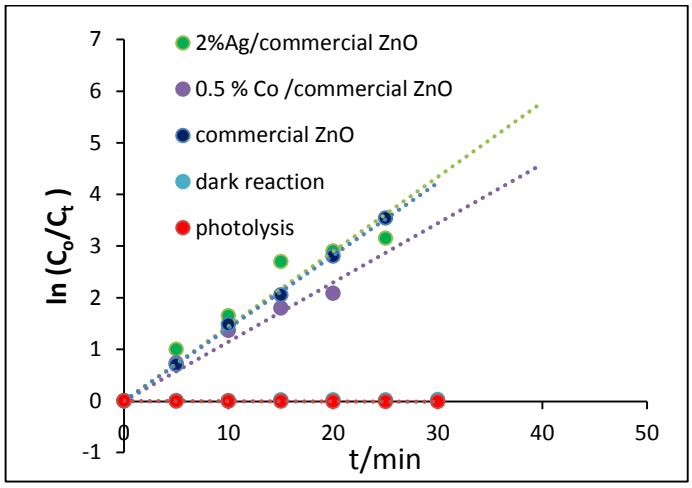

4-1: Preliminary Experiments with naked and metalized Commercial ZnO .

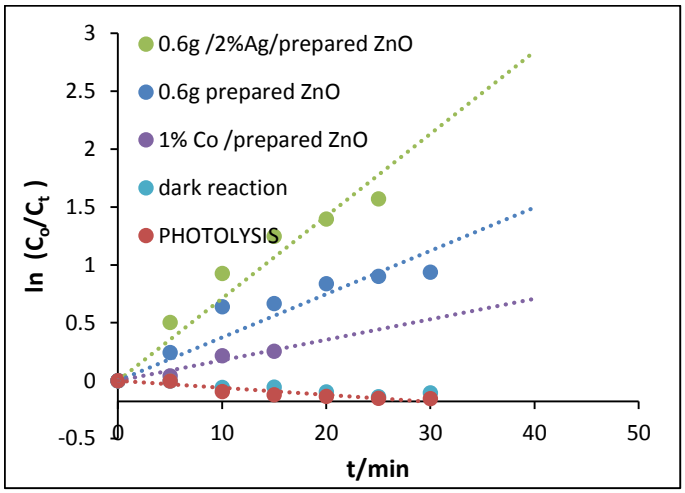

4-2: Preliminary Experiments with naked and metalized prepared ZnO .

In the dark reaction under O_2, the reaction did not occur because no (e^-- h^+) pairs generated in absence of UV-light, moreover, the reaction was never obtained in the absence the catalyst (photolysis process). (show eq$_s$ 4.1 and 4.2).

$$ZnO_{com.\ or\ prep.} + dye + O_2 \xrightarrow{(\text{dark reaction})} N\,R \qquad 4\text{-}1$$

$$hv + dye + O_2 \longrightarrow N.R \qquad 4\text{-}2$$

from the other hand , the catalytic reaction was occurred in eqs. From 4.3 to 4.6 .

$$ZnO_{com.} + dye + O_2 + hv \longrightarrow R. \qquad 4\text{-}3$$

$$ZnO_{pre.} + dye + O_2 + hv \longrightarrow R. \qquad 4\text{-}4$$

$$M\ (Co\ or\ Ag\ ) / ZnO_{com} + dye + hv \longrightarrow R. \qquad 4\text{-}5$$

$$M\ (Co\ or\ Ag\ ) / ZnO_{pre} + dye + hv \longrightarrow R. \qquad 4\text{-}6$$

So, the essential requirements of photo catalytic reaction was used a dye , ZnO (com. or pre.) or metalized (Co or Ag)/ZnO (com. or pre.), O_2 and UV light, because these parameters that enhanced the creation of (e^- - h^+) pairs, play a vital role for generation a hydroxyl radical (·OH) that pushes the photo reaction. These

results are in agreement with the principles of the photoreaction of methanol with presence of TiO_2 [187].

4.2 Characterization of Naked and metalized of ZnO Commercial and prepared.

4.2.1 Atomic Absorption Spectrophotometry (A.A.)

According to A.A results, the Co and Ag were completed through loading on commercial ZnO and prepared ZnO at 3 h by photodeposition process. In this process, the loaded of Co and Ag on commercial ZnO and prepared ZnO surface was carried out through two and one separated steps respectively. Generally, these steps were described in the following mechanisms [188, 189].

$$ZnO + h\nu \longrightarrow e^-_{CB} + h^+_{VB} \qquad 4\text{-}7$$

$$Co^{II} + 2e^-_{CB} \longrightarrow Co^0 \qquad 4\text{-}8$$

$$Ag^I + 1e^-_{CB} \longrightarrow Ag^0 \qquad 4\text{-}9$$

4.2 .1 Fourier Transform Infrared Spectroscopy (FTIR)

ZnO spectra in Figs (3-7 and 3-8) show that the essential peaks of ZnO occurred as a stretching vibrations of the O-H around 3446-3450 cm^{-1} , and the strong band around 500 cm^{-1} was assigned to the stretching band of Zn-O . Hence, the previous results referred to create of ZnO [190.]. In FT-IR spectra, new bands around 1383-1384 cm^{-1} and 1386-1388 cm^{-1} were obtained when cobalt and silver were loaded on commercial and prepared ZnO surfaces [191].

4.2.2 X-Ray Diffraction Spectroscopy (XRD)

From the XRD analysis, the calculated values of mean crystallite sizes and crystallite sizes of Co(0.500)/ commercial ZnO were more than those values for naked commercial ZnO. Moreover, the calculated values of mean crystallite sizes and crystallite sizes of Co(1.00)/ prepared ZnO that calcination at (500) ^oC were more than those values for naked prepared ZnO that calcination at (500) ^oC. See figure 4-3.From the other hand, the results for XRD with loaded Ag on commercial and prepared ZnO was found that the calculated values of mean crystallite sizes and crystallite sizes of Ag (4.00)/ commercial ZnO were more than those values for naked commercial ZnO and prepared ZnO that calcination at (500) ^oC . Note figure 4-4.

This is due to the location and incorporation of Co (II) and Ag(I) with Zn(II) in ZnO lattice. Moreover the ionic radius of (Co^{2+} = 0.745 Å) has relatively the same value of Zn^{2+} therefore, at low amount of Co, that increases the size of crystal ,Because the Ag (I) has low an ionic radius (Ag^{1+} = 0.115 Å) (192-193) that will lead to the need to high amount of it 4% of Ag to give a high crystal size .

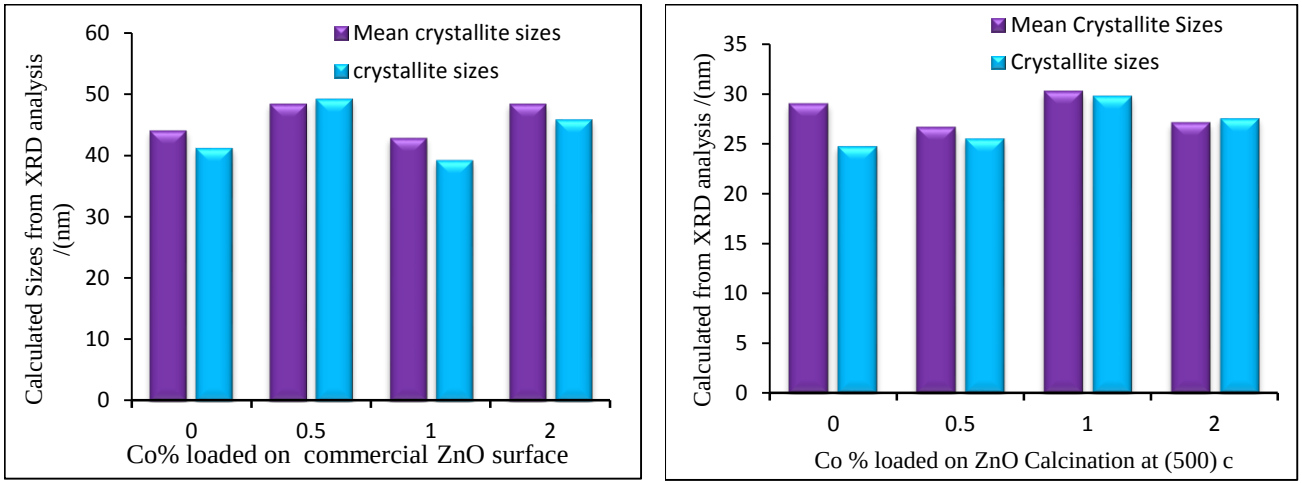

Figure 4-3: Relationship Between Calculated Sizes from XRD Analysis and Different Percentage of (a) Co Loaded on commercial ZnO Surface and (b) Co Loaded on ZnO calcination at (500) ºC Surface Plot.

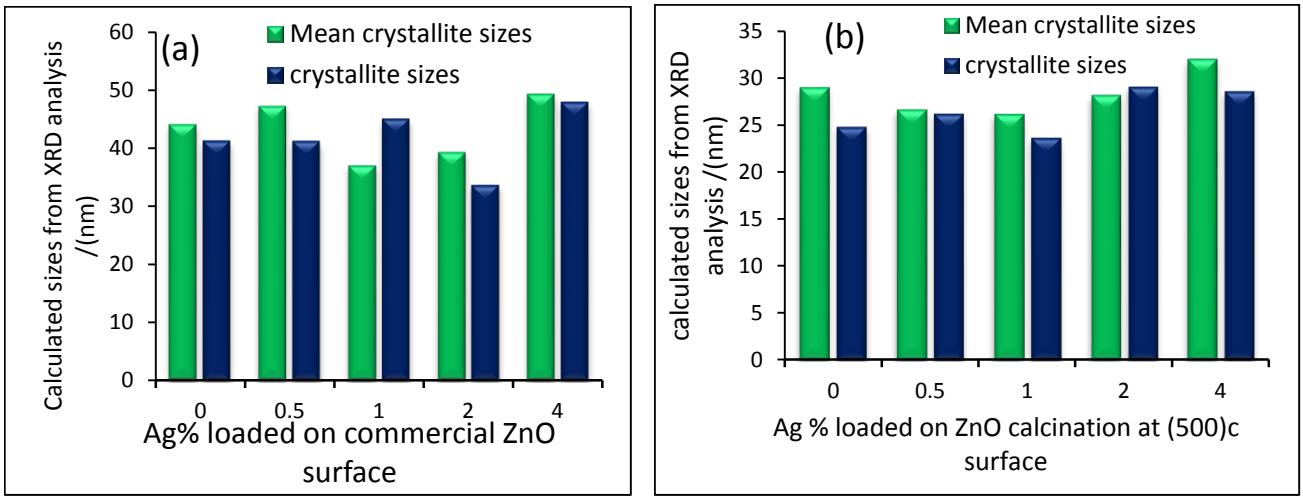

Figure 4-4: Relationship Between Calculated Sizes from XRD Analysis and Different Percentage of (a) Ag Loaded on commercial ZnO Surface and (b) Ag Loaded on ZnO calcination at (500)ºC Surface Plot.

4.2.3 Atomic Force Microscopy (AFM)

AFM images indicate that the shape of naked and metalized ZnO are semi spherical. The values of particle sizes for all samples are found to be less than values of mean crystallite size and crystallite size.

4.3 Effect of Different Parameters on Photocatalytic decolorization of Methyl Green.

This study intends to determine concerned on determined the different parameters on photodecolorization of dye with the presence naked and 2% Ag loaded on commercial and prepared ZnO only, because of the % of Co decreases the efficiency of photoreaction, therefore the studies which uses using Co are few.

4.3.1 Effect of Initial methyl green Concentration

In general, the successful application of the photocatalytic decolorization system requires the investigation of the effect of initial dye concentration on the photocatalytic efficiency, as the industrial or the lab wastewater is found in different concentrations. Hence, in this project, the effect of initial Methyl Green dye concentration on the photo catalytic decolorization rates that were catalyzed by the commercial or the prepared ZnO were also investigated.

The effect of this dye was studied in the range of (25- 100) ppm . At a fixed pH and the fixation amount of catalyst, the results plotted in figure 4-5(a), show that the photo-decolorization efficiency was increased with the increase of the concentration of methyl green dye and up to a maximum value 50 ppm, then decreased with the increase of dye concentration with the presence of naked and 2% Ag loaded on commercial ZnO respectively. This behavior is due to the increase of the quantity of intermediates that increased the photoreaction well, then the apparent rate constant declines.That interpenets to depress of the optical density in the solution and the amount of photons that must reach to catalyst's surface in photoreaction is depress[194].

On the other hand, the results in figure 4-5(b), the apparent rate constant of dye decolourization was inversely proportional with increasing the initial dye concentrations at ranged (25-100) ppm with the presence of naked and 2% Ag loaded on prepared ZnO that calcinated at 500 ^{o}C. The maximum value of the apparent rate constant was 25 ppm for naked and 2% Ag loaded on prepared ZnO, which refers to be the decolorization of methyl green dye which is in good

agreement with the Langmuir- Hinshelwood model [195] and the reaction is the pseudo-first-order [196-198].

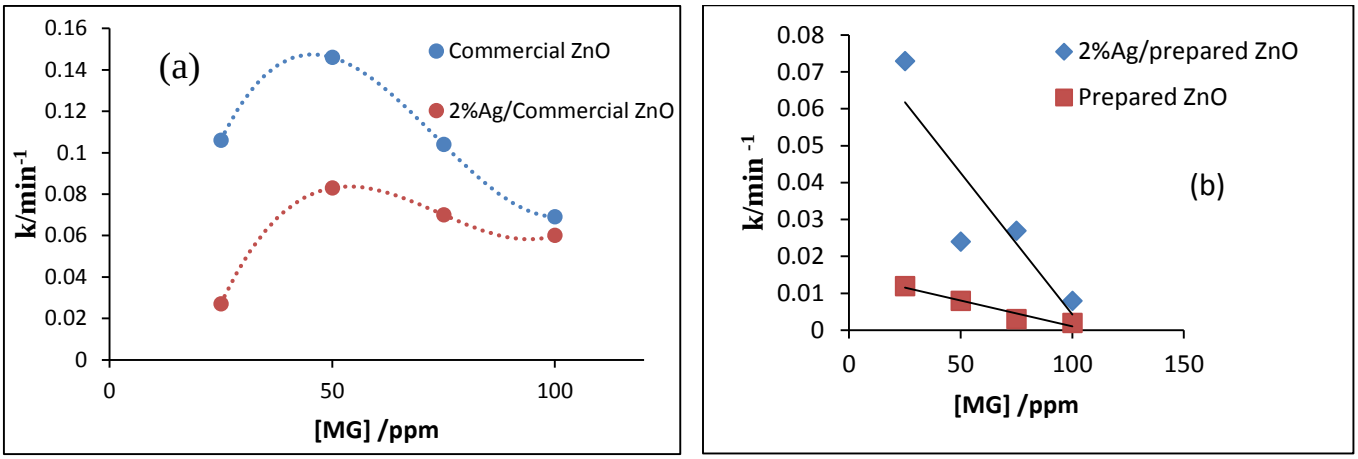

Figure 4-5: Relationship between the apparent rate constant verse methyl green concentrations with a)naked and 2% Ag loaded on Commercial ZnO and b) naked and 2% Ag loaded on prepared ZnO.

4.3.2 Effect of dosage Catalyst

For the economic removal of methyl green dye from the wastewater must find the optimum amount of catalyst for determining the efficient decolourization. The results are plotted in figure 4-6. The photodecolorization efficiency increased with the increase of the dosage of catalyst up to a maximum value at (0.6g/200 ml and 0.7g/200 mL for naked and 2% Ag loaded on prepared ZnO that calcination at 500 ^{o}C (figure 4-6 b), and the maximum value at (0.7g/200 mL) for naked and 2% Ag loaded on commercial ZnO in(figure 4-6 a) respectively. This behavior can be explained on the basis that on increasing catalyst dosage the active site on the catalyst surface increases. These results are in agreement with other previous observations [20].

After that, the apparent rate constant decreased with the increase of catalyst dosage. The increase of the catalyst dosage above the maximum level increases the number of particle suspended in aqueous solution of methyl green dye that increases the turbidity of the suspension. As a result there will be a decrease in the

penetration of irradiation and, hence, the photoactivated volume of suspension decreases and that leading to screening effect [162,159,199].

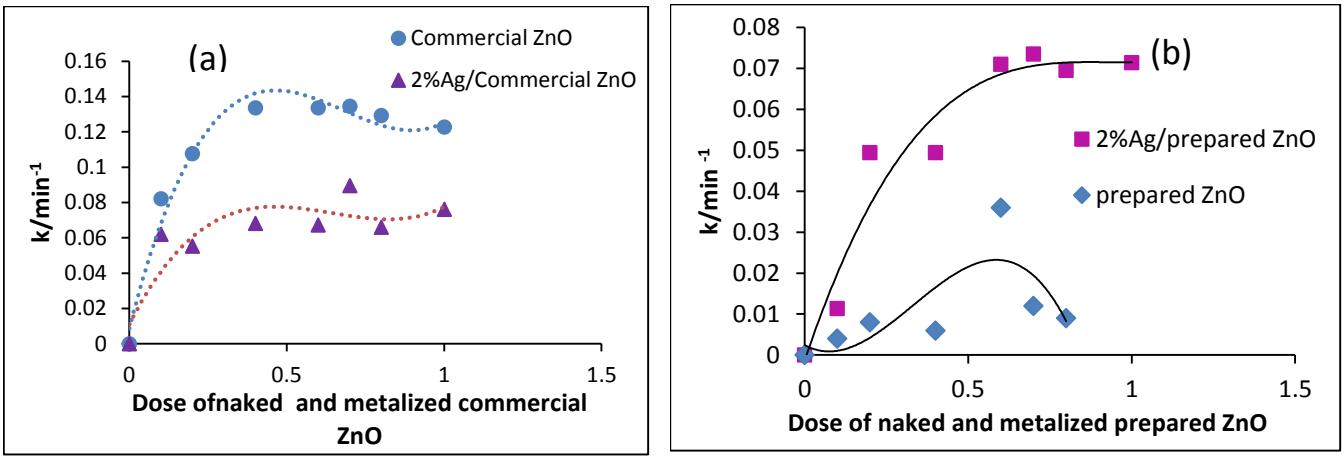

Figure 4-6: Relationship between the apparent rate constant verse dose of a)naked and 2% Ag loaded on Commercial ZnO and b) naked and 2% Ag loaded on prepared ZnO.

4.3.3 Effect of pH of Solution

Due to the amphoteric property of many semiconductor oxides, it is very important to investigate the effect of pH in the dye solution on the reactions that take place on the semiconductor surfaces, as pH is a main factor that influences the surface charge profile of the photocatalysts as shown in the following equations[200-202]:

$ZnOH + H^+ \longleftrightarrow ZnOH_2^+$ acidic media 4-10

$ZnOH + {}^-OH \longleftrightarrow ZnO^- + H_2O$ basic media 4-11

According to figure 4.7(a and b).The decolorization of methyl green obtained the strongly dependent on the pH of solution because of the reaction of heterogeneous photocatalytic which happends on the surface of semiconductors. Hence, the decolorization of dye increases with the increase of the pH of solution until 10 for ZnO commercial and 5.40 for each Ag (2.00) /ZnO commercial, naked and Ag (2.00)/ loaded on prepared ZnO that calcinated at 500 ^oC respectively. In other the word, this behavior could be explained on the basis of zero point charge (ZPC)[203]. The zero point charge was nearly equal to 9.00 for ZnO [204], but its value always deviated by depending on the type of the used dye.

With the increase of the pH of solution the surface of catalyst will be negatively charged by adsorbed hydroxyl ions. The presence of large quantities of adsorbed OH^- ions on the surface of catalyst favor for formation of OH• radical , in spite of

the increasing of the speed of hydroxyl radicals formation, but that was due to increase the ability of an anion Cl^- to react with hydroxyl radicals and lead to inorganic radical ions($ClO^{-\cdot}$). This inorganic radical anion has a lower reactivity than hydroxyl radicals, hence, it does not share in the dye decolourization or degradation [205].

On the other hand, the decolorization of methyl green decreases dramatically at strong acid media (pH=2.1) for ZnO. This could be explained by the photocorrosion of ZnO as shown in the following equations(4-12 and 4-13) [206].

$$ZnO + h\nu \longrightarrow e^-_{CB} + h^+_{VB} \qquad 4\text{-}12$$

$$ZnO + 2h^+_{VB} \longrightarrow Zn^{2+} + 1/2O_2 \qquad 4\text{-}13$$

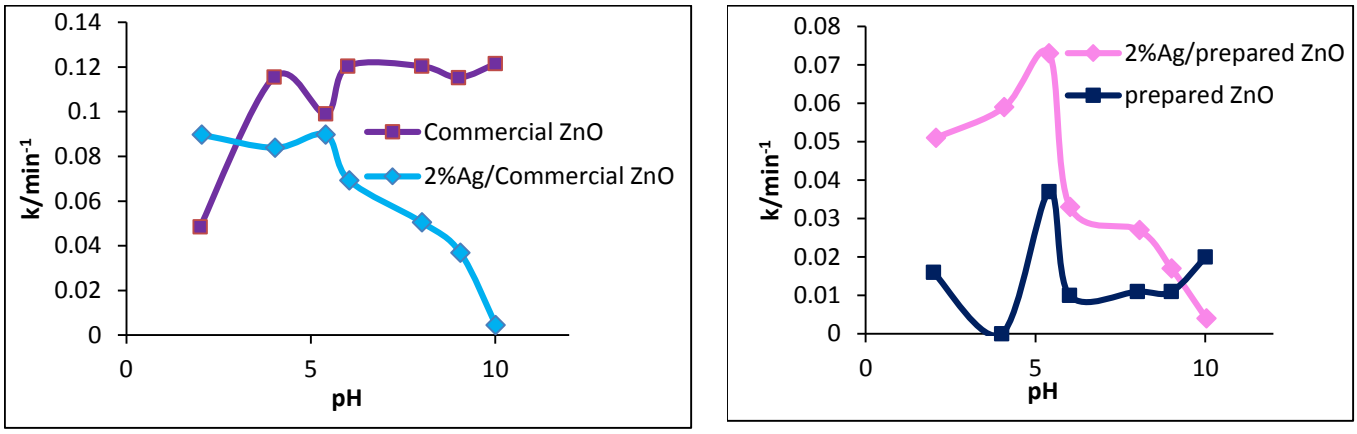

Figure 4-7: Relationship between the apparent rate constant verse initial pH of solution in precence a)naked and 2% Ag loaded on Commercial ZnO and b) naked and 2% Ag loaded on prepared ZnO.

4.3.4 Effect of Temperature

The study of the effect of temperature on photocatalytic decolorization of methyl green in aqueous solution was determined in the range from 278.15 K to 298.15 K. The produced results, in figure 4-8 (a and b), show that the deolorization efficiency of methyl green increased with the increasing of the temperature. The increase in temperature would lead to generation of the free radicals . Thereby, the rise in temperature enhanced the reaction to compete more efficiently than the electron-hole recombination [207]**.** The apparent activation energies decreased with metalized the ZnO surface from 24.914 to 6.185 kJ/mol with loading 2% Ag on surface of commercial ZnO, and the values decreased also when 2% Ag loaded

on surface of prepared ZnO from 19.69 to 10.375 kJ/mol. This case enhanced the photoreaction.

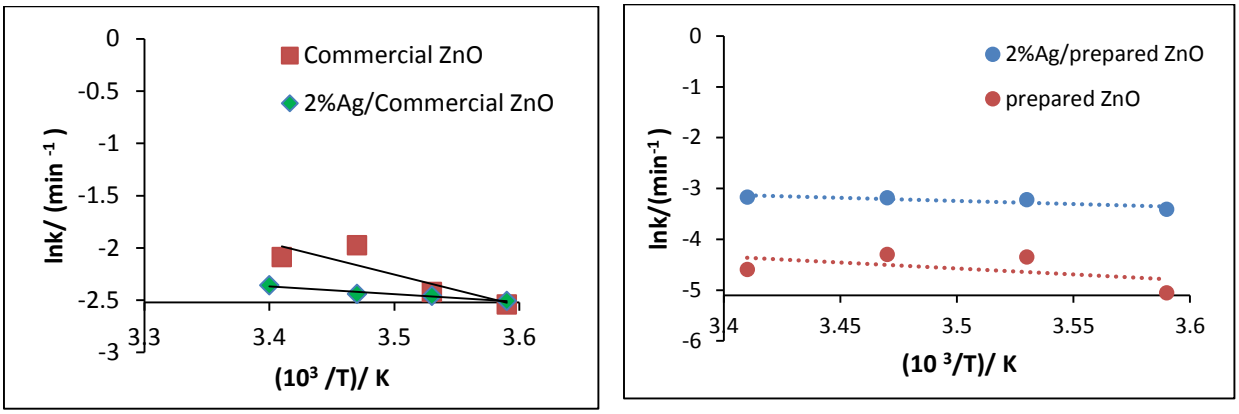

Figure 4-8: Relationship between the ln k verse 1/T in presence a)naked and 2% Ag loaded on Commercial ZnO and b) naked and 2% Ag loaded on prepared ZnO.

From figure 4.9 (a and b), the apparent rate of reaction constant increased with the increases of temperature. Hence the photo-decolourization of methyl green dye was endothermic reaction, and the positive values of enthalpy decreased with metalized ZnO. Moreover, the entropy was less which attributed to the decrease in randomness, and the reaction was not spontaneous (positive of ΔG) . Tabbara and Jamal [205] explained the results of thermodynamics functions for photoreaction in agreement with results of this work. However, at temperature more than 288.15 K the rate of reaction decreased, thereby the solution started to depress of dye adsorption on active sites of ZnO surface. Moreover, the solubility of oxygen in water was less. This decrease the number of produced hydroxyl radical [186].

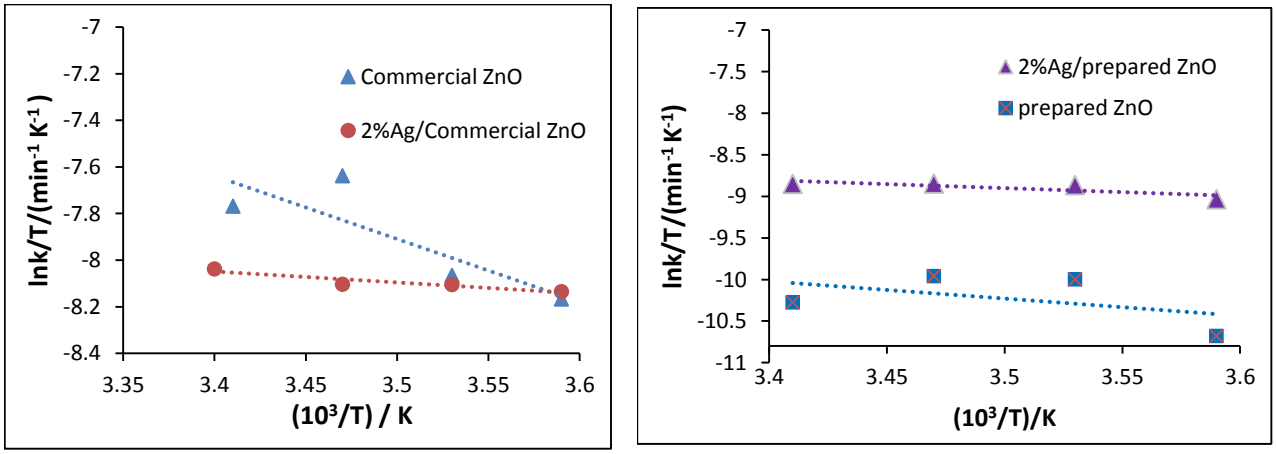

Figure 4-9: Relationship between the (ln k/T) verse 1/T in presence a)naked and 2% Ag loaded on Commercial ZnO and b) naked and 2% Ag loaded on prepared ZnO.

4.4 Effect of Solar radiation

Because sunlight in Iraq is available in most of the year day, the solar light could be effectively employed to remove the pollutants or dyes by photocatalytic decolorization method from wastewater. The influence of solar light on the decolorization of methyl green dye was determined at different intervals as shown in figures 4-10 and 4-11. From these results, the photo decolorization reaction of methyl green by solar light was fast compared with the photodecolorization reaction of it with presence of the UV-A. That attitude takes place of thermal reaction with photo reaction under solar irradiation. Thereby the P.E.D of solar reaction was low, which indicates the increase of the recombination.

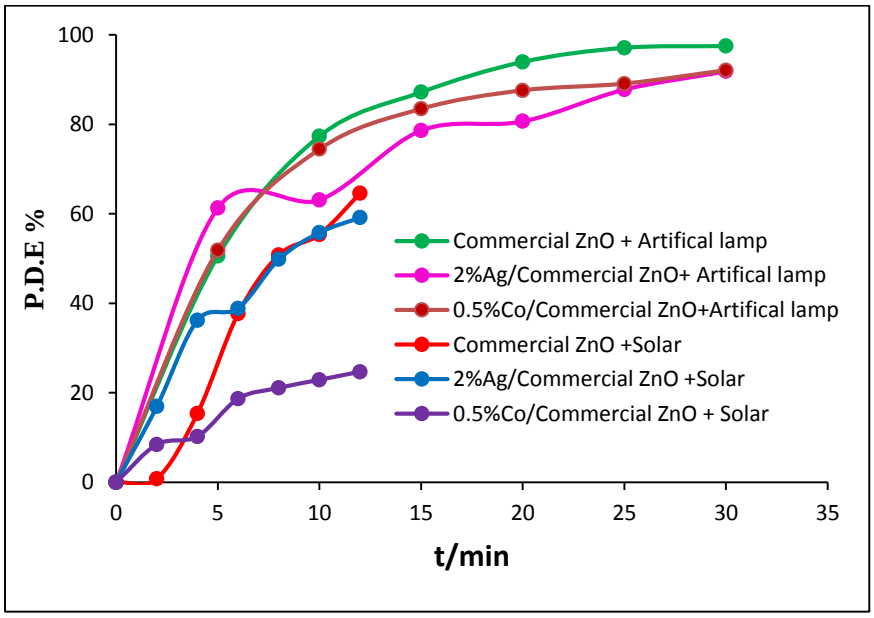

Figure 4-10: Relationship between P.D.E verse time in presence naked and metallized commercial ZnO with UV-A and Solar irradiation.

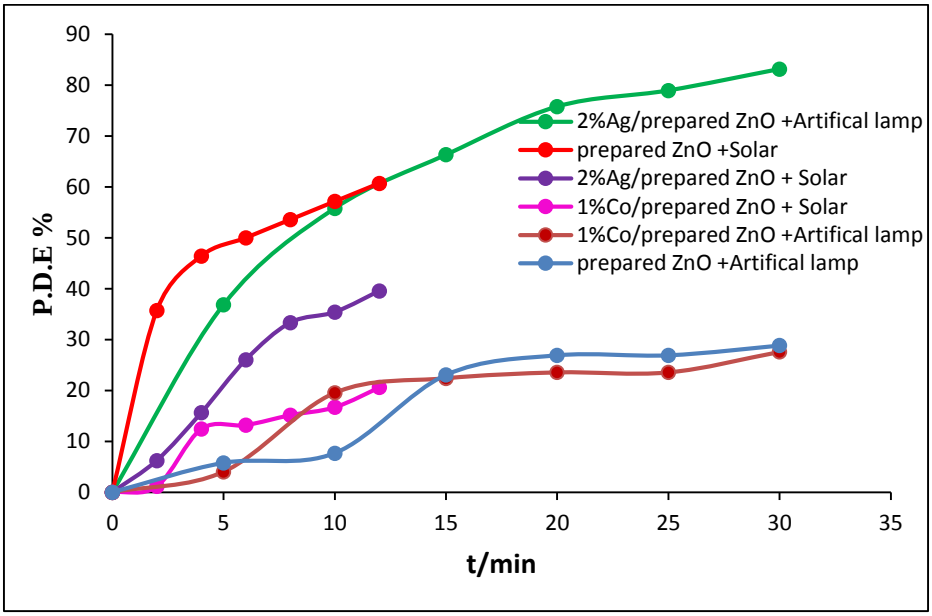

Figure 4-11: Relationship between P.D.E verse time in presence naked and metallized prepared ZnO with UV-A and Solar irradiation.

4.5 Suggested mechanism:

The mechanism of photodecolorization of methyl green dye underwent series of chain reactions, when the photon of UV-A light focuses on the solution that contain methyl green dye with ZnO either commercial or prepared. Hence, the photoelectron and photohole $(e^- - h^+)_{exciton}$ were created, then the photohole and photoelectron are share in different series of reductive-oxidative reactions as follow in scheme (4.1)

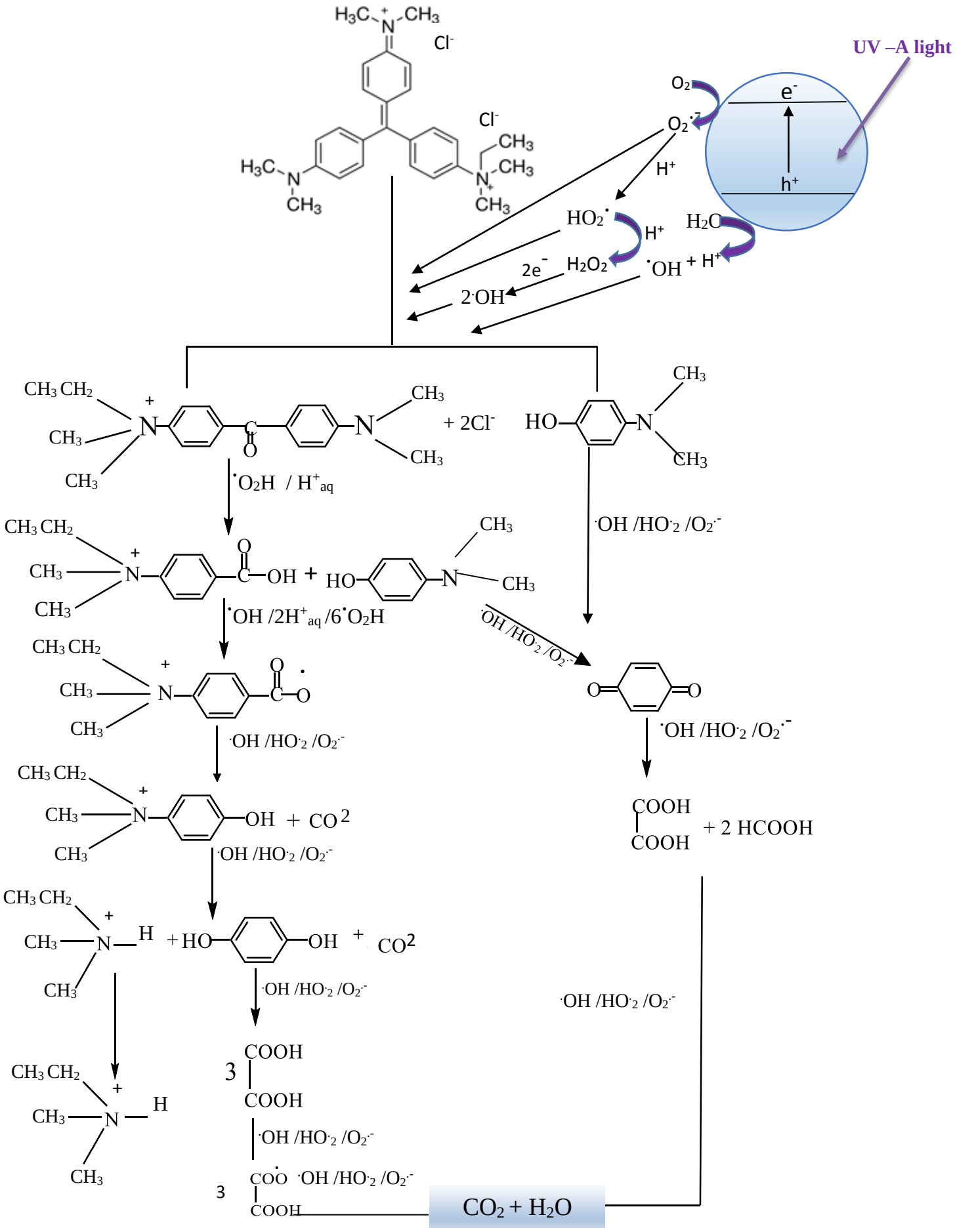

Scheme (4.1): Schematic diagram for more accepted mechanism (Dye/semiconductor/ UV light system)(modified from reference [208].

CHAPTER FIVE

CONCLUSIONS AND RECOMMENDATIONS

5.1 Conclusions:

This study focused on the photocatalytic decolourization of aqueous methyl green solution with naked and metalized of commercial and prepared ZnO. The main conclusions can be summarized as follows:

1. The atomic absorption measurements prove that the added metal (Co and Ag) was completely photodeposited on commercial and prepared ZnO surface after 3 h.
2. The FT-IR spectra show that the ZnO was really created. So, the stretching vibrations of the O-H around 3446-3450 cm^{-1}, and the strong band around 500 cm^{-1} is beyond the stretching band of Zn-O. Moreover, the new bands around 1383-1384 cm^{-1} and 1386-1388 cm^{-1} were obtained when cobalt and silver loaded on commercial and prepared ZnO surfaces respectively.

3. The mean crystallite sizes and crystallite sizes of naked and metallized (Co or Ag) of commercial and prepared ZnO surface is calculated by depending on the XRD data. The mean crystallite sizes and crystallite sizes for naked commercial ZnO were increased with loading 0.5%Co, but decreased with loading 2%Ag . Moreover, the mean crystallite sizes and crystallite sizes for naked prepared ZnO were increased with loading 1%Co and 2%Ag. That is ascribed to agglomerate the particles with increase the amount of metals.

4. AFM images indicate that the shapes of naked and metalized commercial and prepared ZnO are semi spherical.

5. The prepared ZnO is calcined in different temperatures, and the best temperature was found equal to 500 ^{o}C.

6. In photoreaction, the best concentration of dye is 50 ppm in the presence of naked and 2% Ag loaded on commercial ZnO, and 25 ppm in the presence of naked and 2% Ag loaded on prepared ZnO.

7. The maximum values of catalysts dose are (0.6g/200 mL and 0.7g/200 mL for naked and 2% Ag loaded on prepared ZnO that calcination at 500 ^{O}C, and the maximum value at (0.7g/200 mL) for naked and 2% Ag loaded on commercial ZnO.

8. The optimum pH of solution is 10 for ZnO commercial and 5.40 for each Ag (2.00) /ZnO commercial, naked and Ag (2.00)/ loaded on prepared ZnO that calcinated at 500 ^{o}C respectively. While, the increased pH is basic medium, there is an an crease of pH as basic medium , which causes an increase of the ability of an anion Cl^{-} in dye structure to react with hydroxyl radicals and lead to inorganic radical ions($ClO^{-\bullet}$).

9. The activation energies of the photocatalytic reaction decrease from ~ 27 to 6.185 kJ/mol after metalized by 2% Ag of commercial ZnO. In addition , the activation energy decreases from ~19.69 to 10.375 kJ/mol after metalized by 2% Ag of prepared.

10. The thermodynamics functions such as ΔH and ΔS were calculated by employing on Eyring equation. The photo decolorization of methyl green dye was endothermic reaction and fewer randomness. ΔG was calculated by Gibbs equation and the reaction was observed to be non- spontaneous reaction.

5.2 Recommendations:

Future studies ,similar to the present study can be done :

1. A study to investigate the Loaded other metals like Pd, Al, Ni and Mg of different percentage of on ZnO surface, then studied the nanoparticles characterizations and the ability to decolorize the other dyes.
2. A Focuses on the preparation of ZnO by the other different methods, then loaded the metals on the surface of it by photodeposition, direct precipitation, hydrothermal method and microwave method.
3. The TEM analysis can be used to investigate the exact amounts of metals that are loaded on ZnO surface, shapes of nanoparticles, and some properties such as thermal and mechanical properties.
4. The SEM analysis, surface area (BET analysis), Band gap measured and thermal analysis can be used to determine the shapes of nanoparticles, particle size and the other important properties.

References

References

1. M. Hoffmann, S. Martin, W. Choi and D. Bahneman, ″Environmental Applications of Semiconductor Photo catalysis", *Chem. Rev.,* vol. 95, pp. 69-96, 1995.
2. R. P. Wayne, ″ Principles and Applications of Photochemistry″, 2nd ed., OUP, Oxford University press, UK , 1991.
3. A. Fujishima, X. Zhang and D. A. Tryk, ″TiO_2 Photocatalysis and Related Surface Phenomena″, *Surface Science Reports*, vol. 63, no. 12, pp. 515–582, 2008.
4. S .N. Frank and A. J. Bard, ″Heterogeneous photocatalytic oxidation of cyanide ion in aqueous solutions at titanium oxide powders″, *J. Phys. Chem.*, vol. 81, no.15, pp.1484-1488,1977.
5. A. Heller, ″Chemistry and Applications of photocatalytic oxidation of Thin Organic Films″, *Acc. Chem. Res.*, vol. 28 , pp. 503-508 ,1995.
6. A. Fujishima, T.N. Rao and D.A. Tryk ,″ Titanium dioxide photocatalysis ″ , *J. Photochem. Photobiol*. C, vol. 1, pp. 1-21, 2000.
7. T. Watanabe, A. Nakajima, R. Wang, M. Minabe, S. Koizumi, A. Fujishima and K. Hashimoto, ″ Photocatalytic Activity and Photoinduced Hydrophilicity of Titanium Dioxide Coated Glass ″ , *Thin Solid Films* , vol.351 , pp.260-263 , 1999.
8. M. C. Lee and W. Choi, ″Solid Phase Photocatalytic Reaction on the Soot/TiO_2 Interface:the Role of Migrating OH Radicals″, *J. Phys. Chem. B* , vol.106, pp. 11818-11822 ,2002.
9. Y. Ishikawa, Y. Matsumoto, Y. Nishida, S. Taniguchi and J. Watanabe,″ *J. Am.Chem. Soc.,* vol. 125, pp. 6558 - 6562, 2003.
10. T. Tatsuma, W. Kubo and A. Fujishima, "Patterning of Solid Surfaces by Photocatalytic Lithography Based on the Remote Oxidation Effect of TiO_2", *Langmuir,* vol. 18, pp. 9632-9634, 2002.
11. R. Gorges, S. Meyer and G. Kreisel, ″ Photocatalysis in Microreactors ″, *J. Photochem. Photobiol. A: Chem.,* vol.167, pp.95-99, 2004.
12. K. Naoi, Y. Ohko and T. Tatsuma , ″TiO_2 Films Loaded with Silver Nanoparticles: Control of Multicolor Photochromic Behavior ″, *J. Am. Chem. Soc.,* vol.126, pp.3664-3668 ,2004 .
13. K. Naoi, Y. Ohko and T. Tatsuma , "Switchable Rewritability of Ag-TiO_2 Nanocomposite Films with Multicolor Photochromism" , *Chem. Commun.,* pp. 1288-1290 , 2005 .

14. S. Teekateerawej , J. Nishino and Y. Nosaka , ″ Design and Evaluation of Photocatalytic Micro-Channel Reactors Using TiO_2-Coated Porous Ceramics ″ , *J. Photochem. Photobiol. A: Chem.* , vol. 179, pp. 263 -268 ,2006.
15. G. Takei, T. Kitamori and H.-B. Kim, ″Photocatalytic Redox-Combined Synthesis of l-Pipecolinic Acid with a Titania-Modified Microchannel chip″, *Catal. Commun.* , vol. 6 , pp.357- 360 ,2005 .
16. E.T. Castellana, S. Kataoka, F. Albertorio and Paul S. Cremer, ″ Direct Writing of Metal Nanoparticle Films Inside Sealed Microfluidic Channels ″, *Anal. Chem.*, vol. 78, pp.107-112, 2006.
17. G. Takei, M. Nonogi, A. Hibara, T. Kitamori and H.-B. Kim, ″Tuning Microchannel Wettability and Fabrication of Multiple-Step Laplace valves ″, *Lab Chip* ,vol. 7, pp.596-602, 2007.
18. H. Nagai, T. Irie, J. Takahashi and S.-i. Wakida , ″ Flexible Manipulation of Microfluids Using Optically Regulated Adsorption/Desorption of Hydrophobic Materials ″, *Biosens. Bioelectr*., vol. 22 ,pp.1968-1973 , 2007.
19. A. Fujishima and K. Honda,″Electrochemical Photolysis of Water at a Semiconductor Electrode ″ , *Nature*, vol. 238, pp. 37-38, 1972.
20. F. H. Hussein, A. F. Halbus, H. A K. Hassan and W.A K. Hussein, ″Photocatalytic Decolourization of Bismarck Brown G Using Irradiated ZnO in Aqueous Solutions ″, *E-Journal of Chemistry*, vol.7,no.2, pp.540-544,2010.
21. K. Loganathan, P. Bommusamy, P. Muthaiahpillai and M. Velayutham, "The Synthesis, Characterizations, and Photocatalytic Activities of Silver, Platinum, and Gold Doped TiO_2 Nanoparticles", *Environ. Eng. Res*., vol. 16, no. 2, pp. 81-90, 2011.
22. F. Hussein, M. Obies and A. Drea ,"Photocatalytic Decolorization of Bismark Brown R by Suspension of Titanium Dioxide″, *Int. J. Chem. Sci.*, vol.8, no. 4, pp. 2736-2746, 2010
23. J. Galvez and S. Rodriguez, Solar Detoxification, 1st ed., United Nations Educational, Scientific and Cultural Organization, Spine CH 1, 2003.
24. S. Shanmuga Priya, M. Premalatha and N. Anantharaman,″Solar photocatalytic Treatment of Phenolic Wastewater- Potential, Challenges and Opportunities″, *ARPN Journal of Engineering and Applied Sciences*, vol.3, no.6, pp.36-41,2008.
25. J. A. Byrne, P. A. Fernandez-Ibanez, P. S.M. Dunlop, D.M. A. Alrousan and J.W. J. Hamilton, ″ Photocatalytic Enhancement for Solar Disinfection of Water: a Review ″, *International Journal of Photoenergy*, vol. 2011,pp.1-12,2011.
26. J .Grzechulska and A. Morawski, ″ Photocatalytic Decomposition of Azo-Dye Acid Black 1 in Water Over Modified Titanium Dioxide″, *Applied Catalysis B: Environmental* ,vol. 36, pp. 45-51,2002.

27. F. Hussein, A. Alkhateeb and J. Ismail, ″Solar Photolysis and Photocatalytic Decolorization of Thymol Blue ″, *E-Journal of Chemistry* , vol. 5, no. 2, pp.243-250, 2008.
28. Z. Sen, "Solar Irradiation Fundamentals", *EOLSS*, vol. 2, pp. 1-15, 2007.
29. B. Saleh and M. Teich,″Fundamentals of Photonics″, *John Wiley &Sons, Inc*., 1991.
30. A. J. BARD,″ Solar Energy Conversion through Photo electrochemistry at Semiconductors″, Proc. R. A. Welch Foundation Conference on Chemical Research XXVIII. Chemistry in Texas: The 30th Year of the Welch Foundation, Nov. 5-7, Houston, Tx, pp. 95-129, 1984.
31. S. Dutta, S. Chattopadhyay and A.Sarkar, ″Role of Defects in Tailoring Structural, Electrical and Optical Properties of ZnO ″ , *Prog Mater Sci* , vol.54 , pp.89–136 ,2009 .
32. H. P. Myers,″ Introductory Solid State Physics ″, *Taylor & Francis* , 1990 .
33. P. W. Atkins, "Physical Chemistry", 7th Ed., Oxford University presses ,Oxford , England , 2002.
34. S. Y. Huang, G. Schlichthorl, A. J. Nozik, M. Gratzel and A. J. Frank, ″ Charge Recombination in Dye-Sensitized Nanocrystalline TiO_2 Solar Cells ″, *J. Phys. Chem. B,* vol.101, pp. 2576 -2582 ,1997 .
35. C. Klingshirn. ,"*ZnO: Material, Physics and Applications*", *Chem Phys Chem* , vol. 86, pp. 782-803, 2007.
36. A. Al-Kdasi, A. Idris, K. Saed and C. Guan, "Treatment of Textile Wastewate by Advanced Oxidation Processes – A review", *Global Nest: the Int. J.* , vol .6, no. 3, pp. 222-230, 2004, and references there in.
37. A. Stasinakis, "Use of Selected Advanced Oxidation Processes (AOPs) For Wastewater Treatment –A mini review", *Global NEST Journal*, vol. 10, no. 3, pp. 376-385, 2008, and references there in.
38. M. Pera-Titus, V. Garc´ıa-Molina, M. Baños, J. Giméneza and S. Espluga, "Decolourization of Chlorophenols by Means of Advanced Oxidation Processes: A General Review", *Applied Catalysis B: Environmental*, vol. 47, pp.219-256, 2004, and references there in.
39. S. Sharma, J. Ruparelia and M. Patel, "A general review on Advanced Oxidation Processes for waste water treatment", Institute of Technology, Nirma University, Ahmed Abad , pp.382 -481, 2011, and references there in.
40. D.G. Crosby, ″Environmental Toxicology and Chemistry ″, New York ,Oxford University Press, 1998.
41. O. Legrini, E Oliveros and A.M. Braun, ″Photochemical Processes for Water Treatment ″, *Chemical Reviews*, vol. 93, pp. 671 -698, 1993.

42. M. H. Habibi, A. Hassanzadeh and A. Zeini-Isfahani, ″Spectroscopic studies of solophenyl red 3BL polyazo dye tautomerism in different solvents using UV-visible, 1H NMR and steady-state fluorescence techniques″, *Dyes and Pigments*, vol.69, pp. 93-101, 2006.
43. T. Hihara, Y. Okada and Z. Morita, ″Azo-hydrazone tautomerism of phenylazonaphthol sulfonates and their analysis using the semiempirical molecular orbital PM5 method ″, *Dyes and Pigments*, vol. 59, pp. 25-41 , 2003
44. P.R. Gogate and A. B. Pandit, ″ A review of imperative technologies for wastewater treatment I:oxidation technologies at ambient conditions″ , *Advances in Environmental Research* ,vol.8 , pp.501-551, 2004 .
45. F. H. Hussein , ″Photochemical Treatments of Textile Industries Wastewater″ ,Advances in Treating Textile Effluent, Peter J.Hauser (Ed.), ISBN: 978-953-307-704-8, InTech , pp. 117-144, 2011.
46. M. Mashkour, A. Al-Kaim, L. Ahmed and F. Hussein, "Zinc Oxide Assisted Photocatalytic Decolorization of Reactive Red 2 Dye", *Int. J. Chem. Sci.*, vol. 9, no.3, pp. 969-979, 2011, and reference there in.
47. A.D Russell, ″Bacterial adaptation and resistance to antiseptics, disinfectants and preservatives is not a new phenomenon″, *Journal of Hospital Infection*, vol. 57, pp.97–104, 2004.
48. L. Palmisano and A.Sclafani , ″Thermodynamics and kinetics for heterogeneous photocatalytic processes″,Heterogeneous photocatalysis, M. Schiavello, (ed.) , *Wiley and Sons, Chichester*, pp.109–132, 1997.
49. A.J. Bard , ″Photoelectrochemistry and Heterogeneous Photocatalysis at Semiconductors ″, *J. Photochem.* , vol.10, pp. 59-75, 1979.
50. H. Van damme and W.K. Hall, ″ Photoassisted De composition of Water at the Gas-Solid Interface on TiO_2″, *J. Amer. Chem. Soc.*, vol. 101, pp. 4373-4374, 1979.
51. B. Kraeutler, C. D. Jaeger and A. J. Bard, ″ Direct Observation of Radical Intermediates in the Photo-Kolbe Reaction - Heterogeneous Photocatalytic Radical Formation by Electron Spin Resonance ″, *J. Amer. Chem. Soc.*, vol.100, pp.4903-4905, 1978.
52. M. Herrmann, ″Heterogeneous photocatalysis: fundamentals and applications to the removal of various types of aqueous pollutants ″, *Journal of Catalysis Today*, vol. 53, no. 1, pp. 115–129, 1999.
53. M. Fox and M. Dulay , "Heterogenous Photocatalysis", *Chem. Rev.*,vol.93, pp.341-357, 1993.
54. Y. Tan, C. Wong and A. Mohamed, "An Overview on the Photocatalytic Activity of Nano-Doped-TiO_2 in the Decolourization of Organic Pollutants", *International Scholarly Research Network*, vol.1, pp. 1-18, 2011.

55. K. Rajeshwar, C. Chenthamarakshan, S. Goeringer and M. Djukic, "Titania-Based Heterogeneous Photocatalysis Materials, Mechanistic Issues, and Implications for Environmental Remediation", *Pure Appl.Chem.*, vol. 73, no. 12, pp. 1849–1860, 2001, and references therein.
56. H. Selecuk, V. Naddeo, L. Rizzo and V. Belgiorno, "Advanced Treatment by Ozonation and Sonolysis for Domestic Wastewater Reuse", *Proceeding of The 10th International Conference on Environmental Science and Technology, Kos Island, Greece*, 5-7 September, pp. B-771 - B-778, 2007.
57. A. Mills and S. Hunte, "An overview of Semiconductor Photocatalysis", *Journal of Photochemistry and Photobiology A: Chemistry*, vol. 108, pp. 1-35, 1997.
58. A. Companion and R. Wyatt, "The Diffuse Reflectance Spectra of Some Titanium dioxides", *J. Phys. Chem. Solids*, vol. 24, pp. 1025-1028, 1963.
59. A. Giwa, P. Nkeonye, K. Bello, G. Kolawole and A. Oliveira Campos, "Solar Photocatalytic Decolourization of Reactive Yellow 81 and Reactive Violet 1 in Aqueous Solution Containing Semiconductor Oxides", *International Journal of Applied Scienceand Technology*, vol. 2, no. 4, pp. 90-105, 2012.
60. M. Mehra and T. Sharma, "Photo Catalytic Decolourization of Two Commercial Dyes in Aqueous Phase Using Photo Catalyst TiO_2", *Advances in Applied Science Research*, vol. 3, no. 2, pp.849-853,2012.
61. B. Pare, P. Singh and S. Jonnalagadda, "Visible Light-Drive Photocatalytic Decolourization and Minieralization of Neutral Red Dye in a Sulurry Photoreactor", *Indian Journal Chemistry Technoogy*, vol. 17, pp. 391-395, 2010.
62. A.O. Adeloye and P. A. Ajibade , ″Towards the Development of Functionalized Polypyridine Ligands for Ru(II) Complexes as Photosensitizers in Dye-Sensitized Solar Cells (DSSCs)″ , *molecules*, vol.19,pp.12421-12460,2014, and references there in.
63. H. Gnaser, B. Huber and C. Ziegler, "Nanocrystalline TiO_2 for Photocatalysis", *Encyclopedia of Nanoscience and Nanotechnology*, vol. 6, pp. 505–535, 2004, and references there in.
64. W. Tai, K. Inoue and J. Oh," Ruthenium dye-sensitized SnO_2/TiO_2 Coupled solar cells″, *Solar Energy Materials & Solar Cells*, vol. 71, pp. 553–557, 2002.
65. C. Shifu, W. Zhao, S. Zhang and W. Liu, ″Preparation, Characterization and Photocatalytic Activity of N-containing ZnO Powder″, *Chem. Eng. J.*, vol.148, pp. 263 -269 ,2009.
66. Z. Li , S. Suyuan , X. Xiao , Z. Bin and M. Alan ″ Photocatalytic Activity and DFT Calculations on Electronic Structure of N-doped ZnO/Ag Nanocomposites ″, *Catal. Commun.* , vol. 12, pp. 890 -894, 2011.

67. Y. Liu, J.H. Yang, Q.F. Guan, L.L. Yang, Y.J. Zhang, Y.X. Wang, B. Feng, J. Cao, X.Y.Liu, Y.T. Yang and M.B. Wei, ″ Effects of Cr-doping on the optical and magnetic properties in ZnO nanoparticles prepared by sol–gel method ″, *J. Alloys Compd*., vol. 486 , pp. 835-838, 2009.
68. D.Y. Wang, J. Zhou and G.Z. Liu, ″Effect of Li-doped concentration on the structure, optical and electrical properties of p-type ZnO thin films prepared by sol–gel method ″, *J. Alloys Compd.*, vol.481, pp.802-805, 2009.
69. J.Wang, W. Chen and M.R.Wang, ″ Properties analysis of Mn-doped ZnO piezoelectric films ″, *J. Alloys Compd*. , vol.449, pp. 44-47 ,2008.
70. CRC Handbook of Chemistry and Physics, 87th ed., Taylor &Francis, pp. 112–114, 2006.
71. H. Skriver and N. Rosengaard , "Surface Energy and Work Function of Elemental Metals", *The American Physical Phenomena*, vol. 46, no. 11, pp. 7157-7168, 1992, and references there in.
72. Y. Liu, L. Guo, W. Yan and H. Liu, "A composite Visible –light Photocatalyst for Hydrogen Production", *Journal of power Sources*, vol. 159, pp. 1300-1304, 2006.
73. M. Kaneko, H. Ueno and J. Nemoto, "Schottky Junction/Ohmic Contact Behavior of an Anoporous TiO_2 Thin Film Photoanode in Contact With Redox Electrolyte Solutions", *Beilstein J. Nanotechnol.*, vol. 2, pp. 127–134, 2011.
74. A. Linsebigler, G. Lu and J. Yates, "Photocatalysis on TiO_2 Surfaces: Principles, Mechanisms, and Selected Results", *Chem. Rev.*, vol. 95, pp.735-758, 1995, and references there in.
75. A. Das, D.Y. Wang, A. Leuteritz, K. Subramaniam, H.C Greenwell, U. Wagenknecht and G. Heinrich, ″ Preparation of zinc oxide free, transparent rubber nanocomposites using a layered double hydroxide filler ″, *J. Mater. Chem*., vol.21, pp.7194-7200, 2011.
76. P. Mason, ″Physiological and medicinal zinc″, *Pharm. J.*, vol.276, pp.271-274, 2006.
77. A. Yadav, V. Prasad, A.A. Kathe, S. Raj, D. Yadav, C. Sundaramoorthy and N. Vigneshwaran, ″Functional finishing in cotton fabrics using zinc oxide nanoparticles ″, *Bull. Mater. Sci*., vol.29, pp.641-645, 2006.
78. Y. Liu, J. Zhou, A. Larbot and M. Persin, ″ Preparation and characterization of nano-zinc oxide ″, *J. Mater. Process. Technol.* , vol.189 ,pp.379-383, 2007
79. S. Mansouri, R. Bourguiga and F. Yakuphanoglu, ″Analytic model for ZnO-thin film transistor under dark and UV illumination ″, *Curr. Appl. Phys*., vol. 12, pp.1619-1623, 2012.

80. K.D. Gunaratne, C. Berkdemir, C.L. Harmon and A.W. Jr. Castelman, ″ Investigating the relative stabilities and electronic properties of small zinc oxide clusters ″, *J. Phys. Chem. A* , vol.116 ,pp.12429-12437 ,2012.
81. T.J. Kuo, C.N. Lin, C.L.Kuo, M.H. Huang, ″Growth of ultralong ZnO nanowires on silicon substrates by vapor transport and their use as recyclable photocatalysts ″, *Chem. Mater*.,vol.19, pp.5143-5147, 2007.
82. S.D. Janitabar and A.R. Mahjoub , ″ Investigation of phase transformations and photocatalytic properties of sol–gel prepared nanostructured ZnO/TiO_2 composites ″, *J. Alloy. Compd*. , vol.486 , pp.805-808 ,2009.
83. M. Safari, M. Rostami, M. Alizadeh, A. Alizadehbirjandi, S. Nakhli and R. Aminzadeh, "Response Surface Analysis of Photocatalytic Decolourization of Methyl Tert- Butyl Ether by Core/Shell Fe_3O_4/ZnO Nanoparticles", *Journal of environmental Health Science and Engenering*, vol. 12, no. 1, pp. 1-12, 2014.
84. N. Daneshvar, S. Aber, M. Dorraji, A. Khataee and M. Rasoulifard, "Preparation and Investigation of Photocatalytic Properties of ZnO Nanocrystals: Effect of Operational Parameters and Kinetic Study", *World Academy of Science, Engineering and Technology*, vol. 29, pp.267-272, 2007, and references there in.
85. M. O. AL Nafie , ″Photocatalytic Decolorization of Bismarck Brown R″, M.Sc. Thesis, College of Sciences, University of Babylon, Iraq, 2011.
86. Ü. Özgür, Ya. I. Alivov, C. Liu, A. Teke, M. A. Reshchikov, S. Doğan, V. Avrutin, S. J. Cho, and H. Morkoç, ″A comprehensive Review of ZnO Materials and Devices″, *Journal of Applied Physics*, vol.98, pp.1-103, 2005.
87. S. Baruah, and J. Dutta, ″Hydrothermal Growth of ZnO Nanostructures″, *Science and Technology of Advanced Materials*, vol. 10, pp.1-18, 2009.
88. D. C. Look, J.W. Hemsky and J.R. Sizelove, ″Residual Native Shallow Donor in ZnO ″, *Physical Review Letters*, vol. 82, no.12,pp. 2552-2555,1999.
89. D. Banerjee, J.Y. Lao, D.Z. Wang, J.Y. Huang, Z.F. Ren, D. Steeves, B. Kimball and M. Sennett, ″ Large-Quantity Free Standing ZnO Nanowires ″, *Appl. Phys. Lett.* , vol 83 , no.10, pp. 2061–2063 ,2003.
90. Y.B. Hahn, ″ Zinc Oxide Nanostructures and Their Applications ″ , *Korean J. Chem. Eng.* , vol. *28*, pp.1797–1813 , 2011 .
91. T. Frade, M.E. Melo Jorge and A. Gomes, ″ One-Dimensional ZnO Nanostructured Films: Effect of Oxide Nanoparticles ″, *Mater. Lett.* , vol. 82, pp.13–15, 2012.
92. R. Wahab, S.G. Ansari, Y.S. Kim, H.K. Seo and H.S. Shin, ″ Room Temperature Synthesis of Needle-Shaped ZnO Nanorods Via Sonochemical Method ″, *Appl. Surf. Sci.*, vol. 253, pp. 7622–7626, 2007.

93. X. Kong, Y. Ding, R. Yang and Z.L. Wang, ″ Single-Crystal Nanorings Formed by Epitaxial Self-Coiling of Polar-Nanobelts ″, *Science* , vol. 303, pp. 1348–1351 ,2004 .
94. Z.W. Pan, Z.R. Dai and Z.L. Wang, ″ Nanobelts of Semiconducting Oxides ″, *Science,* vol. 291, pp.1947–1949, 2001.
95. J.J. Wu, S.C. Liu, C.T. Wu, K.H. Chen and L.C. Chenm , ″ Hetero structures of ZnO–Zn coaxial Nano cables and ZnO Nanotubes ″, *Appl. Phys. Lett.,* vol. 81, pp.1312–1314, 2002.
96. W.J. Chen, W.L. Liu, S.H. Hsieh and T.K. Tsai, ″ Preparation of Nano sized ZnO Using α Brass ″, *Appl. Surf. Sci*., vol. 253, pp.6749–6753, 2007.
97. J. Liu , X. Huang , J. Duan, H. Ai and P. A Tu , ″Low-Temperature Synthesis of Multiwhisker-Based Zinc Oxide Micron Crystals″, *Mater. Lett.,* vol. 59, pp.3710–3714 , 2005 .
98. Y. Huang, J. He, Y. Zhang, Y. Dai, Y. Gu, S. Wang and C. Zhou, ″Morphology, Structures and Properties of ZnO Nanobelts Fabricated by Zn-powder Evaporation without Catalyst at Lower Temperature ″ , *J. Mater. Sci.* , vol. 41, pp.3057–3062, 2006 .
99. B. Nikoobakht , X. Wang, A. Herzing and J. Shi, ″Scable Synthesis and Device Integration of Self-Registered one-Dimensional zinc oxide Nanostructures and Related Materials ″ , *Chem. Soc. Rev.* , vol. 42, pp. 342–365 ,2013.
100. L.C. Tien , S.J. Pearton, D.P. Norton and F. Ren,″Synthesis and Microstructure of Vertically Aligned ZnO Nanowires Grown by High-Pressure-Assisted Pulsed-Laser Deposition ″, *J. Mater. Sci*., vol.43, pp. 6925–6932, 2008.
101. J. Cui, ″Zinc Oxide Nanowires ″, *Mater. Charact*. , vol. 64, pp.43–52, 2012.
102. T. Xu, P. Ji, M. He and J. Li, ″ Growth and Structure of Pure ZnO Micro/Nanocombs″, *J. Nanomater*., vol. 2012, 2012.
103. W.S. Chiua, P.S. Khiew, M. Clokea, D. Isaa, T.K. Tana, S. Radimanb, R. Abd-Shukorb, M.A. Abd–Hamid, N.M. Huangc and H.N. Limd, ″Photocatalytic Study of Two-Dimensional ZnO Nanopellets in the Decomposition of Methylene Blue ″, *Chem. Eng. J*. , vol.158, pp.345–352 , 2010 .
104. M. Jose-Yacaman, C. Gutierrez-Wing, M. Miki,D.Q. Yang , K.N. Piyakis and E. Sacher, ″ Surface Diffusion and Coalescence of Mobile Metal Nanoparticles ″, *J. Phys. Chem. B* , vol. 109, pp. 9703–9711 ,2005.
105. V. Polshettiwar, B. Baruwati and R.S. Varma , ″ Self Asssembly of Metal Oxides into Three-Dimensional Nanostructures: Synthesis and Application in Catalysis ″, *ACS Nano* , vol. 3,pp. 728–736 , 2009.
106. Q. Xie, Z. Dai, J. Liang , L. Xu, W. Yu and Y. Qian, ″Synthesis of ZnO Three-Dimensional Architectures and Their Optical Properties ″, *Solid State Commun.,* vol.136, pp. 304–307 , 2005.

107. J. Liu, X. Huang, Y. Li, K.M. Sulieman, F. Sun and X. He, ″Selective Growth and Properties of Zinc Oxide Nanostructures ″, *Scr. Mater,* vol. 55, pp. 795–798, 2006.
108. M. Bitenc and Z.C. Orel, ″Synthesis and Characterization of Crystalline Hexagonal Bipods of Zinc Oxide ″, *Mater. Res. Bull.*, vol. 44, pp. 381–387, 2009.
109. J. Zheng , Z.Y. Jiang, Q. Kuang , Z.X. Xie , R.B. Huang and L.S. Zheng, ″Shape-controlled fabrication of porous ZnO architectures and their photocatalytic properties ″, *J. Solid State Chem.*, vol.182 ,pp.115-121 ,2009.
110. S. Suwanboon, A. Amornpitoksuk , A. Haidoux and J.C. Tedenac, ″Structural and optical properties of undoped and aluminium doped zinc oxide nanoparticles via precipitation method at low temperature ″, *J. Alloys Compd.*, vol.462 , pp.335-339, 2008.
111. X. Wei and D. Chen, ″ Synthesis and characterization of nanosized zinc aluminate spinel by sol–gel technique ″, *Mater. Lett.* , vol.60, pp.823-827, 2006.
112. M. Salavati-Niasari, N. Mir and F. Davar, ″ ZnO nanotriangles :Synthesis, characterization and optical properties ″, *J. Alloys Compd*., vol.476,pp.908-912, 2009.
113. P. Tonto, O. Mekasuwandumrong, S. Phatanasri, V. Pavarajarn and P. Praserthdam, ″Preparation of ZnO Nanorod by Solvothermal Reaction of Zinc Acetate in Various Alcohols″, *International Journal of Ceramics*, vol. 34, no. 1, pp. 57–62, 2008.
114. M. Singhal, V. Chhabra, P. Kang and D. O. Shah, ″Synthesis of ZnO Nanoparticles for Varistors Application Using Zn-substituted Aerosol of Microemulsion ″, *Journal of Mater. Res. Bull*., vol. 32, no. 2, pp. 239–247, 1997.
115. Y. F. Guan and A. J. Pedraza, ″Synthesis and Alignment of Zn and ZnO Nanoparticles by Laser-Assisted Chemical Vapor Deposition ″ , *Journal of Nanotechnology*, vol. 19, p. 045609, 2008.
116. F. Rataboul, C. Nayral, M. J. Casanove, A. Maisonnat and B. Chaudret, ″Synthesis and characterization of Monodisperse Zinc and Zinc Oxide Nanoparticles from the Organometallic Precursor $[Zn(C_6H_{11})_2]$ ″ , *Journal of Organomet. Chem.,* vol. 643, pp. 307, 2002.
117. M. Z. Shoushtari, S. Parhoodeh and M. Farbod , ″Fabrication and Characterization of Zinc Oxide Nanoparticles by DC arc Plasma ″ , *Journal of Phys.: Conf. Ser.*, vol. 100, pp. 052017, 2008.
118. K. Sakai, S. Oyama, K. Noguchi, A. Fukuyama, T. Ikari and T. Okada, ″Optical Properties of Nanostructured ZnO Crystal Synthesized by Pulsed-Laser Ablation ″ , *Journal of Physica E,* vol. 40, no. 7, pp. 2489–2493, 2008.

119. Y. R. Uhm, B. S. Han, M. K. Lee, S. J. Hong and C. K. Rhee, ″Synthesis and Characterization of Nanoparticles of ZnO by Levitational Gas Condensation″, *Journal of Mater. Sci. Eng. A*, vol. 449–451, pp. 813–816, 2007.
120. A. Da˛browski , ″ Adsorption _ from theory to practice ″, *Advances in Colloid and Interface Science* ,vol.93,pp.135-224,2001,and references there in .
121. C. H. Giles ,″Adsorption from Solution at the Solid Liquid Interface″, London, 1983.
122. J. M. Herrmann, ″Heterogeneous Photocatalysis Fundamentals and Applications to the Removal of Various Types of Aqueous Pollutants″, *Catalysis Today*, vol. 53, pp.115-129,1999.
123. V. Parmon, A. Emeline and N. Serpone, "Glossary of Terms in Photocatalysis and Radiocatalysis", *International Journal of Photoenergy*, vol. 4, pp. 91-131, 2002.
124. A. W. Adamson, ″Physical Chemistry of Surfaces ″ , *Wiley, New York* , 1982.
125. N. D. Spencer and J. H.Moore , ″Encyclopedia of Chemical Physics and Physical Chemistry ″ ,*Bristol , Philadelphia*, 2001.
126. C. Anderson and A.J. Bard, ″An Improved Photocatalyst of TiO_2/SiO_2 Prepared by a Sol-Gel Synthesis″ , *Journal of Physical Chemistry* ,vol.99, pp.9882-9885,1995.
127. S. Sakka , "Application of Sol-Gel Technology", *Kluwer Academic Publishers*, Massachusetts, USA, 2005.
128. H. Al-Ekabi and N. Serpone , ″Kinetic Studies In Heterogeneous Photocatalysis. Photocatalytic Degradatlon of Chlorinated Phenols in Aerated Aqueous Solutions Over TiO_2 Supported on AGlass Matrix″, *Journal of Physical Chemistry*, vol.92, pp.5726-5731,1988,and references there in .
129. T. N. Obee and S. O. Hay, ″ Effects of Moisture and Temperature on the Photooxidation of Ethylene on Titania ″, Environ. *Sci. & Technol.*,vol. 31,pp.2034-2038 ,1997.
130. C. P. Chang, J. N. Chen and M. C. Lu, ″Heterogeneous Photocatalysis″, *Journal of Environmental Science and Health Part A–Toxic/Hazardous Substances and Environ. Engineering*, vol. 38 , no. 6 ,pp. 1131-1143 ,2003.
131. S. G. Chen., R. T. Yang, F. Kapteijen and J. A. Moulijn, ″A new Surface Oxygen Complex on Carbon Toward a Unified Mechanism for Carbon Gasification Reactions ″ , *Industrial and Engineering Chemistry Research* ,vol. 32,pp. 2835-2840,1993.
132. J. C. Santos, P. Cruz, T.Regala, F.D. Magalhaes and A. Mendes, ″High-Purity Oxygen Production by Pressure Swing Adsorption ″ , *Industrial and Engineering Chemistry Research*, vol. 46, pp.591- 599,2007.

133. M. L. Zhang, T.C.An, J.M.Fu, G.Y.Sheng, X.M.Wang, X.H.Hu and X.J. Ding, ″Photocatalytic Decolourization of Mixed Gaseous Carbonyl Compounds at Low Level on Adsorptive TiO_2/SiO_2 Photocatalyst Using a Fluidized Bed Reactor ″, *Chemosphere*, vol. 64, pp.423-431,2006.
134. M. A. Behnajady and N. Modirshahla, ″Kinetic Study on Photocatalytic Decolourization of C.I. Acid Yellow 23 by ZnO Photocatalyst ″ , *Journal of Hazardous Materials,* vol. 133, pp.226- 232,2006.
135. J. Mo, Y. Zhang, Q. Xu, J.J. Lamson and R. Zhao,″Photocatalytic Purification of Volatile Organic Compounds in Indoor Air: ALiterature Review ″ , *Atmospheric Environment* , vol. 43 pp. 2229–2246,2009.
136. M. A. Behnajady and N. Modirshahla, ″ Nonlinear Regression Analysis of Kinetics of the Photocatalytic Decolorization of an Azo Dye in Aqueous TiO_2 Slurry ″, *Photochemical and Photobiological Sciences*, vol. 5, pp.1078–1081,2006.
137. T. K. Tseng, Y. S.Lin, Y.J. Chen and H. Chu , ″A review of Photocatalysts Prepared by Sol-Gel Method for VOCs Removal ″, *International Journal of Molecular Sciences*, vol. 11, pp. 2336- 2361,2010.
138. M. P. de Lara-Castells and J. L. Krause, ″Periodic Hartree–Fock Study of the Adsorption of Molecular Oxygen on a Reduced TiO_2 (110) Surface ″, *Journal of Chemical Physics*, vol. 115, no.10, pp.4798- 4810, 2001.
139. M. P.de Lara-Castells and J. L.Krause, ″Theoretical Study of the UV induced Desorption of Molecular Oxygen from The educed TiO_2 (110) surface″, *Journal of Chemical Physics*, vol.118, no.11, pp.5098- 5105, 2003.
140. M. Anpo, M. Che, B. Fubini, E.Garrone, E. Giamello and M. C. Paganini, ″Generation of Superoxide Ions at Oxide Surfaces ″ , *Topics in Catalysis*, vol. 8,pp. 189-198,1999.
141. T. Berger, M. Sterrer, O. Diwald and E. Knozinger, ″Charge Trapping and Photo Adsorption of O_2 on Dehydroxylated TiO_2 Nanocrystals—an Electron Paramagnetic Resonance Study ″ , *Journal of Chemical Physics and Physical Chemistry* , vol. 6,pp. 2104-2112,2005.
142. I.M. Banat, P. Nigam, D. Singh and R. Marchant, ″ Microbial Decolorization of Textiledye-Containing Effluents: A review ″, *Bioresource Technol*., vol. 58, pp. 217–227, 1996.
143. T. Robinson, G. McMullan, R. Marchant and P. Nigam, ″Remediation of Dyes in Textile Effluent: a Critical Eeview on Current treatment Technologies with a Proposed Alternative ″, *Bioresour. Technol*, vol.77, pp. 247–255 , 2001.
144. S. Moosvi, H. Keharia and D.Madmwar, ″ Decolourization of textile dye Reactive Violet 5 by a newly isolated bacterial consortium RVM 11.1 ″, *World*

Journal of Microbiology and Biotechnology,vol.21, pp. 667-672 ,2005 ,and references there in.

145. C. O. Neill, F.R. Hawkes, D.L. Hawkes, N.D. Lourenco, H.M. Pinheiro and W. Delee, ″Colour in Textile Effluents—Sources, Measurement, Discharge Consents and Simulation: A review ″, *J.Chem. Technol. Biotechnol*. , vol.74, pp.1009–1018, 1999.
146. Q. Sun and L. Yang , ″The Adsorption of Basic Dyes from Aqueous solution on Modified Peat-resin Particle ″ ,*Water Res*. , vol.37,pp.1535–1544 , 2003.
147. G. McKay, ″The Adsorption of Dye Stuffs from Aqueous Solution using Activated Carbon: Analytical Solution for Batch Adsorption Based on External Mass Transfer and Pore Diffusion ″, *Chem. Eng. J.* , vol. 27 , pp. 187–196 , 1983.
148. S.J. Allen, ″Types of adsorbent materials ″,Use of Adsorbents for the Removal of Pollutants from Wastewaters , in: G. McKay (Ed.) ,CRC, Boca Raton, USA , pp. 59–97,1996.
149. P. Pengthamkeerati, T. Satapanajaru, N. Chatsatapattayakul, P.Chairattanamanokorn and N. Sananwai, ″Alkaline Treatment of Biomass Fly Ash for Reactive Dye Removal from Aqueous Solution ″,*Desalination*, vol. 261, no. 1-2, pp. 34–40, 2010.
150. F. P. Zee and S. Villaverde, ″ Combined Anaerobic–Aerobic Treatment of Azo Dyes—a Short Review of Bioreactor Studies ″ ,*Water Research*, vol.39, pp. 1425 -1440 ,2005.
151. C. M. So, M. Y. Cheng, J. C. Yu and P. K. Wong, ″ Degradation of Azo Dye Procion Red MX-5B by Photocatalytic Oxidation ″ , *Chemosphere*, vol.46, pp. 905 -912 , 2002.
152. S.P.Bhutani, ″Organic Chemistry Selected Topics ″, 1st Ed., (Reprinter),Ane Books india ,New Delhi,2008.
153. F. J. Green,″ The Sigma–Aldrih Handbook of Stains, Dyes, and Indicators ″, Aldrich Chemical, Milwaukee, Wis, USA, 1990.
154. T. Geethakrishnan and P.K. Palanisamy, ″ Degenerate Four-Wave Mixing Experiments in Methyl green Dye-Doped Gelatin Film ″ , *Optik - International Journal for Light and Electron Optics* , vol. 117 , pp.282-286 , 2006.
155. F. Hussein and R. Rudham, "Photocatalytic Dehydrogenation of Liquid Alcohols by Platinized Anatase", *J. Chem. Soc, Faraday Trans.1*,vol. 83, pp. 1631-1639, 1987.
156. L. Ahmed, F. Hussein and Ali Mahdi, "Photocatalytic Dehydrogenation of Aqueous Methanol Solution by Bare and Platinized TiO_2 Nanoparticles", *Asian Journal of Chemistry;* vol. 24, no. 12, pp.5564-5568 , 2012.

157. F. Hussein and R. Rudham, "Photocatalytic Dehydrogenation of Liquid Propan-2-ol by Platinized Anatase and Other Catalysts", *J.Chem. Soc, Faraday Trans.1*,vol. 80, pp. 2817-2825, 1984.
158. J. Herrmann, "Heterogeneous Photocatalysis: Fundamentals and Applications to the Removal of Various Types of Aqueous Pollutants", *Catalysis Today*, vol. 53, pp. 115-129, 1999, and references there in.
159. F. Hussein and T. Abass, "Solar Photocatalysis and Photocatalytic Treatment of Textile Industrial Wastewater", *Int. J. Chem. Sci*., vol. 8, no. 3, pp. 1409-1420, 2010.
160. V. Parmon, A. Emeline and N. Serpone, "Glossary of Terms in Photocatalysis and Radiocatalysis", *International Journal of Photoenergy*, vol. 4, pp. 91-131, 2002.
161. C. Uyguner and M. Bekbolet, "Photocatalytic Decolourization of Natural Organic Matter: Kinetic Considerations and Light Intensity Dependence", *International Journal of Photoenergy*, vol. 6, pp. 73- 80, 2002.
162. F. Hussein and T. Abass, "Photocatalytic Treatment of Textile Industrial Wastewater", *Int. J. Chem. Sci*., vol. 8, no. 3, pp. 1353- 1364, 2010.
163. A. Prevot, C. Baiocchi , M. Brussino , E. Pramauro , P. Savarino , V.Augugliaro, G. Marcì and L. Palmisano, "Photocatalytic Decolourization of Acid Blue 80 in Aqueous Solutions Containing TiO2 Suspensions", *Environ. Sci. Technol*., vol. 35, no. 5, pp. 971–976, 2001, and reference there in.
164. C. Turchi and D. Ollis, "Photocatalytic Decolourization of Organic Water Contaminants: Mechanisms Involving Hydroxyl Radical Attack", *Journal of Catalysis*, vol. 122, pp. 178-192, 1990.
165. C. Sahoo, A. K. Gupta and A. Pal, ″ Photocatalytic Degradation of Methyl Red Dye in Aqueous Solutions Under UV Irradiation Using Ag^{+} Doped TiO_2 ″ , *Desalination* , vol. 181, pp. 91-100 , 2005.
166. N. Daneshvar, S. Aber, M. S. Seyed Dorraji, A. R. Khataee, and M. H. Rasoulifard, ″Preparation and Investigation of Photocatalytic Properties of ZnO Nanocrystals: Effect of Operational Parameters and Kinetic Study ″, *World Academy of Science Engineering and Technology*, vol. 29, pp. 267–272, 2007.
167. M. S. Gonclaves, A. M. Oliverira-Campose, E. M. Piinto, P. M. Plasencia and M. J.Querioz ,″Photochemical Treatment of Solutions of Azo Dyes Containing TiO_2 ″ *Chemosphere*, vol.39, pp. 781 -786 , 1999.
168. H. C. Yatmaz, A. Akyol, M. Bayramoglu, ″ Kinetics of the Photocatalytic Decolorization of an Azo Reactive Dye in Aqueous ZnO Suspensions ″, *Ind. Eng. Chem. Res.*, vol. 43 , pp.6035-6039 ,2004.

169. U. I. Gaya, A. Abdullah, Z. Zainal and M. Z. Hussein, ″ Photocatalytic Degradation of 2, 4-dichlorophenol in Irradiated Aqueous ZnO Suspension ″ , *Int. J. Chem.*, vol.2, p180 , 2010.
170. M. Mashkour, A. Al-Kaim, L. Ahmed and F. Hussein, "Zinc Oxide Assisted Photocatalytic Decolorization of Reactive Red 2 Dye", *Int. J. Chem. Sci*., vol. 9, no.3, pp. 969-979, 2011.
171. P. Atkins and J. Pula, ″Atkin's Physical Chemistry″, 8th Ed., Oxford University Press, UK, 2006.
172. S. Somasundaram, K. Sekar, V. Kumar Gupta and S. Ganesan, ″Synthesis and Characterization of Mesoporous Activated Carbon from Rice Husk for Adsorption of Glycine from Alcohol-Aqueous Mixture ″, *Journal of Molecular Liquids*, vol. 177, pp. 416 –425, 2013.
173. M. R. Samarphandi, M. Zarrabi, M. N. sepehr, A. Amrane, G. H. Safari and S. Bashiri, ″Application of Acidic Treated Pumice as an Adsorbent for the Removal of Azo Dye from Aqueous Solution: Kinetic, Equilibrium and Thermodynamic Studies ″ , *Journal of Iranian. Environ. health sci. Eng*, vol. 9, no. 5, pp. 33–44, 2012.
174. D. Sharma, S. Sharma, B. S. Kaith, J. Rajput, and M. Kaur, ″Synthesis of ZnO nanoparticles using surfactant free in-air and microwave method,″ *Journal of Applied Surface Science*, vol. 257, no. 22, pp. 9661–9672, 2011.
175. D. Duonghong, E. Borgarello and M. Gratzel," Dynamics of Light- Induced Water Cleavage in Colloidal Systems" *J. Am. Chem. Soc*., vol.103, no. 16, pp.4685- 4690,1981.
176. D. Moore and R. Reynolds, ″X-Ray Diffraction and the Identification and Analysis of Clay minerals ″, 2nd Ed., Oxford University Press, Oxford, UK, CH 3, 1997.
177. A. Patterson, "The Scherrer Formula for X-Ray Particle Size Determination", *Physical Review*, vol. 56, pp. 978-982, 1939.
178. A. Monshi, M. Foroughi and M. Monshi, "Modified Scherrer Equation to Estimate More Accurately Nano-Crystallite Size Using XRD ", *World Journal of Nano Science and Engineering*, vol. 2, pp.154-160, 2012.
179. X. Pan, I. Medina-Ramirez, R. Mernaughc and J. Liu, "Nano Characterization and Bactericidal Performance of Silver Modified Titania Photocatalyst", *Colloids and Surfaces B: Biointerfaces*, vol.77, pp. 82–89, 2010.
180. B. Barrocas, O. C. Monteiro, M. E. Melo Jorge and S. Sério, ″Photocatalytic Activity and Reusability Study of Nanocrystalline TiO2 films prepared by sputtering technique ″, *Journal of Applied Surface Science*, vol. 264, pp. 111–116, 2013.

181. R.G.Sartale, G.D. Saratale, J.S.Chang and S.P.Govindwar,″ Ecofriendly Degradation of Sulfonated Diazo Dye C.I. Reactive Green 19A Using Micrococcus Glutamicus NCIM-2168 ″, *Bioresource Technology*, vol. 100, pp.3897-3905 , 2009 .
182. M. Montalti, A. Credi, L. Prodi and M. T. Gandolfi, ″Handbook of Photochemistry ″, 3rd Ed., Taylor & Francis Group, London New York,LLC, CH12, pp. 601-603, 2006.
183. S. Ahmed, "Photo Electrochemical Study of Ferrioxalate Actinometry at A Glassy Carbon Electrode", *Journal of Photochemistry and Photobiology A: Chemistry* ,vol. 161, pp. 151-154, 2004.
184. J. Rabek, ″Experimental methods in the Photochemistry and Photophysics ″, part 2 ,John Wiley & Sons , Chichester, CH IV, pp. 59-63,1982.
185. R. Haberk, J. Herzfeld and R. Griffin, "Photocalorimetry. Enthalpies of Photolysis of trans- Azobenzene, Ferrioxalate and Cobalt ioxalate Ions, Chromium Hexacarbonyl, and Dirhenium Decarbonyl″, *Journal of the American Chemical Society*, vol. 100, no. 4, pp. 1298-1300, 1978.
186. M. A. Tabbara and M. M. Jamal, "A kinetic Study of the Discoloration of Methylene Blue by Na_2SO_3, Comparison with NaOH", *Journal of the University of Chemical Technology and Metallurgy*, vol. 47, no. 3, pp.275-282, 2012.
187. L. Ahmed, F. Hussein and Ali Mahdi, "Photocatalytic Dehydrogen-ation of Aqueous Methanol Solution by Bare and Platinized TiO_2 Nanoparticles*", Asian Journal of Chemistry*; vol. 24, no. 12, pp. 5564-5568 , 2012.
188. M. F. Houcine , F. A. Harraz, A. A. Ismail , S.A. Al-Sayari and M.S. Al-Assir, " Mesoporous Ag/ZnO Multilayer Films Prepared by Repeated Spin-Coating for Enhancing its Photonic Efficiencies ", *Surface & Coatings Technology*, vol. 263, pp. 44–53, 2015.
189. A. M. Valenzuela, O. S. Flores, O. Ríos-Bernỹ, E. Albiter and S. Alfaro, "Photocatalytic Deposition of Metal Oxides on Semiconductor Particles: A Review", Molecular Photochemistry - Various Aspects, S. Saha , Ed. InTech, 2012.
190. H. Kleinwechter, C. Janzen, J. Knipping, H. Wiggers and P. Roth, ″Formation and Properties of ZnO Nanoparticles from Gas Phase Synthesis Pprocesses″, *J. Mater. Sci.* , vol. 37, pp. 4349–4360, 2002 .
191. M . R Vaezi , ″Highly textured ZnO thin films: An Economical Fabrication, Doping by Mn^{2+} and Sn^{2+} and Approachment for Optical Devices″, *Materials and Design*, vol. 28, pp.1065-1070, 2007.
192. B. Pal and P. K. Giri, ″High Temperature Ferromagnetism and Optical Properties of Co Doped ZnO Nanoparticles″, *J. Appl. Phys.* vol. 8, pp. 084322-1 - 084322- 8 , 2010.

193. R.S. Zeferino, M.B. Flores and U. Pal, ″Photoluminescence and Raman scattering in Ag-doped ZnO nanoparticles ″, *J. Appl. Phys*., vol. 109, pp. 14308-1 - 14308-6 ,2011 .
194. L. B. Reutergårdh and M. Langphasuk, "Photocatalytic Decolourization of Reactive Azo Dye: A comparison between TiO_2 and CdS Photocatalysis", *Chemosphere,* vol. 35, no. 3, pp. 585-596, 1977, and references there in.
195. J. Kumar and A. Bansal , ″Dual Effect of Photocatalysis and Adsorption in Degradation of Azorubine Dye Using Nanosized TiO_2 and Activated Carbon Immobilized with Different Techniques ″, *International Journal of ChemTech Research*, vol.2, no.3, pp 1537- 1543, 2010.
196. B. Neppolian, S. Sakthivel, B. Arabindoo, M. Palanichamy and V. Murugesan, ″ Degradation of Textile Dye by Solar Light Using TiO_2 and ZnO Photocatalysts ″, *Journal of Environmental Science and Health* , vol. A34, pp.1829–1838,1999.
197. S. Sakthivel, B. Neppolian, M.V. Shankar, B. Arabindoo, M. Palanichamy and V. Murugesan, ″Solar Photocatalytic Degradation of Azo Dye: Comparison of Photocatalytic Efficiency of ZnO and TiO2 ″,*Solar Energy Mater. Solar Cells* , vol. 77, pp. 65–82 ,2003.
198. J. Bandara, K. Tennakone and P.P.B. Jayatilaka, ″ Composite Tin and Zinc Oxide Nano crystalline Particles for Enhanced Charge Separation in Sensitized Degradation of Dyes ″, *Chemosphere* , vol. 49 , pp. 439–445, 2002.
199. N. Daneshvar , D. Salari and A. R. Khataee, ″Photocatalytic degradation of azo dye acid red 14 in water: investigation of the effect of operational parameters ″ ,*Photochem. J. Photobiol. A. Chem.*, vol. 157, pp. 111-116, 2003.
200. F. Zhang, J. Zhao, T. Shen, H. Hidaka, E. Pelizzetti and N. Serpone , ″TiO2-Assisted Photodegradation of Dye Pollutants II . Adsorption and Degradation Kinetics of Eosin in TiO_2 Dispersions Under Visible Light Irradiation ″, *Applied Catalysis B: Environmental*, vol. 15, pp. 147–156, 1998.
201. S. K. Kavitha and P. N. Palanisamy, ″Photocatalytic andsonophotocatalytic degradation of reactive red 120 using dye sensitized TiO_2 under visible light ″, *International Journal of Civil and Environmental Engineering* , vol. 3, pp. 1–6, 2011
202. H. K. Singh, M. Muneer and D. Bahnemann,″ Photocatalysed Degradation of aherbicide derivative ,bromacil ,in aqueous suspensions of Titanium Dioxide ″, *J. Photochem. Photobiol. Sci.,* vol.2, pp.151-169, 2003.
203. M. Movahedi, A. R. Mahjoub and S. Janitabar-Darzi, *J. Iran. Chem. Soc*., vol.6, pp. 570, 2009.

204. Z. He, S.Song, H.Zhou, H.Ying and J.Chen, ″C.I. Reactive Black Decolorization by combined sonolysis andozonation ″, *Ultrason .Sonochem* , vol.14, pp.298–304.,2007.
205. A.Nezamzadeh-Ejhiehand E.Shahriari,"HeterogeneousPhotodecolourization of Methyl Green Catalyzed by Fe(II)-o-Phenanthroline/Zeolite Y Nanocluster ", *International Journal of Photoenergy*, pp. 1-10, 2011,and references there in.
206. S. Sakthivel, B. Neppolian, M. V. Shankar, B. Arabindoo , M. Palanichamy and V. Murugeasan , ″ Solar photocatalytic degradation of azo dye: comparison of photocatalytic efficiency of ZnO and TiO_2 ″, *Sol. Energy Mater Sol. Cells*, vol. 77,pp.65-82 ,2003.
207. B. R. Lars and I. Mallika, ″Photocatalytic Decolourization of Reactive Azo dye A comparison Between TiO_2 and Us Photocatalysis″ ,*Chemosphere*, vol.35,pp. 585–596,1997.
208. B. Neppolian, H.C. Choi, S. Sakthivel, B. Arabindoo and V. Murugesan, ″Solar Light Induced and TiO_2 Assisted Degradation of Textile Dye Reactive Blue 4 ″ , *Chemosphere*, vol.46,pp.1173-1181,2002.

Appendix (A)

UV-visible absorption spectra

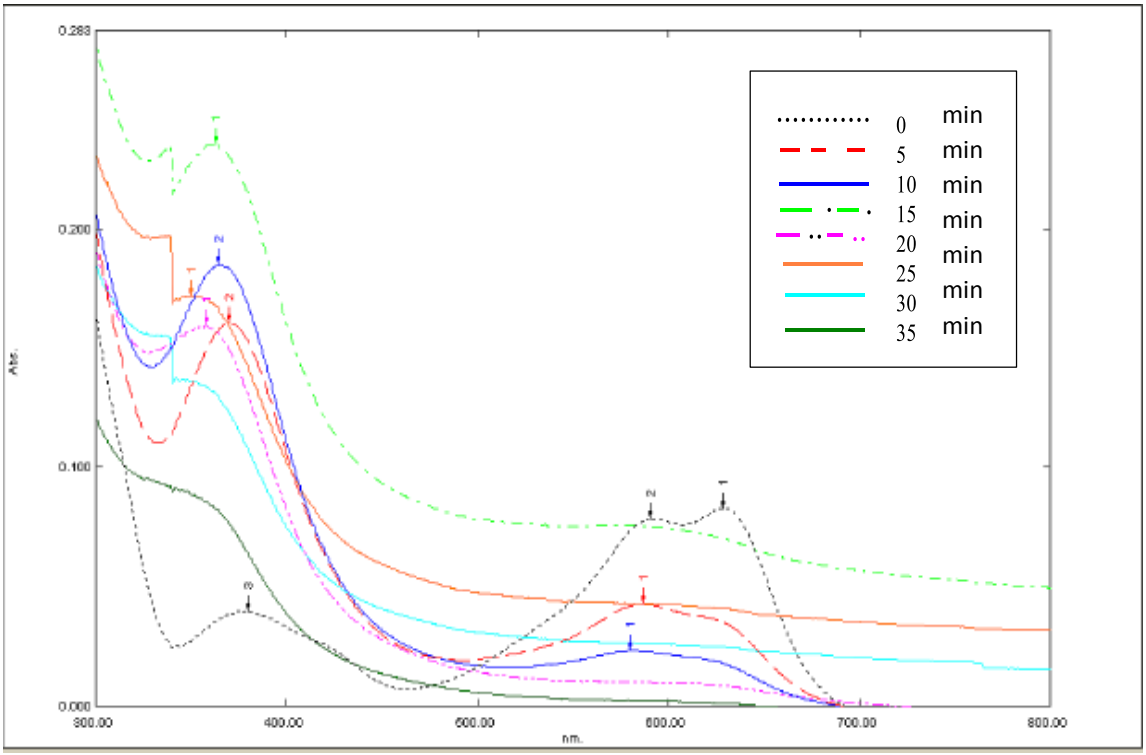

Figure 1 : UV-visible absorption spectra of methyl green with Commercial ZnO.

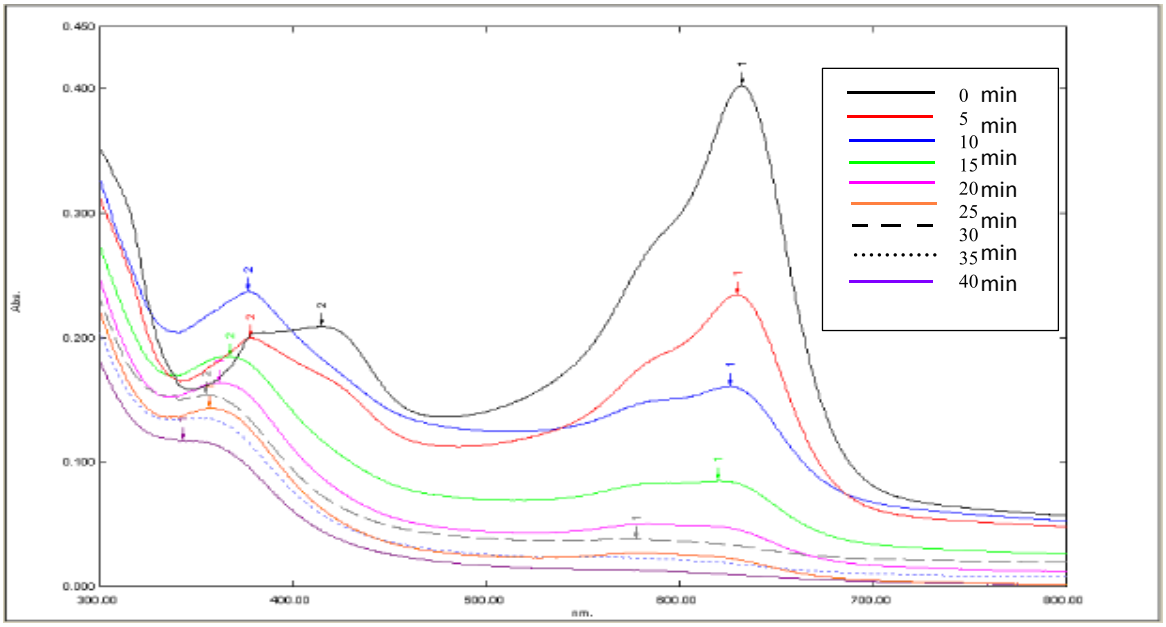

Figure 2 : UV-visible absorption spectra of methyl green with Co (0.50)/ Commercial ZnO.

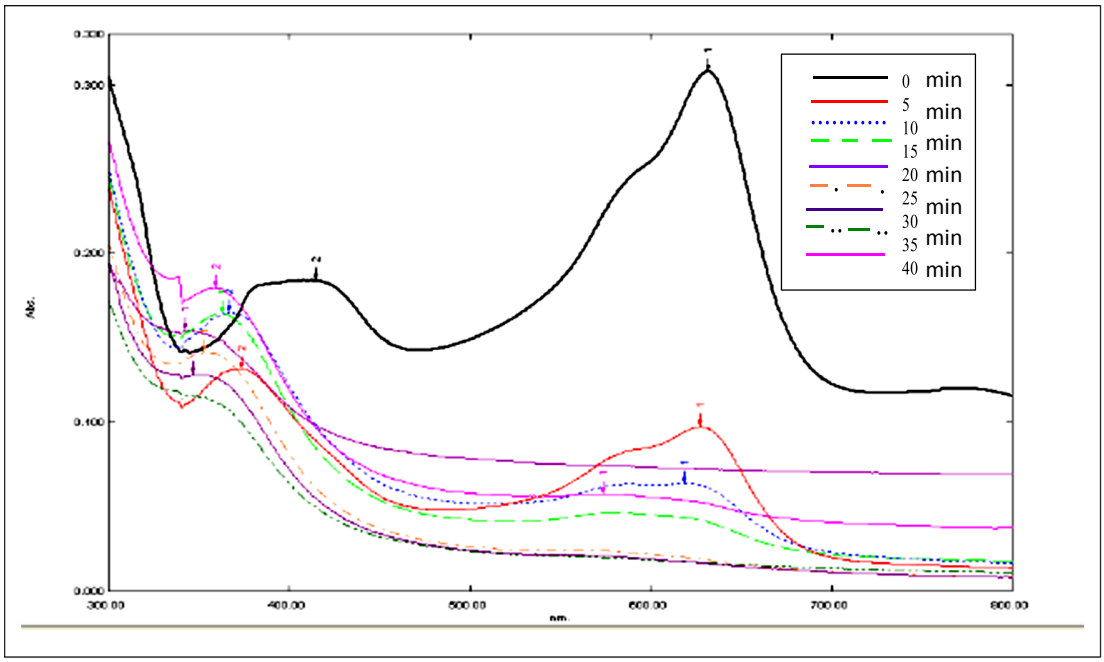

Figure 3: UV-visible absorption spectra of methyl green with Ag(2.00)/ Commercial ZnO

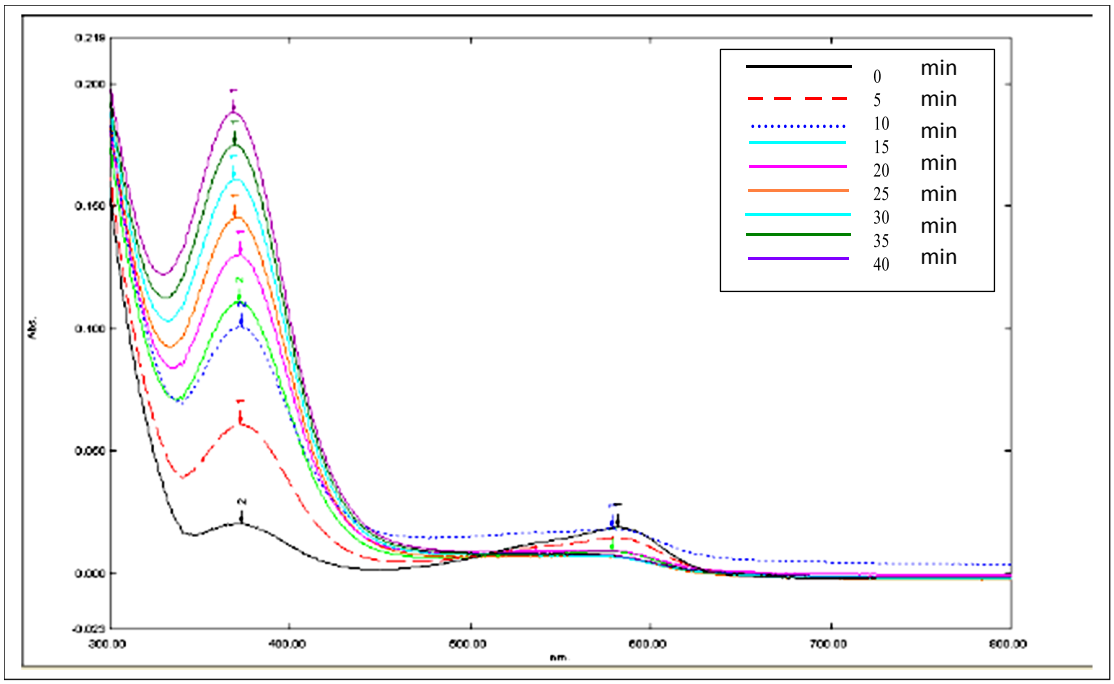

Figure 4: UV-visible absorption spectra of methyl green with ZnO prepared and calcinated at (500)^{o}C.

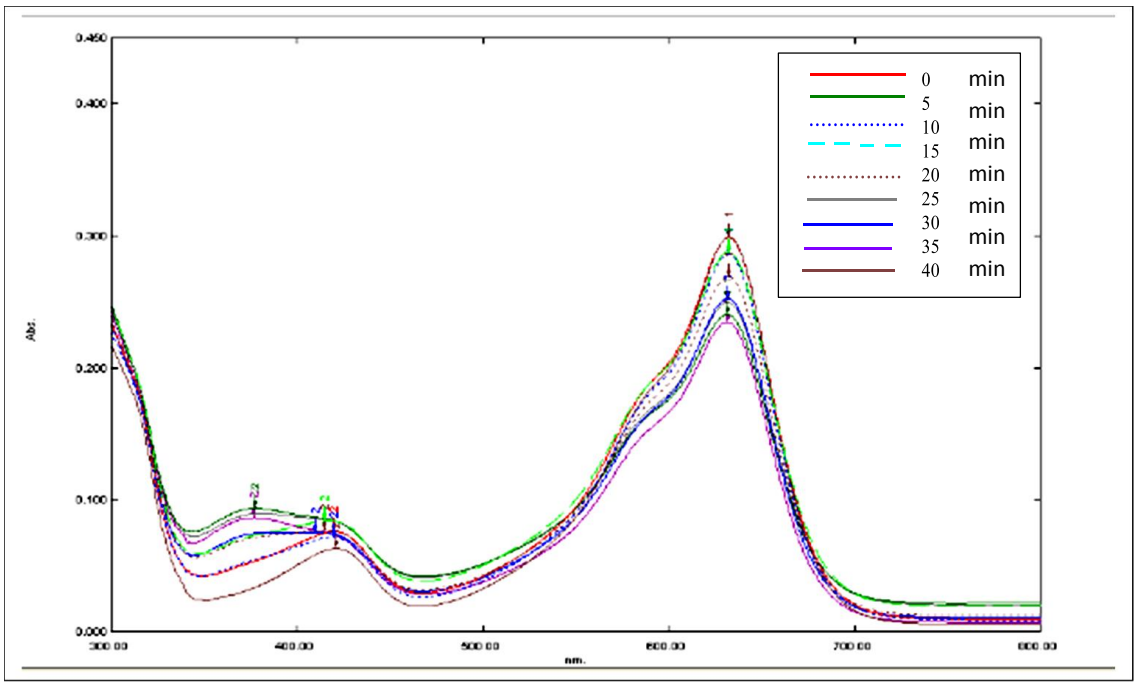

Figure 5 : UV-visible absorption spectra of methyl green with Co (1.00)/ZnO prepared and calcinated at (500)^{O}C.

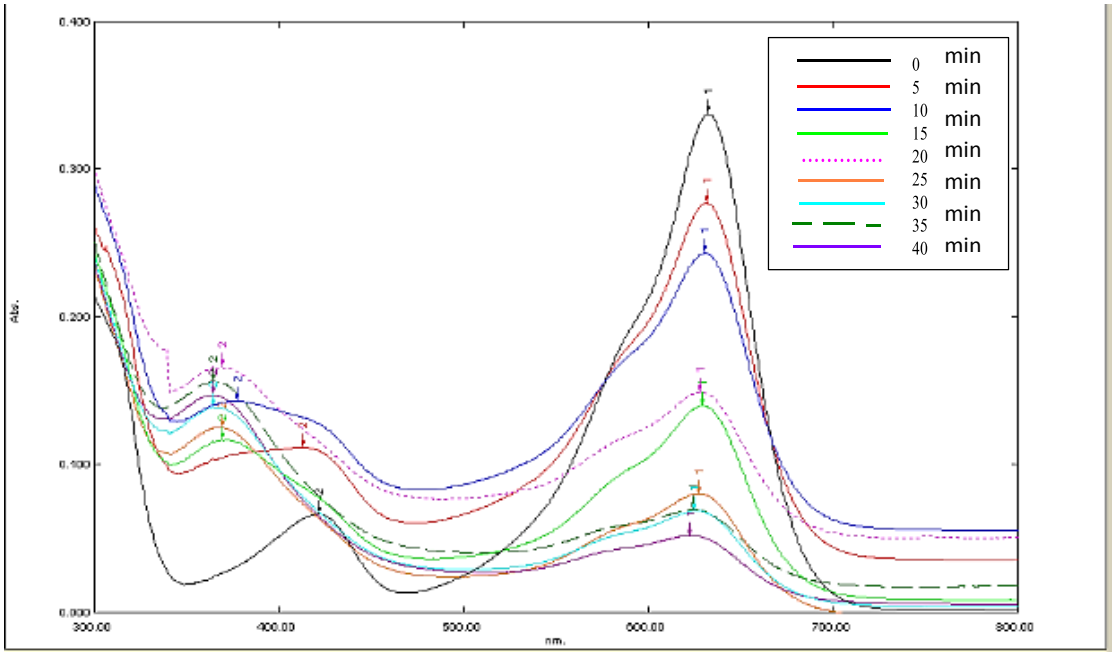

Figure 6 : UV-visible absorption spectra of methyl green with Ag (2.00)/ZnO prepared and calcinated at (500)^{o}C

Fourier Transform Infrared Spectroscopy (FTIR)

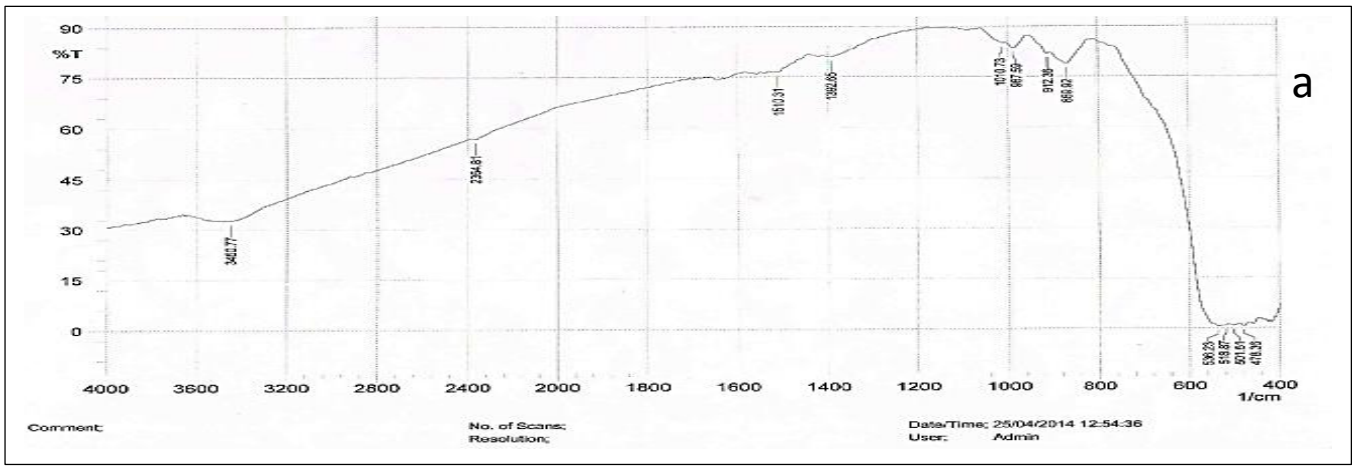

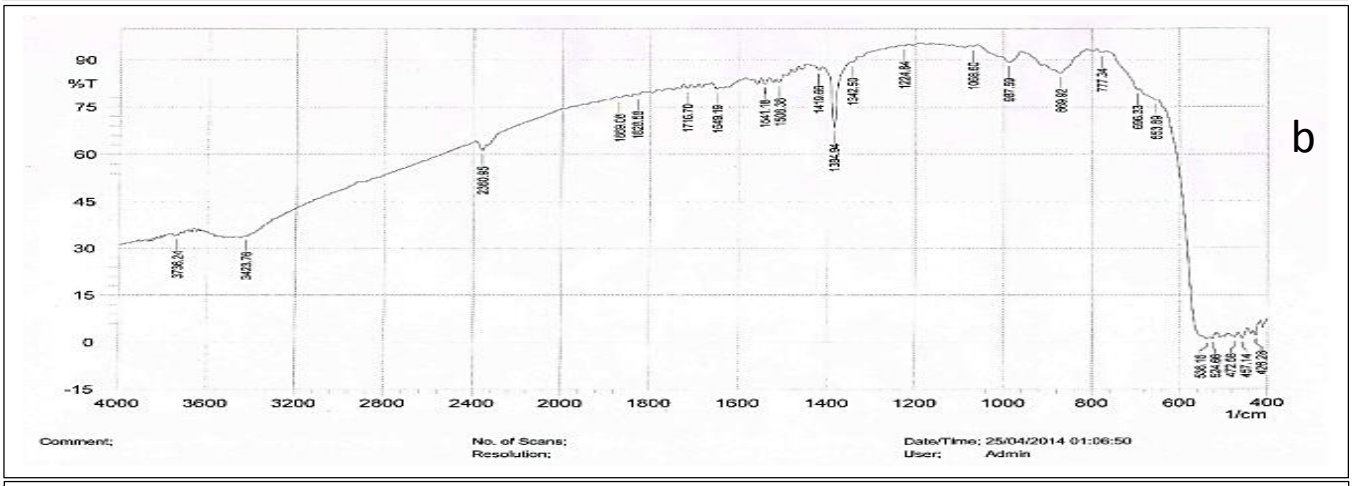

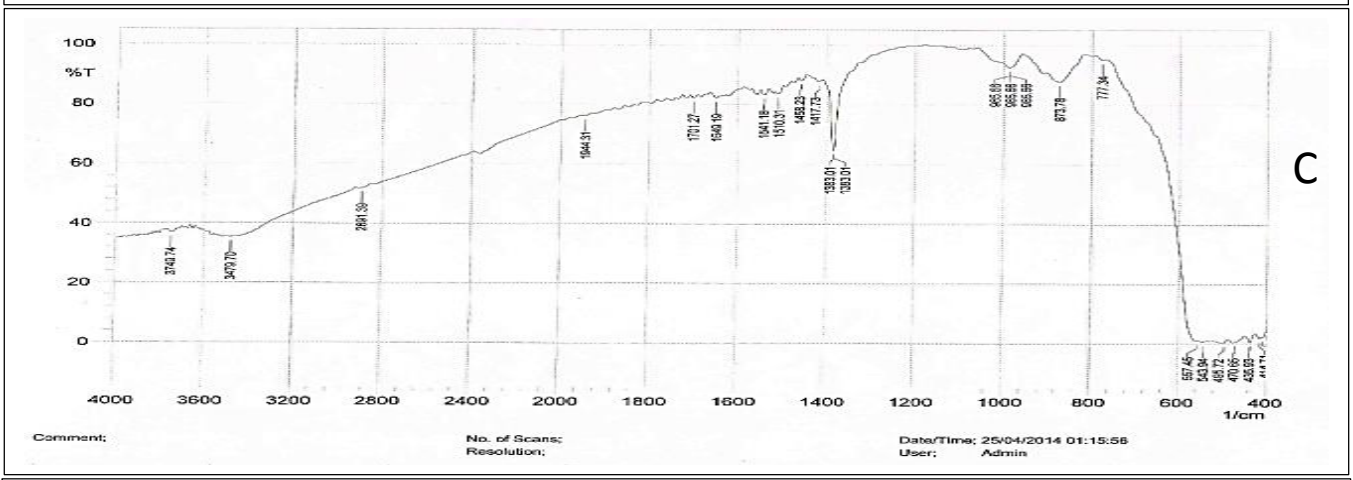

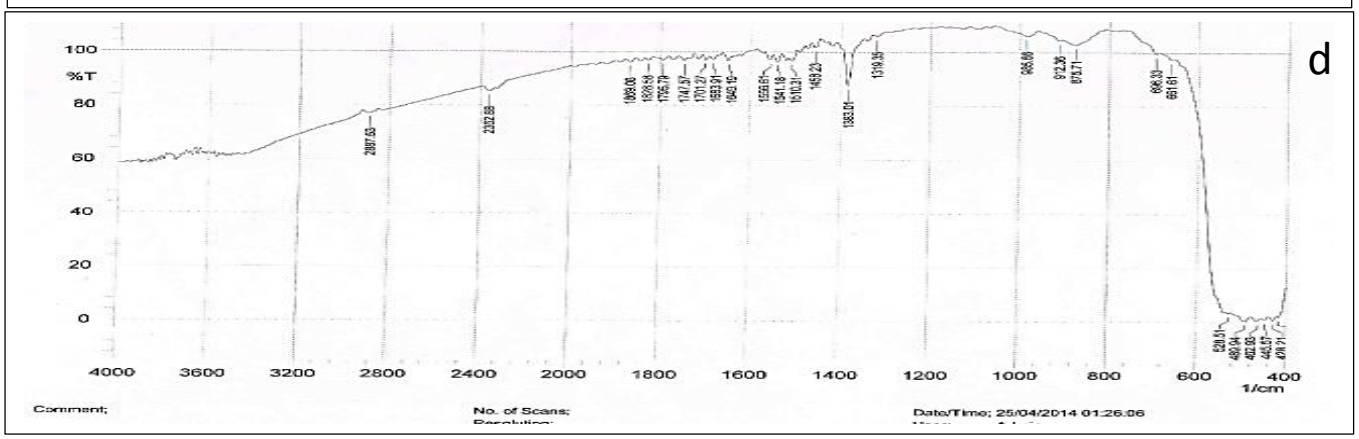

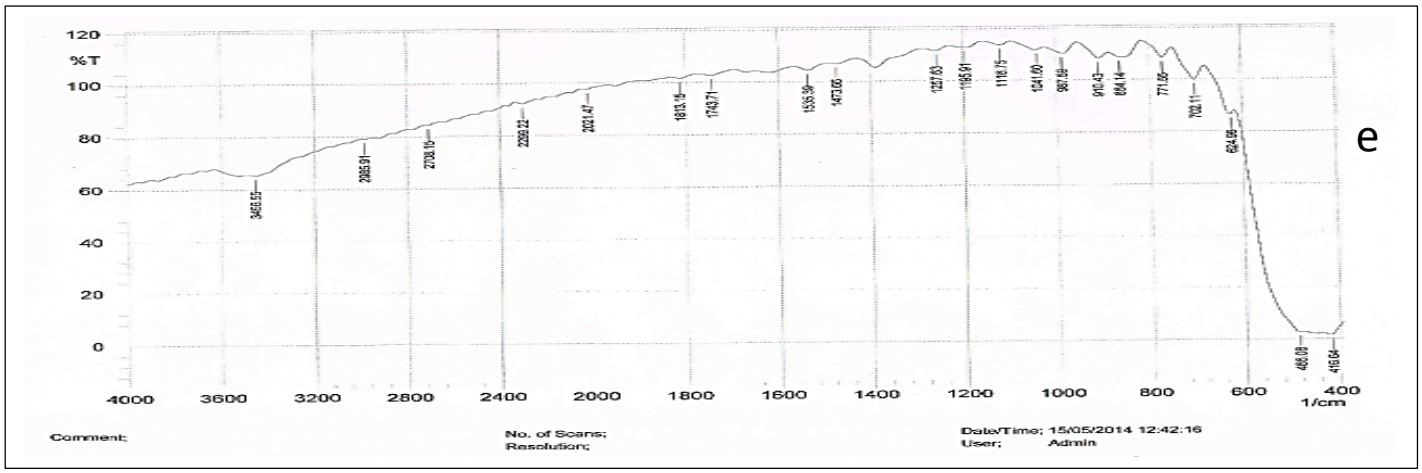
%T
1/cm
Comment:
No. of Scans;
Resolution;
Date/Time; 15/05/2014 12:42:16
User; Admin

e

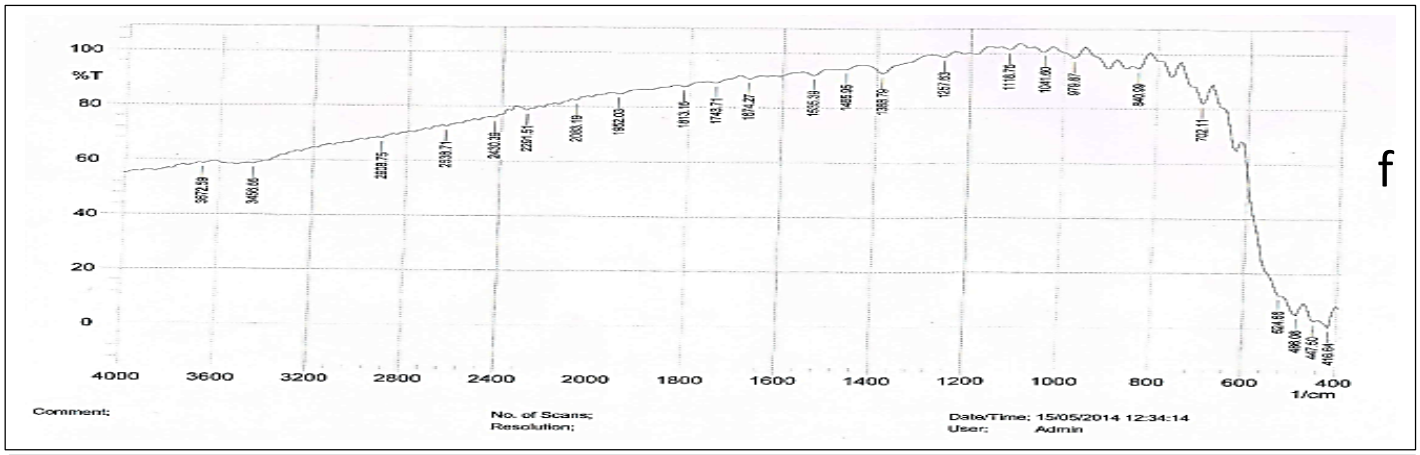
%T
1/cm
Comment:
No. of Scans;
Resolution;
Date/Time; 15/05/2014 12:34:14
User; Admin

f

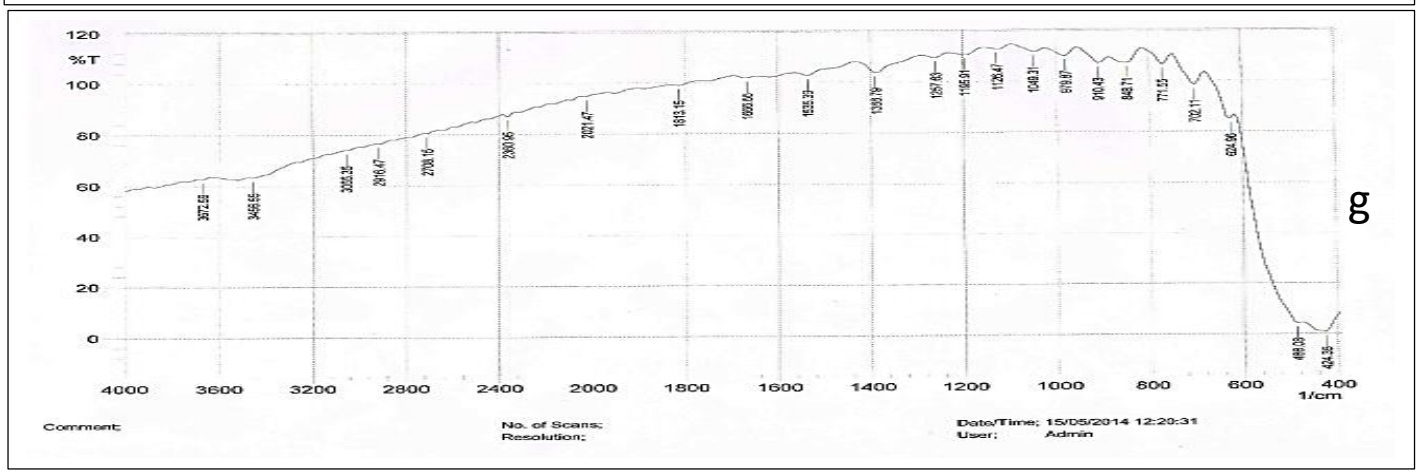
%T
1/cm
Comment:
No. of Scans;
Resolution;
Date/Time; 15/05/2014 12:29:31
User; Admin

g

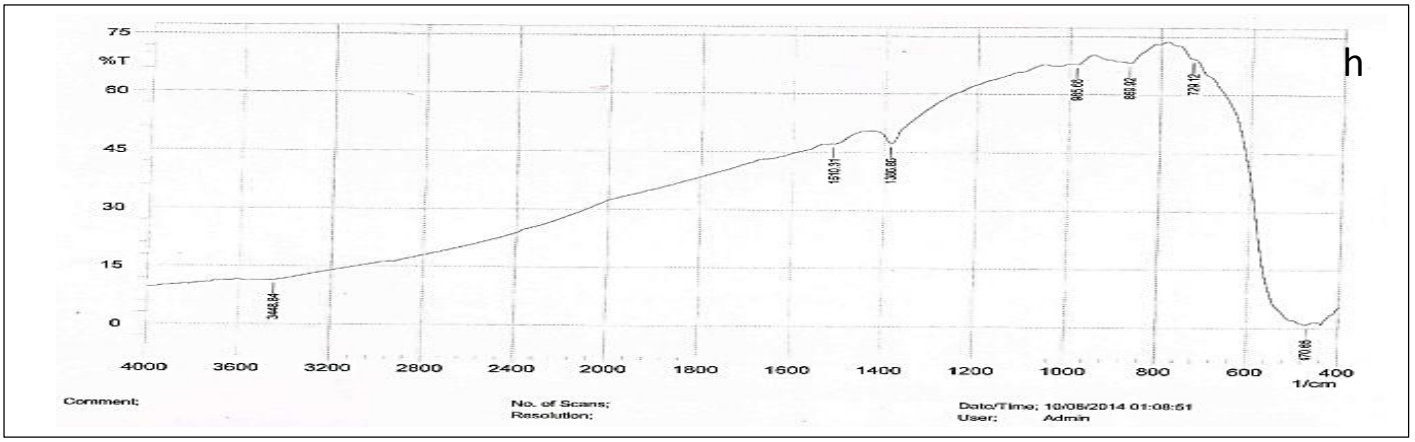
%T
1/cm
Comment:
No. of Scans;
Resolution;
Date/Time; 16/05/2014 01:08:51
User; Admin

h

Figure 7 : FT-IR Spectra for Naked and Different Percentage of Co and Ag Loaded on Commercial ZnO, at a)Naked Commercial ZnO, b) Co(0.5)/ Commercial ZnO , c)Co (1.00)/ Commercial ZnO , d) Co(2.00)/ Commercial ZnO , e)Ag(0.5)/ Commercial ZnO, f) Ag(1.00)/Commercial ZnO ,g)Ag (2.00)/Commercial ZnO , h)Ag (4.00)/Commercial ZnO .

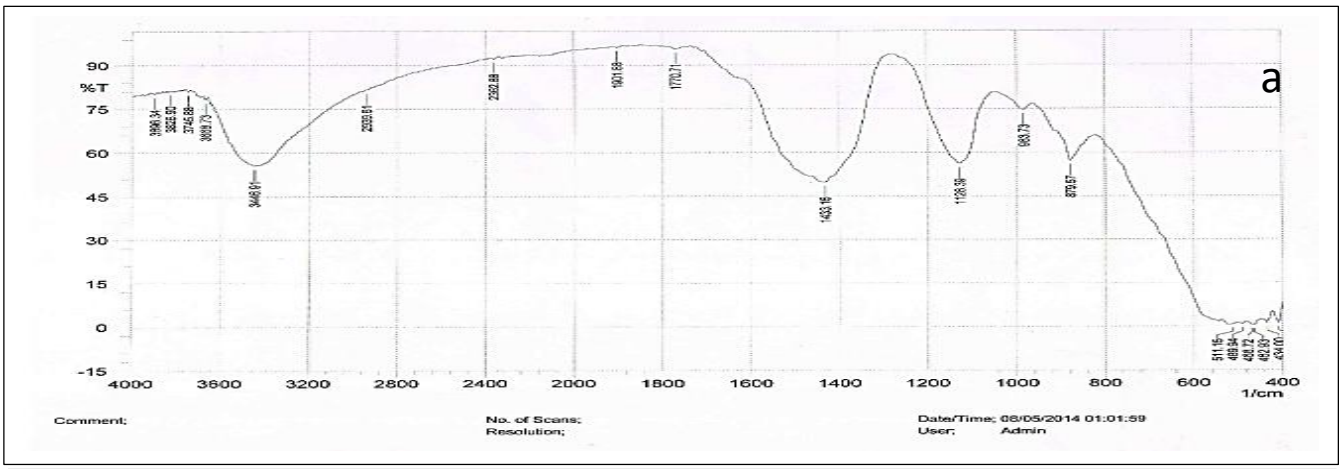

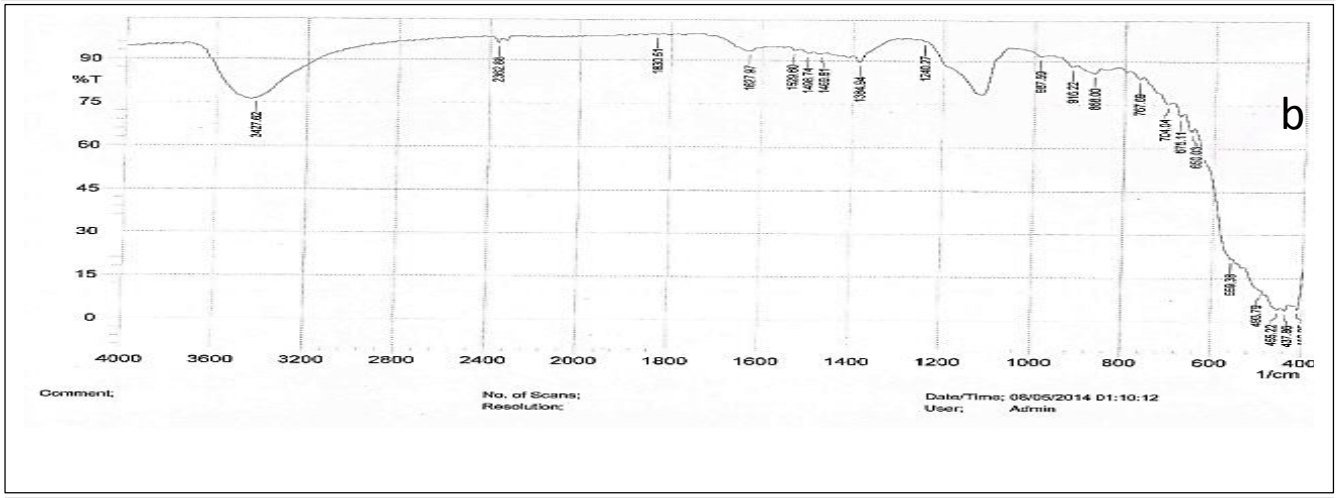

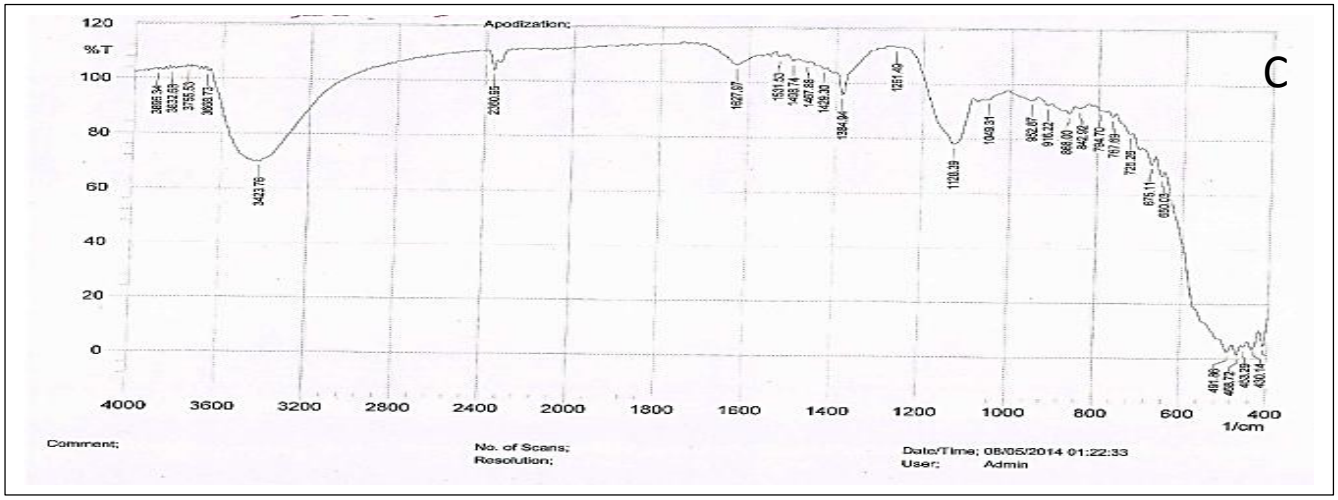

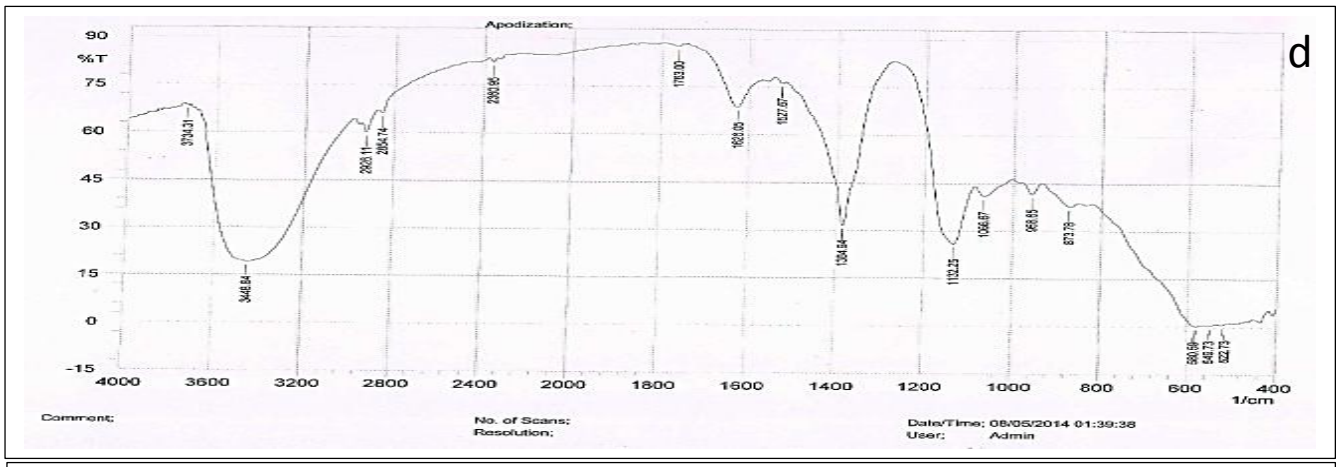
d
Apodization;
%T
1/cm
Comment;
No. of Scans;
Resolution;
Date/Time; 08/05/2014 01:39:38
User; Admin

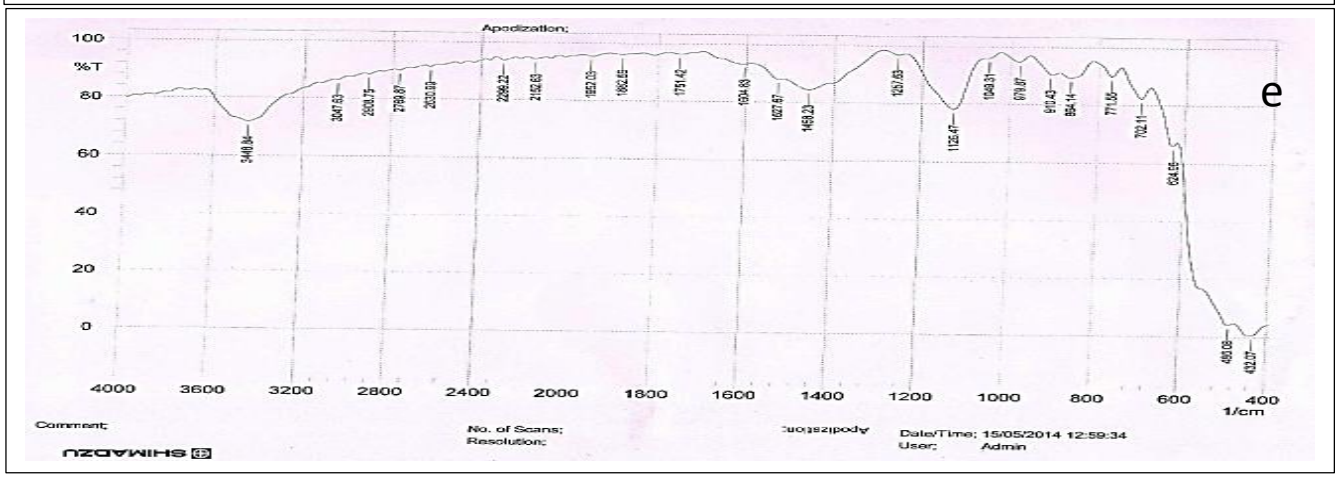
e
Apodization;
%T
1/cm
Comment;
No. of Scans;
Resolution;
Date/Time; 15/05/2014 12:59:34
User; Admin

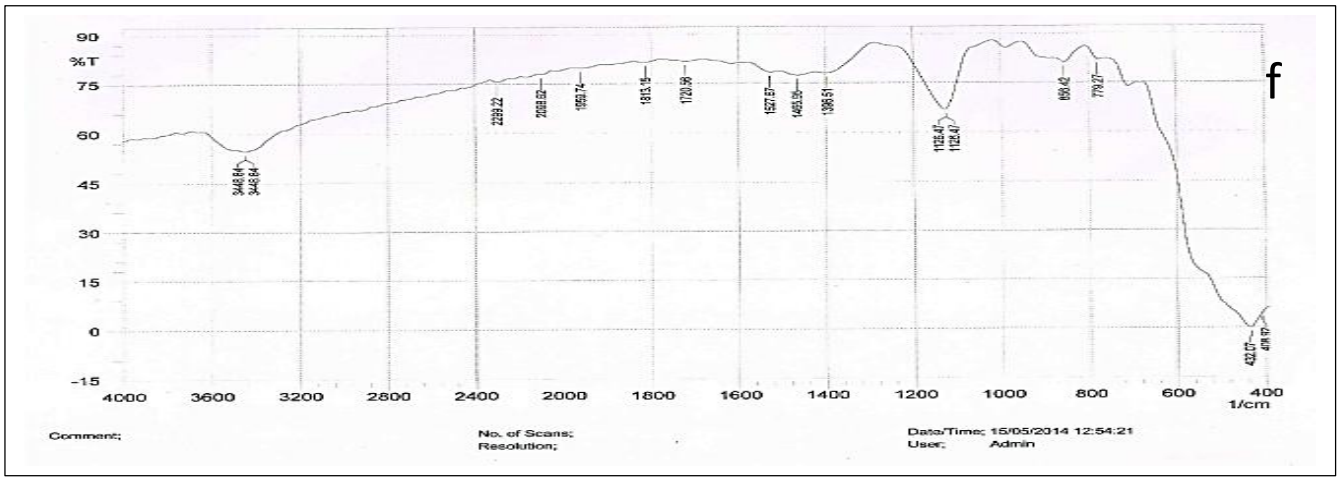
f
%T
1/cm
Comment;
No. of Scans;
Resolution;
Date/Time; 15/05/2014 12:54:21
User; Admin

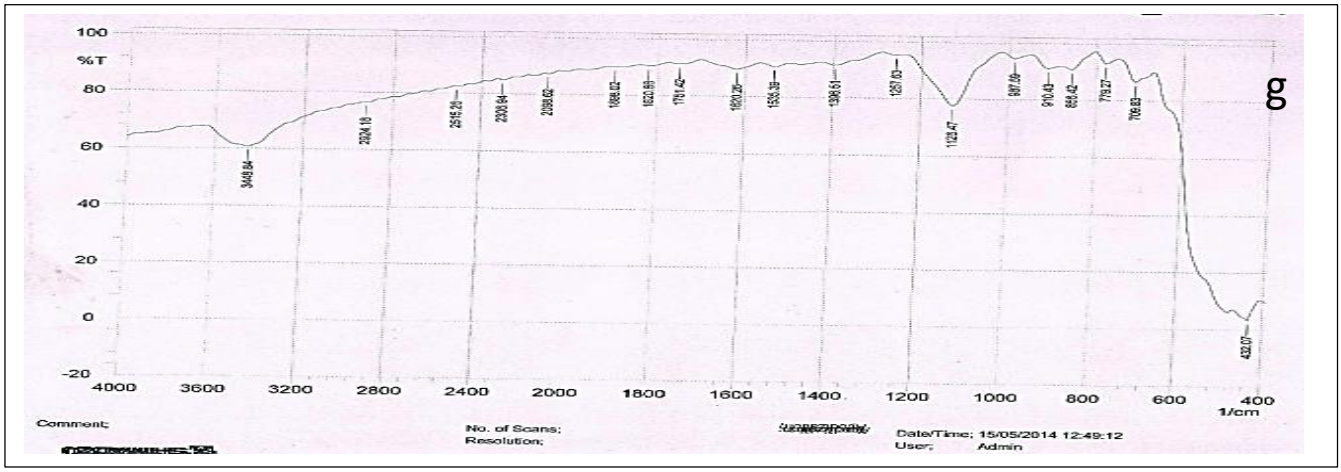
g
%T
1/cm
Comment;
No. of Scans;
Resolution;
Date/Time; 15/05/2014 12:49:12
User; Admin

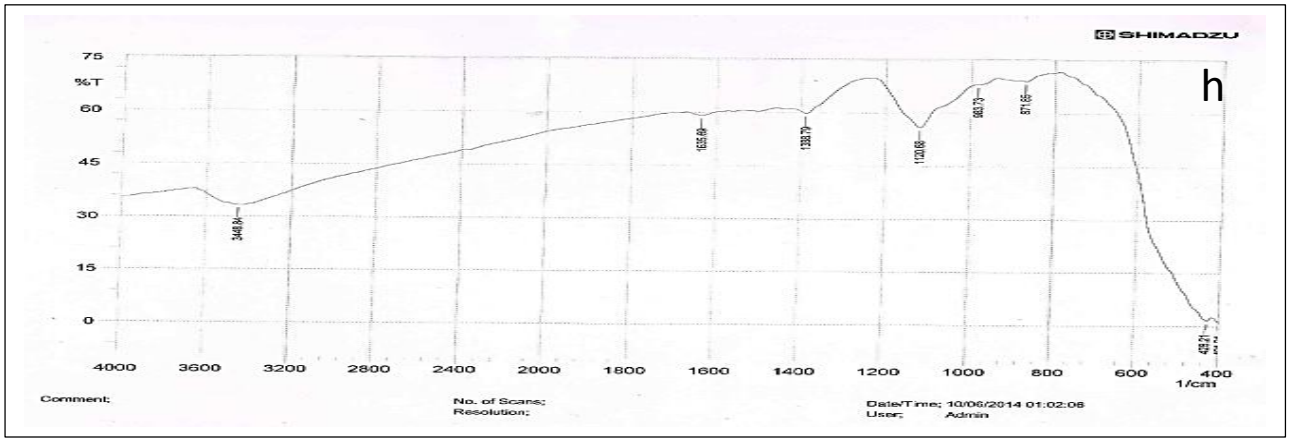

Figure 8 : FT-IR Spectra for Naked and Different Percentage of Co and Ag Loaded on ZnO Calcination at (500)ºC, at a)Naked ZnO at (500) ºC, b) Co(0.5)/ ZnO at (500)ºC, c)Co (1.00)/ ZnO at (500)ºC, d)Co(2.00)/ ZnO at (500)ºC , e)Ag(0.5)/ ZnO at (500)ºC ,f)Ag(1.00)/ZnO at (500)ºC ,g)Ag (2.00)/ZnO at (500)ºC, h)Ag (4.00)/ZnO at (500)ºC.

X-Ray Diffraction Spectroscopy (XRD)

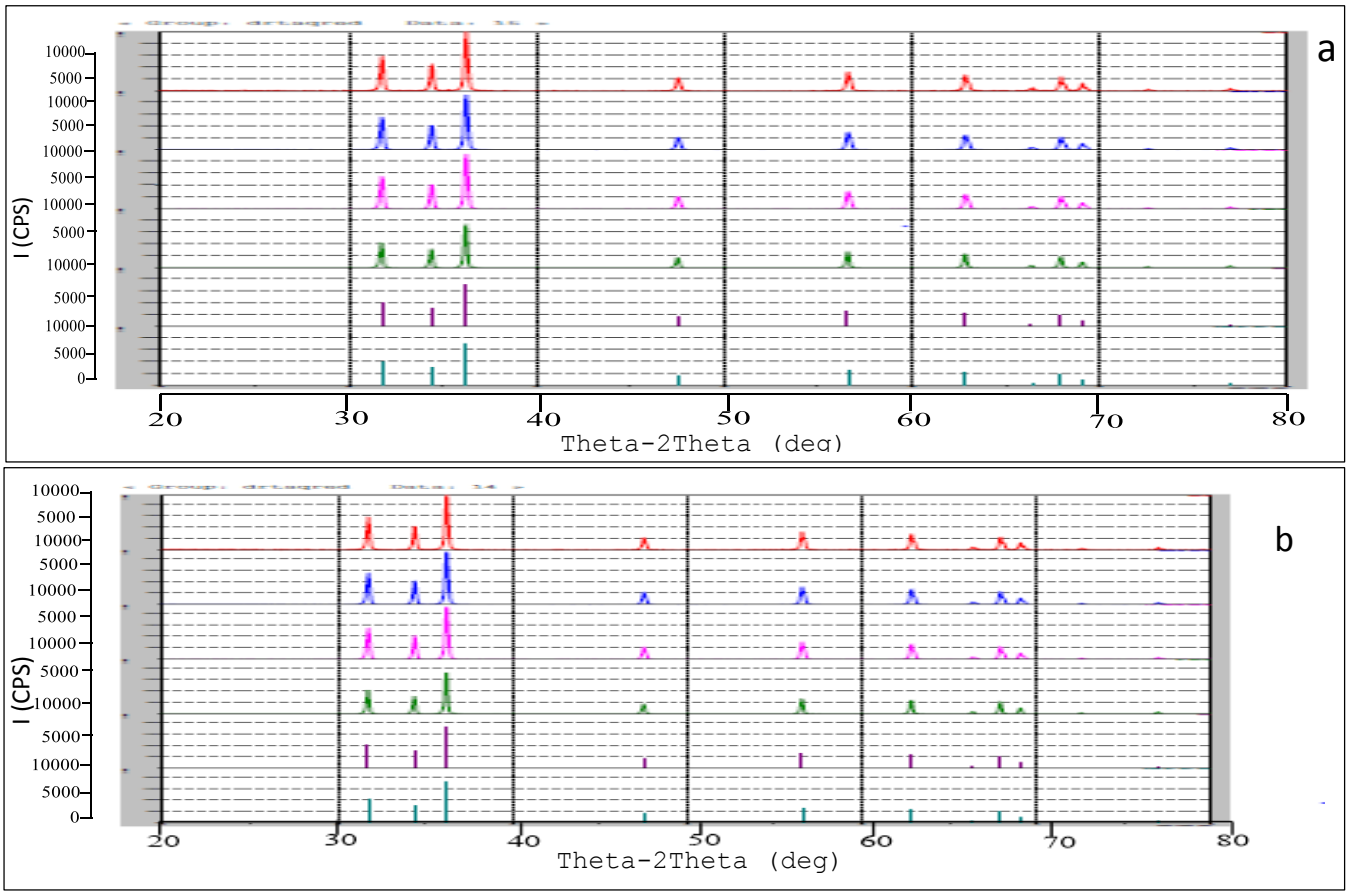

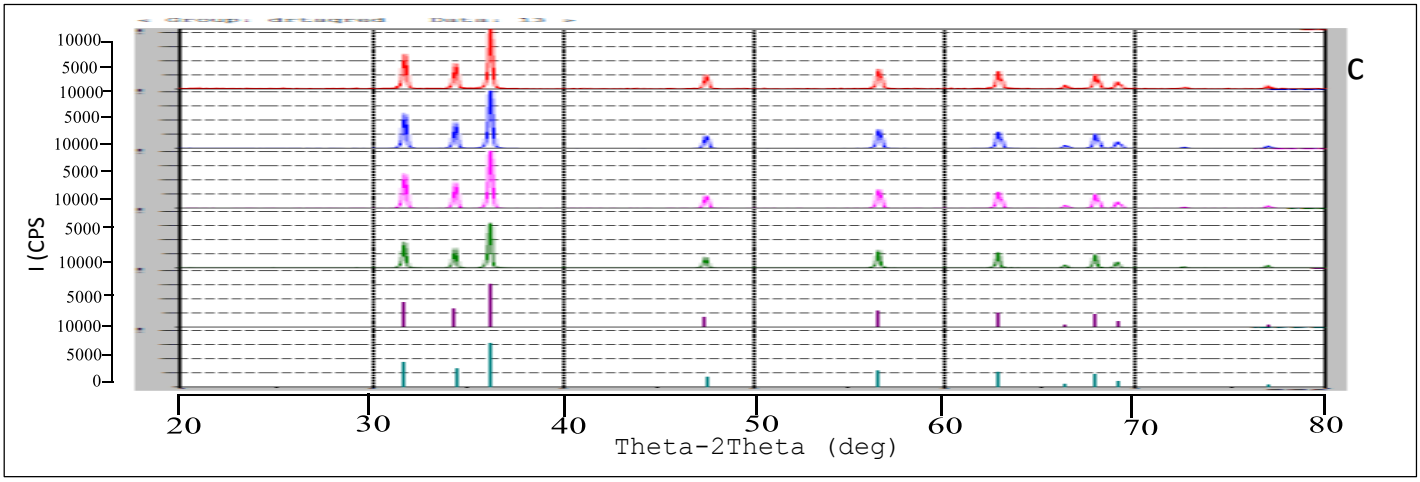
c
I (CPS
10000
5000
0
20
30
40
50
60
70
80
Theta-2Theta (deg)

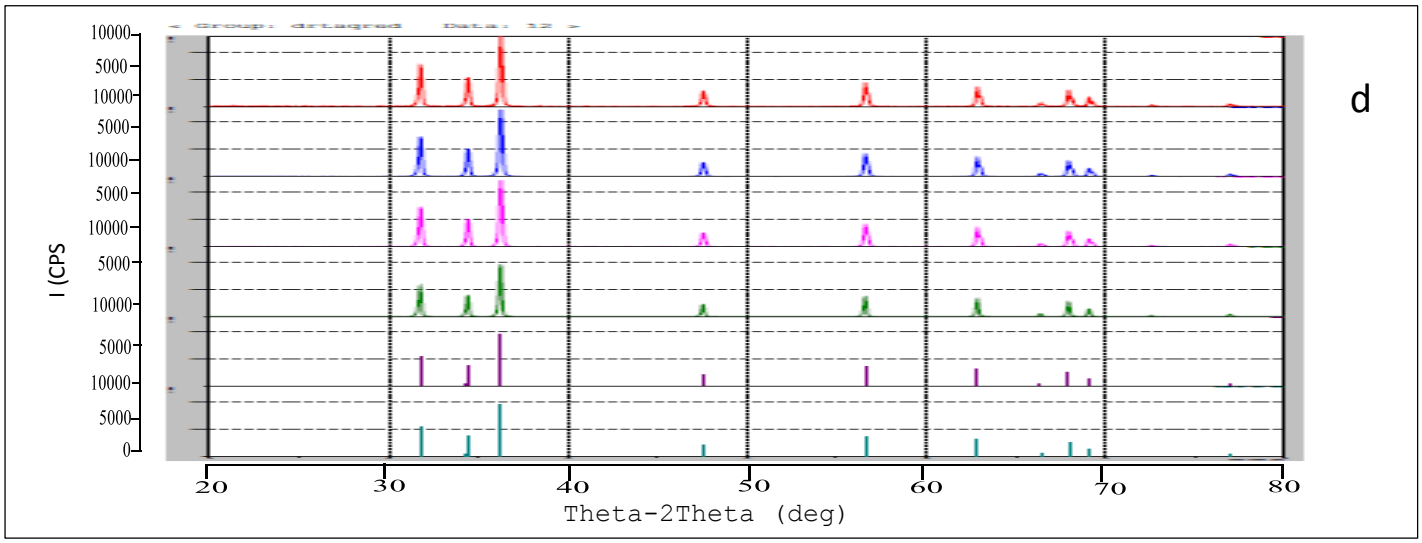
d
I (CPS
10000
5000
0
20
30
40
50
60
70
80
Theta-2Theta (deg)

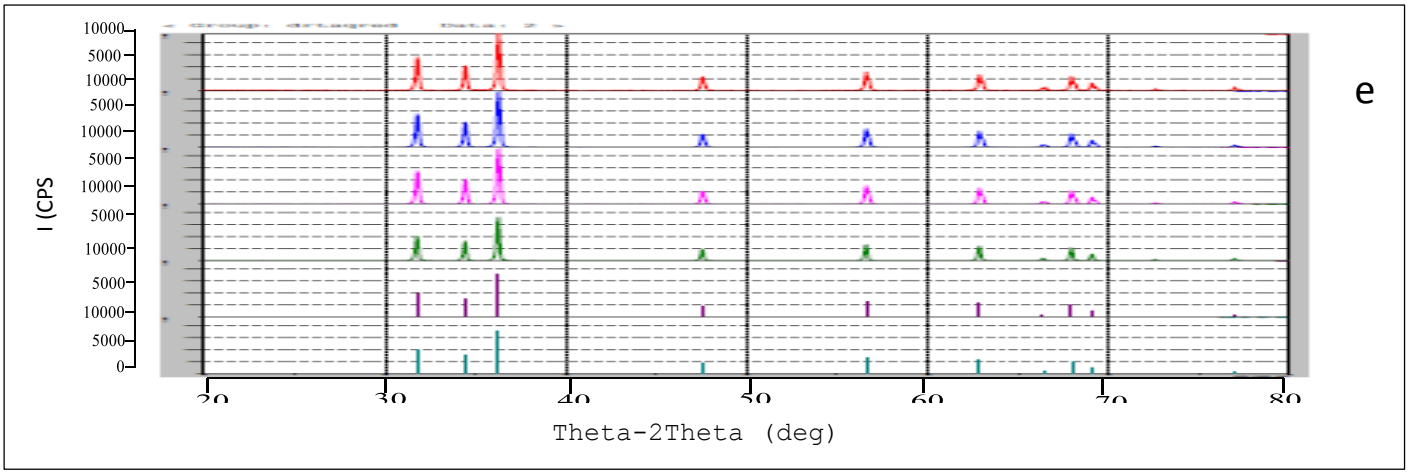
e
I (CPS
10000
5000
0
Theta-2Theta (deg)

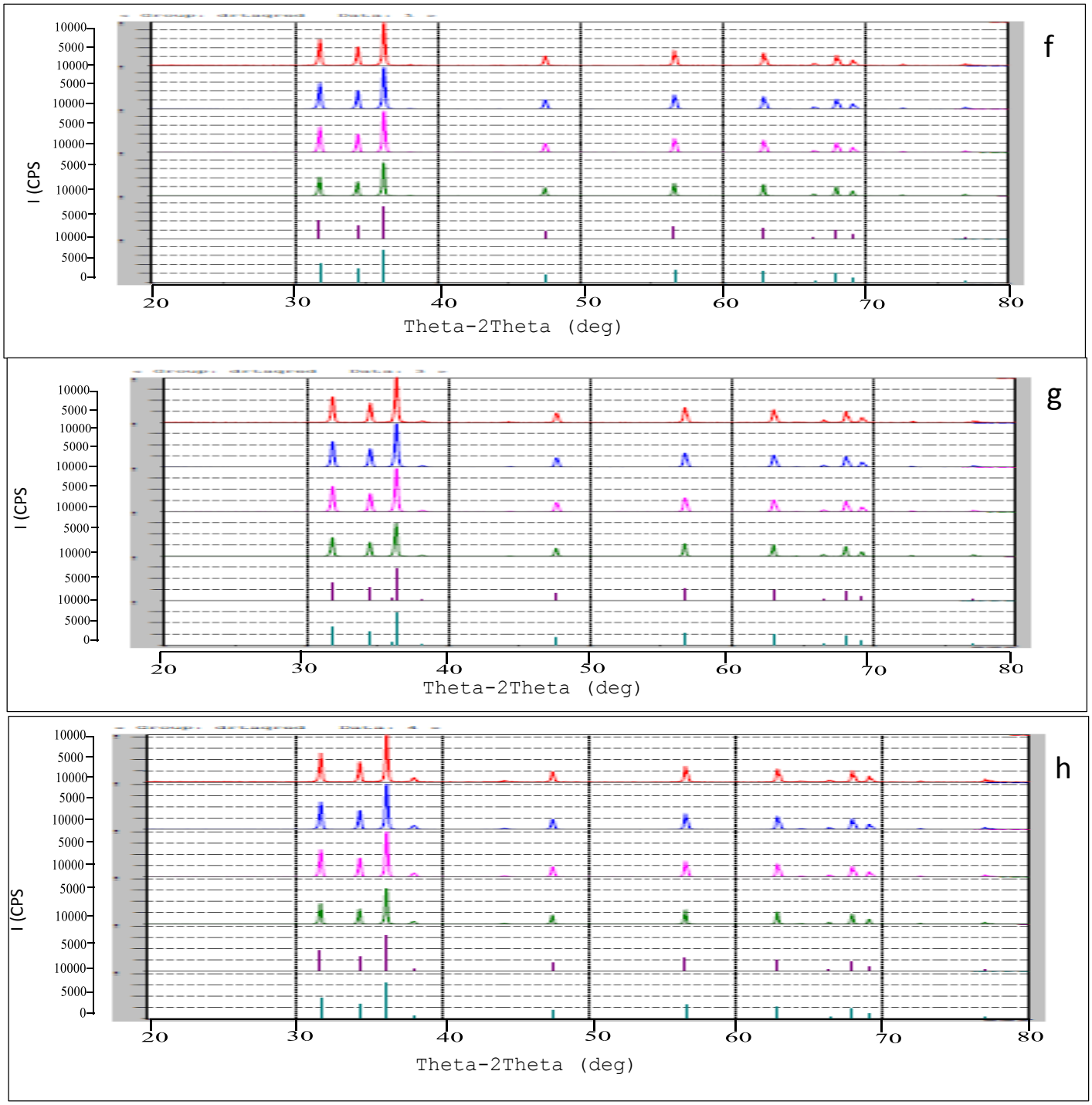

Figure 9 : X-Ray diffraction Spectra for Naked and Different Percentage of Co and Ag Loaded on Commercial ZnO, at a)Naked Commercial ZnO, b) Co(0.5)/ Commercial ZnO, c)Co (1.00)/ Commercial ZnO , d) Co(2.00)Commercial ZnO, e)Ag(0.5)/ Commercial ZnO, f) Ag(1.00)/Commercial ZnO, g)Ag (2.00)/Commercial ZnO , h)Ag (4.00)/Commercial ZnO .

Appendix (A)

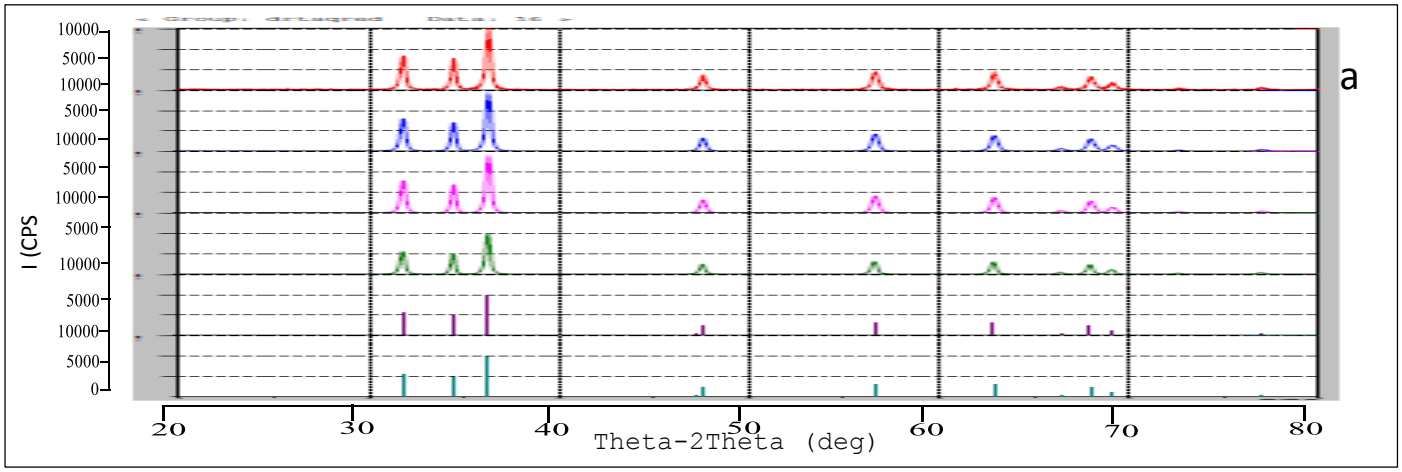
a
I (CPS
10000
5000
0
20
30
40
50
60
70
80
Theta-2Theta (deg)

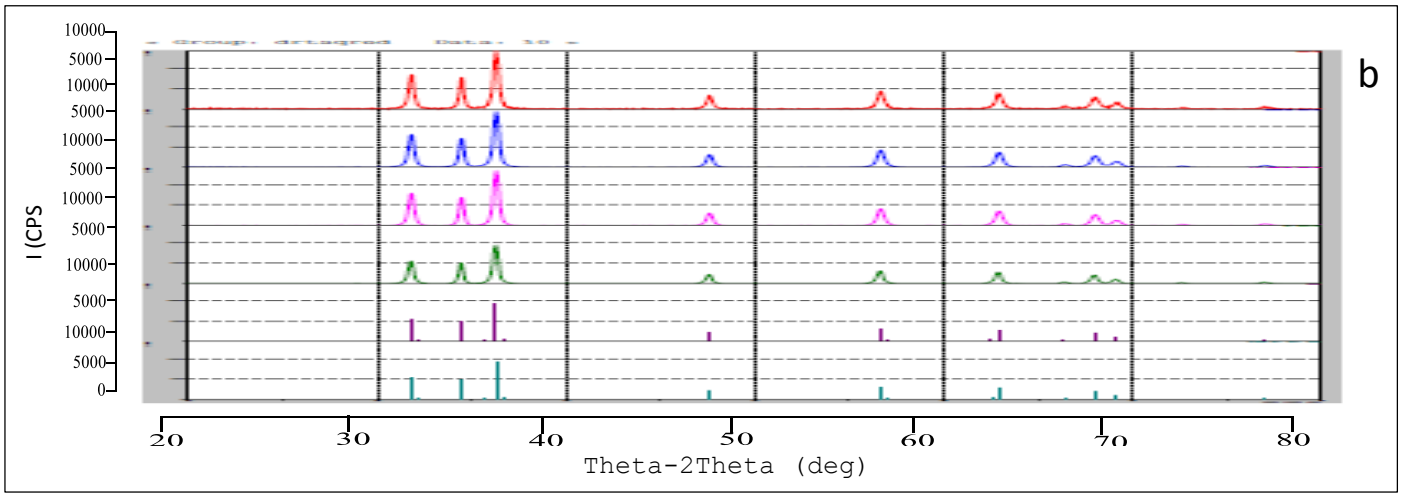
b
I (CPS
10000
5000
0
20
30
40
50
60
70
80
Theta-2Theta (deg)

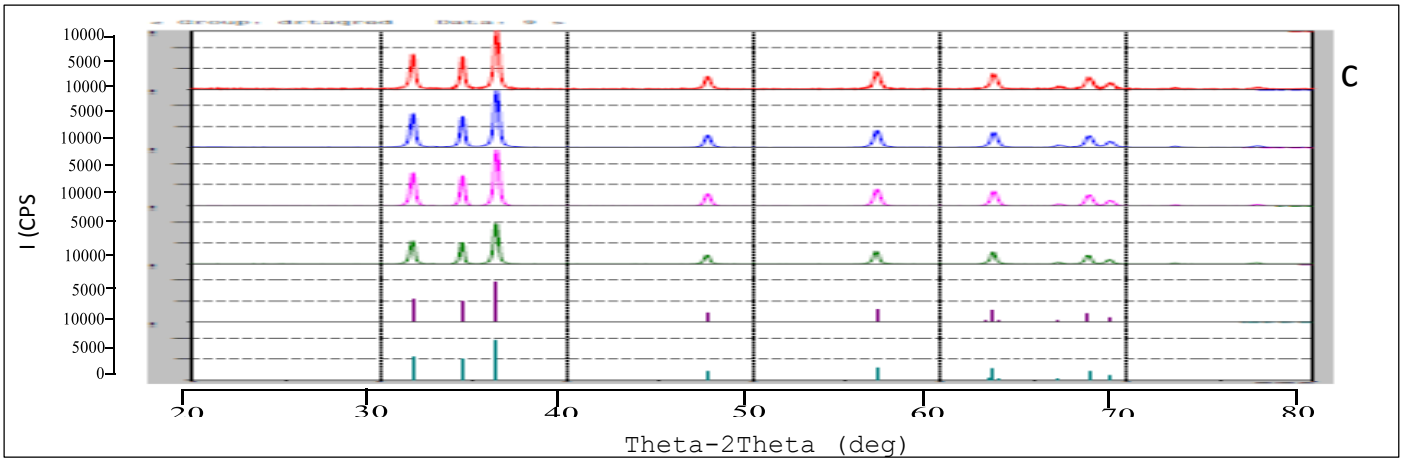
c
I (CPS
10000
5000
0
20
30
40
50
60
70
80
Theta-2Theta (deg)

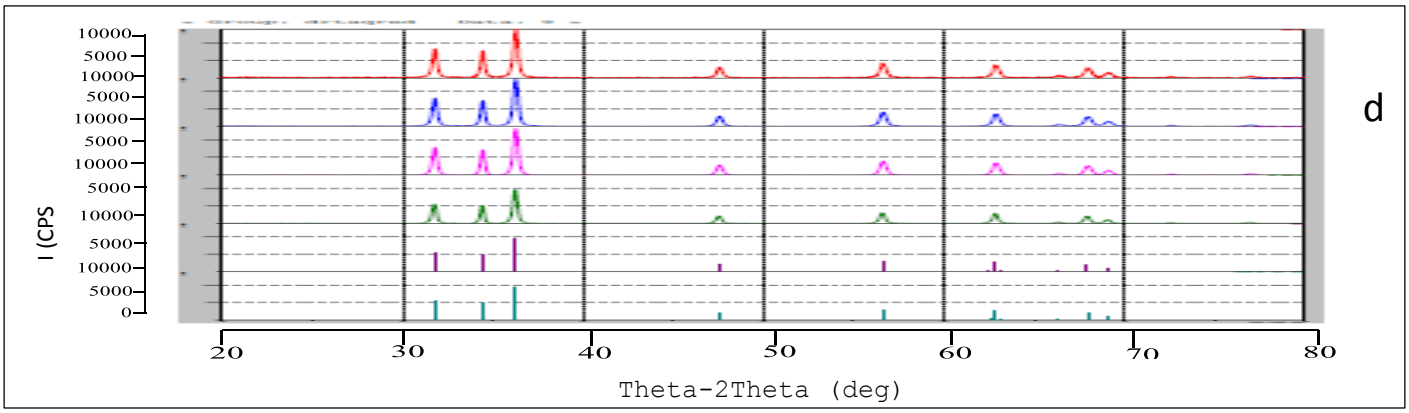
d
I (CPS
10000
5000
0
20
30
40
50
60
70
80
Theta-2Theta (deg)

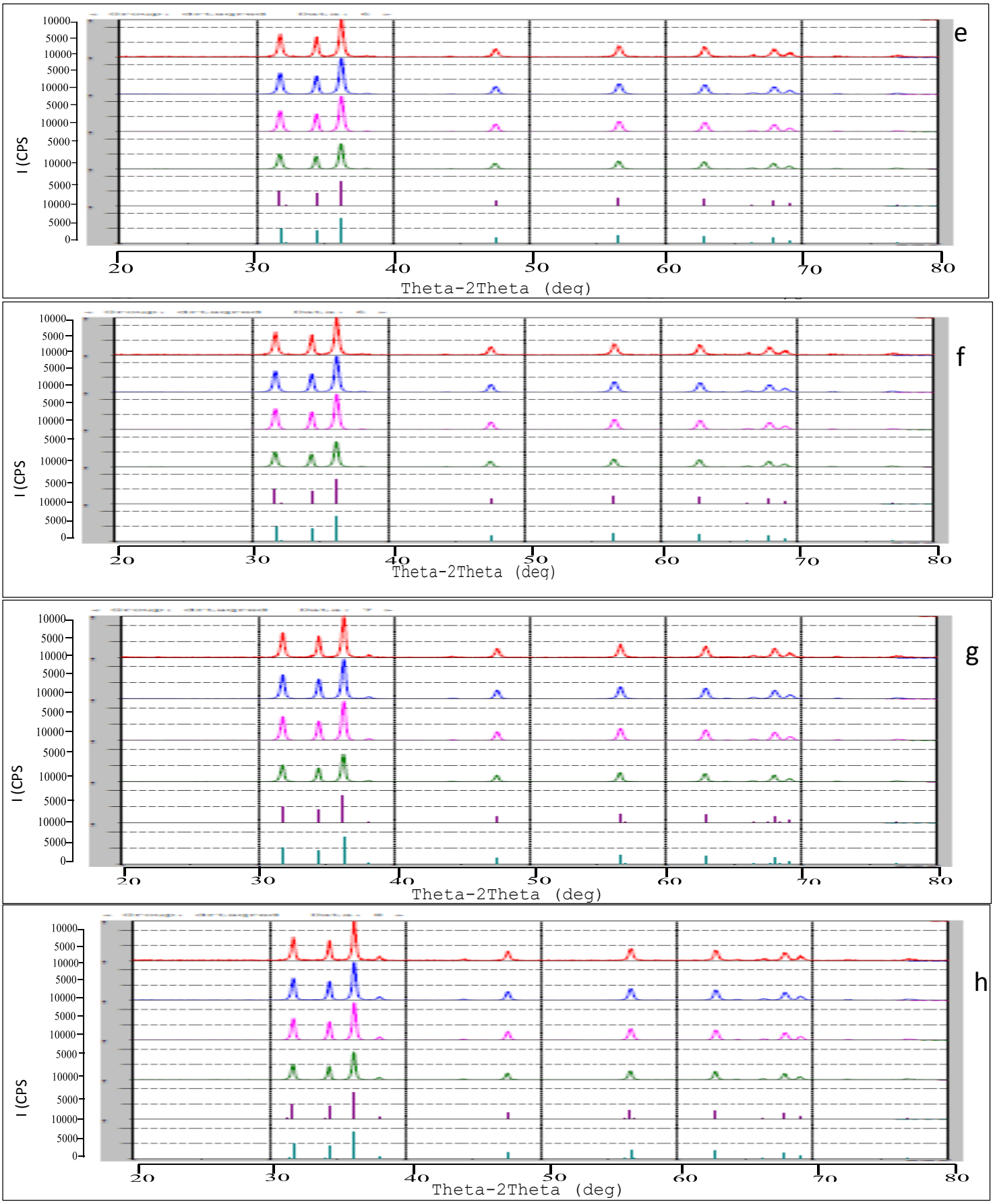

Figure 10 : X-RAY diffraction Spectra for Naked and Different Percentage of Co and Ag Loaded on ZnO Calcination at (500)^{O}C, at a)Naked ZnO at (500)^{O}C, b) Co(0.5)/ ZnO at (500)^{O}C c)Co (1.00)/ ZnO at (500)^{O}C, d)Co(2.00)/ ZnO at (500)^{O}C , e)Ag(0.5)/ ZnO at (500)^{O}C ,f)Ag(1.00)/ZnO at (500)^{O}C ,g)Ag (2.00)/ZnO at (500)^{O}C, h)Ag (4.00)/ZnO at (500)^{O}C

Appendix (B)

Table 1: The change of adsorption time in absence of radiation with ln $(C_o/C_{t)}$.

Adsorption time/min	Ln C_o/Ct	
	ZnO commercial	ZnO calcination at (500) ^OC
0	0	0
5	0.006	-0.003
10	0.009	-0.057
15	0.018	-0.054
20	0.019	-0.095
25	0.02	-0.137
30	0.024	-0.103

Table 2 : The change of adsorption time in presence of radiation with ln $(C_o/C_{t)}$.

Adsorption time/min	Ln $(C_o/C_{t)}$ at different methyl green concentration /ppm	
	50 ppm	25 ppm
0	0	0
5	-0.001	-0.001
10	-0.003	-0.093
15	-0.005	-0.121
20	-0.011	-0.134
25	-0.007	-0.151
30	-0.011	-0.154

Table 3 : The change of irradiation time on different methyl green concentrations with Commercial ZnO with C_t .

Irradiation Time /min	C_t at different methyl green concentration /ppm			
	25	50	75	100
0	16.21	32.631	47.263	46
5	5.526	16.131	29.657	31.947
10	3.157	7.394	18.157	21.894
15	1.368	4.184	11.157	15.315
20	1.684	1.973	5.789	10.289
25	1.421	0.947	3.236	9.526
30	1.21	0.815	1.973	5.684

Table 4: The change of irradiation time on different methyl green concentrations with Commercial ZnO with ln (C_o/C_t) .

Irradiation Time /min	ln (C_o/C_t) at different methyl green concentration /ppm			
	25	50	75	100
0	0	0	0	0
5	1.076	0.704	0.466	0.364
10	1.635	1.484	0.956	0.742
15	2.472	2.053	1.443	1.099
20	2.264	2.805	2.099	1.497
25	2.434	3.539	2.681	1.574
30	2.594	-	3.175	2.09

Table 5: Relationship between apparent rate constant with Commercial ZnO and Concentration of methyl green.

Methyl green Conc./ppm	k/min^{-1}
25	0.106
50	0.146
75	0.104
100	0.069

Table 6 : The change of irradiation time on different concentrations of methyl green with Commercial ZnO with Photocatalytic decolourization efficiency (PDE) .

Irradiation Time / min	P.D.E at different methyl green concentrations			
	25	50	75	100
0	0.000	0.000	0.000	0.000
5	65.909	50.564	37.249	30.549
10	80.519	77.338	61.581	52.402
15	91.558	87.177	76.391	66.704
20	89.61	93.951	87.75	77.631
25	91.233	97.096	93.151	79.29
30	92.532	97.5	95.824	87.643

Table 7 : The change of irradiation time on different dosages of Commercial ZnO with C_t .

Irradiation Time/min	C_t at different dosages						
	0.1	0.2	0.4	0.6	0.7	0.8	1
0	39.631	37.315	32.263	33.5	34.289	34.894	34.184
5	27.815	22	17.657	18	17.236	18.342	16.105
10	18.5	13.5	9.552	9.71	8.657	8.894	6.736
15	12.026	7.368	4.842	4.657	3.947	4.131	3.657
20	8.026	4.236	2.052	2.157	2.026	2.236	2.684
25	4.921	2.578	1.157	0.815	1.105	1.105	2.605
30	3.184	1.447	0.552	0.815	0.763	1.078	5.236

Table 8 : The change of irradiation time on different Dosage of Commercial ZnO with $\ln(C_o/C_t)$.

Irradiation Time/min	$Ln(C_o/C_t)$ at different dosages						
	0.1	0.2	0.4	0.6	0.7	0.8	1
0	0.000	0.000	0.000	0.000	0.000	0.000	0.000
5	0.354	0.528	0.602	0.621	0.687	0.643	0.752
10	0.761	1.016	1.217	1.238	1.376	1.366	1.624
15	1.192	1.622	1.896	1.972	2.161	2.133	2.234
20	1.596	2.175	2.754	2.742	2.828	2.747	2.544
25	2.086	2.672	3.327	3.715	-	3.452	2.574
30	2.521	3.249	4.066	3.715	-	3.476	-

Table 9 : The Relation ship between apparent rate constant of Methyl green with ZnO Commercial and dosage .

Dosage	k /(min^{-1})
0	0
0.1	0.082
0.2	0.107
0.4	0.133
0.6	0.133
0.7	0.134
0.8	0.129
1	0.122

Table 10 : The change irradiation time on different dosages of Commercial ZnO with photocatalytic decolourization efficiency(PDE).

Irradiation Time/min	P.D.E at different dosages						
	0.1	0.2	0.4	0.6	0.7	0.8	1
0	0.000	0.000	0.000	0.000	0.000	0.000	0.000
5	29.814	41.043	45.269	46.268	49.731	47.435	52.886
10	53.32	63.822	70.391	71.013	74.75	74.509	80.292
15	69.654	80.253	84.991	86.095	88.488	88.159	89.299
20	79.747	88.645	93.637	93.558	94.09	93.589	92.147
25	87.583	93.088	96.411	97.564	96.776	96.832	92.378
30	91.965	96.121	98.287	97.564	97.774	96.907	84.68

Table 11 : The change of irradiation time at different value of pH for Commercial ZnO with C_t .

Irradiation Time/min	C_t at different pH						
	2	**4**	**5.4**	**6**	**8**	**9**	**10**
0	31.631	42.184	26.236	37	29.605	24.289	19.605
5	24.973	25.131	15.815	20.184	16.236	13.526	10.026
10	20.105	14.894	9.947	11.263	9.236	7.552	5.473
15	16.236	8.315	6.131	6.394	4.763	3.973	3.026
20	12.5	4.578	3.578	3.473	2.21	2.052	1.552
25	9.631	2.157	2.078	1.789	1.552	1.315	0.894
30	7.21	1.289	1.342	0.894	0.868	0.921	0.605
35	5.5	0.921	0.842	0.578	0.5	0.868	0.552
40	3.5	0.394	0.184	0.947	0.21	0.447	0.236

Table 12 : The change of irradiation time at different value of initial pH with commercial ZnO with ln(C_o/C_t) .

Irradiation Time/min	ln (C_o/C_t) at different pH						
	2	**4**	**5.4**	**6**	**8**	**9**	**10**
0	0.000	0.000	0.000	0.000	0.000	0.000	0.000
5	0.236	0.517	0.506	0.606	0.6	0.585	0.67
10	0.453	1.041	0.969	1.189	1.164	1.168	1.275
15	0.666	1.623	1.453	1.755	1.827	1.81	1.868
20	0.928	2.22	1.992	2.365	2.594	2.47	2.535
25	1.189	2.972	2.535	3.028	2.948	2.915	3.087
30	1.478	3.487	2.972	3.722	3.529	3.272	3.477
35	1.749	-	3.439	4.157	4.081	-	-
40	-	4.671	-	-	4.946	-	-

Table 13 : Apparent rate constant with initial pH by commercial ZnO.

pH	k/ min^{-1}
2	0.048
4	0.115
5.40	0.099
6	0.12
8	0.12
9	0.115
10	0.121

Table 14 : The change of irradiation time on different initial pH with Commercial ZnO with photocatalytic Decolourization efficiency (PDE) .

Irradiation Time/min	P.D.E at different pH						
	2	**4**	**5.4**	**6**	**8**	**9**	**10.00**
0	0.000	0.000	0.000	0.000	0.000	0.000	0.000
5	21.048	40.424	39.719	45.448	45.155	44.312	48.859
10	36.439	64.691	62.086	69.559	68.8	68.905	72.080
15	48.668	80.286	76.629	82.716	83.911	83.640	84.563
20	60.482	89.145	86.359	90.611	92.533	91.549	92.086
25	69.550	94.884	92.076	95.163	94.755	94.582	95.436
30	77.204	96.943	94.884	97.581	97.066	96.208	96.912
35	82.612	97.816	96.790	98.435	98.311	96.424	97.181
40	88.935	99.064	99.297	97.439	99.288	98.158	98.791

Table 15 : The change of irradiation time at different temperature of methyl green solution with Commercial ZnO with C_t .

Irradiation Time/min	C_t at different temperature /K			
	278.15	283.15	288.15	293.15
0	8.578	8.184	34.289	22.736
5	4.921	4.71	17.236	11.236
10	3.526	3.21	8.657	5.631
15	2.078	2.263	3.947	2.868
20	1.421	2	2.026	1.868
25	0.921	1.289	1.105	1.263
30	0.763	0.842	0.763	1.105
35	0.578	0.789	-	1
40	0.5	0.578	-	0.894

Table 16 : The change of irradiation time at different temperature of methyl green solution with Commercial ZnO with $\ln(C_o / C_t)$.

Irradiation Time/min	$\ln(C_o/C_t)$ at different temperature/ K			
	278.15	283.15	288.15	293.15
0	0.000	0.000	0.000	0.000
5	0.555	0.552	0.687	0.704
10	0.889	0.935	1.376	1.395
15	1.417	1.285	2.161	2.07
20	1.797	-	2.828	2.498
25	2.231	-	3.434	2.89
30	2.419	-	3.805	-
35	2.695	-	-	-
40	2.842	-	-	-

Table 17 : The change of lnk with ln k .

$(10^3/T)/K$	Lnk /(min^{-1})
3.59	-2.538
3.53	-2.419
3.47	-1.973
3.41	-2.087

Table 18 :The change of ln (k/T)with (1/T)

$(10^3/T)/K$	Lnk/T/$(min^{-1} K^{-1})$
3.59	-8.17
3.53	-8.07
3.47	-7.36
3.41	-7.77

Table 19 : The activation kinetic parameters of the decolourization of methyl green dye with commercial ZnO .

E_a kJ mol^{-1}	$\Delta H^{\#}$ kJ mol^{-1}	$\Delta S^{\#}$ kJ mol^{-1} K^{-1}	$\Delta G^{\#}_{288.15}$ kJ mol^{-1}
24.914	22.489	-0.184	75.675

Table 20 : The change of irradiation time on different Temperture of methyl green solution with Commercial ZnO with photocatalytic Decolourization efficiency (PDE) .

Irradiation Time/min	P.D.E at different temperature/ K			
	278.15	283.15	288.15	293.15
0	0.000	0.000	0.000	0.000
5	42.638	42.443	49.731	50.578
10	58.895	60.771	74.75	75.231
15	75.766	72.347	88.488	87.384
20	83.435	75.562	94.09	91.782
25	89.263	84.244	96.776	94.444
30	91.104	89.71	97.774	95.138
35	93.251	90.353	98.004	95.601
40	94.171	92.926	98.234	96.064

Table 21: Different Percentage of Co Loaded on commercial ZnO Surface.

Co%	k/min^{-1}
0	0.141
0.5	0.114
1	0.107
2	0.087

Table 22 : Different Percentage of Ag Loaded on Commercial ZnO Surface .

Ag%	k/min^{-1}
0	0.141
0.5	0.099
1	0.108
2	0.144
4	0.085

Table 23 : The change of C_t with irradiation time on different dye concentrations for with (2.00)Ag /Commercial ZnO.

Irradiation Time /min	C_t at different methyl green concentration /ppm			
	25	50	75	100
0	3.815	10.342	10.21	10.736
5	3.5	4	7.578	6.078
10	3.421	3.815	7.105	3.947
15	2.184	2.21	3.105	3.184
20	1.947	2	2.184	2.868
25	1.868	1.263	1.605	2.605
30	1.815	0.842	1.368	2.473
35	1.71	0.736	1.078	2.315
40	1.657	0.578	1	2.157

Table 24 : The change of irradiation time on different methyl green concentrations with Ag(2.00)/ commercial ZnO with ln (C_o/C_t) .

Irradiation Time /min	ln (C_o/C_t) at different methyl green concentration /ppm			
	25	50	75	100
0	0.000	0.000	0.000	0.000
5	0.086	0.949	0.298	0.568
10	0.109	0.997	0.362	1
15	0.557	1.542	1.19	1.215
20	0.672	1.643	1.542	1.319
25	0.714	2.102	1.85	1.416
30	0.742	-	2.009	1.467

Table 25 : apparent rate constant for Ag (2.00)/commercial ZnO with Concentration .

Dye Concentration /ppm	k/min^{-1}
25	0.027
50	0.087
75	0.07
100	0.06

Table 26 : The change of irradiation time on different concentration of methyl green with Ag (2.00)/Commercial ZnO with photocatalytic Decolourization efficiency (PDE) .

Irradiation Time/min	P.D.E at different methyl green concentration			
	25	50	75	100
0	0.000	0.000	0.000	0.000
5	8.275	61.323	25.773	43.382
10	10.344	63.104	30.412	63.235
15	42.758	78.625	69.587	70.343
20	48.965	80.661	78.608	73.284
25	51.034	87.786	84.278	75.735
30	52.413	91.857	86.597	76.96

Table 27: The change of irradiation time on different dosages of Ag (2.00)/ Commercial ZnO with C_t .

Irradiation Time/min	C_t at different dosages						
	0.1	**0.2**	**0.4**	**0.6**	**0.7**	**0.8**	**1**
0	7.552	6.631	7.105	7.973	10.342	6.815	7.026
5	4.157	3.947	3.552	3.868	4	3.657	3.289
10	3.105	2.815	2.552	2.789	3.815	2.105	1.789
15	2.631	2.421	1.973	2.342	2.21	2.052	1.736
20	2.368	2.236	1.868	2.131	2.000	1.921	1.684
25	1.894	2.157	1.815	2.078	1.263	1.842	1.552
30	1.815	2.105	1.71	1.736	0.842	1.789	1.526
35	1.657	2.026	1.578	1.684	0.736	1.657	1.421
40	1.605	1.947	1.447	1.631	0.578	1.578	1.342

Table 28 : The change of irradiation time on different dosages of Ag (2.00)/ Commercial ZnO with $ln(C_o/C_t)$.

Irradiation Time/min	$Ln(C_o/C_t)$ at different dosages/ (mg/200mL)						
	0.1	0.2	0.4	0.6	0.7	0.8	1
0	0	0	0	0	0	0	0
5	0.596	0.518	0.693	0.723	0.949	0.629	0.758
10	0.888	0.856	1.023	1.05	0.997	1.174	1.367
15	1.054	1.007	1.28	1.225	1.542	1.2	1.397
20	1.59	1.086	1.335	1.319	1.643	1.266	1.428
25	1.382	1.122	1.364	1.344	2.102	1.308	1.509

Table 29: The Relation ship between rate constant and dosage of Ag(2.00)/ ZnO commercial.

Catalyst dosages/ g	(k /min^{-1})
0.0	0
0.1	0.062
0.2	0.055
0.4	0.068
0.6	0.067
0.7	0.089
0.8	0.066
1.0	0.076

Table 30 : The change of irradiation time on different dosages of Ag (2.00)/Commercial ZnO with photocatalytic Decolourization efficiency (PDE) .

Irradiation Time/min	P.D.E at different catalyst dosages						
	0.1	0.2	0.4	0.6	0.7	0.8	1
0	0.000	0.000	0.000	0.000	0.000	0.000	0.000
5	44.95	40.48	50	51.49	61.32	46.33	53.18
10	58.89	57.54	64.07	65.02	63.1	69.11	74.53
15	65.16	63.49	72.22	70.63	78.63	69.88	75.28
20	68.64	66.27	73.7	73.27	80.66	71.81	76.03
25	74.91	67.46	74.44	73.93	87.79	72.97	77.9

Table 31 : The change of irradiation time at different value of pH with Ag(2.00)/ commercial ZnO with C_t .

Irradiation Time/min	C_t at different pH						
	2	**4**	**5.4**	**6**	**8**	**9**	**10**
0	13.552	9.71	10.342	6.236	5.236	4.157	1.921
5	5.578	4.684	4	2.973	5.236	2.71	1.736
10	3.578	2.21	3.815	1.815	5.236	2.289	1.71
15	2.684	2.105	2.21	1.763	5.236	2.105	1.736
20	2.315	2.026	2	1.71	5.236	2.052	1.736
25	2.157	1.763	1.263	1.578	5.236	2	1.736
30	2.078	1.578	0.842	1.368	5.236	2	1.71
35	2.052	1.421	0.736	1.315	5.236	2	1.657
40	2	1.315	0.578	1.263	5.236	2	1.578

Table 32 : The change of irradiation time at different value of pH with Ag (2.00)/ commercial ZnO with $\ln(C_o/C_t)$.

Irradiation Time/min	$\ln (C_o/C_t)$ at different pH						
	2	**4**	**5.4**	**6**	**8**	**9**	**10**
0	0	0	0	0	0	0	0
5	0.887	0.729	0.949	0.74	0.771	0.427	-
10	1.331	1.479	0.997	1.233	0.793	0.596	-
15	1.619	1.528	1.542	1.263	0.911	0.68	0.1
20	1.766	1.566	1.643	1.293	0.962	0.705	0.1
25	1.837	1.706	2.102	1.373	0.989	0.731	0.1
30	-	-	-	-	-	-	0.116
35	-	-	-	-	-	-	0.147
40	-	-	-	-	-	-	0.196

Table 33: Relationship between apparent rate constant and initial pH with Ag (2.00)/ commercial ZnO.

pH	k/min^{-1}
2	0.089
4	0.083
5.4	0.089
6	0.069
8	0.05
9	0.036
10	0.004

Table 34: The change of irradiation time on different initial pH of solution with photocatalytic Decolourization efficiency (PDE) with Ag (2.00)/commercial ZnO.

Irradiation Time/min	P.D.E at different pH						
	2	**4**	**5.4**	**6**	**8**	**9**	**10**
0	0	0	0	0	0	0	0
5	58.834	51.761	61.323	52.32	53.768	34.81	9.589
10	73.592	77.235	63.104	70.886	54.773	44.936	10.958
15	80.194	78.319	78.625	71.729	59.798	49.367	9.589
20	82.912	79.132	80.661	72.573	61.809	50.632	9.589
25	84.077	81.842	87.786	74.683	62.814	51.898	9.589
30	84.66	83.739	91.857	78.059	62.814	51.898	10.958
35	84.854	85.365	92.875	78.902	64.321	51.898	13.698

Table 35 : The change of irradiation time at different temperature of solution with C_t with Ag (2.00)/ Commercial ZnO.

Irradiation Time/min	C_t at different temperature /K			
	278.15	283.15	288.15	293.15
0	7.526	7.5	9.526	7.763
5	5.763	3.868	9.526	4.131
10	3.315	1.578	9.526	2.368
15	1.947	1.447	9.526	1.789
20	1.342	1.052	9.526	1.421
25	1.105	1.026	9.526	1.21
30	0.894	0.947	9.526	1.157
35	0.842	0.868	9.526	1.131
40	0.789	0.815	9.526	1.052

Table 36 : The change of irradiation time at different temperature of Ag (2.00)/commercial ZnO with $\ln(C_o/C_t)$.

Irradiation Time/min	$\ln(C_o/C_t)$ at different temperature/ K			
	278.15	283.15	288.15	293.15
0	0	0	0	0
5	0.266	0.662	0.744	0.63
10	0.819	1.558	1.129	1.187
15	1.351	1.645	1.296	1.467
20	1.724	1.963	1.797	1.697
25	1.918	1.988	1.979	-
30	-	2.068	-	-

Table 37: Relationship between lnk and $(10^3/T)$ with Ag (2.00)/commercial ZnO .

$(10^3/T)/K$	Lnk /(min^{-1})
3.59	-2.505
3.53	-2.458
3.47	-2.439
3.4	-2.357

Table 38 : Relationship between ln (k/T) and$(10^3/T)/K$ with Ag (2.00)/Commercial ZnO .

$(10^3/T)/K$	$Lnk/T/(min^{-1} K^{-1})$
3.59	-8.134
3.53	-8.104
3.47	-8.103
3.4	-8.037

Table 39: The activation kinetic parameters of the decolourization of methyl green dye with Ag(2.00)/commercial ZnO.

E_a kJ mol^{-1}	$\Delta H^{\#}$ kJ mol^{-1}	$\Delta S^{\#}$ kJ mol^{-1} K^{-1}	$\Delta G^{\#}_{303.15}$ kJ mol^{-1}
6.185	3.879	-0.251	79.969

Table 40 : The change of irradiation time on different Temperature of Solution with Ag (2.00)/ commercial ZnO photocatalytic with decolourization efficiency (PDE) .

Irradiation Time/min	P.D.E at different temperature/ K		
	278.15	288.15	293.15
0	0	0	0
5	23.426	52.486	0.63
10	55.944	67.679	1.187
15	74.125	72.651	1.467
20	82.167	83.425	1.697
25	85.314	86.187	84.406
30	88.111	88.121	85.084

Table 41: The change of irradiation time on different temperatures of calcination with prepared ZnO with C_t .

Irradiation	C_t at different temperatures of calcination		
Time/min	**300 ºC**	**500 ºC**	**700 ºC**
0	2.657	4	1.105
5	1.447	2.421	0.921
10	1.052	1.552	0.894
15	1.078	1.315	0.973
20	1.078	1.315	0.894
25	1.026	1.236	0.921
30	1	1.184	0.947
35	0.947	1.052	1
40	-	0.868	1

Table 42 : The change of irradiation time on different temperatures of calcination with prepared ZnO with ln C_o/C_t .

Irradiation	Ln Co/ C_t at different temperatures of calcination		
Time/min	**300 ^{O}C**	**500 ^{O}C**	**700 ^{O}C**
0	0	0	0
5	0.607	0.502	0.182
10	0.926	0.946	0.211
15	0.926	1.111	0.126
20	0.901	1.111	0.211
25	0.901	1.173	0.182
30	0.951	1.217	0.154
35	0.977	1.335	0.1
40	0.031	1.527	0.1

Table 43 : The effect of Calcination on the apparent rate constant with prepared ZnO

t/^{o}C	**k/min^{-1}**
0	0
300	0.074
500	0.081
700	0.013

Table 44 : The change of irradiation time on different temperatures of calcination with prepared ZnO with photocatalytic decolorization efficiency (P.D.E) .

Irradiation	P.D.E at different temperatures of calcination		
Time/min	300 ºC	500 ºC	700 ºC
0	0	0	0
5	45.544	39.473	16.666
10	60.396	61.184	19.047
15	60.396	67.105	11.904
20	59.405	67.105	19.047
25	59.405	69.078	16.666
30	61.386	70.394	14.285
35	62.376	73.684	9.523
40	64.356	78.289	9.523

Table 45 : The change of irradiation time on different methyl green concentrations for prepared ZnO and calcinated at (500)^{o}C with Ct.

Irradiation	C_t at different methyl green concentration /ppm			
Time/min	25	50	75	100
0	1.368	1.736	1.578	1.289
5	1.289	1.447	1.552	1.289
10	1.263	1.447	1.473	1.263
15	1.052	1.447	1.447	1.263
20	1	1.447	1.447	1.263
25	1	1.394	1.447	1.21
30	0.973	1.394	1.447	1.21
35	0.868	1.368	1.447	1.21
40	0.842	1.315	1.447	1.21

Table 46 : The change of irradiation time on different methyl green concentrations for prepared ZnO and calcinated at (500) ^{o}C with ln (C_o/C_t).

Irradiation	ln (C_o/C_t)at different methyl green concentration /ppm			
Time/min	25	50	75	100
0	0	0	0	0
5	0.059	0.182	0.016	0.02
10	0.08	0.182	0.068	0.041
15	0.0262	0.182	0.087	0.041
20	0.313	0.182	0.087	0.063
25	0.313	0.219	0.087	0.063
30	0.34	0.219	-	-
35	0.454	0.238	-	-
40	0.485	0.277	-	-

Table 47 : Apparent rate constant for prepared ZnO and calcinated at (500)^{o}C with methyl green Concentration .

Methyl green Concentration /ppm	k/min^{-1}
25	0.012
50	0.008
75	0.003
100	0.002

Table 48 : The change of irradiation time on different concentration of prepared ZnO and calcinated at (500)^{o}C with photocatalytic decolourization efficiency (PDE)

Irradiation	P.D.E at different dye concentration			
Time/min	25	50	75	100
0	0	0	0	0
5	5.769	16.666	1.666	-
10	7.692	16.666	6.666	2.04
15	23.076	16.666	8.333	4.081
20	26.923	16.666	8.333	4.081
25	26.923	19.696	8.333	6.122
30	28.846	19.696	8.333	6.122

Table 49 : The change of irradiation time on different dosages with prepared ZnO and calcinated at (500)^{o}C with C_t .

Irradiation	C_t at different dosage						
Time/min	**0.1**	**0.2**	**0.4**	**0.6**	**0.7**	**0.8**	**1**
0	4.289	2.657	1.078	1.95	1.368	1.74	1.66
5	4.263	2.394	1.052	1.53	1.289	1.53	1.63
10	4.21	2.368	1.026	1.03	1.263	1.5	1.61
15	4.078	2.236	1	1	1.052	1.45	1.45
20	3.947	2.184	0.947	0.84	1	1.42	1.37
25	3.763	2.105	0.921	0.79	1	1.39	1.34
30	3.684	2.078	0.894	0.76	0.973	1.37	1.32
35	3.657	2	0.868	0.76	0.868	1.34	1.29
40	3.631	1.973	0.868	0.76	0.842	1.34	1.29

Table 50 : The change of irradiation time on different dosages with prepared ZnO and calcinated at (500)^{O}C with ln(C_o/C_t) .

Irradiation Time/min	Ln(C_o/C_t) at different dosages						
	0.1	0.2	0.4	0.6	0.7	0.8	1
0	0	0	0	0	0	0	0
5	0.006	-	0.024	0.243	0.059	0.129	0.016
10	0.018	0.115	0.05	0.64	0.08	0.146	0.032
15	0.05	0.172	0.075	0.666	0.262	0.182	0.135
20	0.083	0.196	0.13	0.838	0.313	0.2	0.191
25	0.13	0.233	0.158	0.902	0.313	0.219	0.211
30	0.152	0.245	0.187	0.936	0.34	0.238	0.231
35	-	0.284	0.217	-	0.454	-	-
40	-	-	-	-	0.485	-	-

Table 51 : Relationship between apparent rate constant and dosage with prepared ZnO and calcinated at (500)^{O}C .

Dosage	(k /min^{-1})
0	0
0.1	0.004
0.2	0.008
0.4	0.006
0.6	0.036
0.7	0.012
0.8	0.009
1	0.008

Table 52: The change of irradiation time on different dosage for prepared ZnO and calcinated at (500)^{O}C with photocatalytic Decolourization efficiency (PDE) .

Irradiation Time/min	P.D.E at different catalyst dosage						
	0.1	0.2	0.4	0.6	0.7	0.8	1
0	0	0	0	0	0	0	0
5	0.613	9.9	2.438	21.62	5.8	12.1	1.6
10	1.84	10.9	4.878	47.3	7.7	13.6	3.2
15	4.907	15.8	7.317	48.65	23	16.7	13
20	7.975	17.8	12.2	56.76	27	18.2	17
25	12.269	20.8	14.63	59.46	29	19.7	19
30	14.11	21.8	17.07	60.81	37	21.2	21

Table 53 : The change of irradiation time at different value of pH with prepared ZnO and calcinated at (500)^{o}C with C_t .

Irradiation Time/min	C_t at different pH						
	2	**4**	**5.4**	**6**	**8**	**9**	**10**
0	6.973	1.684	1.947	2.052	2.105	2.105	2.105
5	6.394	1.657	1.526	1.684	1.736	1.763	1.71
10	5.763	1.657	1.026	1.684	1.71	1.71	1.71
15	5.473	1.657	1	1.657	1.71	1.684	1.526
20	4.894	1.657	0.842	1.631	1.71	1.684	1.473
25	4.578	1.657	0.789	1.605	1.71	1.684	1.473
30	4.263	1.657	0.763	1.578	1.71	1.684	1.473
35	3.868	1.657	0.763	1.526	1.71	1.684	1.473
40	3.552	1.657	0.763	1.447	1.71	1.684	1.473

Table 54 : The change of irradiation time at different value of pH with prepared ZnO and calcinated at (500) ^{o}C with ln(C_o/C_t) .

Irradiation Time/min	ln (C_o/C_t) at different pH						
	2	4	5.4	6	8	9	10
0	0	0	0	0	0	0	0
5	0.09	0.02	0.24	-	0.19	0.19	0.21
10	0.19	0.02	0.64	0.2	0.21	0.21	0.21
15	0.24	0.02	0.67	0.21	0.21	0.22	0.32
20	0.35	0.02	0.84	0.23	0.21	0.22	0.36
25	0.42	0.02	0.9	0.25	0.21	0.22	0.36
30	0.49	0.02	0.94	0.26	-	0.22	-
35	0.59	-	-	-	-	-	-
40	0.67	-	-	-	-	-	-

Table 55 : Relationship between apparent rate constant with prepared ZnO and calcinated at (500) ^{o}C and initial pH solution .

pH	k/min^{-1}
2	0.016
4	0
5.4	0.037
6	0.01
8	0.011
9	0.011
10	0.02

Table 56 : The change of irradiation time on different pH of solution with prepared ZnO and calcinated at (500) ^{o}C with photocatalytic Decolourization efficiency (PDE) .

Irradiation Time/min	P.D.E at different pH						
	2	**4**	**5.4**	**6**	**8**	**9**	**10**
0	0.0	0.0	0.0	0.0	0.0	0.0	0.0
5	8.3	1.56	21.6	17.9	17.5	17.5	18.7
10	17.4	1.56	47.3	17.9	18.7	18.7	18.7
15	21.5	1.56	48.6	19.2	18.7	20	27.5
20	29.8	1.56	56.8	20.5	18.7	20	30
25	34.3	1.56	59.5	21.8	18.7	20	30
30	38.9	1.56	60.8	23.1	18.7	20	30

Table 57 : The change of irradiation time at different temperatures of prepared ZnO and calcinated at (500)ºC with C_t .

Irradiation Time/min	C_t at different temperature /K			
	278.2	283.15	288.15	293.15
0	1.184	1.289	1.342	1.105
5	1.052	1.105	1.131	0.973
10	1.052	1.078	1.131	0.947
15	1.052	1.052	1.131	0.947
20	1.052	1.052	1.131	0.947
25	1.052	1.052	0.894	0.947
30	1.052	1.052	0.868	0.947
35	1.052	1.052	0.868	0.947
40	1.052	1.052	0.868	0.947

Table 58: The change of irradiation time at different temperatures with prepared ZnO and calcinated at(500)ºC with $\ln(C_o / C_t)$.

Irradiation Time/min	$\ln(C_o/C_t)$ at different temperature/ K			
	278.15	283.15	288.15	293.15
0	0.000	0.000	0.000	0.000
5	0.117	0.154	0.17	0.126
10	0.117	0.178	0.17	0.154
15	0.177	0.202	0.17	0.154
20	0.117	0.202	0.17	0.154
25	0.117	-	0.405	-
30	-	-	-	-

Table 59: Relationship between lnk and 10^3/T for solution with prepared ZnO and calcinated at 500 ºC.

$(10^3/T)/K$	ln k/min^{-1}
3.59	-5.051
3.53	-4.35
3.47	-4.297
3.41	-4.595

Table 60 : Relationship between ln (K/T) and (10^3/T) for solution with prepared ZnO and calcinated at 500 ^{O}C.

$(10^3/T)/K$	Lnk/T/(min^{-1} K^{-1})
3.59	-10.679
3.53	-9.996
3.47	-9.961
3.41	-10.275

Table 61: The activation kinetic parameters of the decolourization of methyl green dye with prepared ZnO and calcinated at (500)^{O}C.

E_a kJ mol^{-1}	$\Delta H^{\#}$ kJ mol^{-1}	$\Delta S^{\#}$ kJ mol^{-1} K^{-1}	$\Delta G^{\#}_{298.15}$ kJ mol^{-1}
19.69	17.272	-0.222	83.461

Table 62 : The change of irradiation time on different Temperatures of prepared ZnO and calcinated at (500) ºC with photocatalytic Decolourization efficiency (PDE).

Irradiation Time/min	P.D.E at different temperatures/ K			
	278.15	283.15	288.15	293
0	0.000	0.000	0.000	0.000
5	11.111	14.285	15.686	11.9
10	11.111	16.326	15.686	14.3
15	11.111	18.367	15.686	14.3
20	11.111	18.367	15.686	14.3
25	11.111	18.367	33.333	14.3
30	11.111	18.367	35.294	14.3

Table 63 : Different Percentage of Co Loaded on surface of prepared ZnO and calcinated at (500) ºC.

Co %	k/min^{-1}
0	0.044
0.5	0.01
1	0.017
2	0.001

Table 64: Different Percentage of Ag Loaded on prepared ZnO and calcinated at (500) ºC Surface .

Ag %	k/min^{-1}
0	0.044
0.5	0.038
1	0.039
2	0.057
4	0.043

Table 65: The change of irradiation time on different dye concentrations with Ag (2.00)/ prepared ZnO and calcinated at (500)ºC with C_t .

Irradiation	C_t at different methyl green concentration /ppm			
Time/min	25	50	75	100
0	2.5	5.657	5.973	13.921
5	1.578	4.947	5.263	13.315
10	1.105	4.421	4.71	13.078
15	0.842	3.894	3.736	12.421
20	0.605	3.526	2.947	11.578
25	0.526	3.052	2.842	11.315
30	0.421	3	2.842	10.789
35	0.368	2.947	2.842	10.315
40	0.315	2.842	2.736	10.000

Table 66 : The change of irradiation time on different dye concentrations with Ag(2.00)/ prepared ZnO and calcinated at (500) ºC with ln (C_o/C_t).

Irradiation	ln (C_o/C_t) at different methyl green concentration /ppm			
Time/min	25	50	75	100
0	0.000	0.000	0.000	0.000
5	0.459	0.134	0.126	0.044
10	0.816	0.246	0.237	0.062
15	1.088	0.373	-	0.114
20	1.418	0.472	-	0.184
25	-	0.617	-	0.207
30	-	-	0.742	0.254

Table 67 : Relationship between apparent rate constant and Concentration with Ag (2.00)/ prepared ZnO that calcinated at (500)ºC .

Methyl green Concentration /ppm	k/min^{-1}
25	0.073
50	0.024
75	0.027
100	0.008

Table 68 : The change of irradiation time on different concentration with Ag (2.00)/ prepared ZnO that calcinated at (500)ºC with photocatalytic decolourization efficiency (PDE) .

Irradiation	**P.D.E at different methyl green concentration**			
Time/min	25	50	75	100
0	0.000	0.000	0.000	0.000
5	36.842	12.558	11.894	4.347
10	55.789	21.86	21.145	6.049
15	66.315	31.162	37.444	10.775
20	75.789	37.674	50.66	16.824
25	78.947	46.046	52.422	18.714
30	83.157	46.976	52.422	22.495

Table 69 : The change of irradiation time on different dosage of Ag (2.00)/ prepared ZnO that calcinated at (500) ºC with C_t .

Irradiation Time/min	**C_t at different dosage**						
	0.1	**0.2**	**0.4**	**0.6**	**0.7**	**0.8**	**1**
0	4.63	3.21	2.26	2.66	2.5	2.37	2.18
5	4.5	3.11	1.76	1.61	1.58	1.32	1.11
10	4.42	3	1.39	1.05	1.11	0.79	0.68
15	4.32	2.95	1.11	0.76	0.84	0.55	0.61
20	4.18	0.95	0.87	0.66	0.61	0.45	0.53
25	3.53	0.89	0.63	0.55	0.53	0.42	0.29
30	3.42	0.66	0.58	0.34	0.42	0.32	0.29
35	3.08	0.61	0.47	0.32	0.37	0.32	0.24
40	2.84	0.53	0.42	0.29	0.32	0.32	0.21

Table 70: The change of irradiation time on different dosages of Ag (2.00)/prepared ZnO and calcinated at(500)^{O}C with $\ln(C_o/C_t)$.

Irradiation Time/min	$\ln C_o/C_t$ at different dosages						
	0.1	**0.2**	**0.4**	**0.6**	**0.7**	**0.8**	**1**
0	0.00	0.00	0.00	0.00	0.00	0.00	0.00
5	0.03	-	0.25	0.5	0.46	0.59	-
10	-	-	0.48	0.93	0.82	1.1	1.16
15	-	-	0.72	1.25	1.09	1.46	1.28
20	-	1.22	0.96	1.4	1.42	1.67	1.42
25	0.27	1.28	1.28	1.57	-	1.73	2.02
30	0.3	1.59	-	-	-	2.01	2.02
35	0.41	1.67	-	-	-	2.01	2.22
40	0.49	1.81	-	-	-	-	-

Table 71: Relationship between dosage of Ag (2.00)/prepared ZnO that calcinated at (500)^{o}C and rate constant.

Dosage	k /min^{-1}
0	0
0.1	0.011
0.2	0.049
0.4	0.049
0.6	0.071
0.7	0.073
0.8	0.069
1	0.071

Table 72: Relationship between irradiation time on different dosage of Ag (2.00)/prepared ZnO that calcinated at (500)^{o}C and photocatalytic Decolourization efficiency (PDE) .

Irradiation Time/min	P.D.E at different dosage						
	0.1	**0.2**	**0.4**	**0.6**	**0.7**	**0.8**	**1**
0	0.000	0.000	0.000	0.000	0.000	0.000	0.000
5	2.84	3.278	22.093	39.603	36.842	44.444	49.397
10	4.545	6.557	38.372	60.396	55.789	66.666	68.674
15	6.818	8.196	51.162	71.287	66.315	76.666	72.289
20	9.659	70.491	61.627	75.247	75.789	81.111	75.903
25	23.86	72.131	72.093	79.207	78.947	82.222	86.746
30	26.14	79.508	74.418	87.128	83.157	86.666	86.746
35	33.52	81.147	79.069	88.118	85.263	86.666	89.156
40	38.64	83.606	81.395	89.108	87.368	86.666	90.361

Table 73: The change of irradiation time at different value of pH with Ag (2.00)/prepared ZnO that calcinated at (500)^{o}C with C_t .

Irradiation Time/min	C_t at different pH						
	2	**4**	**5.4**	**6**	**8**	**9**	**10**
0	4.263	3.236	2.5	1.236	1.368	0.973	0.684
5	2.684	2.315	1.578	1.078	0.973	0.921	0.684
10	1.973	1.657	1.105	0.842	0.947	0.789	0.657
15	1.815	1.263	0.842	0.71	0.815	0.763	0.657
20	1.631	0.947	0.605	0.631	0.71	0.684	0.631
25	1.315	0.789	0.526	0.552	0.631	0.631	0.605
30	1.131	0.763	0.421	0.526	0.605	0.631	0.605
35	1.052	0.631	0.368	0.5	0.552	0.631	0.578
40	0.973	0.578	0.315	0.473	0.5	0.631	0.578

Table 74: The change of irradiation time at different value of pH for Ag (2.00)/ prepared ZnO that calcinated at (500) ºC with $\ln(C_o/C_t)$.

Irradiation Time/min	$\ln(C_o/C_t)$ at different pH						
	2	4	5.4	6	8	9	10
0	0.000	0.000	0.000	0.000	0.000	0.000	0.000
5	0.462	0.334	0.459	0.136	-	0.055	-
10	0.77	0.669	0.816	0.384	0.367	0.209	0.039
15	0.853	0.94	1.088	0.554	0.517	0.243	-
20	0.96	1.228	1.418	0.672	0.655	0.352	0.08
25	1.175	1.41	-	0.805	0.773	0.432	-
30	-	-	-	-	0.815	-	0.122
35	-	-	-	-	0.906	-	-
40	-	-	-	-	1.006	-	0.167

Table 75: Relationship between pH of Ag (2.00)/ prepared ZnO that calcinated at (500) ºC and apparent rate constant.

pH	k/min^{-1}
2	0.051
4	0.059
5.4	0.073
6	0.033
8	0.027
9	0.017
10	0.004

Table 76: The change of irradiation time on different pH of Ag (2.00)/ prepared ZnO that calcinated at (500)^{o}C with photocatalytic Decolourization efficiency (PDE)

Irradiation Time/min	P.D.E at different pH						
	2	**4**	**5.4**	**6**	**8**	**9**	**10**
0	0.000	0.000	0.000	0.000	0.000	0.000	0.000
5	37.037	28.455	36.842	12.765	28.846	5.405	-
10	53.703	48.78	55.789	31.914	30.769	18.918	3.846
15	57.407	60.975	66.315	42.553	40.384	21.621	3.846
20	61.728	70.731	75.789	48.936	48.076	29.729	7.692
25	69.135	75.609	78.947	55.319	53.846	35.135	11.538
30	73.456	76.422	83.157	57.446	55.769	35.135	11.538
35	75.308	80.487	85.263	59.574	59.615	35.135	15.384
40	77.16	82.113	87.368	61.702	63.461	35.135	15.384

Table 77: The change of irradiation time at different temperatures with Ag (2.00)/ prepared ZnO that calcinated at (500)^{o}C with C_t .

Irradiation Time/min	C_t at different temperature /K			
	278.15	283.15	288.15	293.15
0	5.078	7.289	4.236	4.368
5	4.105	5.973	3.131	3.184
10	3.5	4.289	2.578	2.657
15	2.947	3.815	2.131	2.263
20	2.578	3.368	2.078	2.052
25	2.236	2.842	2.026	1.921
30	1.973	2.789	1.921	1.763
35	1.894	2.736	1.894	1.71
40	1.842	2.684	1.842	1.842

Table 78: The change of irradiation time at different temperatures of Ag (2.00)/ prepared ZnO that calcinated at (500)ºC with ln(C_o /C_t) .

Irradiation Time/min	Ln(C_o/C_t) at different temperature /K			
	278.2	283.15	288.15	293.15
0	0.000	0.000	0.000	0.000
5	0.212	0.199	0.302	0.316
10	0.372	0.53	0.496	0.496
15	0.544	0.647	0.686	0.657
20	0.677	0.771	0.711	0.755
25	0.82	0.941	-	-
30	0.945	-	-	-

Table 79: Relationship between lnk and (1/T) with Ag (2.00)/prepared ZnO and calcinated at 500 ºC.

$(10^3/T)K$	Lnk /min^{-1}
3.59	-3.408
3.53	-3.218
3.47	-3.184
3.41	-3.17

Table 80 : Relationship between ln (k/T) and (10^3 /T) with Ag (2.00)/prepared ZnO that calcinated at 500 ºC.

$(10^3/T)$ /K	Lnk/T/(min^{-1} K^{-1})
3.59	-9.036
3.53	-8.864
3.47	-8.847
3.41	-8.85

Table 81: The activation kinetic parameters of the decolourization of methyl green dye with Ag(2.00)/prepared ZnO that calcinated at (500)ºC.

E_a kJ mol^{-1}	$\Delta H^{\#}$ kJ mol^{-1}	$\Delta S^{\#}$ kJ mol^{-1} K^{-1}	$\Delta G^{\#}_{306.15}$ kJ mol^{-1}
10.37	4.949	-0.243	79.343

Table 82 : The change of irradiation time on different Temperatures of Ag (2.00) / prepared ZnO that calcinated at (500)ºC with photocatalytic decolourization efficiency (PDE) .

Irradiation Time/min	P.D.E at different temperature /K			
	278.15	283.15	288.15	293.15
0	0.00	0.00	0.00	0.00
5	19.17	18.05	26.086	27.108
10	31.088	41.155	39.13	39.156
15	41.968	47.653	49.689	48.192
20	49.222	53.79	50.931	53.012
25	55.958	61.01	52.173	56.024
30	61.139	61.732	54.658	59.638
35	62.964	62.454	55.279	60.834
40	63.73	63.176	56.521	57.831

Table 83 : The change of irradiation time with prepared ZnO and metalized ZnO calcination at (500)ºC by using solar irradiation with Ct .

Irradiation Time/min	C_t at different Concentration		
	ZnO (500)^{O}C	Co (0.50)/ZnO	Ag(2.00)/ZnO
		(500) ^{O}C	(500) ^{O}C
0	0.736	6.763	2.526
2	0.473	6.684	2.368
4	0.394	5.921	2.131
6	0.368	5.868	1.868
8	0.342	5.736	1.684
10	0.315	5.631	1.631
12	0.289	5.368	1.526
14	0.263	5.21	1.447
16	0.263	5.157	1.368

Table 84 : The change of irradiation time with prepared ZnO and metalized ZnO calcination at (500)^{o}C with using solar irradation with lnC_o/C_t .

Irradiation Time/min	Ln C_o/C_t at different Concentration		
	ZnO (500) ^{O}C	Co (0.50)/ZnO (500) ^{O}C	Ag(2.00)/ZnO (500) ^{O}C
0	0.000	0.000	0.000
2	0.441	-	0.064
4	0.624	-	0.169
6	0.693	0.141	0.301
8	0.767	0.164	0.405
10	0.847	0.183	0.437
12	0.934	0.23	0.503
14	0.029	0.26	-
16	0.134	-	-

Table 85 : The change of apparent rate constant with prepared ZnO and metalized ZnO calcination at(500)^{O}C with using solar irradiation with % Metal .

Matel% loaded on prepared ZnO and calcinated at (500) ^{o}C	k/min^{-1}
ZnO (500) ^{o}C	0.08
Co (1.00)/ZnO (500) ^{o}C	0.019
Ag (2.00)/ZnO (500) ^{o}C	0.044

Table 86 :The change of irradiation time with prepared ZnO and metalized ZnO calcination at(500)^{o}C with using solar irradiation with PDE .

Irradiation Time/min	P.D.E at different Concentration		
	ZnO (500) ^{O}C	Co (0.50)/ZnO (500) ^{O}C	Ag(2.00)/ZnO (500) ^{O}C
0	0.000	0.000	0.000
2	35.714	1.167	6.25
4	46.428	12.451	15.625
6	49.999	13.229	26.041
8	53.571	15.175	33.333
10	57.142	16.731	35.416
12	60.714	20.622	39.583
14	64.285	22.957	42.708
16	67.857	23.735	45.833

Table 87: The change of irradiation time with naked ZnO and metalized Commercial ZnO with using solar irradiation with C_t .

Irradiation Time/min	C_t at different Concentration		
	ZnO Commercial	Co (0.50)/ZnO Commercial	Ag(2.00)/ZnO Commercial
0	3.421	4.368	7.921
2	3.394	4.000	6.578
4	2.894	3.921	5.052
6	2.131	3.552	4.842
8	1.684	3.447	3.973
10	1.526	3.368	3.500
12	1.210	3.289	3.236
14	1.000	3.157	3.052
16	0.684	3.105	2.894

Table 88 : The change of irradiation time with naked ZnO and metalized Commercial ZnO with using solar irradiation and ln C_o/C_t .

Irradiation Time/min	Ln C_o/C_t at different Concentration		
	ZnO Commercial	Co (0.50)/ZnO Commercial	Ag(2.00)/ZnO Commercial
0	0.000	0.000	0.000
2	-	-	0.185
4	-	0.108	-
6	0.473	-	0.492
8	0.708	0.236	0.689
10	0.807	0.259	0.816
12	1.038	0.283	-
14	1.229	0.324	-

Table 89: Relationship between apparent rate constant with using solar irradiation and % Metal .

Matel% loaded on ZnO Commercial	k/min^{-1}
ZnO Commercial	0.085
Co (0.50)/ZnO	0.024
Ag (2.00)/ZnO	0.083

Table 90: Relationship between irradiation time with naked ZnO and metalized ZnO with using solar irradiation and PDE.

Irradiation Time/min	**P.D.E at different Concentration**		
	ZnO Commercial	**Co (0.50)/ZnO**	**Ag(2.00)/ZnO**
		Commercial	**Commercial**
0	0.000	0.000	0.000
2	0.769	8.433	16.943
4	15.384	10.240	36.212
6	37.692	18.674	38.870
8	50.769	21.084	49.833
10	55.384	22.891	55.813
12	64.615	24.698	59.136
14	70.769	27.710	61.461
16	80.000	28.915	63.455

الخلاصة

يتكون هذا العمل من ثلاثة أجزاء. **الجزء الأول** يتضمن تحضير أوكسيد الخارصين ,وتلدينه بدرجة حرارة 500 م^{o} بالإضافة الى معدنة كل من أوكسيد الخارصين التجاري والمحضر بنسب تحميل مختلفة من الكوبلت والفضة بطريقة الترسيب الضوئي. وقد تم التحقق من خواص أوكسيد الخارصين المجرد والممعدن باستعمال تقنية الاشعة تحت الحمراء،وحيود الاشعة السينية وتحليل مجهر القوة الذرية بالإضافة الى اجراء تحليل الامتصاص الذري لكل من أوكسيد الخارصين التجاري والمحضر الممعدنيين.

اظهر تحليل الاشعة تحت الحمراء بأن اهتزازات المط لمجموعة الهيدروكسيل وقعت عند 3446 سم$^{-1}$ وهنالك حزمة قوية عند 500 سم$^{-1}$ أشارت الى وجود حزمة مط للأوكسجين- الخارصين، وهذا تاكيد الى تكون أوكسيد الخارصين .

كما ظهرت حزمة جديدة عند 1383-1384 سم$^{-1}$ تحميل الكوبلت على سطحي أوكسيد الخارصين التجاري والمحضر. ومن جهة أخرى تكونت حزمة جديدة عند 1386-1388 سم$^{-1}$ عند تحميل الفضة على سطحي أوكسيد الخارصين التجاري والمحضر .

تم الاستفادة من فحوصات الأشعة السينية لحساب معدل الحجوم البلورية والحجوم البلورية لأوكسيد الخارصين التجاري والمحضر- المجرد والممعدن بوساطة معادلة شيرر.

ازدادت معدل الحجوم البلورية والحجوم البلورية لأوكسيد الخارصين التجاري المجرد مع تحميل 0.5% كوبلت وقلت مع تحميل 2% فضة . اشارت صور مجهر القوة الذرية الى ان معظم الأشكال لأوكسيد الخارصين التجاري والمحضر- المجرد والممعدن شبه كروية. بالإضافة الى ذلك ان معظم حجوم الجسيمات كانت أقل من معدل الحجوم البلورية والحجوم البلورية .

الجزء الثاني، تضمن دراسة تأثير العوامل المختلفة على الإزالة اللونية لصبغة المثيل الاخضر مع وجود أوكسيد الخارصين التجاري والمحضر - المجرد والممعدن .هذه العوامل تتضمن كمية ونوع العناصر المحملة ، وتركيز الصبغة ، وكمية العامل المساعد ، والدالة الحامضية الابتدائية للمحلول ودرجة الحرارة.

الجزء الثالث تضمن نفس العوامل في الجزء الثاني ولكن باستخدام العامل المساعد (أوكسيد الخارصين المحضر المحروق عند 500 م^{o} -المجرد والممعدن**).**

درس التحفيز الضوئي للأزالة اللونية للمثيل الاخضر بوجود اوكسيد الخارصين المجرد والممعدن عند الشروط المثلى . تم دراسة تأثير التركيز الابتدائي للمثيل الاخضر باستخدام تراكيز مختلفة من (25-100) ppm. ووجد ان التفاعل يخضع للمرتبة الأولى الكاذبة .

عينت كمية أوكسيد الخارصين التجاري المجرد والممعدن بالفضة، وكانت افضل قيمة تساوي (0.7)غم /200 مللتر. ومن جهة أخرى وجد ان افضل قيمة لأوكسيد الخارصين المحضر كانت

تساوي (0.6) غم /200 مللتر والتي ازدادت الى (0.7) غم/200 مللتر بتحميل الفضة بنسبة 2% على سطح أوكسيد الخارصين المحضر .

ان أفضل دالة حامضية ابتدائية لمحاليل المثيل الاخضر المحفزه ضوئيا تساوي الى (10, 5.40,5.40 ,5.40) لأوكسيد الخارصين التجاري المجرد، والمحمل بـ 2% فضة ، وأوكسيد الخارصين المحضر، والمحمل بـ 2% فضة على التوالي .

تم التحقق من تأثير درجة الحرارة بوساطة استخدام معادلة ارينوس، وقد وجد انه بزيادة درجة الحرارة من (293.15-278.15) كلفن تزداد سرعة التفاعل، لذلك فأن تفاعل الأزالة اللونية الضوئية لصبغة المثيل الاخضر تفاعل ماص للحرارة. بالإضافة الى ذلك وجد ان قيمة طاقة التنشيط تساوي (29.14) كيلو جول /مول بوجود أوكسيد الخارصين التجاري، وتساوي (6.185) كيلو جول /مول بوجود أوكسيد الخارصين المحمل بالفضة (2%)، و (10.375 ،19.690) كيلو جول /مول بوجود أوكسيد الخارصين المحضر واوكسيد الخارصين المحضرالمحمل بالفضة (2%) على التوالي. وجد ان قيم الانتروبي قليلة نتيجة الى نقصان العشوائية وان التفاعل غير تلقائي.

جمهورية العراق
وزارة التعليم العالي والبحث العلمي
جامعة كربلاء - كلية العلوم – قسم الكيمياء

تحضير ووصف وتطبيق أوكسيد الخارصين لمعالجة صبغة المثيل الأخضر

رسالة مقدمة الى

مجلس كلية العلوم /جامعة كربلاء وهي جزء من متطلبات نيل شهادة

الماجستير في الكيمياء

تقدمت بها

اعتماد صالح فاضل الحسناوي

بأشراف

أ. م. د. لمى مجيد أحمد

1436 هـ **2015 م**